

**Impact of Ceramides and Penetration Enhancers on the
Nanostructure of Stratum Corneum Lipid Model Membranes**

D i s s e r t a t i o n

zur Erlangung des akademischen Grades

doctor rerum naturalium (Dr. rer. nat.)

vorgelegt der

Naturwissenschaftlichen Fakultät I
Biowissenschaften

der Martin-Luther-Universität Halle-Wittenberg

von

Frau Tanja Nadine Engelbrecht
geboren am 09.04.1983 in Zschopau

Gutachter /in

1. Prof. Dr. R. Neubert
2. Prof. Dr. B. Dobner
3. Prof. Dr. G. Brezesinski

Tag der Verteidigung: Halle (Saale), 24.07.2012

Contents

1	Introduction and Outline	6
2	Theoretical Background and Basic Concepts	8
2.1	The Human Skin	8
2.2	Stratum corneum - Main permeation barrier of human skin.....	11
2.2.1	The SC lipids	12
2.3	Insights into the molecular structure of the skin penetration barrier.....	16
2.4	Penetration enhancers	23
2.5	Methodology in Stratum corneum research and principles of the employed techniques	28
2.5.1	Neutron diffraction	28
2.5.2	Other techniques used.....	40
3	Results Represented by Accepted Publications	45
3.1	The influence of different CER subclasses on the lamellar nanostructure of SC lipid model membranes	45
3.1.1	Impact of phytosphingosine-type CER[NP] on the assembly of SC lipids in ternary model membranes (Manuscript: Soft Matter)	45
3.1.2	Study of an artificial CER[EOS] pendant containing a saturated, branched ω - acyl chain (Manuscript: Soft Matter)	55
3.2	Lipophilic penetration enhancers: Their impact on the SC lipid bilayer architecture and modes of action	70
3.2.1	Structure of SC lipid model bilayers in presence of oleic acid (Manuscript: Biophysica et Biochimica Acta – Biomembranes)	70
3.2.2	Isopropyl myristate: Influence on the lamellar architecture of oriented SC lipid model membranes and mode of action (Manuscript: Skin Pharmacology and Physiology)	80
4	Final Discussion and Perspectives	89
4.1	The SC lipid bilayer morphology and the influence of phytosphingosine- and sphingosine-type CER species	89
4.2	Mode of action of two representative lipophilic penetration enhancers on the lamellar architecture of SC lipid multilayers.....	94
4.3	Perspective	99
5	Summary	101
5.1	English version	101

5.2	German version.....	103
6	Appendix	106
6.1	List of Substances	106
6.2	Composition of the oriented SC lipid model membranes studied in the present thesis.....	109
6.3	The effect of OA on the SC lipid architecture: DSC measurements	110
6.4	The impact of IPM on the SC lipids: FT Raman spectroscopy	111
7	References	113
8	Publications	127
9	Acknowledgement.....	130
10	Curriculum Vitae.....	131
11	Eidesstattliche Erklärung	133

Symbols and abbreviations

Å	Angstrom
AP	alpha-hydroxy phytosphingosine
AS	alpha-hydroxy sphingosine
a.u.	arbitrary units
b_{coh}	bound coherent scattering length
b_{incoh}	bound incoherent scattering length
B_0	static magnetic field
BA	behenic acid
CER	ceramide
CHOL	cholesterol
ChS	cholesterol sulphate
cm	centimetre
°C	degree Centigrade
D	deuterium
d	lamellar (bilayer) repeat distance
DMSO	dimethyl sulfoxide
DSC	differential scanning calorimetry
EFADS	essential fatty acid deficiency syndrome
e.g.	for example
EM	electron microscopy
EOS	omega-hydroxy sphingosine esterified with linoleic acid
EOS_branched	omega-hydroxy sphingosine esterified with C10-methyl branched palmitic acid
Eq.	equation
ν	stretching mode
f	frequency
FE	fully extended
FFA	free fatty acid
F_h	structure factor (also SF)
Fig.	figure
FT	Fourier transform
^1H	hydrogen, protium

^2H	deuterium
HZB	Helmholtz-Zentrum für Materialien und Energie Berlin
I	intensity
I	nuclear spin
i.e.	id est
ILL	Institut Laue-Langevin
IPA	isopropyl alcohol
IPM	isopropyl myristate
IPM- d_3	isopropyl myristate-14,14,14- d_3
K	Kelvin
kHz	kilohertz
λ	lambda, wavelength
LAM	longitudinal acoustic mode
LPP	long periodicity phase
MD	molecular dynamics
mm	millimetre
mbar	millibar
mg	milligram
ml	millilitre
m/m	mass ratio
mol/mol	molar ratio
ω	omega
OA	oleic acid
OA- d_2	oleic acid-9,10- d_2
nm	nanometre
NMR	nuclear magnetic resonance
^2H NMR	deuterium nuclear magnetic resonance
NSLD	neutron scattering length density
PA	palmitic acid
RH	relative humidity
$S_{CD}(n)$	order parameter of the carbon-deuterium bond
SA	stearic acid
SANS	small angle neutron diffraction
SAXD	small angle X-ray diffraction

SC	Stratum corneum
SF	structure factor (also F_n)
SLD	scattering length density
SPP	short periodicity phase
θ	theta, scattering angle
T	temperature
v/v	volume ratio
WAXD	wide angle X-ray diffraction

1 INTRODUCTION AND OUTLINE

The outermost layer of mammalian skin, the Stratum corneum (SC) forms a protecting barrier of outstanding importance for the organism. It exhibits a unique structure of cornified cells embedded in an extracellular matrix with lipophilic character. Mainly composed of sphingolipids termed ceramides (CER), free fatty acids (FFA) and cholesterol (CHOL), this lipid matrix is arranged in highly organized and well ordered multiple lipid bilayers containing almost no free water. When the first reports came up stating that the major barrier for transepidermal water loss and penetrating actives is constituted by the lipid lamellae of the SC intercellular matrix, the latter became a topic of great interest in the field of SC research.

Obstacles provided by biological material like excised skin hinder elucidating the molecular morphology of the SC lipid matrix. These difficulties (e.g. the complexity and chemical variability of the lipids present in the SC, disturbing other material like proteins or ethical issues related to the use of excised human skin) led to an increase in the usage of synthetic SC lipids in SC research. To allow for a systematic evaluation of the relevance of single CER species, multilamellar model membranes containing simplistic mixtures of synthetic SC lipids represent a suitable approach as shown in numerous previous works [1-6]. Such a systematic determination of the impact of particular CER subclasses is important for a detailed insight into mechanisms of skin diseases. This knowledge supports the development of new therapeutic approaches. In addition, enhanced understanding regarding the function of different SC lipids in the process of barrier formation and maintenance helps to develop new carrier systems being able to overcome the penetration barrier more efficiently.

This work aimed at investigating the alterations in the molecular architecture of oriented SC lipid model matrices occurring due to the presence of different ceramide subspecies (section 3.1), or taking place after addition of lipophilic penetration enhancers to the model systems (section 3.2). For that purpose, SC lipid model membranes with different compositions were prepared, usually containing one or two CER species besides one FFA component and CHOL. Despite their simplicity, such simplistic models are suitable for determining structure–function relationships, especially for particular CER species. In a first approach (Chapter 3.1.1), the impact of the short-chain CER[NP] on the bilayer morphology of a newly established ternary model system was elucidated in order to confirm the protruding influence of the phytosphingosine-type CER species on the lamellar architecture that was already suggested

previously [7]. In Chapter 3.1.2, a new artificial CER[EOS] with a methyl-branched saturated ω -acyl chain was characterized regarding its thermotropic phase behaviour, and the resulting bilayer structure of a model membrane containing the artificial compound was studied in comparison to the membrane based on native CER[EOS].

To clarify the molecular mode of action of penetration enhancers affecting the lipophilic penetration pathway, two representative model compounds were chosen. First, the effect of unsaturated oleic acid (OA) on the lamellar nanostructure of a well-described quaternary model membrane was studied (Chapter 3.2.1). Benefitting from selective deuterium labelling, the exact molecular assembly of OA inside the model bilayers and its mode of action as penetration enhancer were elucidated. In addition, the pharmaceutically used synthetic liquid wax isopropyl myristate was investigated with regard to its effects on the structure of SC lipid bilayers on a nanoscale (Chapter 3.2.2). Again, selective deuteration was advantageous for the purpose of localizing the enhancer molecules in the bilayer unit cell and to elucidate IPM's enhancer activity on a molecular scale.

The experimental results of this thesis are presented as they were accepted for publication in international peer-reviewed scientific journals. Chapter 4 contains a comprehensive discussion of the results, and in section 5 a summary is given. An Appendix (Chapter 6) was provided for additional information.

2 THEORETICAL BACKGROUND AND BASIC CONCEPTS

The following chapter represents an introduction in the fundamental concepts of the topic of interest, namely the mammalian skin, its components and morphology, its complex function, and further its importance for terrestrial life. Special focus is placed on the outermost skin layer, the Stratum corneum (SC), with the different ideas of structural SC lipid organization being highlighted. Furthermore, the substance class of penetration enhancers is introduced. Finally, the technical and methodological approaches relevant for this thesis are presented.

2.1 The Human Skin

Covering an average area of about 2 m², the skin is the largest organ of the adult human individual. It represents a natural barrier between the inner body and the external environment, protecting the human organism against harmful outer influences, which can be of chemical (e.g. penetrating substances or drugs), physical (e.g. heat or cold), microbial, or mechanical (e.g. pressure) nature. Furthermore, the skin is essentially involved in the maintenance of water balance and thermoregulation of the organism through permanent adaption of perspiration and blood flow. Apart from its relevance in sustaining body homeostasis, the skin moreover plays an important role in further processes, such as signal transduction, and acts as sensory organ due to the presence of various specific receptors [8]. Generally, the human skin is composed of three consecutive layers: the inner subcutis (hypodermis), the dermis (corium), and the outer epidermis. A schematic representation of the anatomical structure of human skin is displayed in Fig. 1.

Accommodating larger blood vessels and nerves than the dermis, the subcutis constitutes the connection between the musculature and periosteum, and the skin. This loose connective tissue mainly consists of lobules of large lipid-containing cells, the *adipocytes*. It serves as an insulating layer, energy reserve, and as protecting cushion against pressure exposure [9]. The hypodermis is followed by the dermis, a supporting tissue containing a network of fibrous protein structures (collagen and elastin fibres), dermal cells (mainly *fibroblasts*), a ground substance containing macromolecules, e.g. proteoglycans and glycoproteins, and is further accommodating structures like blood vessels, nerve endings, skin appendages like sweat glands, sebaceous glands, and hair follicles [10]. Due to its complex composition and the spe-

cific ultrastructure of the fibrous systems, the dermis allows for stability as well as elasticity of the skin [11, 12]. Additionally, extensive vascularization ensures the nutrition of the dermis itself and the adjacent epidermis.

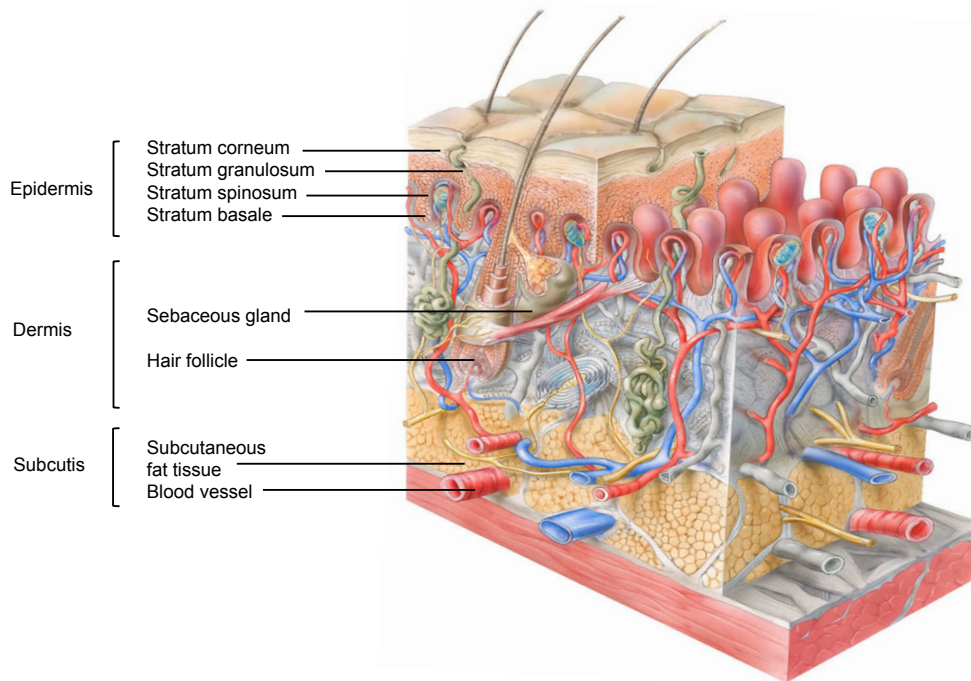


Fig. 1: Schematic representation of a cross section of human skin (adapted from Skin Care Forum [13]).

The upper part of the dermis (papillary dermis) exhibits small upward protuberances, which allow for improved adhesion between dermis and epidermis. The latter forms the outer layer of the skin and can be divided in different parts, which are in inside-to-outside direction the Stratum basale, Stratum spinosum, Stratum granulosum, and the SC.

The epidermis represents a continuously self-renewing tissue. It mainly consists of *keratinocytes*, which are subjected to a distinct differentiation process, and other cell types like dendritic antigen-presenting cells that are relevant for immune response (Langerhans cells), Merkel cells, and melanocytes. Descending from the basal layer where a continuous cell proliferation, i.e. mitosis of stem cells, ensures the permanent regeneration of the epidermis, the keratinocytes pass towards the skin surface to be eventually desquamated. During this migration they undergo several morphological and biochemical changes. Hemidesmosomes accomplish the anchorage of the basal cells to the underlying basement membrane. While keratinocytes located in the basal layer have a cell nucleus and exhibit a columnar form, the cells located upwards, e.g. in the Stratum spinosum, possess a more cubic or polygonal

shape, and increasingly flatten the more they progress towards the outer epidermal layer, the SC. Simultaneously to this change in shape, the cells start to produce the structural protein keratin, which is arranged inside the cell bodies in bundles of filaments (tonofibrils). The latter strongly contribute to the stability and adherence of the epidermis by forming the cytoskeleton and the desmosomes, which represent intercellular junctions between the keratinocytes allowing for a cohesive cell assembly (see Fig. 2). In the next layer, the Stratum granulosum or granular layer, the keratinocytes are subject to apoptosis: most organelles and the cell nucleus disappear, while the cell body is increasingly filled with granules of keratohyalin, an assembly of keratin and another protein, the profilaggrin. The keratinocytes now exhibit a flattened shape and are arranged parallel to the skin surface [9].

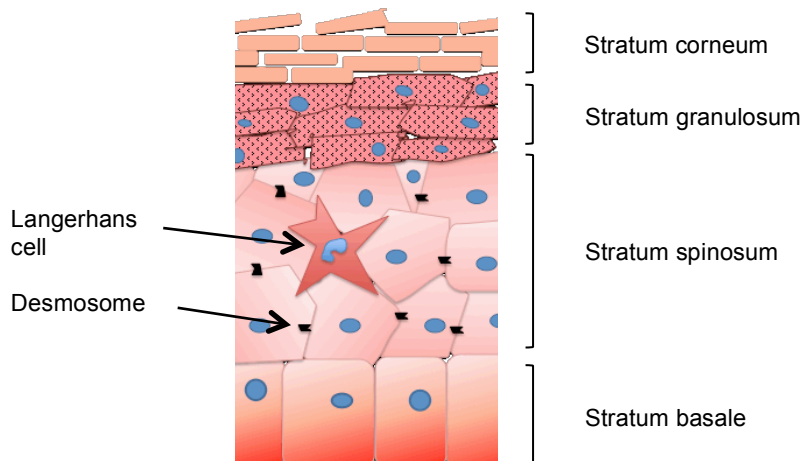


Fig. 2: Sketch of the epidermis of human skin.

Specific cell organelles enriched with lamellar structures appear in the upper layers of Stratum spinosum and in Stratum granulosum, the so-called Odland bodies [14]. These membrane-coating granules contain lamellar stacks of lipids and enzymes, which get discharged into the intercellular space by the cells of the uppermost granular layer. This secretory process is realized by fusion of the lipid-containing granules with the plasma membranes, which subsequently results in the release of disk-shaped lipid aggregates into the extracellular space. [15-18]. It was shown that this lipid extrusion step is significantly important for the proper formation of the intercellular lipid matrix present in the SC [19].

The SC, the outermost non-viable sheath of human skin accommodates the so-called *corneocytes*, the cornified and flattened remaining cell bodies of the keratinocytes, which have reached their final differentiation state and are densely filled with

keratin. The formerly disk-like intercellular lipids now have fused, giving way to the formation of continuous, uninterrupted lipid multilayers. Finally, the superficial corneocytes get desquamated. Due to this regeneration, the whole epidermis is renewed about every 28 days.

2.2 Stratum corneum - Main permeation barrier of human skin

Despite its diminutive thickness of approximately 9-13 μm , which is equivalent to about 15-30 cell layers [20-22], the uppermost epidermal layer, the SC, was early recognized to be highly important for protection of the organism [23], but it was the work of Scheuplein and co-workers which manifested the SC to constitute the main permeation barrier of the skin [24].

Already in the 60s, the SC was realized to feature a well-ordered structure [25]. The SC consists of dead keratin-enriched corneocytes embedded in organized lamellar lipid layers, with the cell bodies being coated by the *cornified envelope* [26]. This mantle is made up of insoluble proteins like involucrin and loricrin, to which a monolayer of intercellular SC lipids is covalently bound via esterified ω -hydroxy groups to form the so-called *lipid envelope* [27]. The latter is assumed to be of importance for the cohesion of the SC [28], which additionally is accomplished by intercellular protein structures, the corneodesmosomes [29].

Due to new insights into SC morphology, the early paradigm of the SC representing just a dense and rigid layer preventing any transport of material has thoroughly changed towards the idea of a highly complex two-compartment system of protein-containing cells inside a lipid-enriched space [30]. One of the first structural approaches describing this morphology was the so-called **Brick and Mortar Model**: in this conception, keratin-filled cells constituting the bricks are embedded in a mortar of intercellular lipids, which are arranged in well-ordered multiple bilayer structures [31]. Now the question arose: Which structural part mainly determines the crucial barrier properties of the SC?

In principle, crossing the skin barrier can take place via different routes, as sketched in Fig. 3. For a long time, drug diffusion through the SC was supposed to mainly take place via a transcellular route [32] through alternating hydrophilic (corneocytes' cell bodies) and lipophilic moieties (see Fig. 3). Later it was realized that the intercellular lipid matrix constitutes the major barrier for molecules traversing

skin, and that its role for drug absorption has to be reconsidered [15, 18, 33]. The intercellular penetration pathway appeared as the favoured way for substances overcoming the skin barrier. Further penetration studies underlined this assumption regarding the importance of the intercellular lipid matrix for the epidermal barrier properties, revealing that SC thickness or quantity of cell layers are of minor importance for percutaneous penetration of model substances [34]. However, beyond the transport-preventing barrier properties, the multilamellar domain of extracellular SC lipids holds a regulatory function by facilitating a controlled transepidermal loss of water in order to guarantee the organism's homeostasis [35].

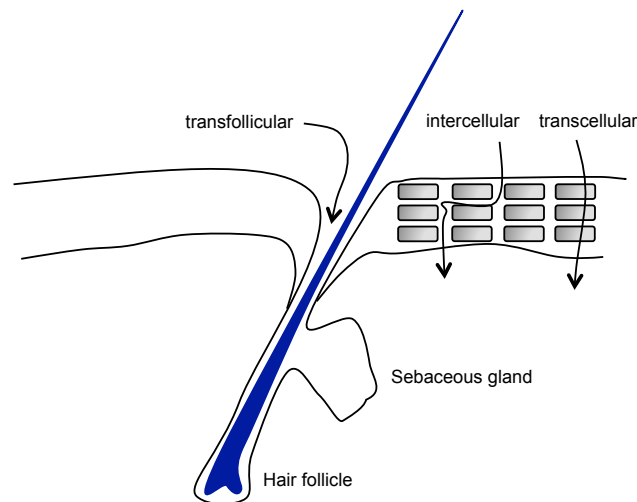


Fig. 3: Schematic representation of main penetration pathways through human SC as reviewed in [36].

The transfollicular skin penetration pathway [37] was shown to play a distinct role in case of application of microparticles [38].

2.2.1 The SC lipids

In the 70s, the first studies addressed the issue of analysing the lipid composition of mammalian epidermal skin [39]. These revealed some characteristics for the uppermost epidermal layer with the most surprising observation being the negligible amount of phospholipids, which actually constitute the main components of all biological membrane structures. Furthermore, it was demonstrated that a distinct group of sphingolipids, the ceramides (CER), are accumulated in the uppermost epidermal layer, and that these compounds represent the quantitatively protruding lipid fraction of the SC [39, 40]. In addition, free fatty acids (FFA) and cholesterol (CHOL) were determined as major SC components of human skin besides small amounts of cholesterol sulphate (ChS) and cholesterol esters [41]. However, the respective SC lipid

amounts underlie inter- and intraindividual variations [41, 42]. The combination of tape-stripping technique with chromatographic procedures allowed for surveying the lipid depth profile within human SC [43]. After a disruption of the SC barrier, e.g. by treatment with detergents or solvents (acetone), the epidermal synthesis of SC lipids gets stimulated. This process slows down as soon as barrier recovery is completed [44].

The skin surface is furthermore covered with a lipophilic film originating from sebaceous glands and the keratinizing epidermal layers, which basically consists of waxes and sterol esters, squalene, sterols, tri-/partial glycerides and fatty acids [45].

2.2.1.1 Ceramides

The ceramides (CER) accumulating in the uppermost epidermal layer during cell differentiation are complex and structurally inhomogeneous lipophilic substances which constitute about 50 % of the SC lipid mass [46]. To this day, 12 subclasses have been determined [47, 48] whose chemical structures are presented in Fig. 4.

In principle, ceramides consist of a long-chain fatty acid species being linked to the amino group of a long-chain sphingoid base via an amide bond. The variation arises from combination of one of the four known bases (sphingosine, phytosphingosine, 6-hydroxy-sphingosine, or dihydrosphingosine) with either of three fatty acid moieties, which can be α -hydroxylated, or ω -hydroxylated, or non-hydroxylated. An older nomenclature which numbered the ceramides according to their chromatographic behaviour and increasing polarity [49, 50] was later replaced by another classification based on a letter code referring to the chemical composition of the ceramide subspecies [51]. Here, the first letter denominates the fatty acid species present in the molecule, i.e. **A** represents an α -hydroxy fatty acid, **N** a non-hydroxy fatty acid, **EO** an esterified ω -hydroxy fatty acid. The second letter indicates the type of N-acylated sphingoid base (**S** for Sphingosine, **P** for Phytosphingosine, **DS** for Dihydrosphingosine, and **H** for 6-Hydroxysphingosine, respectively).

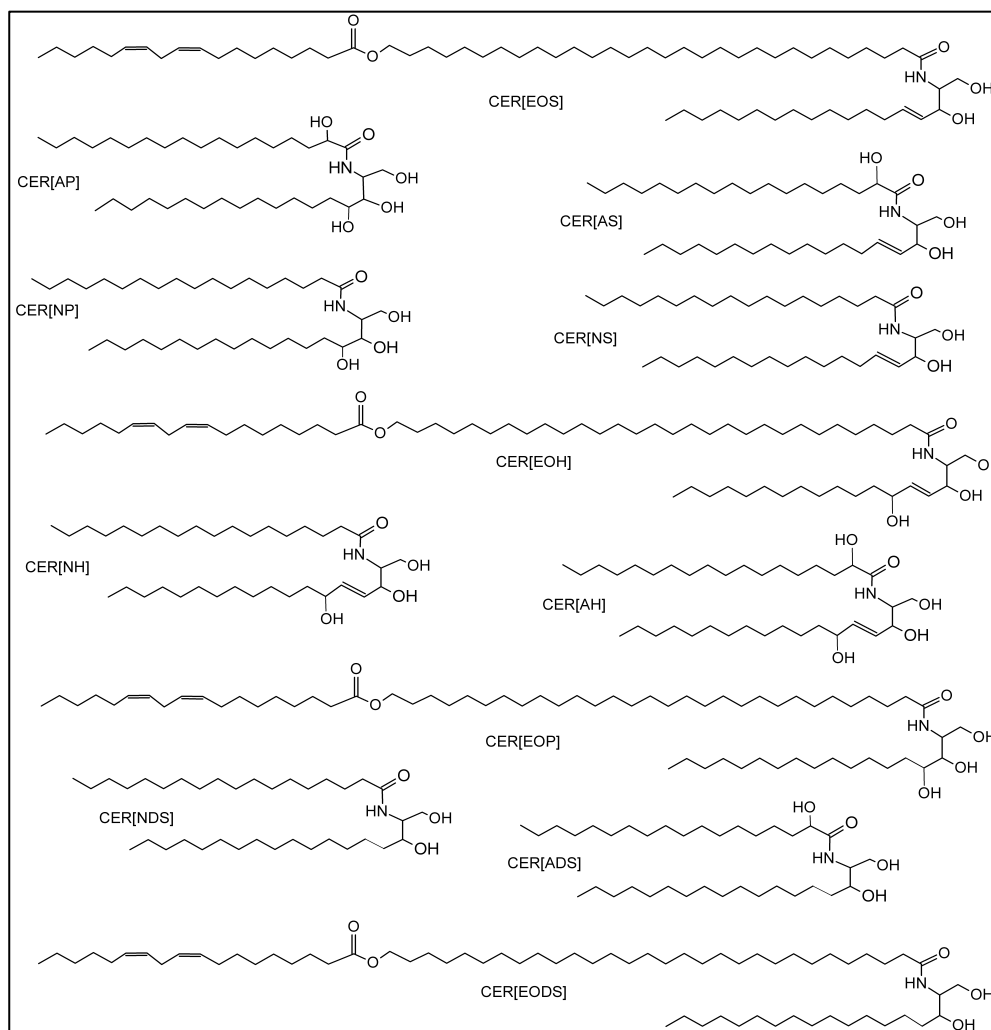


Fig. 4: The chemical structures of the ceramide (CER) subclasses identified in human SC according to [47, 48].

Wertz et al. [50] determined the most abundant alkyl chain lengths of the sphingoid base to be C18-C22, while the most frequently occurring chain lengths of the amide-bound fatty acids vary between C18-C26. However, a subsequent study analysing the SC ceramide subspecies of human forearm skin revealed slightly longer chain lengths for the sphingoid bases, and even proved the presence of odd carbon numbers [47]. The most remarkable structure is owned by the long-chain ω -esterified ceramide species, where the amide-bound fatty acids, primarily C30 and C32, are additionally esterified via their ω -hydroxy group to another fatty acid, mainly the double-unsaturated linoleic acid [50]. This results in one extremely elongated alkyl chain.

Albeit correlations between skin barrier properties and the ceramide content in epidermal tissues suggest a considerable function of those sphingolipids for the maintenance of the skin penetration barrier [52], the exact role of each ceramide subclass is not yet completely enlightened. However, several pathological states of

skin, e.g. atopic dermatitis and psoriasis, are found to be associated with a clearly decreased epidermal level of the long-chain CER[EOS] [53, 54]; the authors concluded a protruding role of this CER subclass for maintaining the skin barrier properties. Besides, the content of CER[NP] and CER[AP] was reported to be diminished in the psoriatic scale [51]. De Paepe et al. [55] stated that epidermal barrier recovery after chemical perturbation was considerably improved after topical treatment of impaired skin with a formulation containing CERIII, CERIIIb, and CERVII (corresponding to the phytosphingosine-based CER[NP], an artificial CER[NP], and CER[AP]) besides other SC lipids. In addition to these studies focusing on the role of particular ceramide subclasses for the epidermal barrier function, there is evidence that the ceramide alkyl chain length determines the properties of the permeability barrier. This was suggested in a permeation study where application of synthetic ceramide species with truncated alkyl chain lengths of C12 (sphingosine base) and C2-C12 (amide bound fatty acid) resulted in enhanced permeation of the model drugs [56].

2.2.1.2 Free fatty acids

Free fatty acids (FFA) present in the interlamellar space of the SC originate from *de novo* synthesis in the epidermis [57]. The most abundant chain lengths were determined to be C16-C26, with C24 dominating [43]. Basically, these FFA represent saturated and straight-chain compounds. At the same time, essential fatty acids only play a minor role in the intercellular FFA fraction of the SC. However, it was shown that supplementation of linoleic acid was capable to normalize the pathologically increased transepidermal water loss (TEWL) occurring in the *essential fatty acid deficiency syndrome* (EFADS) [58, 59]. This correlation presumably arises from the esterified essential fatty acid species linked to the long-chain ω -hydroxy acyl ceramides [60], whose importance for the SC lipid matrix integrity was outlined above. However, the FFA of the intercellular SC space were determined to contribute significantly to the maintenance of a proper permeation barrier, the more so since the skin barrier recovery after acetone-disruption and simultaneous inactivation of the FFA synthesis was considerably enhanced after application of FFA [61].

2.2.1.3 Cholesterol

This sterol is ubiquitary in mammalian biological membranes and constitutes one of the three main components of the human SC intercellular lipid matrix. Its bulky steroid framework of four condensed cycloalkanes with an alkyl chain is accompa-

nied by an OH group representing the comparatively small hydrophilic head group. CHOL present in the intercellular space of the SC descends from epidermal *de novo* synthesis, and its importance for the formation of a competent penetration barrier was highlighted before [62]. In that study, the epidermal synthetic activity for CHOL was clearly enhanced after acute barrier abrogation, which resulted in increased production of epidermal CHOL and finally in recovery of the normal barrier function. Moreover, when the epidermal biosynthesis of CHOL is prohibited, the process of barrier recovery is significantly prolonged as reported by Feingold et al., which indicates the importance of this sterol for the skin integrity [63].

Further, CHOL was found to markedly influence the phase behaviour of other lipids. In a molecular dynamics (MD) simulation study, the extremely well ordered and rigid structure of fatty acids was significantly smoothed in presence of the sterol, with distinct fluidizing effects being introduced to the rigid fatty acid assembly [64]. On the other hand, CHOL presumably condenses the lamellar arrangement of phospholipids and stabilizes the liquid-ordered (Lo) phase [65]. Such a bilateral action of CHOL when mixed with phospholipids, i.e. that it liquefies the lipids below the phase transition temperature, but has a condensing effect on the lipids above the main phase transition temperature [66], was also attested for the interaction of CHOL with SC lipids like CER[AP], palmitic acid, and ChS [67].

Besides free CHOL, also a small amount of ChS can be found in the SC, which decreases towards the upper SC layers. ChS is assumed to be of importance for the cohesion and stability of the inner SC lipid layers [68]. However, it furthermore seems to play an essential role for the desquamation process of the uppermost epidermal cell layers: in X-linked ichthyosis patients, ChS levels are significantly increased in the upper SC compared to healthy skin, which is due to a lacking degradation of ChS to CHOL since the enzyme steroid sulphatase is missing [69, 70]. This defect results in an abnormally dry and scaly appearance of the skin, with large scales instead of single cells getting desquamated.

2.3 Insights into the molecular structure of the skin penetration barrier

Ever since the cognition that the main penetration barrier of the human skin resides in its outermost layer and the discovery of the main SC components, the structural characteristics of this superficial epidermal mantle became a key issue in SC

research: How can such a thin skin layer constitute such an efficient penetration barrier? General knowledge was already available, e.g. it was accepted that the protein-enriched SC cells are embedded in a coherent and extremely hydrophobic matrix of lipids [71]. This early **two-compartment model** or **Brick and Mortar Model** of the human SC based on results received from freeze-fracture studies [30, 72] provided first hints that the SC interstices are largely made up of broad sheets of lamellar material. It was stated that the freeze fracture technique offers some advantages over other methods commonly applied in SC research, e.g. conventional thin section electron microscopy (EM) which suffers from artefacts being introduced by fixation and processing of skin samples [73]. But despite this perception, thin section electron microscopy has been frequently applied as valuable tool for investigating the SC structure on a submicron scale [16, 74].

One of the first studies, which focused on the molecular morphology of the intercellular space of SC and provided evidence of its bilayer structure was the one of Madison et al. [75]. Using the more reactive oxidizing agent ruthenium tetroxide for fixation, the authors were able to prove the presence of alternating electron-dense and electron-lucent bands described as broad-narrow-broad sequences, and determined a lamellar spacing of approximately 130 Å for the SC lipid bilayer structures. The sequenced patterns were likewise observed by Swartzendruber et al. [76], who came up with the **Stacked Monolayer Model** (see Fig. 5) in order to explain the occurrence of such band structures, which differed in width in the transmission electron microscopic images.

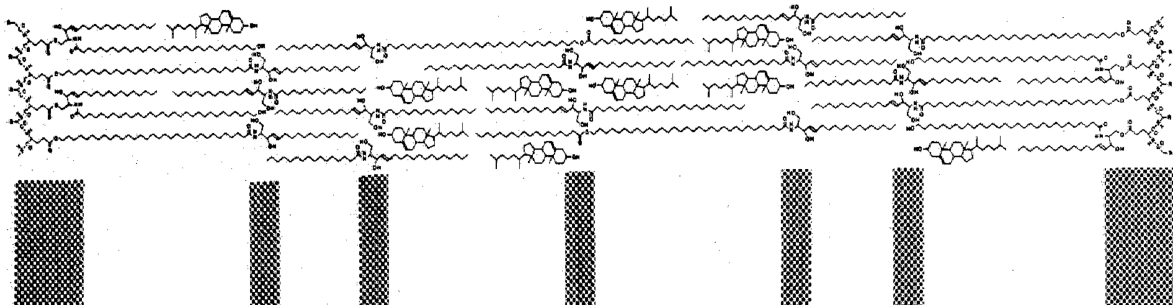


Fig. 5: Structural assembly of the intercellular SC lipid matrix according to the Stacked Monolayer Model [76].

The authors reasoned that, due to a fully extended configuration adopted by the ceramides, the outstretched lipid chains from the neighbouring bilayer might contribute to the formation of an embedded half of another bilayer, i.e. a lipid mono-

layer, by strong interdigitation. Such an alkyl chain assembly would then account for the observed narrow lucent bands coexisting with the broad structures, which were believed to be associated with “normal” lipid bilayers [76]. This work provided an important first insight into the unique ultrastructure of the extracellular SC lipid domains. Yet, the question about the route small molecules take on their way through the intercellular SC lipid matrix in order to leave or enter the human organism was not answered by the model of Swartzendruber et al. [76]. Potts et al. observed a strong correlation of water permeation and the number of *gauche* conformers in isolated porcine SC. The authors proposed that the diffusion of water molecules through lipid membranes occurs via defects provided by *gauche*-conformer “holes” inside otherwise intact lamellar structures [77]. This idea of defects or “holes” in the highly ordered matrix enabling substance diffusion was already introduced before [78] and can be found in the **Domain Mosaic Model** postulated by Forslind [79]. Here, these defects are thought to appear as lipids in a liquid state and are denoted by the authors as “grain borders”. According to this model, the SC lipids form a multilamellar two-phase system of crystalline domains embedded in a continuous liquid-crystalline matrix, the grain borders [79]. While the former are believed to be almost impermeable to water, the latter represent the site of water diffusion with decreased resistance against traversing molecules. As depicted in the sketch of Fig. 6, such a structural arrangement results in a mosaic-like distribution of gel domains in each of the stacked bilayer planes.

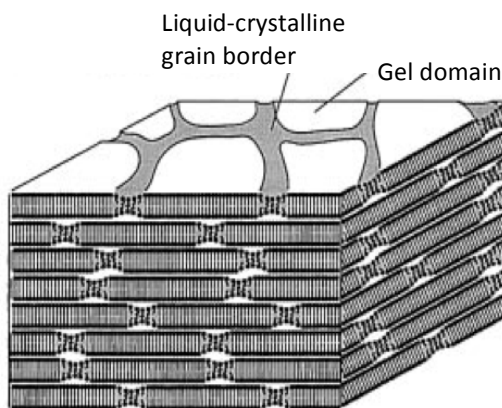


Fig. 6: The Domain Mosaic Model postulated by Forslind [79].

In the direction normal to the multilayer surface, the water-penetrable liquid-crystalline grain border regions are randomly distributed. As a result, compounds diffusing through the SC extracellular lipid regions would have to overcome a single bilayer through such a liquid-crystalline domain, subsequently passing through the polar interlamellar space before entering the next lamellar sheet [79-81].

Another attempt to describe the SC lipid architecture on a molecular scale was introduced as the **Single Gel Phase Model** by Norlén [82]. Based on the idea that the hydrophobic intercellular matrix of the SC is constituted by a single continuous gel-phase membrane structure with basically no phase separations occurring, the model was assumed to ideally explain the impermeability of the skin barrier, since interfaces between segregated lipid domains offering improved permeability are lacking. The SC lipids are thought to exhibit poor mobility due to dense packing, and the water content is expected to be very low. Further, the high compositional variation of the SC lipid matrix was proposed to account for broad phase transitions, which may also contribute to optimal barrier properties even under varying environmental conditions [82]. Although the ceramides may adopt either hairpin or splayed conformation or a mixture of both, and orthorhombic and hexagonal chain packing coexists, the SC lipid matrix is still regarded to remain in a single-phase arrangement according to this model, which is presented in Fig. 7.

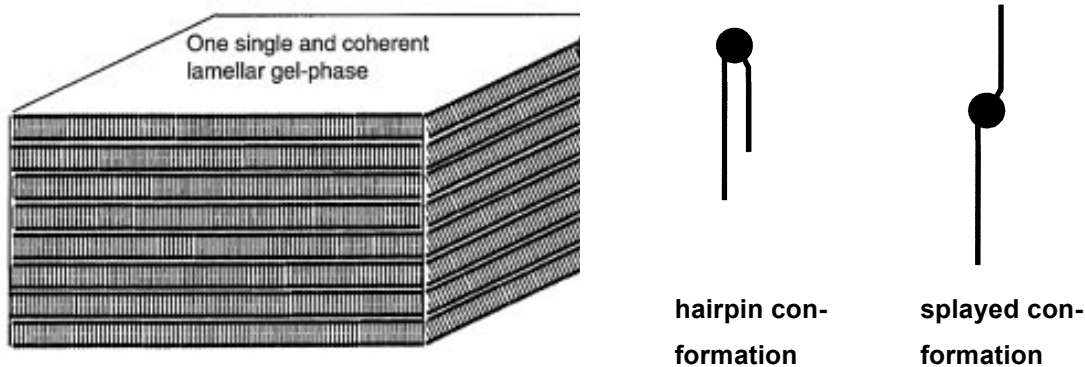


Fig. 7: The SC lipid assembly and the possible ceramide conformations as postulated by Norlén [82].

The assumed absence of phase separations distinguishes the Single Gel Phase model likewise from the aforementioned models and another interesting structural model, the **Sandwich Model** introduced by Bouwstra et al. [83]. The authors thereby made an attempt to clarify the structural arrangement of the SC lipids inside the surprisingly large lamellar structure of approximately 130 Å periodicity [84], which had already been observed before in human as well as murine SC [75, 85] and that occurred besides a smaller phase with a spacing of about 60 Å in small angle X-ray diffraction (SAXD) studies on human SC [84]. In accordance to the sequenced broad-narrow-broad pattern, Bouwstra et al. postulated a three-layer SC lipid assembly which results in the formation of the overall lamellar spacing of 130 Å, the so-called long periodicity phase (LPP). According to their model that is depicted in Fig. 8, the

authors assume the lipid matrix of the SC to consist of a discontinuous and laterally distributed narrow fluid sublattice in the central bilayer region, which is surrounded by two crystalline sublattices. The increasing crystallinity towards the outer bilayer areas results from the long-chain immobile saturated alkyl chains of the ceramide species in hairpin conformation located in this lamellar region. In contrast, the ω -acyl ceramides' unsaturated side chains, CER5 (corresponding to CER[AS] with an amide-bound C16 fatty acid [80]) and CHOL account for the formation of the liquid monolayer in the central bilayer region which corresponds with the narrow sequence reported by Swartzendruber [76]. The authors emphasized that due to the comparatively small amount of SC lipids forming this fluid moiety, the liquid domains do not have continuous properties but are distributed laterally throughout the lamellar matrix [83]. It has to be noted that first, the sandwich model does not take into consideration the different conformational possibilities known to be adopted by the ceramides, and second, the expected exposure of hydrophilic head groups from CER[AS] and CHOL assembled in the central liquid bilayer moiety to hydrophobic alkyl chains may be considered as unlikely [80].

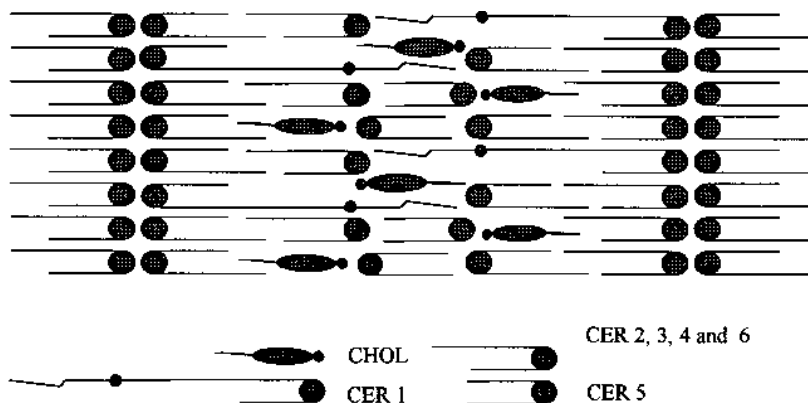


Fig. 8: The Sandwich Model by Bouwstra et al. [83].

The sandwich model regarding the structural alignment of the SC lipids in the LPP is strongly founded on the presence of the long-chain ω -esterified ceramide subspecies CER[EOS], [EOP] and [EOH].

Since the structural models described so far are not able to give reasons for the phenomena occurring under excess hydration of the SC lipid matrix, another approach, the **Armature Reinforcement Model** was postulated by Kiselev et al. [4] in order to explain the reported disappearing 1st order reflection of isolated porcine SC under excess hydration [86]. As already suggested in Norlén's Single Gel Phase Model, the authors also consider different conformational states for the ceramides.

Especially the fully extended (FE) conformation is assumed to play an important role for the membrane integrity and water diffusion resistibility of the SC intercellular lipid matrix. As further emphasized in [3], a change from FE to hairpin conformation - a phenomenon termed chain flip transition of the ceramide molecules - takes place under excess water conditions and accounts for the appearance of a hydrated intermembrane space of about 1 Å. Under partial hydration of the lipid lamellae the FE state provides the steric contact and consequently the adhesion between adjacent bilayers as to be seen in Fig. 9.



Fig. 9: The principle of the Armature Reinforcement Model [3].

In fully hydrated state, the enhanced interlamellar water amount would cause an unfavourable high-energetic state required for the hydration of the hydrophobic alkyl chains of the ceramide molecules in FE conformation. Therefore, the hairpin conformation is energetically preferred under excess of water and the chain flip of one ceramide alkyl chain is conceivable [3, 4].

Finally, Norlén recently introduced a new structural conception of the skin permeability barrier based on results from cryo-electron microscopy on vitreous sections (CEMOVIS) of biological material *in situ* combined with molecular modelling and EM simulation [87, 88]. The electron micrographs revealed the presence of bilayer repeating units of about 110 Å in width consisting of asymmetric sub-units of 65 Å and 45 Å spacing. Those appeared as alternating broad and narrow bands. This lipid organization was explained with a fully extended conformation adopted by the short-chain ceramide molecules such as CER[NP], and an asymmetric distribution of CHOL and FFA. While CHOL is presumably accommodated in the bilayer containing the sphingoid part, FFA have high affinity to the lamellae formed by the amide-bound acyl chain of the ceramide molecules. Such an assembly has not been described before and might sufficiently explain the skin's resistibility against mechanical influences (bending, stretching) and its low permeability, as stated by the authors [88].

The structural models briefly described in this context provide different views regarding the occurrence of phase separation, and the existence of liquid lipid domains inside the SC lipid matrix. Since the ultimate experimental proof for the correctness of each model with respect to the *in vivo* conditions of mammalian SC is

lacking due to experimental obstacles connected with structural investigation of biological material, the aforementioned models are debated vigorously [80, 89]. A particular issue that is controversially discussed is the SC lipid arrangement in the LPP. Whereas there are experimental findings indicating a trilamellar broad-narrow-broad arrangement with sublattice spacings of 50-30-50 Å [84, 90], other results received from EM studies on porcine SC lipids claim the presence of uniform size for the three sublattices of the trilayer structure [91]. The authors reasoned that the impression of a narrow central lamellar structure might result from the stronger accumulation of reduced ruthenium due the localization of the unsaturated linoleate groups in this lamellar region. Indeed, the possibility of artefacts introduced during sample processing and fixation for conventional transmission EM has been addressed in other studies [92].

The lamellar structure of the LPP is frequently discussed in association with the presence of the long-chain ω -acyl ceramides. However, its existence, and its molecular structure are debated controversially. From diffraction experiments with SC lipids isolated from pig epidermal skin, McIntosh and co-workers concluded that the CER[EOS] subspecies must play a key role for the formation of the lamellar structure of the LPP [93]. In addition, Bouwstra et al. proposed that not only porcine SC lipids [94], but also lipids extracted from human SC form the LPP, as long as an ω -acyl ceramide with its exceptional long and unsaturated acyl chain is present [95]. It was moreover reported that lamellar models composed of extracted human CER's, CHOL and FFA closely resemble the intercellular bilayer arrangement previously proposed for intact human SC, where two lamellar structures referred to as short periodicity phase (SPP) with a spacing of about 60 Å, and the LPP of about 120 Å spacing co-exist [95, 96]. Yet, the authors reasoned that the clearly diminished formation of the LPP in mixtures lacking CER[EOS] provides direct evidence for the key role of this particular ceramide subclass for a proper SC barrier function [94, 97]. A similar conclusion was drawn for synthetic SC lipid mixtures consisting of equimolar amounts of CER, FFA and CHOL: for a proper formation of the LPP, de Jager et al. stated that CER[EOS] is required in the ceramide fraction [98-100]. The authors furthermore identified the FFA to advance the creation of the 130 Å phase in mixtures of synthetic SC lipids, while in contrast, the addition of FFA to isolated SC lipids diminished the LPP formation in favour of the SPP assembly. Although the LPP was reported to occur in the SC of all species examined by X-ray diffraction [94, 96, 97], also contro-

versial results disproving the existence of the LPP are found in literature [92, 101]. In particular, recent neutron diffraction studies of multilamellar models consisting of synthetically derived SC lipids do not corroborate the existence of the LPP in CER[EOS] based model membranes [1, 102].

Summing up, a plurality of structural models considering the molecular architecture of the skin penetration barrier exists. Despite the diversity of techniques applied in the field of SC research, a general tendency towards the use of model systems based on synthetic SC lipids with defined chemical structure can be observed. Such systems can overcome difficulties related to the use of biological material, e.g. the limited availability of excised skin human skin due to ethical requirements, and the chemical variability of lipids extracted from human SC [98-100, 103]. Beyond that, the use of more simplistic and less sophisticated models became increasingly established and was proven to represent a valuable tool providing detailed insights into the role of single SC lipid species [1, 102]. Based on this approach, the present work elucidates the impact of different ceramide subclasses and penetration modulators on the SC lipid matrix on a molecular level. Such information is essentially needed for a better understanding of possibilities to maintain the skin barrier function, or to overcome the SC in terms of dermal or transdermal drug delivery.

2.4 Penetration enhancers

The application of topical formulations often aims at strengthening the skin penetration barrier against perturbing outer influences. However, in some cases, least-wise an intermittent derogation may be desirable, e.g. for improving the dermal or transdermal effect of drugs which need to penetrate into deeper skin layers or to traverse the skin [104]. In both cases, the amount of substance overcoming the skin barrier can be increased via several ways. One possibility to achieve this is the chemical penetration enhancement by applying so-called penetration enhancers. For a more extensive description of other ways to promote drug transport through the skin, in particular of physical methods, see [104, 105].

Although a plurality of substances is known to feature enhancing effects on dermal drug penetration, their exact mode of action on the molecular level is not yet completely clarified. Since the main skin penetration barrier resides in the SC, several ways of interaction with the SC components have been proposed, in particular dis-

solution of skin lipids, increase of lipid fluidity, increase of drug solubility in the skin, alteration of molecular lipid conformation, skin protein denaturation, and disruption of the skin water structure. Yet, these processes presumably have to be regarded not as separate but mutually depending actions [106].

Generally, one distinguishes between penetration enhancers, which, due to their hydrophobic character, preferentially interact with the lipophilic part of the SC lipids, i.e. the hydrocarbon chains, and substances affecting the SC lipid head groups as sketched in Fig. 10. The former are referred to as lipophilic penetration enhancers, the latter are termed hydrophilic penetration enhancers. Consequently, lipophilic penetration enhancers are able to promote lateral diffusion processes via the lipophilic pathway along the SC lipids' hydrocarbon tails, whereas hydrophilic enhancers impact the hydrophilic penetration pathway [107]. However, it was realized that such a strict differentiation does not apply to all cases. The manipulation of SC lipid head group interplay by means of a hydrophilic penetration enhancer was found to simultaneously alter the properties of the lipophilic parts of the lipids and vice versa. This explains the observed promotion of lipophilic drug penetration when enhancers interacting with the hydrophilic lipid part are applied [104].

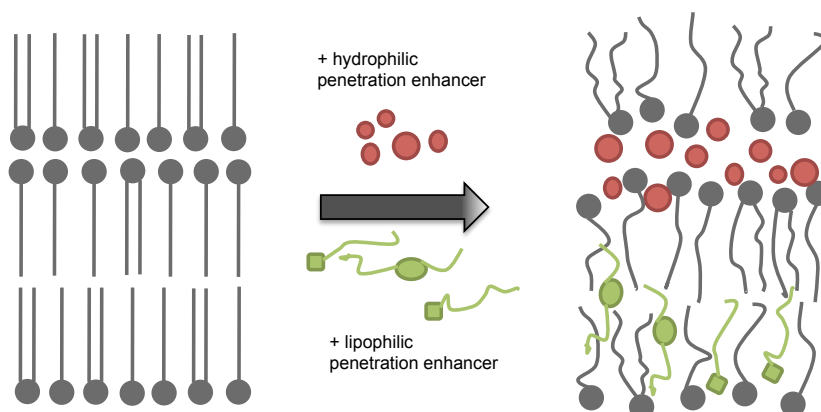


Fig. 10: Schematic representation of the SC intercellular lipid matrix and possible ways of interaction with penetration enhancers, modified according to [107].

One of the most efficient substances enhancing the diffusion of hydrophilic drugs is water. Its effect is pharmaceutically used in e.g. occlusive vehicles or in transdermal therapeutic systems. The usual water content of human SC varies between 10% [108] and 20% of the tissue dry weight [109] and can increase to a severalfold under excess hydration conditions, e.g. occlusion [109]. Such an extensive SC hydration results in simultaneous changes in the lipid phase state as reported in a differential scanning calorimetry (DSC) study [110]. Water was concluded to interact

with the SC lipid head groups and appeared to loosen the lipid packing [110]. This results in an increased fluidity of the SC lipids, which then presumably accounts for the decreased resistance of the skin barrier towards diffusion of actives.

Another potent penetration enhancer for hydrophilic, but also lipophilic substances is the aprotic solvent dimethyl sulphoxide (DMSO). Its high polarity founded on the S-O bond accounts for the excellent dissolving properties of DMSO, making it a powerful cosolvent for numerous substances [104]. Different suggestions for the enhancer activity of DMSO and its mode of action exist. Interaction with the protein components of SC and simultaneous change of keratin conformation was reported [111]. On the other hand, DMSO apparently influences the intercellular lipid lamellae by increasing the number of *gauche* conformers, which appeared in an increase in lamellar disorder as revealed by Fourier transform (FT) Raman spectroscopy [112]. A considerable aspect of DMSO's enhancer activity is presumably founded on such lipid-fluidizing and disordering effects, as further corroborated by molecular dynamics (MD) simulations of a ceramide-based bilayer [113]. The authors reported a significant decrease in bilayer thickness and simultaneous increase of the area per lipid at high concentrations of DMSO. The experimental results indicated DMSO to induce a gel-to-liquid-crystalline phase transition due to extensive interactions of the polar DMSO molecules with the SC lipid head groups at the expense of lipid-lipid interactions. Hence, the lamellar SC lipids featuring such an altered liquid-crystalline structure represent a weaker barrier to the permeating agents [113]. The ability of DMSO to induce the formation of water pores in phospholipid membranes [114] could not be proven in the ceramide-based system, but the enhancer presumably lowers the membrane bending rigidity in a way comparable to phospholipid membranes [113]. The main disadvantage of DMSO is its irritant potential when applied in the comparatively high doses of about 60 % required for relevant enhancer activity [109, 115, 116]. Further hydrophilic penetration enhancers, which have been studied extensively, are alkanols [117-120] and urea [121]. The former substance class presumably increases drug diffusion through the skin via combined mechanisms of improving the solubility of permeants being poorly soluble in the vehicle, increasing the drug partitioning into the SC lipid layers, and augmenting the permeant's thermodynamic activity in the vehicle due to formation of an supersaturated solution [109]. For propylene glycol, which acts as a co-solvent, a *solvent-drag* mechanism is discussed [122]. On

the other hand, the enhancer activity of urea is presumably based on its hydrating, in higher concentrations keratolytic effects [109].

In addition, a variety of lipophilic penetration enhancers exist. The percutaneous penetration of substances was shown to increase after application of different unsaturated fatty acids. From a structural point of view, one expects fatty acids to strongly interact with the lipid part of the SC, with an incorporation of those amphiphilic molecules into the intercellular lipid lamellae being thoroughly conceivable. In the work of Aungst et al., the most pronounced effect in terms of enhanced penetration of the model drug naloxone was detected for fatty acid compounds exhibiting either short-chain or unsaturated structure [106]. The authors explained this result with the intercellular SC lipid matrix being made up of tightly packed and mainly long-chain fatty acids and ceramides. Such a dense arrangement is more efficiently disrupted by short-chain or unsaturated fatty acids than by the long-chain species. Among the fatty acids studied, the monounsaturated species oleic acid (OA) was early recognized as a very potent penetration promoter for acyclovir [123], dihydroergotamine [124], 5-flourouracil [125], piroxicam [126] and several other drugs [127], underlining OA's capability of improving flux of both lipophilic and hydrophilic substances. Spectroscopic measurements revealed the *cis*-unsaturated C18 fatty acid to strongly influence the SC lipid ordering by perturbation of the lamellar structure [128, 129]. The bulky *cis* unsaturated structure apparently requires more space and consequently affects the surrounding lamellar lipid arrangement drastically. In contrast, the C18 fatty acid with *trans* unsaturation was shown to have almost no effect on the permeation properties of salicylic acid [130].

In addition, phase separation was reported to occur and is assumed to substantially contribute to OA's activity as penetration enhancer [131, 132]. Such separated and fluid domains being rich in OA would offer a significantly decreased resistance against substances traversing the skin barrier [126] and are therefore regarded to account for the penetration enhancer activity of OA. However, despite their potential, the application of fatty acids, particularly of linoleic acid as penetration enhancers is limited due to their skin irritation potential which emerges at higher concentrations [133, 134]. Furthermore, the application of OA as penetration enhancer was found to alter the surface properties of corneocytes, i.e. formation of pores was facilitated. In addition, a likewise observed decrease in the density of Langerhans cells might der-

ogate the skin's immune competency [135]. Therefore, the noncritical use of permeation promoters should be avoided.

Fatty acid esters were also highlighted as potent lipophilic penetration enhancers in numerous experiments. Isopropyl myristate (IPM) increased both piroxicam flux through excised rat skin [136] and permeation of nicorandil through excised hairless rat skin [137]. The latter work compared various esters in terms of their ability to act as penetration enhancers, e.g. isopropyl butyrate/hexanoate/decanoate/palmitate. It was further demonstrated that IPM increases the estradiol flux through excised human skin [138], and that there is a synergistic effect depending on the deployed cosolvent. In that study, isopropyl alcohol (IPA) together with IPM showed the most pronounced enhancement effect. Furthermore, the authors found that IPM was largely retained inside the SC and has high affinity to the SC intercellular lipids due to its distinct lipophilic character [138]. Comparable synergies were also reported for the combination of IPM with propylene glycol in an *in vitro* study of diclofenac sodium penetration. The enhancement effect of IPM was attributed to its affinity to the intercellular lipid matrix of the SC and its ability to liquefy the SC lipids [139], which was already demonstrated before in the work of Leopold et al. [140]. Another group approved IPM's high impact on the lipid moieties of the SC by combined DSC, wide-angle x-ray diffraction (WAXD) and small-angle x-ray diffraction (SAXD) studies, and reported reduced transition temperatures and lowered transition enthalpies, but surprisingly also a more densely packed lateral lipid arrangement. The decreased permeation of hydrocortisone in presence of IPM in the vehicle was assumed to be due to lower solubility of the drug in IPM [141]. However, when IPA was used as enhancer, drug flux was increased, and combined application of IPM and IPA led to even more enhanced drug permeation. Both additives were supposed to have a high affinity to the intercellular SC lipid layer, thereby altering its structural properties, but IPA's disordering and fluidizing effects seem to counteract the observed stabilizing action of IPM [141]. The authors concluded synergistic enhancer action of IPM and IPA. From further SAXD and WAXD studies, the authors deduced a structural idea of IPM being incorporated in the SC lipid bilayers with the isopropyl group anchored in the polar bilayer moiety and the C14 alkyl group pointing towards the bilayer center [142]. Also the short-chain esters, e.g. ethyl acetate, were found to be capable to enhance the flux of different substances through rat skin *in vitro* [143]. A disruption of the lipid packing with increased lipid fluidity was assumed to represent the mode of

action of the applied esters. Finally, also novel ester compounds, e.g. N-acetyl proline esters, have been successfully synthesized and were proven to promote benazepril and hydrocortisone penetration into hairless mouse skin [144].

Other lipophilic compounds, which improve cutaneous absorption of substances via the lipophilic pathway, are the naturally occurring and non-aromatic terpenes [145]. Especially the cyclic monoterpenes and terpenoids have been subject of interest in several penetration studies. Yamane and co-workers highlighted the effect of 1,8-cineole and d-limonene on the *in vitro* permeability of 5-flourouracil and the drug's partitioning into the SC in a DSC study [125]. The results suggested that 1,8-cineole exhibited a higher effect than d-limonene, and that the mode of action presumably is based on interaction with and interruption of the well-ordered SC lipid matrix.

2.5 Methodology in Stratum corneum research and principles of the employed techniques

2.5.1 Neutron diffraction

The technique of neutron diffraction is a versatile instrument for the study of structure and dynamics, which also applies to biological samples. Due to their specific properties, neutrons may provide structural insights that are hardly obtained by using other techniques, e.g. X-ray or light scattering. Neutrons are subatomic particles constituting the atomic nucleus together with the protons, and have a mass of 1.675×10^{-27} kg and a spin I of $1/2$. Neutrons for research are produced either in a fission reactor (fission of ^{235}U), or in a spallation source (bombardment of a heavy metal target with accelerated subatomic particles, e.g. protons). Since the neutron flux of present fission reactor facilities is comparably low in relation to synchrotron facilities producing high-intense photon radiation, measuring time in neutron diffraction studies is unequally longer for collection of complete data sets with sufficient statistics. The neutron diffraction experiments performed in this work were carried out at the reactor sources of either Helmholtz-Zentrum Berlin für Materialien und Energie (HZB), or Institut Laue-Langevin (ILL) in Grenoble.

As non-charged particles, neutrons are enabled to penetrate matter deeply due to the small probability of interaction [146]. In contrast to X-rays, which are scattered by the electrons, neutrons interact with the atomic nucleus and are scattered isotrop-

ically [147]. Hence, while the ability of elements to scatter X-rays increases with the atomic number throughout the periodic table, such a correlation does not exist for neutrons [148]. Particularly hydrogen, a light atom that is almost invisible for X-rays, is a strong scatterer for neutrons. This makes neutron diffraction a valuable instrument to investigate structure and dynamics in biological samples being rich in hydrogen. Moreover, neutrons show isotope-sensitivity, i.e. even different isotopes of one element may have different scattering power for neutrons, for which hydrogen (^1H) and deuterium (^2H , D) are the most prominent examples [147]. The possibility to distinguish between components differing in their ability to scatter neutrons in one single sample, the so-called *contrast*, is of great advantage for the study of biological systems like lipids and proteins [149-151].

According to the particle-wave-dualism [152], neutrons exhibit a wave character in addition to their particle properties. The neutron wavelength λ is defined as

$$\lambda = \frac{h}{\vec{p}} = \frac{h}{m \cdot \vec{v}} \quad \text{Eq. 2-1}$$

where h is the Planck's constant, \vec{p} represents the neutron's momentum, m is the neutron's mass and \vec{v} is the neutron's velocity. Depending on the moderator used, the neutron wavelength λ may be shifted towards desired values. Thermal neutrons are received in a reactor by the cooling water surrounding the reactor core, and a "hot source" moderator like graphite produces neutrons with higher energies and shorter wavelengths, while the use of a "cold source" like liquid hydrogen produces low energy neutrons with longer wavelengths. For the purpose of structural studies of matter, λ usually has the dimension of Å, which is the typical order of magnitude of most interatomic distances. This allows for studying the structure of condensed matter.

The neutron's momentum is further given by

$$\vec{p} = \hbar \cdot \vec{k} \quad \text{Eq. 2-2}$$

where Planck's constant h is reduced to $\hbar = h/2\pi$, and \vec{k} is the neutron wave vector, defined by $|\vec{k}| = 2\pi/\lambda$.

In the course of a simple neutron diffraction experiment, the sample to be studied is placed in a collimated neutron beam with defined neutron wavelength λ , received by appropriate positioning of a monochromator. Incoming neutrons interact with the sample and thereby experience a change in their momentum, which appears

as a change of neutron direction and/or velocity. Hence, monitoring the variation of the neutron's momentum provides information regarding the structure and dynamics of the sample matter. In order to describe this momentum change, a momentum transfer vector, the *scattering vector* \vec{Q} , was introduced. \vec{Q} is defined as the vector difference between the incident neutron wave vector \vec{k}_1 and the scattered neutron wave vector \vec{k}_2 :

$$\vec{Q} = \vec{k}_1 - \vec{k}_2 \quad \text{Eq. 2-3}$$

In addition to a change in direction, the value of \vec{k} might also change due to *energy* exchange between incoming neutrons and nuclei of the sample matter. The neutron's energy change E is defined according to the law of energy conservation:

$$\Delta E = E_1 - E_2 = \hbar^2 \cdot \frac{\vec{k}_1^2}{2m} - \hbar^2 \cdot \frac{\vec{k}_2^2}{2m} \quad \text{Eq. 2-4}$$

with m being the neutron mass. When $E = 0$, the scattering process is considered as completely elastic. Consequently, we have $|\vec{k}_1| = |\vec{k}_2|$, and receive according to Eq. 2-3:

$$|\vec{Q}| = 2\vec{k}_1 \cdot \sin \theta \quad \text{Eq. 2-5}$$

In the case of crystalline matter, Bragg peaks arise at values of \vec{Q} equivalent to the reciprocal spacing of the lattice:

$$|\vec{Q}| = \frac{2\pi}{d} \quad \text{Eq. 2-6}$$

Here, d represents the spacing between the crystal lattice planes.

Given that $|\vec{k}| = 2\pi/\lambda$, the known Bragg equation is received:

$$\lambda = 2d \cdot \sin \theta \quad \text{Eq. 2-7}$$

It represents the conditions for constructive interference to occur when neutron waves with a wavelength λ in the range of the atomic spacings hit a set of equidistant crystal lattice planes separated by the distance d [146]. At this point, the different phenomena of *scattering* and *diffraction* are to be outlined for clarity. *Scattering* occurs when radiation hits and subsequently interacts with matter. Given that the material lacks an organized lattice arrangement, e.g. randomly dispersed particles in a

distinct medium, the scattered waves cover different distances and consequently differ in their relative phases. This provides information about particle size, shape and interaction. However, *diffraction* takes place when waves impinge on ordered material, i.e. a crystal structure. It therefore represents a special case of scattering, where - according to Bragg's law - constructive interference of waves scattered by the well-ordered lattice planes of a crystalline sample appears as a so-called Bragg maximum at a distinct scattering angle 2θ . The scattered waves remain in phase since the path length difference equals an integer multiple of the wavelength λ . This correlation, and a sketch of a typical neutron diffraction experimental set-up are presented in Fig. 11. The feasibility to obtain diffraction patterns directly from the intact SC intercellular lipid domains was demonstrated in the late 80's, indicating the presence of highly ordered structures [85].

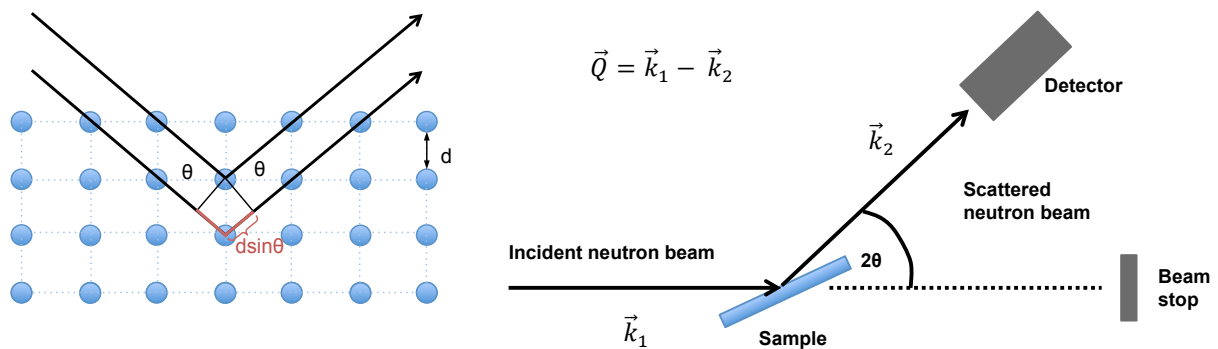


Fig. 11: (Left) Schematic drawing of neutron scattering from ordered crystalline matter, as given by Bragg's law. The incident neutron waves (hitting the crystal lattice planes in the angle θ from the left) are scattered to the right. The scattering planes are separated by the interplanar distance d . The path length difference between the waves interfering constructively is equal to $2d \sin \theta$. (Right) Typical set-up of a neutron diffraction experiment as performed in the present thesis. \vec{k}_1 designates the incoming wave vector, \vec{k}_2 represents the scattered neutron wave vector, and \vec{Q} is the scattering vector. The change of energy of the scattered neutron wave, ΔE , was disregarded.

Assuming a neutron scattering process from a single, fixed nucleus, the incoming neutron wave can be regarded as plane wave ψ_1 while the scattered wave ψ_2 has spherical character. Now the characteristics of ψ_2 strongly depend on the atomic nucleus' scattering power, described by the neutron scattering length b , which can be considered as atomic or isotopic constant with typical dimensions in the range of 10^{-12} cm. The square of the latter is proportional to the total scattering cross section σ_s , roughly spoken the effective area an atom's nucleus presents to the incoming neutron wave for the elastic scattering process [146]. As mentioned before, the val-

ues of coherent scattering length b_{coh} differ significantly for ^1H ($-0.374 \cdot 10^{-12}$ cm) and ^2H ($0.667 \cdot 10^{-12}$ cm). One can easily imagine that both isotopes are well distinguishable for neutrons, which is often utilized as will be explained later. A problem is the large incoherent scattering cross section b_{inc} of various isotopes, e.g. ^1H , which gives rise to difficulties in scattering studies of biological material due to increased background signals [147]. In neutron diffraction experiments like the ones performed during the present thesis, the quantity of neutrons scattered is counted with respect to the scattering direction. The spatial distribution of the neutron intensity I recorded on the detector area provides knowledge about the atomic distribution, i.e. the scattering length density (SLD), and hence about the molecular structure of the material, since all atoms in the sample jointly contribute to the scattering process.

2.5.1.1 Neutron diffraction studies of oriented lipid model membranes

The neutron diffraction experiments for this thesis were performed using two instruments situated at different research facilities (see Fig. 12): the Membrane Diffractometer V1 located at the cold source of the reactor BER II of Helmholtz-Zentrum Berlin (HZB), and the Small Momentum Transfer Diffractometer D16 located at a cold source of High Flux Reactor (HFR) at Institut Laue-Langevin Grenoble (ILL).

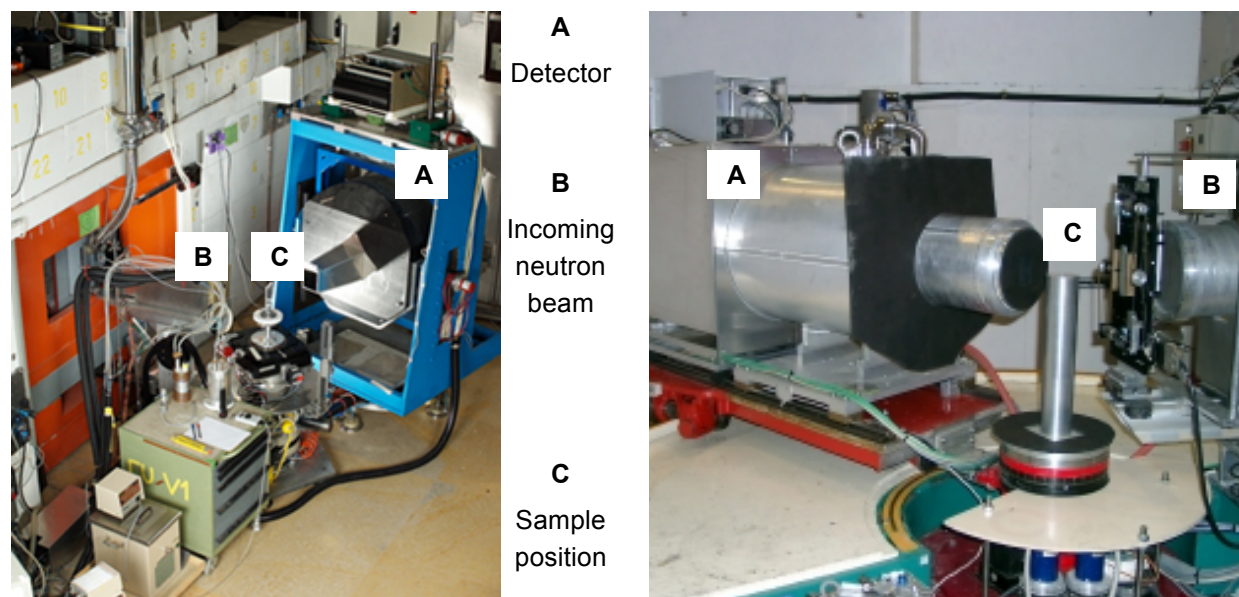


Fig. 12: (Left) The Membrane Diffractometer V1 at HZB, Berlin. (Right) The Small Momentum Transfer Diffractometer D16 at ILL, Grenoble. The three major components are marked.

Both instruments are comparable in their experimental set-ups and thus suitable for investigating the model systems studied in the present thesis. Defined neutron wavelengths λ for the experiments were received by appropriate positioning of a pyrolytic graphite monochromator, and equalled $\lambda = 5.23 \text{ \AA}$ at V1, and $\lambda = 4.741 \text{ \AA}$ or $\lambda = 4.752 \text{ \AA}$, respectively, at D16. Sample-to-detector distances amounted to 95.0 cm or 101.5 cm at D16, and 102.38 cm at V1. The two-dimensional position-sensitive ^3He detector MILAND employed to record the scattered neutron intensity I at D16 previously had an area of $256 \times 256 \text{ mm}^2$, spatial resolution $2 \times 2 \text{ mm}^2$ before it was upgraded to $320 \times 320 \text{ mm}^2$, spatial resolution $1 \times 1 \text{ mm}^2$. At V1, the detecting unit likewise is a two-dimensional position-sensitive ^3He detector with an area of $200 \times 200 \text{ mm}^2$ and $1.5 \times 1.5 \text{ mm}^2$ spatial resolution. For measurements in reflection mode, the planar SC lipid model membranes to be studied were placed in the neutron beam as depicted in Fig. 11. To achieve reproducible and comparable results, the samples were kept inside lockable measurement chambers under distinct envi-

ronmental conditions prior to and during the diffraction measurements. A temperature (T) of 32°C was chosen for all experiments to be as close as possible to *in vivo* conditions of the skin surface. In addition, the diffraction behaviour of particular model membranes was studied at higher T values. The SC lipid model membrane inside the sample chamber was exposed to a relative humidity (RH), set to either 58 % or 99 % by using either saturated salt solutions as described elsewhere [153], or using thermostated water reservoirs inside the sample chambers. The resulting vapour inside the chamber was furthermore varied for three different D₂O/H₂O ratios (100/0, 50/50, and 8/92 mol/mol) in order to change the solvent scattering density with respect to the scattering density of the SC lipids. This procedure, the concept of *contrast variation* achieved by varying the neutron contrast between the studied material and the water vapour, has been highlighted before [154, 155]. To reach equilibrium conditions, the model membranes were left for at least 8 to 10 hours of equilibration prior to the diffraction experiments. This was proven to be a sufficient time interval for equilibration of the SC models investigated here, with no further changes in height and position of the Bragg maxima (Fig. 13).

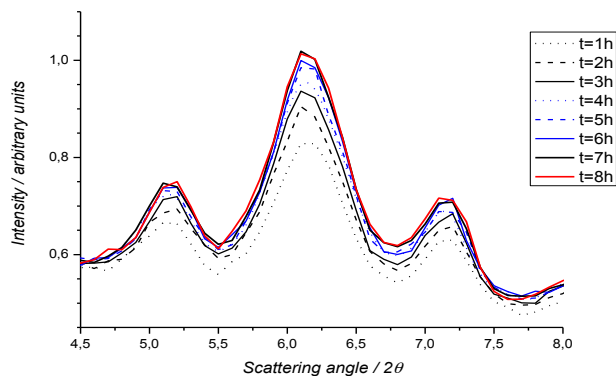


Fig. 13: $\theta - 2\theta$ -Scan recorded during the equilibration (58 % RH, 100 % D₂O, 32°C) of a SC lipid model membrane (composition: CER[EOS]/ CER[AP]/ behenic acid (BA)/ CHOL, 23/10/33/33 (m/m) Already after 7 hours, no changes in peak intensity are detected any more.

After 7 hours of equilibration time at a temperature of 32 °C, no further changes in peak intensity were detectable. The measurements were carried out either as rocking scans (ω -scan), where the incident neutron beam was rotated by an angle $\omega = \pm 2^\circ$ around the expected position of the Bragg maximum with the neutron intensity being recorded at the respective position 2θ for each diffraction order, or as continuous $\theta - 2\theta$ -scans.

2.5.1.2 Data reduction and evaluation

Assuming an elastic scattering event with $|\vec{k}_1| = |\vec{k}_2|$ as mentioned above, the momentum transfer \vec{Q} is correlated with the scattering angle 2θ by

$$Q = \frac{4\pi \cdot \sin\theta}{\lambda} \quad \text{Eq. 2-8}$$

The intensity I of scattered neutrons in arbitrary units (a.u.) was recorded as a function of the scattering angle 2θ , and the resulting Bragg maxima were fitted with Gaussians in order to determine the integrated peak intensity I_h . The latter is correlated with the amplitude of the structure factor F_h by

$$|F_h| = \sqrt{h \cdot I_h \cdot A_h(\theta)} \quad \text{Eq. 2-9}$$

where I_h is the intensity of the h th peak, h is the Lorentz factor used for intensity correction for the purpose of being independent on the geometry of data collection [156], and $A_h(\theta)$ represents the specimen absorption correction. According to [157], $A_h(\theta)$ is accessible by

$$A_h(\theta) = \frac{\sin\theta}{2\mu L} \cdot \left(1 - \exp\left(-\frac{2\mu L}{\sin\theta}\right) \right) \quad \text{Eq. 2-10}$$

with the linear absorption coefficient μ and the thickness L of the lamellar sample. Considering a stack of centrosymmetric bilayers, the Fourier transform of all observed structure factors F_h of 1st - h^{th} order correlates with the distribution of **neutron scattering length density** (NSLD) inside the model bilayer $\rho_s(x)$ [158]:

$$\rho_s(x) = a + b \cdot \frac{2}{d} \cdot \sum_{h=1}^{h_{max}} F_h \cdot \cos\left(\frac{2\pi \cdot h \cdot x}{d}\right) \quad \text{Eq. 2-11}$$

In this correlation, a and b represent free coefficients for normalization; d is the lamellar spacing between the scattering planes, i.e. the width of the unit cell, h is the diffraction order and F_h is the h^{th} order structure factor. The $\rho_s(x)$ provides detailed information regarding the distribution of neutron scattering length density, and therefore of the atoms inside the studied material. Consequently, the NSLD profiles directly reveal the assembly of the SC lipids inside the bilayer unit cell on a molecular scale. However, its calculation is solely possible if the amplitude *and* the phase of the Fourier coefficients are known. Evaluating the signs of the F_h , known as the *phase*

problem, is not trivial. Yet, in the case of neutrons, the signs of the structure factors can be easily determined by the *isomorphous replacement method*, i.e. the introduction of atoms, which effectively change the neutron contrast of the sample [146]. Commonly, this is realized by the aforementioned D₂O/H₂O contrast variation, assuming water diffusion into the interlamellar spaces with considerable bilayer hydration [157]. In the case of centrosymmetric bilayers with identical composition of the lamellar leaflets as supposed for the samples investigated in the course of the present thesis, the phase problem reduces to the possibilities of – or + [159]. In the linear correlation of the amplitude of F_h and the D₂O content present in the water vapour surrounding the sample and diffusing into the interlamellar space, the slope corresponds with the structure factor's phase (presented in Fig. 14):

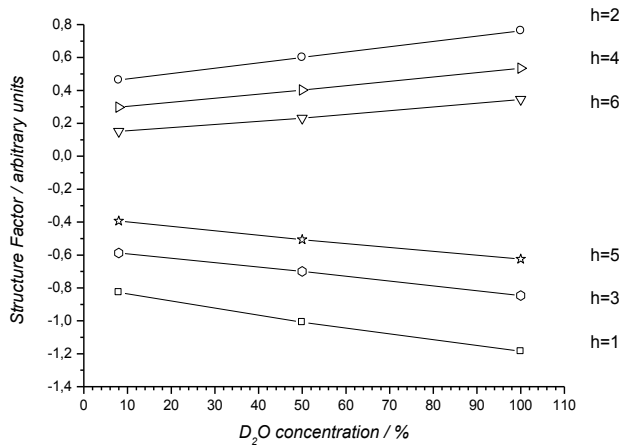


Fig. 14: The amplitude of the structure factors F_h for the diffraction orders $h=1-6$ in relation to the D₂O content, recorded for a quaternary SC lipid model membrane composed of CER[EOS]_branched, CER[AP], BA, CHOL (23/10/33/33 m/m). The F_h phase were assigned as -,+, -,+, -,+ for the diffraction orders 1-6.

The unit cell of the SC lipid bilayer is considered to be constituted by several multiatomic submolecular groups contributing to the overall distribution of scattering length density, which is an image of the distribution of the structure factor F_h in reciprocal space. These groups can be represented by Gaussian functions of certain width. Fully resolving the image of the bilayer unit cell requires recording of preferably *all* F_h yielded by the studied structure [160]. As stated by Kiselev and co-workers the resolution of the Fourier transform for a model bilayer with a spacing d is limited by the number of available diffraction orders h_m [4]:

$$Resolution_{FT} = \frac{3.8 \cdot d}{2\pi h_m} \approx 0.6 \cdot \frac{d}{h_m} \quad \text{Eq. 2-12}$$

Consequently, the signals from two molecular groups can be resolved by Fourier transform if they are separated by a certain distance Δx , and if a sufficient number of F_h is detected. However, only limited numbers of F_h are available in neutron dif-

fraction experiments, since higher order diffraction peaks often disappear in the background due to structural disorder and fluctuation effects. Disregarding higher order Bragg maxima that might be observable results in artificially decreased number of Fourier terms and consequently in truncation artefacts due to the Fourier synthesis [158]. Consequently, the space resolution of the Fourier synthesis and hence, the information regarding the SC lipid bilayer structure are limited.

All $\rho_s(x)$ presented here are calculated on a relative scale in arbitrary units (a.u.), since a and b are unknown coefficients. Calculating NSLD profiles on a “relative absolute scale” requires exact specification of the volume of molecular groups [158, 161], and knowledge about the exact amount of water molecules per lipid head group [162-164]. Since CER-based model bilayers are poorly penetrable for water [4], these values can not be determined with high accuracy. Consequently, calculating the profiles $\rho_s(x)$ on an absolute scale is omitted due to the resulting large error.

The application of neutron diffraction for localizing a specifically deuterated compound has been reported in numerous works [149, 163, 165, 166]. The determination of the deuterium label position requires the acquisition of diffraction data for both the model membrane containing the protonated lipid, and the model membrane with the deuterated compound. Then, the positive contribution of the deuterium label to the overall scattering length density, i.e. the density distribution of the deuterium label across the bilayer, is extracted by calculating the difference F_{h_diff} of all structure factors received for the deuterated sample (F_{h_deut}) and the ones for the protonated sample (F_{h_prot}):

$$F_{h_diff} = F_{h_deut} - F_{h_prot} \quad \text{Eq. 2-13}$$

and by a Fourier transform of the F_{h_diff} according to Eq. 2-14

$$\rho_{s_diff}(x) = a + b \cdot \frac{2}{d} \cdot \sum_{h=1}^{h_{max}} F_{h_diff} \cdot \cos\left(\frac{2\pi \cdot h \cdot x}{d}\right) \quad \text{Eq. 2-14}$$

For these calculations, the NSLD profiles were scaled to the sum of the F_h to allow for comparability between the protonated and the deuterated sample. Localisation of the deuterium label, represented by the distribution of the difference structure factor F_{h_diff} in reciprocal space, is received from determining the position of the maxima occurring in the $\rho_{s_diff}(x)$ by Gaussian fits.

2.5.1.3 Preparation of oriented multilamellar samples for the neutron diffraction studies

The preparation of highly oriented multiple stacks of SC lipid bilayers on a quartz substrate was performed according to the technique described before [167]. A list of the SC lipids and other substances used for sample preparation can be found in chapter 6 (Appendix). Appropriate amounts of SC lipids were dissolved in a solvent mixture composed of chloroform and methanol, 2:1 (v/v) to yield a total lipid concentration of 10 mg/ml, and then combined in the required ratio to receive the SC lipid mixtures to be investigated. A volume equalling 12 mg of the SC lipid mixture was applied onto a planar quartz glass with an area of $2.5 \times 6.5 \text{ cm}^2$ by means of an air-brush instrument (Harder & Steenbeck, Norderstedt, Germany). After solvent evaporation at room temperature and atmospheric pressure, the lipid film was kept under reduced pressure ($<50 \text{ mbar}$) for at least 12 hours to remove solvent traces. Subsequently, three alternating heating and cooling cycles were performed to improve sample quality, with the chosen temperature depending on the respective SC lipid mixture and its main phase transition temperature (determined by *differential scanning calorimetry*, DSC, see section 2.5.2.2). This so-called *annealing procedure* aims at creating a one-dimensional crystal structure with a state of high lamellar order. As described in the preceding section, well-oriented SC lipid model membranes are essentially needed in order to be able to record as many orders of diffraction as possible: The less ordered the bilayer assembly is, the less structure factors are available [164]. Consequently, the errors connected with the Fourier synthesis will increase and the image of atomic distribution inside the model bilayers is less detailed. A measure for the sample quality with respect to the presence of a one-dimensional crystal structure is the *mosaicity*, which can be determined by ω -scans. In this set-up, the scattered intensity is recorded as function of the incident neutron beam angle α , and the scattering angle 2θ is fixed on the h th order peak. The mosaicity indicates the misorientation of domains present in the mixture of SC lipids assembled in bilayers by a certain angle $\tau = \alpha - \theta$ from perfect orientation $\tau = 0^\circ$ [168], schematically presented in Fig. 15. According to Bragg's equation $\lambda = 2d \cdot \sin\theta$, maximum intensity is recorded if $\alpha = \theta$.

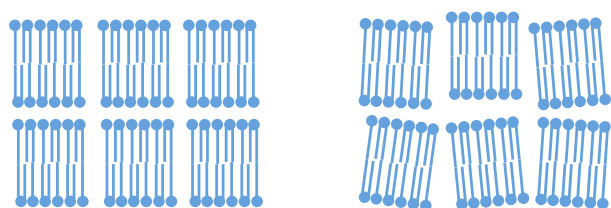


Fig. 15: (Left) Sketch of a perfect one-dimensional lamellar structure with low mosaicity. (Right) Crystallite domains with differing orientations result in high sample mosaicity, with a wide angular distribution of bilayer normal vectors [168].

Sample composition was kept simple for the diffraction experiments in the course of this thesis. This resulted from the severalfold better sample quality observed for the simplistic ternary or quaternary SC lipid mixtures compared to more complex models, as to be seen in Fig. 16. Whereas the simplistic systems showed a state of high lamellar order indicated by the presence of sharp diffraction signals up to the 7th order, the more complex mixture exhibits strong phase separation and only few broad diffraction signals. Based on such low-quality diffraction data received for the complex SC lipid models as exemplary shown in Fig. 16, the information regarding the bilayer nanostructure is limited and consequently insufficient for exact analysis. A list of the composition for all studied SC lipid model membranes can be found in the Appendix 6.2.

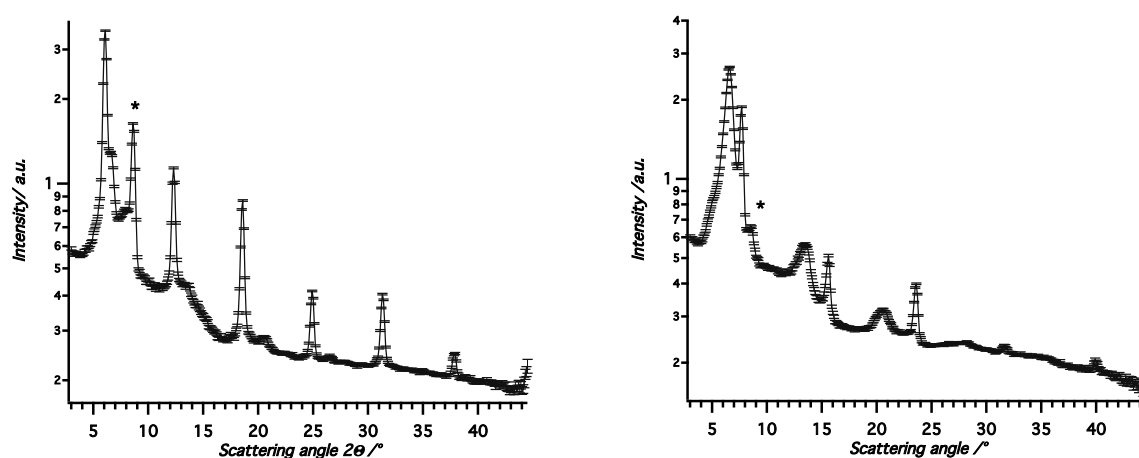


Fig. 16: Diffraction patterns recorded at 100 % D₂O, 32°C, 58 % RH for (Left) a quaternary sample containing CER[EOS]_{branched}, CER[AP], BA, CHOL (23/10/33/33, m/m) and (Right) a SC model membrane of complex composition (see Appendix 6.2). The asterisk (*) marks the signal of phase-separated CHOL crystals.

It is of utmost importance to understand the impact of distinct lipid classes to the SC lipid matrix architecture on a molecular scale. Model membranes with simplistic composition were shown to provide the better and more reproducible approach for the purpose of gaining an insight into the bilayer assembly on a nano-scale, while more sophisticated systems are less favourable [113]. This applies in particular to the investigation of the influence of either particular SC lipid species or even penetration

enhancers on the structural properties of SC lipid bilayers. Although it might be challenging to approximate the more physiological lipid composition of the intercellular matrix of human SC, the multiple constituents influencing the overall bilayer architecture complicate the extraction of information regarding the contribution of a single component to such a complex structure. This problem can be overcome by using simplistic but realistic sample compositions, where the influencing factors are minimized to few components [1, 89, 102, 169].

2.5.2 Other techniques used

2.5.2.1 Raman spectroscopy

Raman spectroscopy is a non-destructive analytical technique based on inelastic scattering of photons by molecules. When radiation of a certain frequency f_1 impinges on a molecule, the main fraction of scattered photons remains on the same energy level (i.e. has the same frequency f_1 and hence the same wavelength). This phenomenon is denoted as *Rayleigh scattering*. Simultaneously, a very small part of the scattered photons exhibit a slightly changed frequency ($f_2 \neq f_1$) due to interaction and energy exchange with the molecule (often $f_1 > f_2$, the so-called *Stokes shift*). The excitation source is usually a high-intense laser due to the low intensity of Raman scattering. By exciting the molecule to oscillate differently than before the photon loses energy, and the shift in energy between the incoming and scattered photon corresponds with the energy required for transferring the molecule from a ground state to a different rotational or vibrational state. The detection of the frequency of the scattered photons (termed wave number, cm^{-1}) allows drawing conclusions about the vibrations and rotation movements of molecular groups [170, 171]. One generally distinguishes between bending modes (movements with varying bond angles) and stretching modes ν (symmetric or asymmetric movements along a bond axis with changing bond lengths). The development of Fourier transform (FT) Raman spectrometers increased the efficiency and sensitivity of the instruments.

Basic precondition for a molecule oscillation to be Raman active is a change of the molecular polarizability during the oscillation. Roughly spoken, the polarizability is the extent of deformation of the electron cloud. Dipoles and more polar molecules hence only show a weak Raman effect since their electron clouds are poorly deformable. In contrast, non-polar molecular groups and especially alkanes show the strongest Raman effect and can be readily studied by means of Raman spectroscopy

[171]. The spectral Raman bands observed after laser excitation are assigned to distinct molecular vibrations. Since they are sensitive to conformational changes in the molecule, the state of order of alkyl moieties, particularly in lipids can be studied [172-174]. A measure for the alkyl chain order is the amount of *trans* and *gauche* conformers present in the hydrocarbon chain. In the crystalline state, the motional freedom is decreased in favour of a highly ordered zig-zag arrangement of the alkyl chain comprising a high number of *trans* conformers and only few *gauche* defects. When the chain disorder increases, the number of *gauche* conformers increases at the expense of *trans* conformers [175]. The analysis of characteristic Raman bands assigned to certain molecular vibrations allows evaluating the *trans/gauche* ratio and hence to draw conclusions regarding the alkyl chain order. Sharp bands in the spectral region $< 300 \text{ cm}^{-1}$ (termed the longitudinal acoustic mode, LAM [176]) indicate *all-trans* chain conformation and result from bending motions of the hydrocarbon chains. Increased numbers of *gauche* defects result in a shift of the LAM to higher wave numbers and band broadening [175]. A highly ordered *trans* hydrocarbon chain terminus is indicated by the CH_3 rocking mode, a sharp peak located at 890 cm^{-1} , while the presence of *gauche* conformers is revealed by a broad peak at lower frequency, usually 870 cm^{-1} [177]. The bands assigned to the symmetric and asymmetric C-H stretching mode, $\nu_{\text{sym}}(\text{CH}_2)$ and $\nu_{\text{asym}}(\text{CH}_2)$, located in the spectral region between 2800 and 3000 cm^{-1} are of particular interest [178, 179]. The position of $\nu_{\text{sym}}(\text{CH}_2)$ is inversely correlated with the alkyl chain order: the higher the frequency, the lower the state of order due to an increased number of *gauche* conformers. Furthermore, the intensity ratio $I(\nu_{\text{asym}}(\text{CH}_2)/\nu_{\text{sym}}(\text{CH}_2))$ is sensitive to the *trans-gauche* ratio [180, 181] and decreases with enhanced alkyl chain disorder and increasing *gauche* defects, respectively.

In addition, analysing the spectral region between 1400 and 1500 cm^{-1} reveals the intermolecular packing behaviour of alkyl chains in one unit cell. A double peak at 1450 and 1460 cm^{-1} represents the CH_2 scissoring mode in the case of a hexagonal packing of the lipid hydrocarbon chains, while factor group splitting with a peak triplet occurs for the orthorhombic chain packing [177].

The Raman experiments for elucidation of the thermotropic phase behaviour of SC lipid mixtures or pure CER subspecies were performed on a Bruker Fourier transform infrared spectrometer RFS 100/S (Bruker Optics, Ettlingen, Germany). The excitation source was a diode pumped Nd:YAG laser with a wavelength $\lambda=1064 \text{ nm}$. The

scattered radiation was detected in an angle of 180° with respect to the incoming beam to avoid detection of the high-intense excitation radiation. The spectra (4 cm^{-1} resolution) were recorded at a laser power of 400 mW at the sample location.

The SC lipid mixtures to be studied, or the pure SC lipids were prepared from organic solutions (solvent mixture: chloroform/methanol 2:1, v/v). The solvent was allowed to evaporate completely, first at room temperature, subsequently at reduced pressure ($<50\text{ mbar}$). After vacuum storage for not more than 24 hours, appropriate amounts of the sample material was transferred into an NMR tube and Raman spectra were recorded under dry conditions in a temperature range from 25°C and 95°C with 5 minutes equilibration between each step. According to the DSC studies, spectra were recorded for two or three heating cycles.

2.5.2.2 Differential scanning calorimetry

Differential scanning calorimetry (DSC) is a technique applied in order to measure heat and commonly used to determine the thermotropic phase behaviour of the studied material. Measuring heat is based on heat exchange and a resulting heat flow due to temperature differences. Since most chemical processes or physical transitions are related with consumption (endothermic processes) or release (exothermic processes) of heat, DSC represents the ideal tool to monitor such sample transitions, particularly the thermotropic phase behaviour of lipids [182].

During a heat flux DSC experiment, sample and reference are both subjected to the same constant change of temperature (heating program with fixed heating rate). In case that thermally activated transitions are initiated in the sample material, a difference in sample and reference temperature $\Delta T \neq 0$ is detected which is proportional to the heat flux difference between sample and reference [183]. The resulting endothermic or exothermic transition peaks recorded at a certain temperature point provide insight into the structural behaviour of the sample material upon temperature change. Extrapolating the peak onset yields the phase transition temperature, while integrating the peak area yields the transition enthalpy. Knowledge of these parameters provides insight into the thermotropic behaviour of the material studied; yet, detailed information about the structural processes taking place on a nanoscale during temperature change cannot be obtained.

All DSC measurements were performed on a Netzsch DSC 200 differential scanning calorimeter (Netzsch Geraetebau, Selb, Germany). Samples were trans-

ferred in aluminium pans and studied in dry state in a temperature range from 20 to 120°C. An empty aluminium pan was used as reference and heated simultaneously. Each of the three heating scans performed for every sample was conducted at a heating rate of 5 K per minute and followed by a cooling scan.

2.5.2.3 ^2H NMR spectroscopy

Nuclear magnetic resonance (NMR) is based on the interaction of a nucleus' magnetic moment with an externally applied strong magnetic field B_0 . This magnetic moment, and consequently the phenomena of NMR, only occur if the nucleus has a non-zero nuclear *spin* ($I \neq 0$), whereat the spin I can be an integer (^2H , deuterium, has a spin $I=1$) or half an integer (^1H has a spin $I=1/2$). In order to have a non-zero spin, the total number of neutrons and/or protons of a nucleus need to be uneven. In contrast, nuclei with an even mass number (even number of neutrons and protons) have a zero spin and consequently do not have a magnetic moment [184]. When the nucleus with $I \neq 0$ experiences the influence of a strong external magnetic field B_0 , its magnetic moment can only adopt discrete permitted orientations $2I+1$ due to quantization, and the nucleus is forced into a precessing movement about the magnetic field. The frequency of this precession is the Larmor frequency and directly dependent on the magnetic field strength. If this state is now influenced by another short electromagnetic impulse directed normally to B_0 and matching the Larmor frequency, the equilibrium precession is disturbed, and transitions between the quantized states are possible. Directly after the short-pulse excitation, the nuclei relax back to the equilibrium state and the change in the magnetic momentum during relaxation is detected by radiofrequency coils, which yields the NMR signal [184]. A preferably short pulse excites a broad range of resonance frequencies, and a Fourier transform of the detected relaxations allows calculating the NMR spectrum. Since the magnetic moments of the excited nuclei are not independent from their environment, but in fact are influenced by their surrounding atomic neighbours which all act as small magnetization sources, shielding effects can occur which result in locally diminished or enhanced resonance frequencies for the same isotope. This leads to the observation of the typical chemical shifts permitting distinction between the different populations of one kind of atom in a molecule and providing information about their chemical environment.

In the powder samples of solid state NMR, all spatial molecular orientations are present, and the anisotropic interactions having a strong impact on the properties of nuclear spins are not averaged by fast molecular motions, like e.g. in solution. The directional dependency of these nuclear spin interactions, and consequently of the nuclear resonance frequency causes the occurrence of the typical broad NMR signals [185].

Since the ^2H nucleus has a nuclear spin $I > 1/2$ (exact: $I=1$), it adopts three permitted spin states in a static magnetic field B_0 . Accordingly, two magnetic resonance transitions exist which are splitted in the NMR spectrum [186]. Due to their non-spherical nuclear charge distribution, nuclei with $I > 1/2$ like ^2H exhibit a *quadrupolar moment*, whose interaction with the molecular electric field causes the *quadrupolar interaction*, an important anisotropic interaction in ^2H NMR spectroscopy where signals are detected as so-called Pake doublets [187]. Lamellar structures like SC lipid model membranes, where the lipids are oriented centrosymmetrically, can be studied by means of ^2H NMR spectroscopy for the purpose of elucidating the particular molecular motions of the individual species of ^2H -labelled molecules, and to investigate the phase behaviour of lipids in complex mixtures [132]. The powder spectra obtained by ^2H NMR spectroscopy contain information regarding structure and dynamics of the molecules studied, yet, the data need to be treated by a “dePaking” algorithm to extract the required information. The quadrupolar splittings $\Delta\nu_Q$, i.e the frequency separation of the doublet corresponding to every single deuterium nucleus can be determined from the depaked spectra [187]. To describe the motional characteristics of the deuterated lipid alkyl chains in a lamellar assembly the order parameter $S_{CD}(n)$ is introduced, defining the orientation of the C-D bond vector at the n th CD_2 group in the perdeuterated compound (beginning at the lipid head, e.g. the carbonyl group). It is correlated to the quadrupolar splitting $\Delta\nu_Q(n)$ by:

$$\nu_Q(n) = \frac{3}{4} \frac{e^2 q Q}{h} S_{CD}(n) \quad \text{Eq. 2-15}$$

where $e^2 q Q / h = 167$ kHz is the quadrupolar coupling constant for the C- ^2H bond. From the carbonyl group towards the alkyl chain terminus $S_{CD}(n)$ decreases due to the increasing mobility of the hydrocarbon, hence, detailed order parameter profiles reveal the state of order along the lipid alkyl chains [188, 189] This makes ^2H NMR spectroscopy a versatile tool for revealing the C-D bond orientation and the degree of order, particularly in lamellar phases [190, 191].

3 RESULTS REPRESENTED BY ACCEPTED PUBLICATIONS

In the following section, the results obtained from experiments performed in the course of the present thesis are presented as they were accepted for publication in peer-reviewed international scientific journals.

3.1 The influence of different CER subclasses on the lamellar nanostructure of SC lipid model membranes

As outlined before, the CER subclasses present in the human SC intercellular lipid matrix at large contribute to the barrier formation. It is probably the broad distribution of alkyl chain lengths, the resulting plurality of CER and the heterogeneity of SC lipid species, which guarantee the integrity and functionality of the penetration-limiting lipid lamellae [82]. However, the role of particular subspecies, e.g. phytosphingosine-based CER and the long-chain ω -acyl CER, gained increasing interest in SC research during the past decades. A new oriented SC model system based on CER[NP], one of the most abundant CER subclasses present in human SC, was established. In an interdisciplinary approach using neutron diffraction and ^2H NMR spectroscopy, the lamellar nanostructure of the model was investigated and compared with the CER[AP] based membrane. In addition, an artificial CER[EOS] descendant with a methyl-branched, saturated ω -acyl chain derived from chemical synthesis was proven to exhibit equivalent properties in terms of thermotropic phase behaviour and membrane bilayer structure like its naturally occurring pendant.

3.1.1 Impact of phytosphingosine-type CER[NP] on the assembly of SC lipids in ternary model membranes (Manuscript: Soft Matter)

Engelbrecht TN, Schroeter A, Hauß T, Demé B, Scheidt HA, Huster D, Neubert RHH: **The impact of ceramides NP and AP on the nanostructure of stratum corneum lipid bilayers. Part I: Neutron diffraction and ^2H NMR studies on multilamellar models based on ceramides with symmetric alkyl chain length distribution.** *Soft Matter*, 2012; 8: 2599-2607
(DOI: 10.1039/c2sm25420d)

Available online:

<http://pubs.rsc.org/en/Content/ArticleLanding/2012/SM/C2SM25420D>

Cite this: *Soft Matter*, 2012, **8**, 2599

www.rsc.org/softmatter

PAPER

The impact of ceramides NP and AP on the nanostructure of *stratum corneum* lipid bilayer. Part I: neutron diffraction and ²H NMR studies on multilamellar models based on ceramides with symmetric alkyl chain length distributionTanja N. Engelbrecht,^a Annett Schroeter,^{*a} Thomas Hauß,^b Bruno Demé,^c Holger A. Scheidt,^d Daniel Huster^d and Reinhard H. H. Neubert^a

Received 23rd February 2012, Accepted 11th April 2012

DOI: 10.1039/c2sm25420d

We investigated the lamellar structure of ternary *stratum corneum* (SC) lipid model systems based on either the phytosphingosine type ceramide (CER) [NP] or CER[AP], supplemented by cholesterol and stearic acid as representative free fatty acid species. For the CER[NP] based membrane, neutron diffraction measurements revealed the coexistence of two lamellar phases, which markedly differ in their hydration properties. CER[NP] forms an extremely rigid and stable bilayer backbone and is at least partly sequestered in a separate phase which coexists with a second lamellar phase. At increased temperature, a structural re-organization of the lipids was observed. One of the lamellar phases disappeared, while the remaining phase *increased* its repeat distance by about 1 Å. Such a behaviour has not been described for SC lipid model membranes based on CER[AP] so far. Further, ²H NMR spectroscopic measurements on two SC lipid model systems based on either CER[NP] or CER[AP] in addition to cholesterol and perdeuterated stearic acid revealed a state of high lamellar order present in both samples, emphasizing the importance of the phytosphingosine-type ceramides for the proper formation of stable SC bilayer structures. However, the CER[NP] based ternary model showed a state of higher lamellar order than the CER[AP] based system. Our results demonstrate that slight changes in the ceramides' head groups (CER[NP] with 3 hydroxyl groups vs. CER[AP] with 4 hydroxyl groups) have a dramatic influence on the morphology of the lipid structures formed by these lipids.

1. Introduction

It is well known that the outermost layer of the mammalian skin, the *stratum corneum* (SC) maintains homeostasis of the organism by protecting the body from various outer influences and uncontrolled water loss. With its intercellular lipid matrix surrounding the corneocytes, the SC is generally accepted to represent the major penetration barrier of the skin.^{1–3} Main constituents of the lipid lamellae are ceramides (CERs) in addition to cholesterol (CHOL) with its derivatives and free fatty acids (FFA),^{4,5} whereby particularly the structural arrangement of these SC lipids in highly ordered and coherent multiple bilayers is regarded to be essential for the maintenance of the skin barrier properties.⁶ The CERs represent a very lipophilic and rigid class of molecules with only small

hydrophilic head groups, and they presumably determine the structure of the lipid lamellae of the SC to a high extent, which results *e.g.* in poor penetrability of mammalian skin for water.⁶ Accordingly, it was found that there is almost no free water present inside the intercellular lamellar sheets of the SC.⁷ With their particular properties, the CER lipids are regarded to be highly important for the proper formation of the penetration barrier.

Current SC research increasingly addresses the issue of identifying specific CER subclasses or SC lipid species playing a key role in the processes of skin barrier formation. There have been numerous attempts to correlate different states of impaired skin with alterations in the content of particular lipid species as reviewed previously.⁸ For the case of atopic dermatitis, a significant reduction in the linoleic-acid containing ω -acylceramide CER[EOS] was found.⁹ The authors concluded an important role of this CER subspecies for the skin barrier properties. Di Nardo and co-workers likewise reported a diminished content of ω -acyl-ceramides in the skin of atopic dermatitis patients¹⁰ as well as a reduced CER[NP] level, which was assumed to account for the impaired trans-epidermal water loss observed for this unphysiological skin state. A strong reduction of the phytosphingosine-based CER[AP] and CER[NP] has also been demonstrated for the psoriatic skin.¹¹

^aInstitute of Pharmacy, Martin Luther University, Wolfgang-Langenbeck-Straße 4, 06120 Halle, Germany. E-mail: annett.schroeter@pharmazie.uni-halle.de; Tel: +49 345 25025

^bInstitute Soft Matter and Functional Materials, Helmholtz-Zentrum-Berlin, Hahn-Meitner-Platz 1, 14109 Berlin, Germany

^cInstitut Laue-Langevin (ILL), 6 Rue Jules Horowitz, 38042 Grenoble Cedex 9, France

^dInstitute of Medical Physics and Biophysics, University of Leipzig, Härtelstraße 16-18, 04107 Leipzig, Germany

From the physicochemical point of view, the phytosphingosine-type CERs show distinct characteristics.^{12,13} It was reported that CER[NP] is capable of forming an extremely strong network of intra- and inter-molecular hydrogen bonds,¹² which accounts for its distinct conformational characteristics and alkyl chain packing behaviour. When comparing the phytosphingoid-type CER[AP] and CER[NP] with sphingosine-based CERs, phase transition temperatures, intermolecular interactions and especially hydrogen bonding networks involving the hydrophilic head groups differ markedly.^{14,15} The authors reasoned that it is the CER head group, which significantly determines the overall behaviour of the studied ternary lipid mixture.

Furthermore, the number and exact position of the hydroxyl groups in the hydrophilic head of the CER molecules was recognized to affect the intermolecular lipid interactions. The additional α -hydroxyl group present in CER[AP] was found to induce a certain steric hindrance to the stabilizing hydrogen bond network mediated by the other hydroxyl groups of the CER head.¹⁶ Consequently, there seems to be a sensitive balance of mutual interaction contributing to the stability of the overall SC lipid structure.

The protruding role of phytosphingosine-type CER[AP] for the formation of stable bilayer structures was also described in the work of Kiselev and co-workers.^{17,18} Direct structural insights into the bilayer architecture of a CER[AP]-based quaternary SC lipid model membrane obtained from neutron diffraction revealed the formation of an extremely stable lamellar backbone with only little free water being present in the intermembrane space. Even under excess hydration, the repeat distance of the model bilayers only increased marginally by about 1 Å. The authors concluded that the polar CER[AP] accounts for the creation of such a rigid bilayer structure by forming strong lateral hydroxyl bonds, which was summarized in the armature reinforcement model. In the fully extended conformation, CER[AP] is assumed to pull the lamellae together, thereby preventing stronger swelling of the bilayers.¹⁷ That work furthermore emphasized the importance of the non-destructive neutron diffraction technique for the purpose of structural investigation of lamellar structures. Additionally, the results obtained by further neutron diffraction experiments underlined that detailed information regarding the specific impact of particular CER species on the lamellar SC lipid assembly can favourably be received by studying simplistic SC model membranes based on mixtures of synthetic SC lipids featuring well-defined head group architecture and defined alkyl chain lengths.^{19,20}

In order to advance our knowledge regarding the influence of phytosphingosine-type CERs on the molecular assembly of SC lipids, the present study focused on highly oriented ternary model membranes based on CER[NP] with symmetric alkyl chain length (stearic acid amide-bound to C18 phytosphingosine base), CHOL and the FFA stearic acid (SA). The system was investigated by means of neutron diffraction at two different temperatures in order to elucidate the bilayer architecture under varying environmental conditions. Additional ²H NMR spectroscopic measurements were performed to study the structure and dynamics of the free SA in the mixture with CHOL and either CER[AP] or CER[NP] in order to analyze potential differences between CER[AP] or [NP] based systems.

2. Experimental

2.1. Materials

CER[NP] (*N*-(octadecanoyl)-phytosphingosine) and CER[AP] (*N*-(α -hydroxyoctadecanoyl)-phytosphingosine) were a gift of Evonik Goldschmidt GmbH (Essen, Germany). Since the substances had a purity of $\geq 96\%$, they were used as received without any further purification. CHOL and SA were purchased from Sigma Aldrich GmbH (Taufkirchen, Germany) and used as received. The perdeuterated SA (SA-*d*₃₅) used for ²H NMR measurements was received from Dr Ehrenstorfer (Augsburg, Germany) and used without further purification. Cholesterol-25,26,26,26,27,27,27-*d*₇ was purchased from Avanti Polar Lipids (Alabaster, AL, USA). Quartz slides (Spectrosil 2000, 25 × 65 × 0.3 mm³) for the neutron diffraction experiments were purchased from Saint-Gobain (Wiesbaden, Germany). Fig. 1 displays the chemical structure of the SC lipids used for the experiments. For the deposition of the lipids onto the quartz surface, an airbrush instrument (Harder & Steenbeck, Norderstedt, Germany) was employed. Chloroform and methanol used as solvents for preparation of the lipid solutions were of analytical grade. All buffer substances were obtained from Sigma Aldrich.

2.2. Sample preparation

2.2.1 Neutron diffraction experiment. Oriented multilamellar model membranes for investigation by means of neutron diffraction were prepared according to the procedure described earlier.²¹ The sample studied by neutron scattering was composed of CER[NP]/CHOL/SA, component mass ratio (m/m) 55/25/20. A total volume of 1.2 ml of the final lipid mixture dissolved in chloroform/methanol (2 : 1 v/v) with a concentration of 10 mg ml⁻¹ was spread over the quartz surface using the airbrush device at constant air flow. The solvent was allowed to evaporate under atmospheric pressure and subsequently under

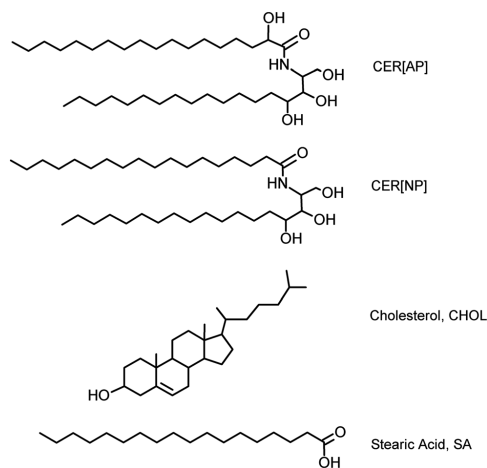


Fig. 1 The chemical structures of the SC lipids prepared as multilamellar SC model membranes.

reduced pressure (<50 mbar), where the samples were kept for 10–12 hours. After the solvent was removed completely, a subsequent annealing procedure was applied, whereby the samples were heated to 80 °C and cooled down to room temperature in water-saturated atmosphere. Such a procedure is often used in sample preparation for neutron diffraction experiments in order to improve the sample quality and state of lamellar order,²² which is of benefit for the peak intensities in the diffraction experiment and for the subsequent data analysis. For a detailed description of the necessity of the annealing procedure see former reports.²³ Until the measurements, the samples were stored at room temperature.

2.2.2 ²H NMR spectroscopy. For the ²H NMR measurements, the sample composition was either CER[NP] or CER[AP] in mixture with CHOL and SA at a mass ratio (m/m) of 55/25/20, where either the stearic acid (SA-*d*₃₅) or the cholesterol (CHOL-*d*₇) was deuterated. Briefly, aliquots of the synthetic SC lipids were dissolved in chloroform/methanol 2 : 1 (v/v) and mixed in the required ratio to yield a total amount of 2.5 mg per sample. After the solvent was evaporated under vacuum (~1 mbar), the remaining lipid film was dispersed in 4 ml of an aqueous buffer solution (10 mM Hepes, 100 mM NaCl, pH 7.4). In order to achieve homogeneity, the lipid dispersion was heated up to 80 °C and shaken for 3 hours with alternating bath ultrasonication and extensive vortexing. The resulting homogeneous lipid dispersion was treated by ultracentrifugation (*T* = 4 °C, 79 000 × *g*) (Beckman Optima L-60, Beckman Coulter GmbH, Krefeld, Germany) in order to separate and remove excessive buffer. The samples were subjected to several freeze–thaw cycles to improve homogeneity, and finally transferred into 5 mm glass vials for NMR measurements.

2.3. Neutron diffraction experiments

The neutron diffraction experiments were performed at the Small Momentum Transfer Diffractometer D16 situated at the cold source of the High-Flux Reactor (HFR) at Institute Laue-Langevin (ILL, Grenoble, France). The neutron wavelength of $\lambda = 4.74$ Å used for our experiment was received by appropriate positioning of a pyrolytic graphite monochromator. A two-dimensional position-sensitive detector (³He, area 256 × 256 mm², spatial resolution 2 × 2 mm²) was used to record the scattered neutron intensity. Diffraction data were collected as rocking scans (ω -scans) with the samples being rocked around the expected Bragg positions ω while the detector was set to a fixed position 2θ at a sample-to-detector distance of 101.5 cm. For equilibration and subsequent measurements, the sample was mounted in lockable chambers. Parameters like temperature (*T*) and relative humidity (RH) were externally controlled. Prior to each measurement, the sample was equilibrated at a temperature of 32 °C (comparable to *in vivo* conditions) and the respective RH until no changes in peak intensity or peak position were detectable. According to previous studies, 6–8 hours are sufficient for equilibrium hydration of such SC lipid model membranes and consequently, this time period was also applied in the present experiment.¹⁸ Measurements were performed at different temperatures, *i.e.* at 32 °C and 80 °C, and under relatively dry and more humid atmospheres (58% RH and 99% RH,

respectively). The comparatively high temperature of 80 °C was chosen to investigate the behaviour of the ternary model membrane near the main phase transition temperature. Since liquid-crystalline lipid bilayers are known to be several-fold more permeable for agents than gel-state lamellar structures,²⁴ it is important to study the structural properties of the SC lipid model lamellae in the liquid-crystalline state.

For each measurement condition, the model membrane was studied at no less than three different D₂O contrasts in order to vary the neutron scattering length density between the lipids and water. For that purpose, the chamber atmosphere was set to three D₂O/H₂O concentrations: 100/0, 50/50 and 8/92 (mol/mol).

The multilamellar sample was exposed to a monochromatic and collimated incoming neutron beam during measurements, while the intensity of scattered neutrons *I* was recorded as a function of the scattering angle 2θ . The correlation of 2θ to Q (scattering vector) is given by $Q = 4\pi\sin\theta/\lambda$, with Q being the resulting vector between the incoming wave vector \vec{k}_i and the scattered wave vector \vec{k}_s , and λ being the neutron wavelength, while θ represents the angle of incident beam. The correlation $d = 2\pi\pi/Q_n$ is used to calculate the repeat distance (periodicity) *d* of a lamellar phase from the positions of a series of equidistant peaks Q_n , where *n* is the diffraction order of the peak.

The commonly applied procedure for the interpretation of neutron diffraction data in order to gain insight into the nano-scaled structure of the model membrane is to calculate the neutron scattering length density (NSLD) profiles $\rho_s(x)$ by a Fourier synthesis of the structure factors F_h according to:

$$\rho_s(x) = a + b \frac{2}{d} \sum_{h=1}^{h_{\max}} F_h \cos\left(\frac{2\pi hx}{d}\right) \quad (1)$$

In this equation, *a* and *b* are unknown coefficients for the relative normalization of $\rho_s(x)$, *d* is the lamellar periodicity and *h* the order of diffraction. The absolute value of F_h was calculated by $|F_h| = \sqrt{hI_hA_h}$, where *h* is the Lorentz correction, A_h is the absorption correction²⁵ and I_h is the integrated intensity of the *h*th peak. To calculate $\rho_s(x)$, at least three to four diffraction orders *h* of one lamellar phase are required. Well-oriented model membranes are essentially needed to record diffraction peaks of higher orders which, however, can be hampered by the poor signal-to-noise (*s/n*) ratio resulting from the strong background due to the large incoherent scattering cross-section of the large number of hydrogen atoms present in the hydrocarbon chains of SC lipids. Raw data treatment and data reduction to intensity vs. 2θ were performed with the *Large Array Manipulation Program* (LAMP, a software package provided by the ILL²⁶). Integration of the Bragg peaks, determination of the peak positions and intensities after background subtraction were performed using the software package IGOR Pro 6.1 (WaveMetrics Inc., Portland, OR, USA).

For the Fourier transform, not only the amplitude but also the phase of each F_h is required. With a Gaussian water distribution assumed to feature a maximum at the position $x = d/2$ (near the hydrophilic head group region), the phase of F_h can be determined using the *isomorphous replacement method* described previously.^{25,27} Since the lamellar lipid arrangement of the SC model membrane investigated here is supposed to be centrosymmetric, the phase problem simplifies to the possibilities +

or – for the phases of F_h and can be solved by measuring the samples at least at three different D_2O/H_2O ratios. A detailed description of this procedure (so-called contrast variation) and of the neutron diffraction data evaluation can be found elsewhere.^{22,25,28}

2.4. 2H NMR experiment

Static 2H NMR spectra were recorded on a Bruker Avance 750 MHz NMR spectrometer (Bruker Biospin GmbH, Rheinstetten, Germany) operating at a resonance frequency of 115.1 MHz for 2H using a single-channel solids probe equipped with a 5 mm solenoid coil. The 2H NMR spectra were accumulated using quadrature phase detection with a phase-cycled quadrupolar echo sequence.²⁹ The spectral width was set to ± 250 kHz. Typical length of a 90° pulse was 3 to 5 μs , and a relaxation delay of 0.8 s or 3 s was applied. The spectra were acquired at temperatures of $32^\circ C$ and $80^\circ C$.

The obtained 2H NMR powder spectra of stearic acid (SA- d_{35}) were depaked³⁰ (using the algorithm of McCabe and Wassall³¹) and the order parameter profiles of the acyl chain were determined from the observed quadrupolar splitting $\Delta\nu_Q(n)$:

$$\Delta\nu_Q(n) = \frac{3}{4} \frac{e^2qQ}{h} S(n) \quad (2)$$

where e^2qQ/h is the quadrupolar-coupling constant (167 kHz for 2H in a $C-^2H$ bond) and $S(n)$ the chain order parameter for the n^{th} carbon position in the chain. Details about the analysis of 2H NMR spectra are found in the literature.³²

3. Results and discussion

3.1. Neutron diffraction experiments on CER[NP]/cholesterol/stearic acid

Fig. 2 displays the diffraction pattern for the sample CER[NP]/CHOL/SA (55/25/20, m/m) recorded at 100% D_2O contrast and at three different measurement conditions. At $32^\circ C$ and 58% RH, obviously two lamellar phases coexist, which are referred to as PI and PII. Five orders of diffraction were detectable for each phase, which differ in their peak shape. The reflections of PI are

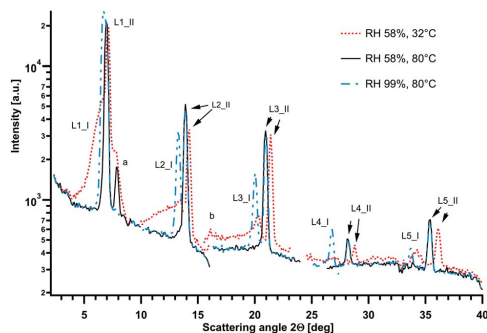


Fig. 2 Neutron diffraction patterns recorded for the ternary sample CER[NP]/CHOL/SA at a D_2O contrast of 100% and different experimental conditions: at $32^\circ C$, 58% RH (red dotted lines), at $80^\circ C$, 58% RH (black solid lines), and $80^\circ C$, 99% RH (blue dash-dotted lines).

smear-out, broad, and less intense, while the diffraction signals attributed to PII are well defined and sharp. As displayed in Table 1, the lamellar repeat distances d are equal to 39.9 ± 0.3 Å for PI, and 38.2 ± 0.1 Å for PII, respectively. Peaks located at $2\theta = 7.8^\circ$ and 16° are attributed to segregated crystalline CHOL, whose occurrence was already described before and is known to not affect the lamellar order of the model membranes.^{20,33,34} From these first findings, we conclude a certain fraction of SC lipids to be sequestered into the additionally occurring lamellar phase PII. However, at $80^\circ C$ and 58% RH, only the peaks attributed to PII are detectable, while PI disappears (see Fig. 2). Simultaneously, PII increases its d -spacing by 0.7 Å to 38.9 Å (Table 1), recognizable by a shift of the diffraction signals towards lower 2θ values. Phase-separated CHOL is still detectable. When the relative humidity is subsequently raised to 99% while the temperature is kept at $80^\circ C$, two coexisting phases are formed again. The reappearing phase is clearly pronounced and exhibits sharp diffraction signals of high intensity up to the 5th order. However, the lamellar repeat distance is increased by 1.2 Å when compared to the phase PI at lower temperature. Phase-separated CHOL is no longer observed, indicating an improved miscibility of this rigid molecule with the other SC lipids at high temperature and high humidity. This can be explained with the increased area per SC lipid molecule due to enhanced head group hydration at higher humidity, which allows for improved CHOL incorporation into the SC lipid lamellae. Under all experimental conditions studied, the lamellar phase PII did neither disappear, nor show any clear response to D_2O contrast variation, *i.e.* the diffraction intensity was not dependent on the D_2O/H_2O ratio (diffraction patterns not shown). In contrast, PI was found to exhibit the expected response to D_2O contrast variation. Two conclusions can be drawn from these experimental findings: first, the SC lipids arranged in PII presumably are virtually shielded from any interactions with the water vapour, which prevents appreciable interlamellar hydration. This does not apply for the SC lipids assembled in PI. Consequently, the lipid arrangement must differ in both phases. Second, temperature-dependent reorganization of the lipid lamellae takes place. One phase, PI, is no longer detectable at $80^\circ C$, while PII persists, but slightly increases its repeat distance. The latter is an atypical behaviour. Usually, the lamellar spacing of phospholipid bilayers decreases at high temperature due to an increased number of *gauche* defects, increased chain fluidity and consequently stronger interdigitation.^{35,36} Such an expected behaviour with decreased bilayer repeat distance at higher temperature was also observed before for SC model membranes based on the more polar CER[AP].³⁷

Table 1 Lamellar d -spacings of the ternary model membrane composed of CER[NP], CHOL and SA (mass ratio 55/25/20) calculated from the neutron diffraction data. Measurements were carried out at $32^\circ C$ or $80^\circ C$, and at RH 58% or 99%. The values for d given in Å are averaged over three D_2O concentrations (n.d.: not detectable)

Temperature	58% RH		99% RH	
	PI	PII	PI	PII
$32^\circ C$	40.0 ± 0.1	38.2 ± 0.1	39.9 ± 0.3	38.2 ± 0.1
$80^\circ C$	n.d.	38.9 ± 0.1	41.1 ± 0.2	38.9 ± 0.1

Since PII did not display considerable contrast variation and the F_h amplitudes do not display changes beyond statistical uncertainty at increasing D₂O concentrations (see Table 2), we cannot determine the F_h signs for PII reliably. However, since there is at least a tendency we assume the signs for the diffraction orders 1–5 as $- + - + -$. The $\rho_s(x)$ received from Fourier synthesis are shown in Fig. 3. In general, a typical bilayer arrangement can be deduced from the calculated profiles. Both, PI and PII exhibit two maxima at the outer edges of the $\rho_s(x)$, which indicate the presence of molecular groups with a positive neutron scattering length, *i.e.* the head groups of SA and CER [NP]. In the central bilayer region at $x = 0$ Å, both profiles exhibit minima, indicating a high density of atoms with negative neutron scattering length (*i.e.* the methylene groups and terminal methyl groups of the lipid alkyl chains). The shape of the membrane profile with the maxima located at $x_{PH} = d/2$ suggests a very small intermembrane space with a thin water layer present as reported previously.¹⁸ The latter preferentially applies for PI, whose head group region features maxima with different intensities at the three D₂O contrasts studied (Fig. 3A). In contrast, the insensitivity of the head group region of PII to D₂O contrast variation becomes apparent in the stable maxima of the $\rho_s(x)$, suggesting the absence of exchanged deuterium in that region, and consequently the absence of interlamellar water (Fig. 3B). To further underline this finding, we calculated the water distribution $\rho_w(x)$ across the lamellar unit cell according to ref. 18 for both PI and PII using eqn (3):

$$\rho_w(x) = \rho_{50\%D_2O} - \rho_{8\%D_2O} \quad (3)$$

The $\rho_w(x)$ presented in Fig. 3C prove that there is practically no water present in the interlamellar space of PII. Accordingly, the observed increase of d for PII at 80 °C does not result from swelling. In contrast, the two maxima in $\rho_w(x)$ of PI reveal the presence of a certain amount of free water in the head group region exchanged by D₂O. These findings underline the completely different hydration characteristics of PI and PII. However, it remains unclear from the present data whether a considerable interlamellar hydration of PII is possible after a longer equilibration time, *e.g.* several days.

Taking into account former reports in the literature, it is most likely that PII is constituted by crystalline phase-separated CER [NP]. Raudenkolb *et al.* investigated pure CER[NP] in water by X-ray diffraction and reported almost identical lamellar spacings and temperature-dependent changes,¹³ as we observed for PII.

Although several studies proved that ternary systems of CER[NP], CHOL and free fatty acid are well miscible,^{15,38} we assume that PII is exclusively formed by segregated ceramide. However, the incorporation of a certain amount of CHOL into the lamellar phase PII cannot be ruled out from the experimental diffraction data. In order to definitely elucidate this, the application of specifically deuterated SC lipids might be helpful. As shown previously,^{23,39,40} selective deuterium labelling allows for the direct localization of the deuterated compounds inside the model bilayers. The coexisting phase PI at 32 °C could either be phase-separated fatty acid,⁴¹ or is made up of SA besides the other membrane components. In the first case, the observed formation of a one-phase system at 80 °C and 58% RH would originate from fluidization of the SA-rich phase and subsequent melting (melting point of SA: about 68 °C³⁸). In the latter case, an improved miscibility of the SC lipids at increased temperature could account for the formation of one single phase at 80 °C and 58% RH.

In the remaining lamellar arrangement of PII, the rigid and lipophilic CER[NP] forms the stabilizing bilayer backbone. Former reports regarding the water impermeability of films composed of CER[NP],¹⁶ and the inaccessibility of the head group region for deuterium exchange⁴⁴ may confirm the assumption of pure CER[NP] constituting PII, and corroborate our experimental finding of lacking contrast variation in that phase. A possible explanation is provided by the results of Dahlen and Pascher⁴² who stated a V-shaped CER conformation for *N*-tetracosanoyl-phytosphingosine with the alkyl chains of asymmetric length pointing in opposite directions and the hydrophilic head group being located in the apex of the angle of 101°. Such a structural conception based on CER[NP] outstretching its two alkyl chains in opposite directions is likewise possible for PII of the ternary model membrane studied here and would explain the lacking contrast variation, with the small ceramide head group shielded from hydration by the outstretched alkyl chains and by the inter- and intramolecular network of hydrogen bonds described for phytosphingosine-type CERs.^{43,44} The lacking response of PII to D₂O contrast variation has not been reported before for the CER[AP]-based,⁴¹ or other CER-based SC lipid model membranes. We therefore conclude that the respective CER species present in the model system influences the lamellar structure and the SC lipid arrangement to a high extent. In addition, the V-shaped CER conformation could also account for the slightly larger d -spacing of PII at 80 °C by expansion of the chain angle.¹³

Due to the low affinity of CER[NP] based model membranes to water, it seems likely that the more humid vapour of 99% RH

Table 2 The amplitudes of the structure factors F_h calculated for PII of the multilamellar sample containing CER[NP], CHOL and SA (mass ratio 55/25/20) at 32 °C and 58% RH

Diffraction order	8% D ₂ O		50% D ₂ O		100% D ₂ O	
	Structure factor	Error	Structure factor	Error	Structure factor	Error
L1	74.16	0.35	73.36	0.23	71.60	0.12
L2	44.83	0.73	45.80	0.55	44.10	0.46
L3	50.82	0.92	50.79	0.89	49.74	0.28
L4	17.50	1.13	17.93	1.03	16.45	0.62
L5	24.91	1.14	24.42	0.95	24.66	0.82

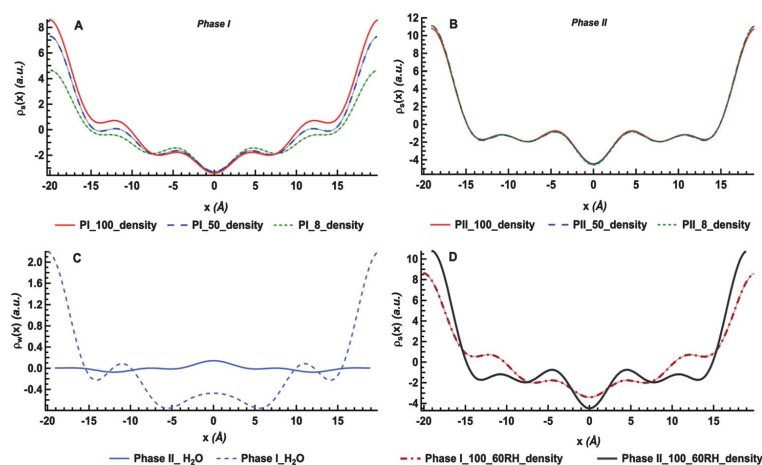


Fig. 3 The calculated NSLD profiles for PI (A) and PII (B) at 32 °C, 58% RH, and 100% (red solid line), 50% (blue dashed line), 8% (green dotted line) D₂O. Note the varying amplitude of the two maxima located at the outer edges in the case of PI (A), which is not observed for PII (B). (C) Water density distribution profile across the membrane for PI (blue dashed line) and PII (blue solid line). (D) Parallel presentation of NSLD profiles for PI (red dashed-dotted line) and PII (black solid line) after F_v normalization to 1. Experimental conditions are equivalent (100% D₂O, 32 °C, 58% RH).

Downloaded by Martin-Luther-Universitaet on 07 June 2012
Published on 17 May 2012 on http://pubs.rsc.org | doi:10.1039/C2SM25420D

induces a distinct hydration pressure to the SC lipids assembled in PII. This would provide a possible explanation for the observed reversible segregation of PI at 80 °C and 99% RH. While presumably a large fraction of CER[NP] remains as PII being still inaccessible for hydration, at least a part of the ceramide and the other model membrane components with a higher affinity to hydration, particularly the fatty acid, presumably form the re-appearing lamellar phase PI at 80 °C and 99% RH. Fig. 4 displays a sketch of the assumed SC lipid assembly of PI and PII at 80 °C and RH 99%. The well-defined diffraction peaks and the state of high lamellar order of PI despite the high temperature suggest that a certain amount of CER[NP] is incorporated into this phase besides CHOL and SA. The repeat distance is increased by about 1 Å in comparison to PI at 32 °C, and D₂O contrast variation results in increasing structure factor amplitudes. This finding indicates that the interlamellar space is hydrated to a certain extent in this phase. In order to allow for such a hydration, the ceramide molecules need to exhibit a less densely packed assembly in comparison to PII. This could be possible due to a significantly weakened hydrogen bond network of the ceramide head group at higher temperature. At this point, it is not clear whether a chain flip resulting in a hair-pin conformation of the ceramide molecules being reported before for the related phytosphingosine-based CER[AP] under excess water^{17,18} is likewise possible for CER[NP]. However, at 80 °C and excess hydration, significant changes in the lateral packing behaviour of the CER[NP] were reported previously with reorganization from orthorhombic to hexagonal chain packing. It was concluded that changes in the hydrogen bond network account for these changes.¹⁶ These findings may explain the re-occurrence of a stable and well-ordered lamellar phase at high temperature and high humidity, as reported in the present work.

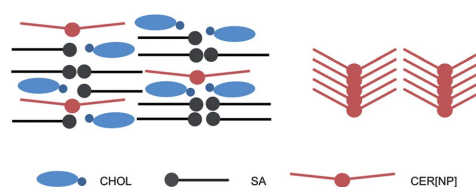


Fig. 4 Sketch of the assumed lamellar lipid assembly present in the phase-separated domains of PI and PII in the ternary SC lipid model membrane containing CER[NP], CHOL and SA at 80 °C and 99% RH. While PII is constituted by crystalline CER[NP] showing a V-shaped conformation, PI is formed by CER[NP], SA and CHOL.

To summarize, we observed a stable and dense bilayer assembly with surprising characteristics upon hydration and heating which suggest a V-shaped CER conformation, and co-existence of two lamellar phases. The distinct properties of CER [NP] probably account for the poorly hydrated but highly ordered bilayer organization present in the investigated SC lipid model membrane. From these findings, we conclude a protruding influence of the phytosphingosine-type ceramides for the proper formation of a stable SC bilayer structure.

3.2. ²H NMR spectroscopy on CER[NP]/cholesterol/stearic acid and CER[AP]/cholesterol/stearic acid

The morphology of the bilayer structure in the presence of CER [NP] was further corroborated by ²H NMR spectroscopy on either perdeuterated SA-*d*₅ or partially deuterated cholesterol-*d*₇ in the ternary mixtures. Typical ²H NMR spectra are shown in Fig. 5. In the CER[NP] containing mixture, the ²H NMR

spectrum of stearic acid shows the typical superposition of Pake doublets indicative of a lamellar and fluid phase state at 80 °C (A) and mainly 32 °C (B). However, at a temperature of 32 °C some molecules in the CER[NP] mixture are in the ordered phase as indicated from a broad plateau underneath the spectrum with a width of approximately ± 65 kHz. The ^2H NMR spectrum of cholesterol- d_7 (C) is dominated by a narrow quadrupolar splitting from the two methyl groups at C26 and C27 and a larger splitting coming from the deuteron attached to C25.

In the CER[AP] containing mixture, the ^2H NMR spectrum of stearic acid at 32 °C (E) represents the superposition of a highly ordered phase with part of the molecules in a more fluid state, however, not comparable to a true liquid-crystalline phase state as shown at 80 °C (D). As again can be seen from a broad plateau underneath the spectrum some molecules are in an ordered phase in the CER[AP] mixture even at the high temperature. The ^2H NMR spectrum of cholesterol- d_7 is again very similar to that in the ternary mixture with CER[NP].

The ^2H NMR spectra do not show any indications that either SA or cholesterol would be present in more than just one phase. If either of the molecules was contained in both the PI and the PII phases, we would have detected two sets of quadrupolar splittings for each deuteron, which was clearly not the case but has been described in the literature.^{45–47} This supports the model that attributes stearic acid and cholesterol to one of the lamellar phases, PI, with no exchange between the two phases (see Fig. 4). While the cholesterol spectra are identical in both mixtures, the ones attributed to the stearic acid vary more significantly between the two systems. Presumably, the structural assembly of the fatty acid is affected to a higher extent by the respective CER species, than the cholesterol. While CER[NP] appears to prefer a fluid phase state, the CER[AP] stabilizes a more rigid gel-like state. This reflects the structural differences of the two molecules.

More structural insights into the PI phase can be obtained from the analysis of the order parameter profiles derived from the ^2H NMR spectra of SA- d_{35} , which are shown in Fig. 6. All order parameters are relatively high and thus indicative of

a tightly packed lamellar structural arrangement. This supports the results received from the neutron diffraction experiments and underlines the high state of lamellar order, which is based on the presence of the CER species. Although the mixture containing CER[AP] appears to stabilize the gel state, at 80 °C it shows lower order parameters than the mixture containing CER[NP]. Highest order parameters are shown for the CER[NP] containing mixture at 32 °C, while the corresponding spectrum of the CER [AP] containing mixture could not be analysed due to the high proportion of a gel state.

Significantly increased order parameters were measured for SA- d_{35} in the mixture containing CER[NP] compared to CER [AP]. The reason for the higher state of order in the presence of CER[NP] compared to the ternary system composed of CER [AP] could be the α -hydroxyl group present in the amide bound stearic acid of CER[AP]. Although phytosphingosine-based ceramides are known to form a strong inter- and intra-molecular hydrogen bond network, also the localization of the hydroxyl groups involved in this network plays a crucial role: while the vicinal hydroxyl groups of CER[NP] and CER[AP] are important for the formation of intermolecular interactions, the α -hydroxy group only present in CER[AP] was found to somehow weaken the head group interaction between the SC lipids.⁴⁸ This influence was corroborated by the ^2H NMR results since the order parameter profiles show higher order parameters for the CER[NP] based model system (Fig. 6).

The NMR order parameters further allow the calculation of geometric parameters for the molecular packing in phase PI (see Table 3).⁴⁹ The stearic acid chains are very much elongated requiring a minimal cross-sectional area in the mixture with CER [NP]. In the mixture with CER[AP], the stearic acid chains are more disordered, however, they still represent a rigid extended conformation. From these geometrical parameters, the fraction of *gauche* conformers in each chain can be calculated⁵⁰ and is also given in Table 3. In the most rigid conformation, stearic acid on average only features ~ 2.2 *gauche* defects, which agrees with a very well ordered free fatty acid. This all confirms the model, according to which the stearic acid is forced into a more rigid and ordered structure when CER[NP] is present: the longer alkyl

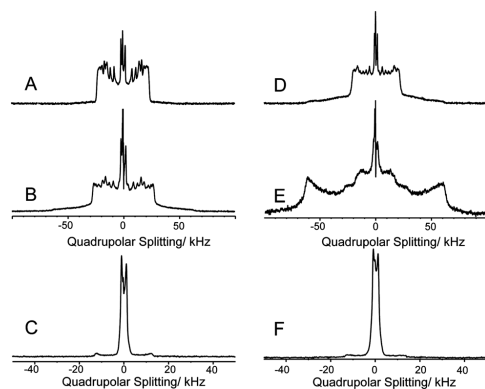


Fig. 5 ^2H NMR spectra of CER[NP]/CHOL/SA- d_{35} at 80 °C (A) and 32 °C (B), CER[NP]/CHOL- d_7 /SA at 80 °C (C), CER[AP]/CHOL/SA- d_{35} at 80 °C (D) and 32 °C (E), CER[AP]/CHOL- d_7 /SA at 80 °C (F).

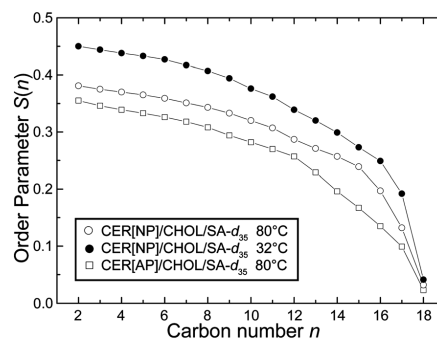


Fig. 6 Order parameter profiles obtained from the ^2H NMR spectra for the stearic acid in CER[NP]/CHOL/SA- d_{35} and in CER[AP]/CHOL/SA- d_{35} at a temperature of 32 °C and 80 °C.

Table 3 Calculated geometric parameters: mean interfacial area of one chain (A) and the chain extent (L_c^a) for the deuterated hydrocarbon chain of SA in the investigated samples

	$T/^\circ\text{C}$	$A/\text{\AA}^2$	$L_c^a/\text{\AA}$	Gauche conformers per chain
NP/CHOL/SA- d_{35}	80	25.2	16.8	3.2
	32	22.5	17.9	2.2
AP/CHOL/SA- d_{35}	80	25.9	15.9	4.0
	32	— ^a	— ^a	— ^a

^a Parameters could not be calculated due to the presence of the gel phase state.

chain extent indicates the prevalence of *trans* conformers, and the smaller area per molecule likewise suggests a more dense packing in comparison with the CER[AP] based system.

In conclusion, SA- d_{35} experiences a distinct influence from the respective CER species present in the mixture. This furthermore supports our assumption considering the molecular arrangement of the SC lipids in this model system based on a V-shaped conformation of CER[NP].

4. Conclusions

The present study investigated ternary SC lipid models containing the phyto-sphingosine-based CER[NP], CHOL and the fatty acid SA. We explored the influence of this sphingolipid species on the lamellar lipid assembly and investigated the samples by means of neutron diffraction and ^2H NMR spectroscopy. Our results indicate that in the presence of CER[NP], phase separation occurs, and a highly ordered lamellar SC model system is formed. Even at high temperature, the system exhibits bilayers with a densely packed and stable lamellar backbone. From the present data, we conclude that the phyto-sphingosine-type CER[NP] exerts a dominating influence on the structure of the ternary SC model: it prevents the model membrane from significant hydration and swelling, probably due to intense intra- and intermolecular head group interactions. Furthermore, it appears that model membranes based on CER[NP] exhibit a completely different temperature-dependent behaviour and different hydration characteristics, when compared to the closely related CER[AP] described in preceding studies.^{37,41} Thus, the CER head group apparently has a significant influence on the arrangement of the membrane lipids. The absence of only one OH group in the CER molecule leads to drastic structural changes as reported here. The interdisciplinary approach of our present study highlights the importance of applying combined techniques in order to elucidate the influence of particular CER species on the structural arrangement of simplistic SC lipid model membranes.

Abbreviations

SC	Stratum corneum
CER	Ceramide
CER[NP]	<i>N</i> -(Nonhydroxyoctadecanoyl)-phyto-sphingosine

CER[AP]	<i>N</i> -(α -Hydroxyoctadecanoyl)-phyto-sphingosine
CER[EOS]	30-Linoyloxy-triacontanoic acid-[(2 <i>S</i> ,3 <i>R</i>)-1,3-dihydroxyocta-dec-4-enyl]-amide
FFA	Free fatty acid
SA	Stearic acid
CHOL	Cholesterol
NSLD	Neutron scattering length density
RH	Relative humidity

Acknowledgements

The authors would like to express their gratitude to Evonik Goldschmidt GmbH (Essen, Germany) for the donation of CER [NP] and CER[AP]. T. Engelbrecht would like to thank the Graduiertenförderung des Landes Sachsen-Anhalt as well as Evonik Goldschmidt for funding. We gratefully acknowledge granting of beam-time and financial assistance by Institute Laue-Langevin (ILL, Grenoble, France). We thank the DFG (German Research Foundation) and the Experimental Physics Institutes of the University of Leipzig for providing measuring time on the Avance 750 MHz NMR spectrometer.

References

- P. M. Elias, *J. Invest. Dermatol.*, 1983, **80**(suppl), 44s–49s.
- P. M. Elias, J. Goerke and D. S. Friend, *J. Invest. Dermatol.*, 1977, **69**, 535–546.
- P. W. Wertz and B. van den Bergh, *Chem. Phys. Lipids*, 1998, **91**, 85–96.
- G. M. Gray and H. J. Yardley, *J. Lipid Res.*, 1975, **16**, 434–440.
- G. Brooks and B. Idson, *Int. J. Cosmet. Sci.*, 1991, **13**, 103–113.
- S. E. Friberg, I. Kayali, W. Beckerman, L. D. Rhein and A. Simion, *J. Invest. Dermatol.*, 1990, **94**, 377–380.
- P. W. Wertz, *Exog. Dermatol.*, 2004, **3**, 53–56.
- L. Coderch, O. Lopez, A. de la Maza and J. L. Parra, *Am. J. Clin. Dermatol.*, 2003, **4**, 107–129.
- G. Imokawa, A. Abe, K. Jin, Y. Higaki, M. Kawashima and A. Hidano, *J. Invest. Dermatol.*, 1991, **96**, 523–526.
- A. Di Nardo, P. Wertz, A. Giannetti and S. Seidenari, *Acta Derm-Venereol.*, 1998, **78**, 27–30.
- S. Motta, M. Monti, S. Sesana, R. Caputo, S. Carelli and R. Ghidoni, *Biochim. Biophys. Acta*, 1993, **1182**, 147–151.
- S. Raudenkolb, W. Hubner, W. Rettig, S. Wartewig and R. H. H. Neubert, *Chem. Phys. Lipids*, 2003, **123**, 9–17.
- S. Raudenkolb, S. Wartewig and R. H. H. Neubert, *Chem. Phys. Lipids*, 2003, **124**, 89–101.
- M. E. Rerek, H. C. Chen, B. Markovic, D. Van Wyck, P. Garidel, R. Mendelsohn and D. J. Moore, *J. Phys. Chem. B*, 2001, **105**, 9355–9362.
- M. E. Rerek, D. van Wyck, R. Mendelsohn and D. J. Moore, *Chem. Phys. Lipids*, 2005, **134**, 51–58.
- P. Garidel, *Phys. Chem. Chem. Phys.*, 2002, **4**, 1934–1942.
- M. A. Kiselev, *Crystallogr. Rep.*, 2007, **52**, 525–528.
- M. A. Kiselev, N. Y. Ryabova, A. M. Balagurov, S. Dante, T. Hauss, J. Zbytovská, S. Wartewig and R. H. H. Neubert, *Eur. Biophys. J.*, 2005, **34**, 1030–1040.
- D. Kessner, M. Kiselev, S. Dante, T. Hauss, P. Lersch, S. Wartewig and R. H. Neubert, *Eur. Biophys. J.*, 2008, **37**, 989–999.
- A. Schröter, D. Kessner, M. A. Kiselev, T. Hauss, S. Dante and R. H. H. Neubert, *Biophys. J.*, 2009, **97**, 1104–1114.
- M. Seul and M. J. Sammon, *Thin Solid Films*, 1990, **185**, 287–305.
- D. L. Worcester and N. P. Franks, *J. Mol. Biol.*, 1976, **100**, 359–378.
- A. Schroeter, M. A. Kiselev, T. Hauss, S. Dante and R. H. H. Neubert, *Biochim. Biophys. Acta, Biomembr.*, 2009, **1788**, 2194–2203.

- 24 A. Carruthers and D. L. Melchior, *Biochemistry*, 1983, **22**, 5797–5807.
- 25 N. P. Franks and W. R. Lieb, *J. Mol. Biol.*, 1979, **133**, 469–500.
- 26 D. Richard, M. Ferrand and G. J. Kearley, *J. Neutron Res.*, 1996, **4**, 33–39.
- 27 S. Dante, T. Hauss and N. A. Dencher, *Biochemistry*, 2003, **42**, 13667–13672.
- 28 J. F. Nagle and S. Tristram-Nagle, *Biochim. Biophys. Acta*, 2000, **1469**, 159–195.
- 29 J. H. Davis, K. R. Jeffrey, M. Bloom, M. I. Valic and T. P. Higgs, *Chem. Phys. Lett.*, 1976, **42**, 390–394.
- 30 E. Sternin, M. Bloom and A. L. Mackay, *J. Magn. Reson.*, 1983, **55**, 274–282.
- 31 M. A. McCabe and S. R. Wassall, *J. Magn. Reson., Ser. B*, 1995, **106**, 80–82.
- 32 D. Huster, K. Arnold and K. Gawrisch, *Biochemistry*, 1998, **37**, 17299–17308.
- 33 M. R. Ali, K. H. Cheng and J. Huang, *Biochemistry*, 2006, **45**, 12629–12638.
- 34 V. Pata and N. Dan, *Biophys. J.*, 2005, **88**, 916–924.
- 35 R. T. Zhang, W. J. Sun, S. Tristram-Nagle, R. L. Headrick, R. M. Suter and J. F. Nagle, *Phys. Rev. Lett.*, 1995, **74**, 2832–2835.
- 36 F. Y. Chen, W. C. Hung and H. W. Huang, *Phys. Rev. Lett.*, 1997, **79**, 4026–4029.
- 37 A. Schroeter, *The role of ceramide [AP] for the structural assembly of stratum corneum lipid model membranes*, Ph.D. thesis, Martin Luther University Halle-Wittenberg, 2010.
- 38 N. Ohta and I. Hatta, *Chem. Phys. Lipids*, 2002, **115**, 93–105.
- 39 T. N. Engelbrecht, A. Schroeter, T. Hauss and R. H. Neubert, *Biochim. Biophys. Acta, Biomembr.*, 2011, **1808**, 2798–2806.
- 40 D. Kessner, M. A. Kiselev, T. Hauss, S. Dante, S. Wartewig and R. H. Neubert, *Eur. Biophys. J.*, 2008, **37**, 1051–1057.
- 41 A. Ruettinger, M. A. Kiselev, T. Hauss, S. Dante, A. M. Balagurov and R. H. Neubert, *Eur. Biophys. J.*, 2008, **37**, 759–771.
- 42 B. Dahlen and I. Pascher, *Acta Crystallogr., Sect. B: Struct. Crystallogr. Cryst. Chem.*, 1972, **28**, 2396–2404.
- 43 P. Garidel, B. Folting, I. Schaller and A. Kerth, *Biophys. Chem.*, 2010, **150**, 144–156.
- 44 I. Pascher, *Biochim. Biophys. Acta*, 1976, **455**, 433–451.
- 45 A. Bunge, P. Müller, M. Stöckl, A. Herrmann and D. Huster, *Biophys. J.*, 2008, **94**, 2680–2690.
- 46 T. Bartels, R. S. Lankalapalli, R. Bittman, K. Beyer and M. F. Brown, *J. Am. Chem. Soc.*, 2008, **130**, 14521–14532.
- 47 S. L. Veatch, O. Soubias, S. L. Keller and K. Gawrisch, *Proc. Natl. Acad. Sci. U. S. A.*, 2007, **104**, 17650–17655.
- 48 E. Corbe, C. Laugel, N. Yagoubi and A. Baillet, *Chem. Phys. Lipids*, 2007, **146**, 67–75.
- 49 A. Vogel, C. P. Katzka, H. Waldmann, K. Arnold, M. F. Brown and D. Huster, *J. Am. Chem. Soc.*, 2005, **127**, 12263–12272.
- 50 A. Vogel, G. Reuther, K. Weise, G. Triola, J. Nikolaus, K. T. Tan, C. Nowak, A. Herrmann, H. Waldmann, R. Winter and D. Huster, *Angew. Chem., Int. Ed.*, 2009, **48**, 8784–8787.

3.1.2 Study of an artificial CER[EOS] pendant containing a saturated, branched ω -acyl chain (Manuscript: Soft Matter)

Engelbrecht T, Hauß T, Süß K, Vogel A, Roark M, Feller SE, Neubert RHH, Dobner B: **Characterisation of a new ceramide EOS species: synthesis and investigation of the thermotropic phase behaviour and influence on the bilayer architecture of stratum corneum lipid model membranes.** *Soft Matter* 2011; 7: 8998-9011 (DOI: 10.1039/c1sm05134b)

Available online:

<http://pubs.rsc.org/en/content/articlelanding/2011/sm/c1sm05134b>

Cite this: *Soft Matter*, 2011, **7**, 8998

www.rsc.org/softmatter

PAPER

Characterisation of a new ceramide EOS species: synthesis and investigation of the thermotropic phase behaviour and influence on the bilayer architecture of stratum corneum lipid model membranesTanja Engelbrecht,^a Thomas Hauß,^b Kevin Süß,^a Alexander Vogel,^c Matthew Roark,^d Scott E. Feller,^d Reinhard H. H. Neubert^{*a} and Bodo Dobner^a

Received 26th January 2011, Accepted 8th July 2011

DOI: 10.1039/c1sm05134b

The lipids of the stratum corneum, particularly the ceramides, are known to play a crucial role for the skin barrier properties. Thereby, the unique ω -acyl ceramide EOS is regarded to be a precondition for the formation of a protective envelope. We report on the chemical synthesis of a new ceramide EOS derivative constituting a saturated and branched ω -acyl chain instead of the naturally occurring ω -esterified linoleic acid moiety, therefore showing an improved stability against oxidative influences. In addition, the thermotropic phase behaviour of the new ceramide was studied using differential scanning calorimetry (DSC) and Fourier transform Raman spectroscopy. The results indicate a phase behaviour similar to the one known for the naturally occurring ceramide EOS. Chain packing behaviour as well as phase transition temperatures are found to be comparable for both ceramide species. Furthermore, the present study addresses the issue of characterising oriented quaternary stratum corneum lipid model membranes based on the new ceramide EOS derivative by means of neutron diffraction. The results indicate the formation of a stable bilayer architecture with membrane parameters comparable to the quaternary model systems containing naturally the occurring ceramide EOS species. Additional molecular dynamics simulations corroborated the findings received from neutron diffraction and the proposed lipid bilayer arrangement.

1. Introduction

With an area of about 2 m², the skin represents the largest organ of the human body. The outermost layer of the skin, the stratum corneum (SC), exhibits a unique morphology consisting of flattened and keratin-filled cells (corneocytes) which are embedded in a continuous multilamellar matrix of lipid membranes.¹ As it is widely accepted that the SC forms the main skin barrier,² it was not until a series of experiments were carried out before it was accepted that in particular the intercellular SC lipid matrix is playing a key role in preventing uncontrolled water loss³ and protecting the organism from environmental, physical or chemical perturbation.^{4,5} Ceramides (CER), free fatty acids (FFA) and cholesterol (CHOL) with its derivatives such as cholesterol sulfate (ChS) are the main constituents of the intercellular SC

lipid matrix while phospholipids being present in all human cell membranes are lacking.⁶ By now, 11 subclasses of CER differing in sphingoid bases and amide-bound fatty acids have been identified.⁷

Detailed knowledge regarding the organisation of the SC lipids on a molecular scale is still lacking. Early studies based on electron micrographs of full thickness skin using ruthenium tetroxide fixation revealed the presence of alternating electron dense and electron lucent bands termed broad-narrow-broad sequences.⁸ Further small angle X-ray diffraction (SAXD) experiments on human SC suggested a lipid arrangement in two lamellar phases with bilayer repeat distances of approximately 65 Å and 130 Å, respectively.⁹ Later, these phases were referred to as the long periodicity phase (LPP) and short periodicity phase (SPP).¹⁰ But due to low availability of human skin (except from surgery) and large inter-individual variations in SC lipid content and composition,¹¹ a different approach in SC research arose. One now tends to use mixtures of synthetic SC lipids with well-defined head group architecture and defined hydrocarbon chain lengths.¹² It was shown that synthetic SC lipid mixtures serve as appropriate models which closely resemble the native SC lipid arrangement, furthermore preventing disturbing influences due to the heterogeneity of CER subspecies present in native skin.¹³ In recent years, the neutron diffraction technique was proven to

^aInstitute of Pharmacy, Martin Luther University, Wolfgang-Langenbeck-Straße 4, 06120 Halle, Germany. E-mail: reinhard.neubert@pharmazie.uni-halle.de

^bInstitute Soft Matter and Functional Materials, Helmholtz-Zentrum-Berlin, Hahn-Meißner-Platz 1, 14109 Berlin, Germany

^cInstitute for Medical Physics and Biophysics, University of Leipzig, Härtelstraße 16-18, 04107 Leipzig, Germany

^dDepartment of Chemistry, Wabash College, 301 W. Wabash Ave, Crawfordsville, IN, 47933, USA

be an attractive tool for structural investigation of highly oriented multilamellar SC model membranes, especially with simple lipid composition.^{14,15} The benefit offered by such less complex models for determining the impact of particular SC lipids on the bilayer architecture was emphasized not only in neutron diffraction studies, but also in other reports.¹⁶ Based on the findings for a quaternary SC model containing the sphingolipid CER[AP] (*N*-(α -hydroxyoctadecanoyl)-phytosphingosine), CHOL, palmitic acid (PA) and ChS, Kiselev and co-workers evaluated the lipid bilayer arrangement¹⁵ and proposed the *armature reinforcement model*,¹⁷ which suggests the formation of a stable membrane structure based on the unique properties of the short-chain CER[AP]. Due to its high polarity founded on four OH groups it creates a stable bilayer backbone probably by strong lateral hydrogen bonds, forcing the other SC lipids to arrange inside the lamellar structure dictated by CER[AP] itself. Furthermore, the specific properties of neutrons allow for localisation of deuterium-labelled molecules. Using this knowledge it was possible to determine the position of *e.g.* fatty acid species¹⁸ or CHOL¹⁹ inside the model bilayers.

Apart from CER[AP], several studies revealed that CER[EOS] also appears to play a distinct role in SC barrier formation. A report of Motta and co-workers²⁰ compared the CER composition of healthy and barrier-impaired psoriatic skin. Results indicated a noticeable decrease in CER[EOS] content in the latter case. As CER[EOS] is regarded to be a prerequisite for the correct formation of the LPP,¹³ the long-chain ω -acyl ceramide was and still is a subject of great interest in SC research.

The objective of the present study was the synthesis of a new artificial CER[EOS] species and its further investigation by means of differential scanning calorimetry (DSC) and Raman spectroscopy. Comprising a C10-methyl-branched palmitic acid instead of an linoleic acid esterified in the ω -position, the substance will accordingly be designated as CER[EOS]_{branched}. Its chemical structure and the formula of its natural pendant CER[EOS] are displayed in Fig. 1. Due to its structure, the synthetic CER[EOS]_{branched} is less sensitive to oxidative influences and therefore easier to handle, making it a more inexpensive alternative to its natural pendant. This may be of importance since ceramides are considered to be useful in treatment of diseased skin and to improve the skin barrier function as reviewed in ref. 21. An early report regarding the positive effects of ceramides on the barrier properties of skin is the one of Imokawa and co-workers.²² They found a clearly improved water-holding capability of lipid-depleted skin after topical application of SC lipids, with the CER application causing the strongest effect. Later, potential repair effects due

to treatment with a synthetic CER species related to CER 2 were reported.²³ Here, *in vitro* measurements revealed a significant decrease of transepidermal water loss (TEWL) of isolated human SC after treatment with the CER solution. Additional hair friction tests also indicated positive effects of CER treatment on the surface properties of hair. Besides few studies underlining the need for topical application of SC lipid mixtures rather than supplementing a single CER species to improve the barrier repair,²⁴ there are also some reports emphasizing the particular role of externally applied acylceramides containing linoleic acid for recovery of a diminished skin barrier.²⁵

Besides the synthesis and characterisation of CER[EOS]_{branched}, we also report on its impact on the SC lipid bilayer assembly. For that purpose, quaternary model membranes containing the new CER, CHOL, CER[AP] and behenic acid were investigated by neutron diffraction and additional molecular dynamics (MD) simulations were performed. The results are discussed in comparison to the findings obtained for the native CER[EOS] species.

2. Experimental

2.1. Materials

The ceramides CER[EOS] (30-linoyloxy-triacontanoic acid-[(2S,3R)-1,3-dihydroxyocta-dec-4-en-yl]-amide) and CER[AP] (*N*-(α -hydroxyoctadecanoyl)-phytosphingosine) were generously provided by Evonik Goldschmidt GmbH (Essen, Germany). A chromatographic procedure was used to increase the purity of CER[EOS] above 96%. Therefore, the substance was treated by using middle pressure liquid chromatography (MPLC) on a silica gel column with a chloroform/methanol gradient. Mass spectrometry was used to prove the identity of CER[EOS] ($M_r = 1011.965 \text{ g mol}^{-1}$). CER[AP] was used as received with a purity above 96%. CHOL and behenic acid (BA) were received from Sigma Aldrich GmbH (Taufkirchen, Germany). The synthetic CER[EOS] species (CER[EOS]_{branched}) was received from chemical synthesis as described in detail in the section "Synthesis of the artificial branched CER[EOS]". All substances needed for synthesis were purchased from Sigma Aldrich GmbH (Taufkirchen, Germany) and used without purification. All solvents were purified and dried before use. Melting points were determined by a Boetius-apparatus and are uncorrected. ¹H-NMR-spectra were recorded on a Gemini 2000 NMR spectrometer. Mass spectrometric data were obtained with a Q-TOF2 mass spectrometer (Waters Micromass, Manchester, U.K.) (ESI-MS) or were recorded on a AMD 402 spectrometer (AMD Intecta GmbH, Harpstedt, Germany) (70 eV, EI-MS). Elemental analysis data for characterisation of the compounds received from chemical synthesis (analysed elements: C, H, N) were determined using a Leco CHNS-932 apparatus. After synthesis, the substance was purified using liquid chromatography on a silica gel column with a chloroform/methanol gradient. The identity of CER[EOS]_{branched} was proven by mass spectrometry ($M_r = 1001.971 \text{ g mol}^{-1}$). Quartz slides (Spectrosil 2000, $25 \times 65 \times 0.3 \text{ mm}^3$) for the neutron diffraction experiments were purchased from Saint-Gobain (Wiesbaden, Germany).

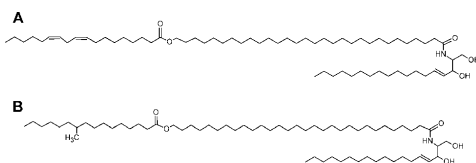


Fig. 1 (a) Chemical structure of native CER[EOS] with ω -linoleic acid side chain. (b) Chemical structure of the methyl-branched CER[EOS] derived from own synthesis.

2.2. Synthesis of the artificial branched CER[EOS]

Synthesis of 10-methylhexadecanoic acid chloride. 13 mmol (3.4 g) of 10-methylhexadecanoic acid and 77 mmol (15 ml) of freshly distilled thionyl chloride were heated for 3 h under reflux. The excess thionyl chloride was distilled off and the residue was dried under reduced pressure over potassium hydroxide. The crude product was used for the next step without further purification.

Preparation of (30-hydroxytriacontan-1-yloxy)-10-methylhexadecanoate (3). 15.8 mmol (7.2 g) of triacontan-1,30-diol were placed in 240 ml of dry chloroform and heated under reflux. Then, 5.54 mmol (1.5 g) of the crude acid chloride dissolved in 50 ml of chloroform were dropped slowly into the boiling solution with stirring. The mixture was heated for further 5 h under reflux. After cooling down the unconsumed triacontan-1,30-diol was filtered off, the solution was evaporated to dryness and the residue was purified by column chromatography using chloroform/heptanes with the gradient technique.

Yield: 2.55 g (65%), white solid, mp 70.5–71 °C, ¹H NMR (CDCl₃, 400 MHz): δ = 0.83 (d, 3H, [–CH(CH₃)–]), 0.89 (t, 3H, [–CH₃]), 1.53–1.59 (m, 6H, [HO–CH₂–CH₂–], [–CO–O–CH₂–CH₂–], [–CH₂–CH₂–CO–O–]), 2.3 (t, 2H, [–CH₂–CO–O]), 3.65 (t, 2H, [HO–CH₂–]), 4.01 (t, 2H, [–CO–O–CH₂–]) ppm. EI-MS for C₄₇H₉₄O₃: 706 [M]⁺, 688 [M – H₂O]⁺. Anal. Calcd for C₄₇H₉₄O₃: C, 79.82%; H, 13.40%; found: C, 79.33%; H, 13.40%.

Synthesis of 30-(10-methylhexadecanoyloxy)triacontanoic acid (4). 1.4 mmol (0.98 g) of the monoester 3 in 50 ml of CH₂Cl₂ were dropped into a slurry of 5.0 mmol (1.9 g) of pyridinium dichromate in 30 ml of CHCl₃ over a period of 3 h at room temperature. The mixture was then stirred for further 72 h at the same temperature. After that the reaction mixture was poured into crushed ice and after phase separation the organic layer was removed. The water phase was extracted twice with 20 ml of chloroform and the combined organic layers were evaporated to dryness. The crude acid was purified by middle pressure chromatography using chloroform/ether as the eluent.

Yield: 0.72 g (71%), white substance, mp 74–75.5 °C, ¹H NMR (CDCl₃, 400 MHz): δ = 0.82 (d, 3H, [–CH(CH₃)–]), 0.87 (t, 3H, [–CH₃]), 1.2–1.4 (m, H, [chain]), 1.52–1.63 (m, 4H, [–CH₂–CH₂–O–CO–], [–CH₂–CH₂–COO–]), 2.27 (t, 2H, [–O–CO–CH₂–]), 2.35 (t, 2H, [HO–CO–CH₂–]), 4.0 (t, 2H, [–CO–O–CH₂–]) ppm. EI-MS for C₄₇H₉₂O₄: 719 (65%, [M – H]⁺), 705 (23%, [M – H, –CH₃]⁺). Anal. Calcd for C₄₇H₉₂O₄: C, 78.27%; H, 12.81%; found: C, 78.09%; H, 12.61%.

Preparation of 10-methylhexadecanoic acid (30-[(3E)-2-hydroxy-1-hydroxymethyl-heptadec-3-en-1-yl]amino)-30-oxo-triacontan-1-yl)ester (5). 1 mmol (0.72 g) of compound 4, 1.5 mmol (0.37 g) of EEDQ and 1.5 mmol (0.44 g) of sphingosine were suspended in 10 ml of dry ethanol and stirred at 50 °C for 48 h. The solvent was removed in vacuum and the residue was purified by column chromatography.

Yield: 0.41 g (41%), white waxy substance, mp 80.5–82 °C, ¹H NMR (CDCl₃, 400 MHz): δ = 0.84 (d, 3H, [–CH–CH₃]), 0.88 (t, 3H, [–CH₃]), 1.08–1.40 (m, 93H, [chain]), 1.48–1.65 (m, 8H, [–CH₂–CH₂–CO–O–], [–CH₂–CH₂–O–CO–], [–CH₂–CH₂–CO–NH–], [–CH₂–CH₂–CH=CH–]), 2.0–2.05 (m, 2H, [–CH₂–CH=

CH–]), 2.21 (t, 2H, [–CH₂–CO–NH–]), 2.28 (t, 2H, [–CH₂–CO–O–]), 3.68–3.72 (m, 2H, [–CH₂–OH]), 3.9–3.95 (m, 1H, [–CH–CH–NH–]), 4.03 (t, 2H, [–CH₂–O–CO–]), 4.28–4.32 (m, 1H, [–CH=CH–CH–OH]), 5.5–5.55 and 5.70–5.78 (2m, 2H, [–CH=CH–]) ppm. ESI-MS for C₆₅H₁₂₇NO₅: 1002.918 [M – H]⁺. Anal. Calcd for C₆₅H₁₂₇NO₅: C, 77.86%; H, 12.77%; N, 1.40%; found: C, 77.26%; H, 12.46%; N, 1.36%.

2.3. Differential scanning calorimetry

The DSC measurements were carried out using a Netzsch DSC 200 differential scanning calorimeter (Netzsch Geratebau, Selb, Germany). The native CER[EOS] as well as CER[EOS]_{branched} were studied in a dry state in a temperature range from 20 to 120 °C. About 2 mg of each substance were placed in sealed aluminium pans. Each ceramide species was measured separately and underwent the temperature program together with a reference (empty aluminium pan), whereby a heating rate of 5 K per minute was chosen. After the heating scan, the sample was cooled down to 20 °C. Subsequently, this temperature cycle was repeated twice.

2.4. Fourier-transform Raman spectroscopy

For the spectroscopic study of CER[EOS]_{branched}, Raman spectra were recorded using a Bruker Fourier transform infrared spectrometer RFS 100/S (Bruker Optics, Ettlingen, Germany). As an excitation source a diode pumped Nd:YAG laser which emits radiation at 1064 nm was used. The scattered radiation was collected at 180° at the source, with the spectra being recorded at a laser power of 400 mW at the sample location and at a resolution of 4 cm^{–1}. The substance CER[EOS]_{branched} was placed in an NMR tube and measured in a dry state over a temperature range from 25 °C up to 95 °C. Prior to recording of the Raman spectra, the sample was allowed to equilibrate for 5 minutes. OPUS, a Bruker software package, was used for data evaluation.

2.5. Neutron diffraction experiments

A method according to ref. 26 was used for sample preparation for the neutron diffraction experiments. Briefly, appropriate amounts of SC lipids were dissolved in a mixture of chloroform/methanol (2 : 1, v/v) and mixed in the required ratio, yielding a total lipid concentration of 10 mg ml^{–1}. The sample composition is listed in Table 1.

A volume of 1200 μl of the lipid solution was spread over the quartz surface, followed by a drying process at room temperature first under atmospheric pressure and then under vacuum. After the complete removal of the organic solvent, a subsequent annealing cycle was applied. Thereby, the sample underwent an alternating heating and cooling process in a water-saturated atmosphere to decrease mosaicity. The necessity of this procedure for creation of an organised multilamellar lipid arrangement was described in detail in ref. 27.

Table 1 Composition of the investigated sample

SC lipid model system	Component ratio (m/m)
CER[EOS] _{branched} /CER[AP]/BA/CHOL	23/10/33/33

Neutron diffraction data were collected by means of the V1 membrane diffractometer at the BER II research reactor of the Helmholtz-Zentrum-Berlin (HZB, Berlin, Germany), situated on a cold source. A neutron wavelength of $\lambda = 5.23 \text{ \AA}$ for the experiments was selected by appropriate positioning of a pyrolytic graphite monochromator. Diffraction patterns were recorded as $\theta - 2\theta$ scans from $2\theta = 0^\circ$ to 45° . A two-dimensional position sensitive ^3He detector ($20 \times 20 \text{ cm}^2$ area, $1.5 \times 1.5 \text{ mm}^2$ spatial resolution) with a sample to detector distance of 102.38 cm was employed. Prior to all neutron diffraction experiments, the samples were equilibrated for 8 up to 12 hours in portable and lockable aluminium cans and kept at a fixed relative humidity (rh) of 57% and at a certain $\text{D}_2\text{O}/\text{H}_2\text{O}$ ratio. Test measurements recorded during the equilibration procedure proved this time period to be adequate for equilibration of the samples, as no further changes in peak intensity and position were observed after 7 hours.

A saturated solution of NaBr inside the chamber was used to adjust the humidity, creating a vapour to which the sample was exposed during equilibration and measurements. For variation of the neutron contrast between the lipid sample and water, the vapour in the sample can was varied for three different $\text{D}_2\text{O}/\text{H}_2\text{O}$ ratios: 100/0, 50/50 and 8/92% (v/v). At all times, temperature inside the can was controlled through a thermostat and kept constant at 32°C , which is comparable to *in vivo* conditions of the skin. The basic principle of diffraction phenomena is given by Bragg's law:

$$n\lambda = 2d \cdot \sin \theta \quad (1)$$

where n is the order of diffraction, λ is the wavelength, d is the spacing between the scattering planes inside the sample and θ is the angle between the incident beam and the diffracting planes, here the membrane planes. The sample studied was exposed to a monochromatic and collimated incoming neutron beam. During the measurements, the intensity I of scattered neutrons was recorded as a function of the scattering angle 2θ . The scattering angle is correlated with the scattering vector Q (momentum transfer) by $Q = 4\pi \cdot \sin \theta / \lambda$, with Q being the resulting vector between the incoming wave vector \vec{k}_i and the scattered wave vector \vec{k}_s . From the positions of a series of equidistant peaks in the diffraction pattern, the periodicity (d -spacing) of a lamellar phase can be calculated by using eqn (2):

$$d = 2n\pi/Q_n \quad (2)$$

where Q_n is the position of a series of equidistant peaks and n is the respective diffraction order. Peaks were fitted with Gaussian functions using the software package IGOR Pro (WaveMetrics Inc., Portland, OR, USA).

For determination of the internal membrane structure, the neutron scattering length density (NSLD) profiles $\rho_s(x)$ were calculated by Fourier transform of the structure factors F_h (see eqn (3)):

$$\rho_s(x) = a + b \frac{2}{d} \sum_{h=1}^{h_{\max}} F_h \cos \left(\frac{2\pi hx}{d} \right) \quad (3)$$

where a and b are coefficients used for relative normalisation of $\rho_s(x)$.²⁸ d is the lamellar repeat distance, h is the order of

diffraction and F_h is the structure factor of the h^{th} peak. Thereby, the absolute value of F_h is accessible as $|F_h| = \sqrt{hI_h}$, with h being the Lorentz correction and I_h being the integrated intensity of the h^{th} peak. As described in ref. 29 and 30, the determination of the signs of F_h (which can only be "+" or "-" for centrosymmetric bilayers) is easily possible by contrast variation, which is done by measuring the samples at no less than three different $\text{D}_2\text{O}/\text{H}_2\text{O}$ ratios and linear correlation between the F_h value and D_2O content. In ref. 15, 19, 29 and 31, a more detailed description concerning the evaluation of the neutron diffraction data is given. The NSLD profiles $\rho_s(x)$ display the density distribution of the neutron scattering length across one centrosymmetric lipid bilayer and allow for detailed insights into the lipid arrangement within such a model membrane.

2.6. Molecular dynamics simulations

All-atom MD simulations of the proposed membrane model consisted of 80 CER[EOS]_branched, 56 CER[AP], 320 BA, and 280 CHOL molecules closely matching the mixture of the experiments. Initial structures of the molecules were built from internal coordinates with the acyl chains in an all-*trans* conformation and roughly parallel for the ceramides. The BA molecules were considered to be neutral since it is known that long saturated fatty acids have a high apparent pK_a in membrane environments.^{32,33} Next the molecules were equally distributed over four individual membranes spaced according to the experimental d -spacing, placed at random lateral positions, and vertically shifted such that the oxygens facing the water were all in the same plane. For each CER[EOS]_branched and CER[AP] molecule one water molecule was placed at a random position between the membranes leading to a total of 136 H_2O molecules resulting in a total number of 65 168 atoms. In this model the very long chain of CER[EOS]_branched completely spans its host membrane with the carboxylic acid ester group between two membranes and the ω -C10-methyl-branched palmitic acid chain embedded in the next membrane while CER[AP] is in a hairpin conformation with both acyl chains inserted in the same membrane.

The forcefield for the ceramides is based on the CHARMM forcefield of sphingomyelin³⁴ with the head group removed and replaced by an OH group whose parameters were taken from the side chain of serine. For BA and CHOL the all-H lipid forcefield, including a refinement of the saturated acyl-chain torsions³⁵ was used and water was represented by the TIP3 model. The simulation was setup and analysed using CHARMM³⁶ while it was run with NAMD³⁷ due to much better parallel performance. The simulation was run under conditions of constant temperature (32°C) and normal pressure (1.013 bar) with periodic boundary conditions where the cell dimensions were allowed to fluctuate in all directions and only their ratio was kept constant in the plane of the membrane. No lateral pressure was applied. The smooth particle-mesh Ewald algorithm was used to compute the electrostatic forces.³⁸ The SHAKE algorithm was used to maintain rigid all bonds involving hydrogen atoms,³⁹ allowing a 2 fs time step. The simulation was run for 517 ns with the initial 217 ns discarded as equilibration. During this equilibration period it was once step-wise heated up to 90°C and continued for 5 ns followed by step-wise cooling back to 32°C to anneal the membrane and reproduce the experimental sample preparation.

To calculate NSLD profiles from MD, the water that was deuterated in the experiments was also considered deuterated in the simulation. The simulation cell was divided into slices perpendicular to the z -axis to create a histogram of atomic distributions along the z -axis. Each bin was parallel to the x - y plane with a width of 1.0 Å. Each trajectory frame was shifted such that the center of mass of one membrane was centered at $z = 0$. In each trajectory frame the number of occurrences of atom a within bin b , n_{ab} , is multiplied by its corresponding scattering length, s_a . The summation was accumulated for each bin over the entire trajectory. Next, the average for each bin was calculated by dividing by the total number of trajectory frames, the area of the simulation unit cell, and the number of bins. The result is a NSLD profile averaged over the entire MD simulation with an effective resolution of 1.0 Å. The same method was also used to compute profiles for a particular molecule species simply by counting only the occurrences of atoms in these molecules.

3. Results and discussion

3.1. Synthesis of compound 5

The synthesis of CER[EOS]_{branched} (Fig. 2) starts from 10-methylhexadecanoic acid chloride **1**. A facile synthesis of 10-methylhexadecanoic acid was already described.⁴⁰ For the preparation of monoester **3** the fatty acid chloride was dropped into a solution of triacontan-1,30-diol **2**⁴¹ in boiling chloroform over a period of 2 h without a base. The main problem in this reaction step was the poor solubility of the diol at room temperature, leading to the preparation of the diester especially with a base as catalyst. This is due to the better solubility of the monoester which then reacts faster to the diester. With an excess of diol **2** and the above discussed procedure, compound **3** was isolated in yields of 65%. The monoester **3** was then oxidized to the corresponding acid **4**. Oxidation with chromtrioxide in half concentrated sulfuric acid⁴² was accompanied by byproducts resulting from esterification of starting alcohol **3** with acid **4** under these conditions. As the method of choice, oxidation with pyridinium dichromate in nearly three-fold excess has been emerged. The purified acid **4** was transformed into the ceramide **5** by activation with EEDQ using dry ethanol as solvent at 50 °C over a period of 24 h.^{43,44}

3.2. DSC measurements

The DSC measurements were performed for both the native and the branched CER[EOS] species for comparison reasons. The thermograms for native CER[EOS] and CER[EOS]_{branched} recorded during the first, second and third heating scan are shown in Fig. 3a and b, respectively. Upon heating, both substances obviously show similar thermotropic phase behaviour with endothermic processes indicated by sharp phase transition peaks. In the case of CER[EOS], the main phase transition peak is located at about 83 °C for the first heating, and the one for CER[EOS]_{branched} was found to be very close to the latter and within the experimental error limits at 81.7 °C. Interestingly, only one transition was detected for native CER[EOS]. Contrary to this, CER[EOS]_{branched} exhibits a pretransition at approximately 72 °C during the first heating. Here, preliminary changes in chain packing of the molecule seem to take place before a sharp peak at 81.7 °C indicates the main phase transition. The latter is well correlated with the melting point of CER[EOS]_{branched} (80.5–82 °C), where the more densely packed chains get disordered which requires more thermal energy.

Table 2 displays the phase transition temperatures found for CER[EOS] and CER[EOS]_{branched}. Remarkably, the pretransitions detected for CER[EOS]_{branched} are clearly shifted to lower temperatures during the second and third heating, namely from 72 °C (first scan) towards 58 °C (second scan) to 56.6 °C (third scan). The same was observed for the main transition peak being moved by more than 2 °C towards lower temperatures. This may be due to a delayed reformation of the original alkyl chain packing, with the initial degree of order not being completely rebuilt prior to the subsequent heating scan. A hysteresis of about 10 °C found upon cooling the sample corroborates this assumption of slow reformation of the gel structure during the cooling process, which is in line with other reports in the literature.^{45,46}

The native CER[EOS] species with the linoleic acid in ω -position shows one pretransition at 77 °C during the second heating scan, which is only visible as a small shoulder during the third sample heating. The temperature of the main phase transition shifts to slightly higher temperatures, from 83 °C to 85 °C. Either partial conformational change from *cis* to *trans* or degradation due to thermal influences presumably accounts for this observation.

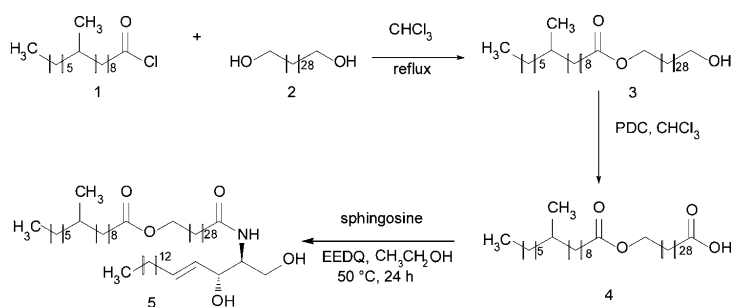


Fig. 2 Chemical synthesis of the new artificial CER[EOS]_{branched} with a methyl-branched palmitoyl side chain.

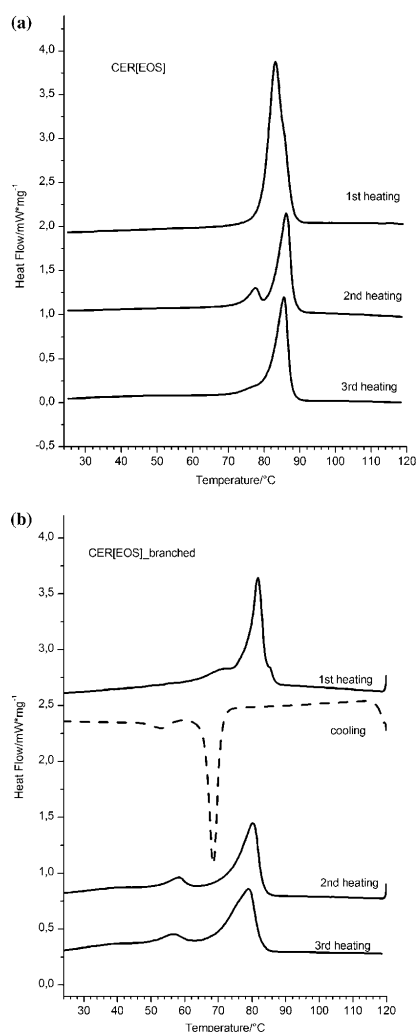


Fig. 3 (a) DSC spectra recorded for CER[EOS]. Shown are the thermograms for the first, second and third heating scans (bold lines). The occurring peaks indicate endothermic phase transitions. (b) DSC spectra recorded for CER[EOS]_{branched}. Displayed are the thermograms for the first, second and third heating scans (bold lines). The dashed line represents the cooling process following the first heating scan. Positive peaks indicate endothermic phase transitions during the heating process, while the negative peak indicates the exothermic process upon cooling the sample. Note the hysteresis of about 10 °C.

Interestingly, exchanging the unsaturated linoleic acid in CER [EOS] against the saturated 10-methyl palmitic acid in CER [EOS]_{branched} does not lead to a higher main phase transition temperature as may be expected. The ω -acyl chains in both substances seem to affect the alkyl chain packing behaviour in

Table 2 Phase transition temperatures found for CER[EOS] and CER[EOS]_{branched}, respectively, with the main phase transition temperature written in bold

	1 st heating	2 nd heating	3 rd heating
CER[EOS]	83 °C	77 °C, 86 °C	76 °C, 85 °C
CER[EOS] _{branched}	72 °C, 81.7 °C	58.2 °C, 80.2 °C	56.6 °C, 79 °C

a similar way. This is surprising, as unsaturated moieties reduce the ratio of *trans* conformers in molecules.^{47,48} A reason for this could be the branching of the ω -acyl chain. As the 10-methyl group is preventing the terminal C6 moiety from contributing to a dense alkyl chain packing, only the C-atoms between the branching and the ester group are involved in forming a dense chain packing. The consequence is a perturbed alkyl chain order comparable to native CER[EOS] containing the ω -linoleic acid, which results in comparable thermotropic phase behaviour for both ceramides.

3.3. Raman experiments

As often reported in the literature, FT-Raman spectroscopy is a valuable tool frequently used for investigating the hydrocarbon chain packing behaviour and phase transitions of lipids, especially ceramides.^{49–51} The Raman spectra of the synthetic pendant CER[EOS]_{branched} recorded at different temperatures are presented in Fig. 4a and b, respectively. Characteristic Raman bands and their assignment according to the literature^{52–55} are summarised in Table 3.

Interesting is the absence of sharp bands at the positions of $<300\text{ cm}^{-1}$ (the longitudinal acoustic mode, LAM) and 890 cm^{-1} (CH_3 rocking mode). Obviously, CER[EOS]_{branched} exhibits no *all-trans* chain conformation as well as no *trans* conformers at the alkyl chain end. In fact, upon raising the temperature to 82 °C, a very broad and low intense peak located at 870 cm^{-1} appears, indicating increased chain motion due to the higher temperature as well as the presence of *gauche* conformation in the chain end position.⁵⁶ Raman studies of the native CER[EOS] species revealed that the chain end also does not show an *all-trans* conformation,⁵⁷ which is probably caused by the presence of the ω -linoleic acid moiety. As CER[EOS]_{branched} features a saturated alkyl chain in the ω -position, the absence of *trans* conformers at the chain end is surprising. The reason could be again the branched 10-methyl-palmitic acid esterified in the ω -position. The higher degree of order expected to occur for the saturated side chain is disturbed by the methyl group, which inhibits a dense chain packing behaviour. Therefore, no characteristic bands of LAM or *trans* conformation of the chain end are detectable. Sharp bands occurring at 1063 cm^{-1} and 1128 cm^{-1} which represent the asymmetric and symmetric C–C stretching modes, respectively, indicate the presence of three or more *trans* conformers in a row and suggest a certain state of alkyl chain order present in the molecule. During heating of CER [EOS]_{branched}, the band intensities of $\nu_s(\text{C–C})$ and $\nu_{as}(\text{C–C})$ decrease due to the enhanced alkyl chain movement and the associated loss of order.

According to ref. 58, vibrational spectroscopic studies do not only allow for insights into intramolecular conformational characteristics but also allow, as especially the CH_2 scissoring

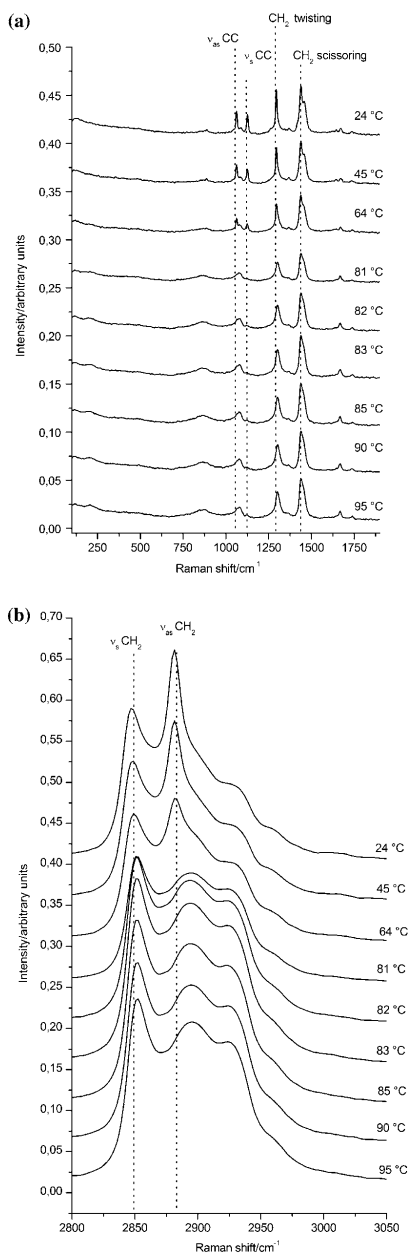


Fig. 4 (a) Raman spectra recorded for CER[EOS]_{branched} at different temperatures in the spectral range from 100 to 1900 cm^{-1} . (b) Raman spectra of CER[EOS]_{branched} in the spectral range of 2800–3050 cm^{-1} at different temperatures as assigned.

Table 3 Characteristic bands of the Raman spectra of CER[EOS]_{branched} (ν represents the stretching mode)

Band position/ cm^{-1}	Band assignment
1063	ν_{as} (C–C), three or more <i>trans</i> bonds in sequence
1128	ν_{s} (C–C), three or more <i>trans</i> bonds in sequence
1295	CH ₂ twisting
1439, 1459	CH ₂ scissoring
2848	ν_{s} CH ₂
2882	ν_{as} CH ₂

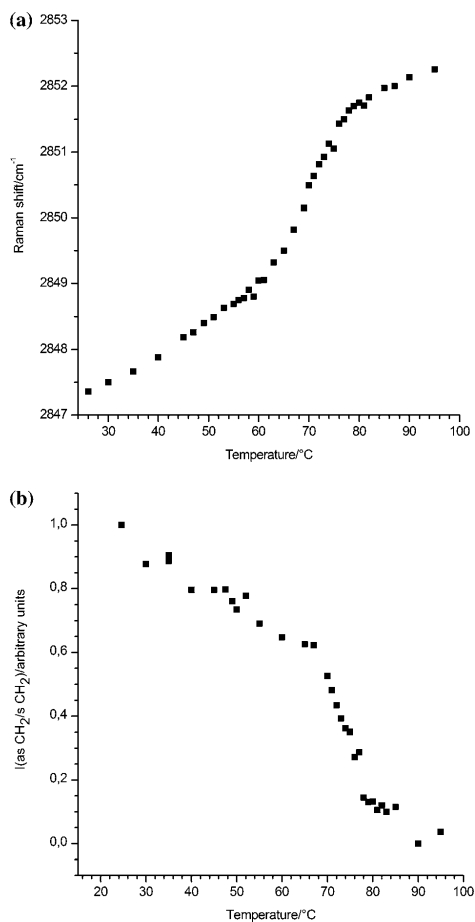


Fig. 5 (a) Temperature dependency of $\nu_{\text{s}}(\text{CH}_2)$. With increasing temperature the band position is shifted continuously to higher wavenumbers. (b) The intensity ratio $I(\nu_{\text{as}}(\text{CH}_2))/I(\nu_{\text{s}}(\text{CH}_2))$ displayed in dependency of temperature. Upon heating, the ratio decreases continuously. Beginning at about 70 °C, a drastic decrease of $I(\nu_{\text{as}}(\text{CH}_2))/I(\nu_{\text{s}}(\text{CH}_2))$ can be observed, with the tendency to reach a zero value at about 80 °C, which indicates the phase transition.

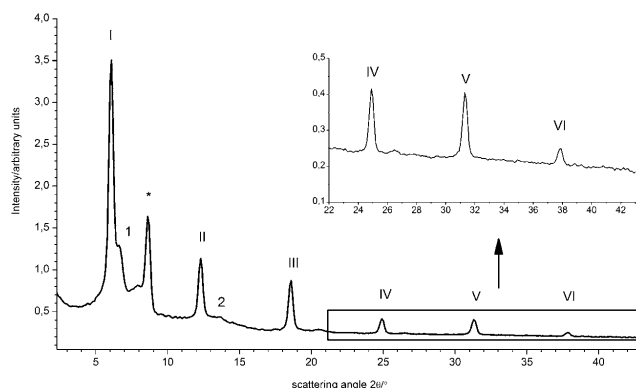


Fig. 6 Neutron diffraction pattern measured as $\theta - 2\theta$ scans of the membrane composed of CER[EOS]_{branched}/CER[AP]/BA/CHOL, 23/10/33/33 (m/m), at 32 °C and 57% rh. Plotted is the measured intensity against the scattering angle 2θ at 100% D₂O. Roman numerals indicate the first to sixth order of diffraction of the oriented model membrane. The asterisk represents the first diffraction order of crystalline CHOL; arabic numerals indicate the first and second diffraction orders of an additional phase. The inset shows the magnification of the fourth to sixth order diffraction peaks.

mode is sensitive to interchain interactions, changes in the lattice packing to be monitored. Clearly visible is the splitting of the CH₂ scissoring mode into a doublet (1439 cm⁻¹, 1459 cm⁻¹) at 24 °C (see Fig. 4a). This doublet was also observed in Raman studies of the native CER[EOS] as reported in ref. 57. As no factor group splitting with the presence of a triplet occurs, an orthorhombic subcell packing can be ruled out. The alkyl chains of CER[EOS]_{branched} must be packed in a hexagonal lattice.

The bands of asymmetric and symmetric CH₂ stretching modes (and $\nu_s(\text{CH}_2)$) are localised at 2882 cm⁻¹ and 2848 cm⁻¹, respectively. In general, the position of the $\nu_s(\text{CH}_2)$ band correlates with the state of the hydrocarbon chain order in the following way: the higher the wavenumber or Raman shift of the band position, the lower the order.⁵¹ As seen in Fig. 5a, the localisation of the $\nu_s(\text{CH}_2)$ band shows a distinct temperature dependency.

The low value of the $\nu_s(\text{CH}_2)$ of 2847 cm⁻¹ (24 °C) indicates a high number of *trans* conformers in the alkyl-chain region.^{59,60} During the heating process the state of the chain order decreases. Starting at about 2847 cm⁻¹ the band is stepwise shifted to higher wavenumbers as the temperature increases, with the final band position located at 2852 cm⁻¹ at 95 °C. A stronger shift can be observed between 65 and 80 °C. In that temperature range, the signal is moved by more than 2 cm⁻¹, indicating a significant loss in the chain order. At 82 °C, the band can be found at the position of 2852 cm⁻¹. The state of disorder is increased, as the chains are molten and possess motional freedom to a high extent at the phase transition temperature.

The intensity ratio $I(\nu_{as}(\text{CH}_2))/\nu_s(\text{CH}_2)$ is another important measure for the relative population of *trans* and *gauche* conformers.^{48,50,60} A decreasing intensity ratio $I(\nu_{as}(\text{CH}_2))/\nu_s(\text{CH}_2)$ can be taken as an increase of *gauche* conformers. As displayed in Fig. 5b, the relative content of *trans* conformers decreases in favour of the *gauche* population during heating, as $I(\nu_{as}(\text{CH}_2))/\nu_s(\text{CH}_2)$ is reduced continuously. Around the phase transition temperature at about 82 °C, this ratio goes towards zero. This is in line with the findings for the naturally occurring

CER[EOS] reported in ref. 57, where $I(\nu_{as}(\text{CH}_2))/\nu_s(\text{CH}_2)$ also decreased and tended to zero around the phase transition temperature.

Summarising, CER[EOS]_{branched} and CER[EOS] exhibit similar phase behaviour. At increased temperature, the relative population of *trans* conformers decreases while the state of the chain disorder is increased. One main phase transition temperature above 80 °C was determined. The reason for the comparable main phase transition temperature of CER[EOS] and CER[EOS]_{branched} is the methyl branch present in the ω -acyl chain of CER[EOS]_{branched} which prevents a closer chain packing and causes a distinct disorder in the terminal C6 moiety. A hexagonal subcell packing was found for CER[EOS]_{branched}.

3.4. Neutron diffraction experiments

Neutron diffraction was applied to elucidate the lipid bilayer architecture of oriented model membranes composed of CER[EOS]_{branched}/CER[AP]/BA/CHOL (23/10/33/33 m/m). The corresponding diffraction pattern is displayed in Fig. 6. For comparison reasons, the sample composition is closely related to the model matrix based on naturally occurring CER[EOS] already described by Schröter and co-workers.²⁷

The well-oriented lamellar system allowed for detection of up to six orders of diffraction associated with the model membrane. Only small amounts of CHOL crystallised into a separate domain indicated by a reflection at $2\theta = 8.71^\circ$.⁶¹ As often reported in the literature^{62,63} this will not affect a proper lamellar arrangement of the other membrane lipid components. Predominantly, a one-phase system was present, as only marginal reflections of a first and second diffraction order of another lamellar phase (termed “small phase” due to the very small intensity measured) were visible. Therefore, following results and their discussion refer to the evaluable main phase. Its lamellar repeat distance averages 48.19 ± 0.01 Å. The corresponding NSLD profiles $\rho_s(x)$ will be displayed on a relative scale

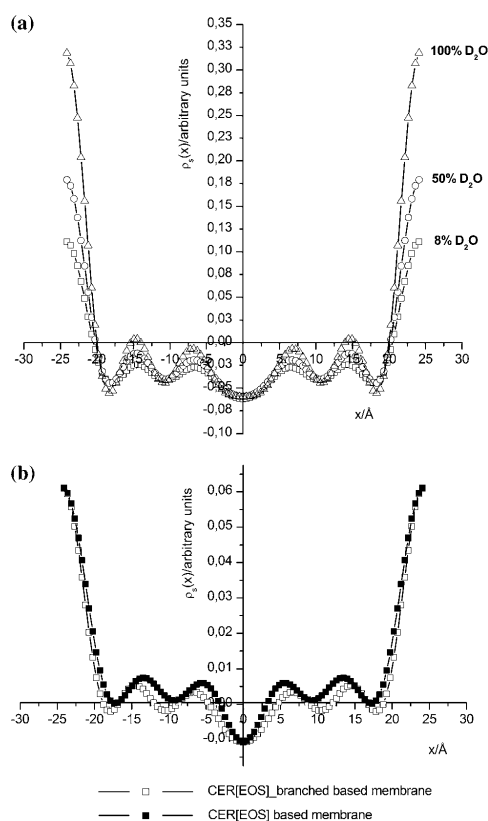


Fig. 7 (a) NSLD profiles for the sample composed of CER[EOS]_{branched}/CER[AP]/BA/CHOL measured at 32 °C and 57% rh. Shown are the profiles for D₂O contents of 100%, 50% and 8% in H₂O. (b) Comparison of the NSLD profiles for the oriented SC model membranes composed of CER[EOS]_{branched}/CER[AP]/BA/CHOL (23/10/33/33 m/m) and CER[EOS]/CER[AP]/BA/CHOL (23/10/33/33 m/m). The experimental conditions were the same for both samples (8% D₂O, *T* = 32 °C and 57% rh).

in arbitrary units. The reason for this is the generation of large errors when calculating an absolute scale due to the low amount of water molecules per lipid as described in detail before.²⁷ Fig. 7a illustrates the NSLD profiles $\rho_s(x)$ for the studied model membrane at different D₂O concentrations, revealing the following results:

(i) The outer edges are formed by two maxima representing a high density of atoms with a positive neutron scattering length. This region is formed by the SC lipid head groups. In agreement with the findings in ref. 14, 15 and 27, the intermembrane space is close to zero due to a very thin water layer, and the membrane thickness is nearly identical to the bilayer repeat distance d .¹⁵

(ii) The minimum in the centre of the profile ($x = 0$ Å) corresponds to the presence of a high density of atoms with

Table 4 The structure factors F_h for the model membrane CER[EOS]/CER[AP]/BA/CHOL (23/10/33/33 m/m) according to ref. 27 and normalisation to 1

Diffraction order h	F_h according to ref. 27	F_h norm
1	-6.656	-0.3301
2	3.764	0.1867
3	-4.692	-0.2328
4	2.227	0.1104
5	-2.825	-0.1401

Table 5 The structure factors F_h for the model membrane CER[EOS]_{branched}/CER[AP]/BA/CHOL (23/10/33/33 m/m) investigated in the present study and normalisation to 1

Diffraction order h	F_h	F_h norm
1	-0.827	-0.2993
2	0.462	0.1673
3	-0.587	-0.2125
4	0.2985	0.108
5	-0.3939	-0.1425
6	0.1517	0.0549

a negative neutron scattering length like hydrogen. The middle of the bilayer is therefore mainly formed by methyl and methylene groups.

In the literature, the presence of ω -acyl ceramides such as CER[EOS] is often regarded as a prerequisite for the formation of the LPP.^{12,13,64} Interestingly, despite the presence of an ω -acyl chain ceramide in the present model membrane, the SC lipids are arranged in a phase with a short periodicity of about 48 Å. This actual finding corroborates former results, where the long-chain CER[EOS] did not induce the formation of the long periodicity phase as long as CER[AP] is present.²⁷ For better comparison of the bilayer architecture for the two quaternary model membranes containing the different CER[EOS] species, it seemed likely to directly contrast the resulting NSLD profiles on one arbitrary scale which is possible due to the similar d -spacing of $d = 48.3 \pm 0.1$ Å found for the membrane comprising native CER[EOS]. For the simultaneous presentation shown in Fig. 7b, the sum of the structure factors F_h derived from ref. 27 as well as the present ones was normalised to 1 and thereby placed on the same relative scale. Results of the normalisation process are displayed in Table 4 and Table 5, respectively.

The following results can be taken from a comparison of the profiles:

(I) Obviously, the lipid arrangement found for both model systems is very similar: Especially in the head group region and in the middle of the bilayer no differences are detectable. The absence of larger differences is not surprising; the more so as the investigated model membranes do not differ substantially regarding their composition. CHOL, BA and CER[AP] are present in the same ratio as CER[EOS], which only varies in the character of the ω -acyl chain.

(II) The only noticeable deviation in both profiles can be found in the area between the bilayer centre and the head group region. In that interval, the $\rho_s(x)$ calculated for the sample containing CER[EOS]_{branched} exhibits a slightly more negative curve

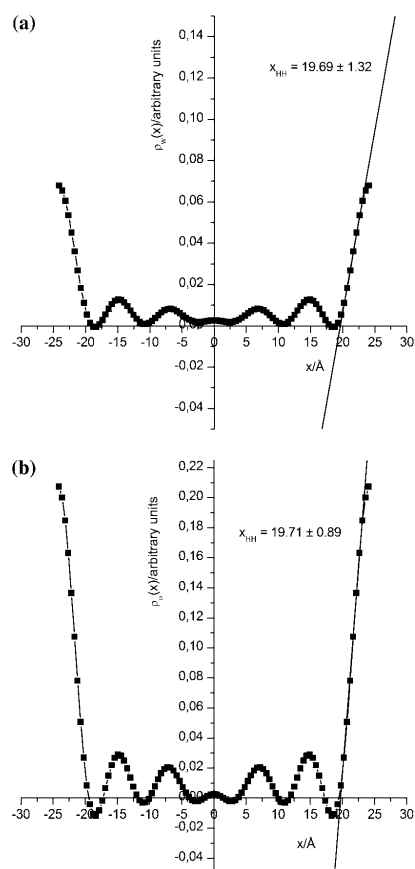


Fig. 8 Water density distribution function ρ_w across the membrane for the quaternary model membrane composed of CER[EOS]_{branched}/CER[AP]/BA/CHOL (23/10/33/33 m/m). (a) Difference profile of 50% D₂O and 8% D₂O. (b) Difference profile of 100% D₂O and 8% D₂O. The results of the linear fit procedure to determine the lipophilic and hydrophilic bilayer regions are added.

progression, while the NSLD profile received for the sample comprising CER[EOS] is slightly lifted towards positive values.

That fact may be explained by taking into account the lipid arrangement proposed for the sample CER[EOS]/CER[AP]/BA/CHOL.²⁷ No LPP is formed and the d -spacing of 48 Å is in the range of a theoretical bilayer formed by two opposing CER[AP] molecules. For a proper arrangement inside the short 48

Å-phase, the long-chain CER[EOS] is supposed to span its ω -acyl chain into the area between the head group region and the bilayer centre of the adjacent membrane. Consequently, the ω -methyl-branched palmitic acid chain of CER[EOS]_{branched} causes more hydrogen atoms to be present in that membrane region than the linoleic acid-containing native CER[EOS]. Hydrogen exhibits a negative neutron scattering length of -3.74 fm,⁶⁵ hence, the sample based on native CER[EOS] should exhibit a more positive neutron scattering length density in the discussed unit cell region while the presence of CER[EOS]_{branched} provokes a more negative value. Considering an average C–C bond length of about 1.5 Å⁶⁶ besides the detected bilayer d -spacing of 48 Å, the above discussed changes in the NSLD profiles should become apparent in the region of about ± 10 to ± 15 Å from the bilayer centre. In fact, the NSLD profiles displayed in Fig. 7b show the slight difference in the region from about ± 5 to ± 15 Å. Thus, the observed characteristics in the $\rho_w(x)$ could arise from the chemical variation present in the ω -acyl chain, as the membrane composition is equivalent.

Regarding the chemical structure of CER[EOS]_{branched} comprising a saturated instead of an unsaturated acyl chain, one could expect the artificial variety to create a stable, more rigid bilayer backbone or to enable the formation of an LPP, thereby exceeding the polar forces of CER[AP] proposed before.^{14,27} However, that assumption was not affirmed by the present results. Apparently, the C10 methyl branch of CER[EOS]_{branched} anticipates the formation of a rigid backbone as being probably needed for the formation of a long phase with 130 Å spacing. The disturbance caused by the methyl branched palmitic acid side chain is most likely comparable to the perturbation by the ω -linoleic acid chain, which results in formation of bilayers with a short periodicity d due to the protruding influence of CER[AP]. These findings are supported by the results received from the DSC measurements and Raman spectroscopy described above. The exchange of CER[EOS] against CER[EOS]_{branched} does not influence the lamellar lipid assembly in terms of enabling the formation of the LPP.

Former studies revealed that SC lipid model membranes exhibit a diminutive intermembrane hydration. The NSLD profiles of the CER[EOS]_{branched} based membrane investigated here show a clear increase of intensity in the head group region at high D₂O content (see Fig. 7a) being proportional to the water density distribution function across the bilayer which indicates that at least some water penetrates into the head group region. To elucidate the bilayer hydration properties, the water distribution function ρ_w across the unit cell was calculated according to ref. 15 and 27 using eqn (4a) or (b):

$$\rho_{w1} = \rho_{100\%D_2O} - \rho_{8\%D_2O} \quad (4a)$$

$$\rho_{w2} = \rho_{50\%D_2O} - \rho_{8\%D_2O} \quad (4b)$$

Table 6 The membrane parameters for the quaternary model membrane based on CER[EOS]_{branched} (derived by eqn 4b)

$d/\text{Å}$	Position of polar head group/Å	$x_{HH}/\text{Å}$	Thickness hydrophobic region/Å	Thickness hydrophilic region/Å
48, 19 ± 0.01	24.1	19.69 ± 1.32	39.4 ± 2.64	4.47 ± 1.32

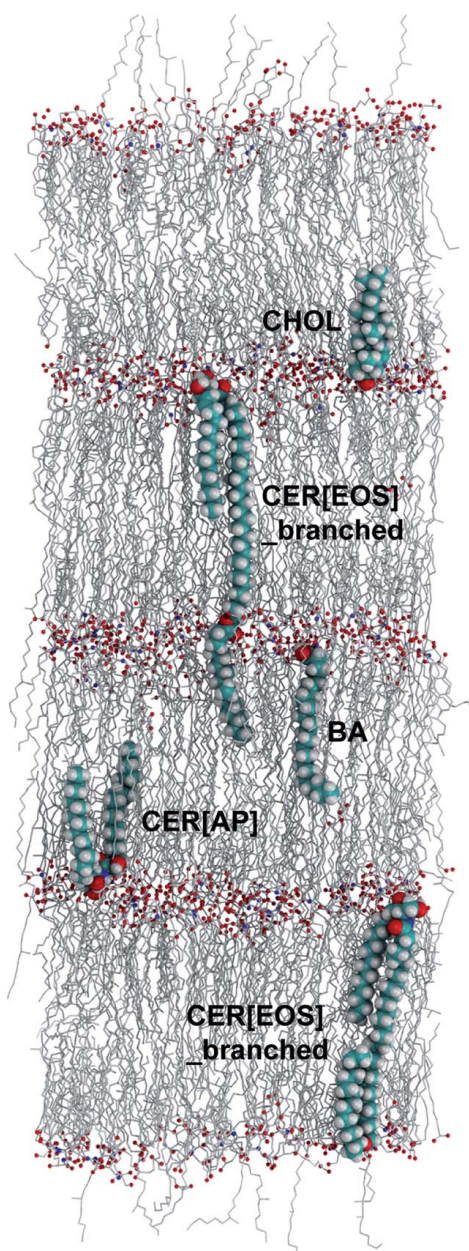


Fig. 9 Snapshot from the end of the MD simulation at 517 ns conducted at 32 °C consisting of CER[EOS]_branched/CER[AP]/BA/CHOL (23/10/33/33 m/m) and H₂O. Heavy atoms of all molecules are shown and color coded (carbons: white, oxygens: red, nitrogens: blue). Representative structures of each molecule species have been selected and are shown in

The results are presented in Fig. 8. As described in ref. 67, the neutron scattering density of water has a zero value at 8% D₂O (v/v) which means that the contribution to the overall NSLD at that D₂O/H₂O ratio derives only from the lipid membrane components, not from any intermembrane water. Consequently, eqn (4a) or (b) can be used to estimate ρ_w . Generally, one can divide the lipid bilayer into a hydrophilic and a hydrophobic part separated by the hydrophilic–hydrophobic boundary x_{HH} . Since only the hydrophilic membrane region is accessible for H₂O/D₂O, x_{HH} should be located at point x , where the water density distribution function ρ_w reaches zero. A linear fit as shown in Fig. 8a and b revealed x_{HH} to be located at $x_{HH} = 19.7$ Å. As eqn (4a) and (b) led to similar values for x_{HH} , the suitability of the method could be proven. For the case of ρ_w , the membrane parameters x_{HH} , position of the polar head groups x_{PH} , thickness of the hydrophilic region as well as the thickness of the hydrophobic region are summarised in Table 6. The bilayer repeat distance d corresponds to the distance between the two maxima. Consequently, the position of the polar head groups is defined as $x_{PH} = d/2$ for our centrosymmetric bilayer. Comparing CER[EOS] and CER[EOS]_branched, similar membrane parameters were detected. Small differences are noticeable for the thickness of the hydrophilic domain, which is slightly reduced in the case of the CER[EOS]_branched based membrane studied here. However, this could be due to the limited space resolution of the diffraction experiment. According to ref. 15, the space resolution $\Delta(x)$ of the Fourier synthesis can be calculated as $0.6 \cdot d/h_m$, where d is the repeat distance and h_m is the number of recorded diffraction peaks. For the present neutron diffraction experiment, 4.8 Å is the calculated space resolution of the Fourier synthesis. This means that only structures (e.g. head groups) separated by more than 4.8 Å can be resolved.

Summarising, one can state that the bilayer assembly of the quaternary lipid model membranes based on either CER[EOS] or CER[EOS]_branched was shown to be comparable. The alteration present in the ω -acyl moiety of CER[EOS]_branched does not induce the formation of the LPP under the chosen conditions.

3.5. Molecular dynamics simulation of the lamellar arrangement of the model membrane

To assess if the proposed model of the ceramide membrane is realistic we performed an all-atom MD simulation. We built four individual bilayers in which both monolayers are symmetric and where the long chain of the CER[EOS]_branched spans the whole membrane with the methyl-branched ω -palmitoyl chain embedded in the next membrane, while CER[AP] was built in a hairpin conformation. A snapshot from the end of this 517 ns simulation is shown in Fig. 9.

a VdW representation with hydrogens present where the color code was changed for better visibility (hydrogens: white, carbons: cyan, oxygens: red, nitrogens: blue). In addition a rare conformation of CER[EOS]_branched where the branched ω -palmitic acid chain is not inserted into the neighboring membrane but folds back onto the molecule is shown in the bottom with the same color code. The figure was prepared with VMD.⁷²

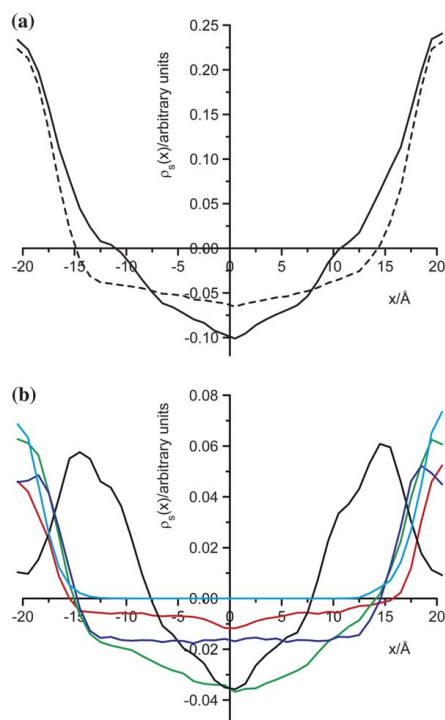


Fig. 10 NSLD profiles calculated from the last 300 ns of the MD simulation of the quaternary membrane based on CER[EOS]_branched with H₂O (considered as D₂O for calculation of the profiles) at 32 °C. (a) Profiles for all molecules (solid line) and all molecules except CHOL (dashed line) are compared where the latter shows a good qualitative agreement with the experimental profile. (b) Profiles for the individual molecule species (CER[EOS]_branched: dark blue, CER[AP]: red, BA: green, CHOL: black, D₂O: cyan) were also compared and show that the observed difference between the experimental profile and the one for all molecules is in fact due to the overrepresentation of CHOL.

During the whole simulation this topology stayed intact even when the temperature was raised to 90 °C for annealing indicating that the proposed model is intrinsically stable. The acyl chains of the molecules only show few gauche-defects as expected and CER[EOS]_branched as well as CER[AP] remained in their starting topology. In Fig. 9, individual molecules with representative structures are highlighted also showing one of only two CER[EOS]_branched that deviated from their starting topology and inserted the branched ω -acyl chain into the same membrane by folding back to the upper part of the chain above the carboxylic acid ester group. However, at the beginning of the simulation the periodic cell quickly increased in the lateral dimensions while shrinking in the vertical dimension which is most likely due to an overrepresentation of CHOL which is sequestered as seen from the experiments. This explanation might seem curious at first since CHOL is best known to increase

the order and thereby the acyl chain length in phospholipids.⁶⁸ However, it has actually been shown that it decreases the order and thereby the acyl chain length of phospholipid membranes below the main phase transition temperature where they are highly ordered and therefore much more similar to the investigated ceramide membranes.⁶⁹ This arises from the structure of CHOL which is a very rigid and also a comparatively short molecule and therefore cannot adapt to the longer chains of the surrounding CER and FFA and rather induces a shortening of these chains leading to the observed changes in the cell dimensions.

The excess of CHOL also has implications for the NSLD profiles that were calculated for the last 300 ns of the simulation. First of all the d -spacing at the end of the simulation is close to 40 Å which is a direct result of the shrinking of the periodic cell. The total profile is shown in Fig. 10a and deviates considerably from the experimental one. To further analyse this difference we calculated NSLD profiles for each individual molecule species which are shown in Fig. 10b. As can be seen the profiles for both CER[AP] and CER[EOS] and for BA are close to the experimental profile while the one for CHOL is leading to the observed differences. Therefore, we calculated the NSLD profile for all components but CHOL (shown in Fig. 10a) and got a good qualitative agreement with the experimental profile except for the smaller d -spacing due to the effect of CHOL on the other membrane constituents.

4. Conclusions

The present study addressed the issue of synthesis of an artificial CER[EOS] species and characterisation of its temperature-dependent phase behaviour in comparison to the naturally occurring CER[EOS]. Furthermore, the internal bilayer architecture of an oriented SC lipid model membrane containing the synthetic ceramide was elucidated and subsequently compared to a quaternary model membrane of equal composition, but containing the native CER[EOS] species. Although there is published data regarding the importance of the presence of an appropriate CER mixture besides FFA for the formation of the long periodicity phase (LPP),^{70,71} its existence is debated controversially and could not be corroborated by the present study. Moreover, the actual findings support former results regarding the protruding influence of CER[AP], as a short 48 Å-phase instead of the LPP was observed. In contrast, X-ray powder diffraction studies revealed pure CER[EOS] to be assembled in a long periodicity phase in excess water.⁵⁷

Furthermore, the new CER[EOS]_branched was shown to serve as an appropriate substitute for native CER[EOS] in terms of formation of well-ordered lipid bilayers with a lipid arrangement equivalent to the model matrix comprising the naturally occurring CER[EOS].²⁷ Since both CER species exhibit comparable thermotropic phase behaviour, research projects dealing with the structural investigation of SC lipid bilayers like the present work could benefit from easy availability, *e.g.* from own chemical synthesis, and improved storage stability with decreased oxidative sensitivity offered by CER[EOS]_branched. Our study underlines the importance of the neutron diffraction technique combined with MD simulation for the purpose of studying simplistic SC lipid model membranes on a nanoscale as

it allows for analysing the influence of particular lipid species on the lamellar assembly.

Acknowledgements

The authors would like to thank Evonik Goldschmidt GmbH (Essen, Germany) for the gift of CER[EOS] and CER[AP], and M. Jung for performing the mass spectrometric measurements. Tanja Engelbrecht would like to thank the Graduiertenförderung des Landes Sachsen-Anhalt for funding. Granting of beamtime and financial assistance by Helmholtz-Zentrum-Berlin (HZB, Berlin, Germany) is gratefully acknowledged. NAMD was developed by the Theoretical and Computational Biophysics Group in the Beckman Institute for Advanced Science and Technology at the University of Illinois at Urbana-Champaign.

References

- 1 P. M. Elias and D. S. Friend, *J. Cell Biol.*, 1975, **65**, 180–191.
- 2 P. W. Wertz and B. van den Bergh, *Chem. Phys. Lipids*, 1998, **91**, 85–96.
- 3 P. M. Elias, *J. Invest. Dermatol.*, 1983, **80**(Suppl.), 44s–49s.
- 4 P. M. Elias, J. Goerke and D. S. Friend, *J. Invest. Dermatol.*, 1977, **69**, 535–546.
- 5 P. M. Elias, N. S. McNutt and D. S. Friend, *Anat. Rec.*, 1977, **189**, 577–593.
- 6 G. M. Gray and H. J. Yardley, *J. Lipid Res.*, 1975, **16**, 434–440.
- 7 Y. Mizutani, S. Mitsutake, K. Tsuji, A. Kihara and Y. Igarashi, *Biochimie*, 2009, **91**, 784–790.
- 8 K. C. Madison, D. C. Schwartzendruber, P. W. Wertz and D. T. Downing, *Invest. Dermatol.*, 1987, **88**, 714–718.
- 9 J. A. Bouwstra, G. S. Gooris, J. A. van der Spek and W. Bras, *J. Invest. Dermatol.*, 1991, **97**, 1005–1012.
- 10 J. A. Bouwstra, F. E. R. Dubbelaar, G. S. Gooris and M. Ponc, *Acta Derm.-Venereol.*, 2000, 23–30.
- 11 L. Norlén, I. Nicander, B. L. Rozell, S. Ollmar and B. Forslind, *J. Invest. Dermatol.*, 1999, **112**, 72–77.
- 12 M. W. de Jager, G. S. Gooris, I. P. Dolbnya, W. Bras, M. Ponc and J. A. Bouwstra, *J. Lipid Res.*, 2004, **45**, 923–932.
- 13 M. W. de Jager, G. S. Gooris, M. Ponc and J. A. Bouwstra, *J. Lipid Res.*, 2005, **46**, 2649–2656.
- 14 D. Kessner, M. Kiselev, S. Dante, T. Hauss, P. Lersch, S. Wartewig and R. H. Neubert, *Eur. Biophys. J.*, 2008, **37**, 989–999.
- 15 M. A. Kiselev, N. Y. Ryabova, A. M. Balagurov, S. Dante, T. Hauss, J. Zbytovská, S. Wartewig and R. H. H. Neubert, *Eur. Biophys. J.*, 2005, **34**, 1030–1040.
- 16 E. Corbe, C. Laugel, N. Yagoubi and A. Baillet, *Chem. Phys. Lipids*, 2007, **146**, 67–75.
- 17 M. A. Kiselev, *Crystallogr. Rep.*, 2007, **52**, 525–528.
- 18 A. Schroeter, M. A. Kiselev, T. Hauss, S. Dante and R. H. H. Neubert, *Biochim. Biophys. Acta, Biomembr.*, 2009, **1788**, 2194–2203.
- 19 D. Kessner, M. A. Kiselev, T. Hauss, S. Dante, S. Wartewig and R. H. Neubert, *Eur. Biophys. J.*, 2008, **37**, 1051–1057.
- 20 S. Motta, M. Monti, S. Sesana, R. Caputo, S. Carelli and R. Ghidoni, *Biochim. Biophys. Acta, Gen. Subj.*, 1993, **1182**, 147–151.
- 21 L. Coderch, O. Lopez, A. de la Maza and J. L. Parra, *Am. J. Clin. Dermatol.*, 2003, **4**, 107–129.
- 22 G. Imokawa, S. Akasaki, M. Hattori and N. Yoshizuka, *J. Invest. Dermatol.*, 1986, **87**, 758–761.
- 23 M. Philippe, J. C. Garson, P. Gilard, M. Hocquaux, G. Hussler, F. Leroy, C. Mahieu, D. Semeria and G. Vanlerberghe, *Int. J. Cosmet. Sci.*, 1995, **17**, 133–146.
- 24 K. De Paep, D. Roseeuw and V. Rogiers, *J. Eur. Acad. Dermatol. Venereol.*, 2002, **16**, 587–594.
- 25 G. Imokawa, Y. Yada, K. Higuchi, M. Okuda, Y. Ohashi and A. Kawamata, *J. Clin. Invest.*, 1994, **94**, 89–96.
- 26 M. Seul and M. J. Sammon, *Thin Solid Films*, 1990, **185**, 287–305.
- 27 A. Schröter, D. Kessner, M. A. Kiselev, T. Hauss, S. Dante and R. H. H. Neubert, *Biophys. J.*, 2009, **97**, 1104–1114.
- 28 J. F. Nagle and S. Tristram-Nagle, *Biochim. Biophys. Acta*, 2000, **1469**, 159–195.
- 29 M. C. Wiener and S. H. White, *Biophys. J.*, 1991, **59**, 162–173.
- 30 N. P. Franks and W. R. Lieb, *J. Mol. Biol.*, 1979, **133**, 469–500.
- 31 D. L. Worcester and N. P. Franks, *J. Mol. Biol.*, 1976, **100**, 359–378.
- 32 D. M. Small, D. J. Cabral, D. P. Cistola, J. S. Parks and J. A. Hamilton, *Hepatology*, 1984, **4**, 77S–79S.
- 33 J. R. Kanicky and D. O. Shah, *J. Colloid Interface Sci.*, 2002, **256**, 201–207.
- 34 M. T. Hyvönen and P. T. Kovanen, *J. Phys. Chem. B*, 2003, **107**, 9102–9108.
- 35 J. B. Klauda, B. R. Brooks, A. D. MacKerell, R. M. Venable and R. W. Pastor, *J. Phys. Chem. B*, 2005, **109**, 5300–5311.
- 36 B. R. Brooks, R. E. Bruccoleri, B. D. Olafson, D. J. States, S. Swaminathan and M. Karplus, *J. Comput. Chem.*, 1983, **4**, 187–217.
- 37 J. C. Phillips, R. Braun, W. Wang, J. Gumbart, E. Tajkhorshid, E. Villa, C. Chipot, R. D. Skeel, L. Kale and K. Schulten, *J. Comput. Chem.*, 2005, **26**, 1781–1802.
- 38 U. Essmann, L. Perera, M. L. Berkowitz, T. Darden, H. Lee and L. G. Pedersen, *J. Chem. Phys.*, 1995, **103**, 8577–8593.
- 39 W. F. van Gunsteren and H. J. C. Berendsen, *Mol. Phys.*, 1977, **34**, 1311–1327.
- 40 B. Dobner, B. Elsner and P. Nuhn, *Pharmazie*, 1989, **44**, 758–760.
- 41 S. Drescher, A. Meister, A. Blume, G. Karlsson, M. Almgren and B. Dobner, *Chem.–Eur. J.*, 2007, **13**, 5300–5307.
- 42 D. F. Jones, *J. Chem. Soc. C*, 1968, 2809–2815.
- 43 B. Belleau and G. Malek, *J. Am. Chem. Soc.*, 1968, **90**, 1651–1652.
- 44 S. Müller and R. R. Schmidt, *J. Prakt. Chem.*, 2000, **342**, 779–784.
- 45 J. M. Holopainen, J. Lemmich, F. Richter, O. G. Mouritsen, G. Rapp and P. K. J. Kinnunen, *Biophys. J.*, 2000, **78**, 2459–2469.
- 46 S. G. Black and G. S. Dixon, *Biochemistry*, 1981, **20**, 6740–6744.
- 47 P. Garidel, *Phys. Chem. Chem. Phys.*, 2006, **8**, 2265–2275.
- 48 A. Tfyli, E. Guillard, M. Manfait and A. Baillet-Guffroy, *Anal. Bioanal. Chem.*, 2010, **397**, 1281–1296.
- 49 M. Wegener, R. Neubert, W. Rettig and S. Wartewig, *Chem. Phys. Lipids*, 1997, **88**, 73–82.
- 50 M. Wegener, R. Neubert, W. Rettig and S. Wartewig, *Int. J. Pharm.*, 1996, **128**, 203–213.
- 51 S. Raudenkolb, S. Wartewig and R. H. H. Neubert, *Chem. Phys. Lipids*, 2003, **124**, 89–101.
- 52 R. G. Snyder, S. L. Hsu and S. Krimm, *Spectrochim. Acta, Part A*, 1978, **34**, 395–406.
- 53 R. G. Snyder and J. R. Scherer, *J. Chem. Phys.*, 1979, **71**, 3221–3228.
- 54 R. Mendelsohn and D. J. Moore, *Chem. Phys. Lipids*, 1998, **96**, 141–157.
- 55 R. Neubert, W. Rettig, S. Wartewig, M. Wegener and A. Wienhold, *Chem. Phys. Lipids*, 1997, **89**, 3–14.
- 56 K. G. Brown, E. Bicknellbrown and M. Ladjadj, *J. Phys. Chem.*, 1987, **91**, 3436–3442.
- 57 D. Kessner, G. Brezesinski, S. S. Funari, B. Dobner and R. H. H. Neubert, *Chem. Phys. Lipids*, 2010, **163**, 42–50.
- 58 R. G. Snyder, G. L. Liang, H. L. Strauss and R. Mendelsohn, *Biophys. J.*, 1996, **71**, 3186–3198.
- 59 R. A. Macphail, H. L. Strauss, R. G. Snyder and C. A. Elliger, *J. Phys. Chem.*, 1984, **88**, 334–341.
- 60 R. W. Wang, J. Guo, G. Baran and S. L. Wunder, *Langmuir*, 2000, **16**, 568–576.
- 61 H. S. Shieh, L. G. Hoard and C. E. Nordman, *Nature*, 1977, **267**, 287–289.
- 62 M. R. Brzustowicz, V. Cherezov, M. Caffrey, W. Stillwell and S. R. Wassall, *Biophys. J.*, 2002, **82**, 285–298.
- 63 J. Y. Huang, J. T. Buboltz and G. W. Feigenson, *Biochim. Biophys. Acta, Biomembr.*, 1999, **1417**, 89–100.
- 64 J. A. Bouwstra, G. S. Gooris, F. E. R. Dubbelaar, A. M. Weerheim, A. P. Ijzerman and M. Ponc, *J. Lipid Res.*, 1998, **39**, 186–196.
- 65 V. F. Sears, *Neutron News*, 1992, **3**, 26–37.
- 66 F. H. Allen, O. Kennard, D. G. Watson, L. Brammer, A. G. Orpen and R. Taylor, *J. Chem. Soc., Perkin Trans. 2*, 1987, S1–S19.
- 67 G. Zaccari, in *Structure and Dynamics of Biomolecules—Neutron and Synchrotron Radiation for Condensed Matter Studies*, ed. E. Fanchon, E. Geissler, J.-L. Hodeau, J.-R. Regnard and P. A. Timmins, Oxford University Press, 2000, vol. IV, pp. 238–250.
- 68 G. V. Martinez, E. M. Dykstra, S. Lope-Piedrafita and M. F. Brown, *Langmuir*, 2004, **20**, 1043–1046.

[View Online](#)

- 69 H. A. Scheidt, D. Huster and K. Gawrisch, *Biophys. J.*, 2005, **89**, 2504–2512.
- 70 M. W. de Jager, G. S. Gooris, I. P. Dolbnya, W. Bras, M. Ponce and J. A. Bouwstra, *Chem. Phys. Lipids*, 2003, **124**, 123–134.
- 71 M. W. de Jager, G. S. Gooris, I. P. Dolbnya, M. Ponce and J. A. Bouwstra, *Biochim. Biophys. Acta, Biomembr.*, 2004, **1684**, 132–140.
- 72 W. Humphrey, A. Dalke and K. Schulten, *J. Mol. Graphics*, 1996, **14**, 33–38.

Downloaded by Martin-Luther-Universität on 16 April 2012
Published on 09 August 2011 on <http://pubs.rsc.org> | doi:10.1039/C1SM05134B

3.2 Lipophilic penetration enhancers: Their impact on the SC lipid bilayer architecture and modes of action

While the maintenance and strengthening of the skin barrier is essential in the treatment of unphysiological states of skin, e. g. atopic dermatitis, a temporary impairment may be desirable to achieve sufficiently high levels of actives applied for dermal or transdermal effects in the treatment of skin diseases. The exact mode of action of penetration enhancers on a molecular scale is still to be elucidated. For that reason, two representative lipophilic penetration promoters, oleic acid and isopropyl myristate were chosen as model substances. Their influence on the bilayer organization of quaternary oriented SC lipid model membranes were studied by means of neutron diffraction. By applying the selectively deuterium-labelled species oleic acid-9,10- d_2 and isopropyl myristate-14,14,14- d_3 , valuable insights regarding the arrangement of the penetration enhancers in the model bilayers and the mode of enhancer activity on a nano-scale were provided.

3.2.1 Structure of SC lipid model bilayers in presence of oleic acid (Manuscript: Biophysica et Biochimica Acta – Biomembranes)

Engelbrecht TN, Schroeter A, Hauß T, Neubert RH: **Lipophilic penetration enhancers and their impact to the bilayer structure of stratum corneum lipid model membranes: neutron diffraction studies based on the example oleic acid.** *Biochimica et Biophysica Acta, Biomembranes* 2001; 1808: 2798-2806
(DOI: 10.1016/j.bbamem.2011.08.012)

Available online:

<http://www.sciencedirect.com/science/article/pii/S0005273611002732>



Lipophilic penetration enhancers and their impact to the bilayer structure of stratum corneum lipid model membranes: Neutron diffraction studies based on the example *Oleic Acid*

Tanja N. Engelbrecht^a, Annett Schroeter^{a,*}, Thomas Hauß^b, Reinhard H.H. Neubert^a

^a Institute of Pharmacy, Martin Luther University, Wolfgang-Langenbeck-Straße 4, 06120 Halle, Germany

^b Institute Soft Matter and Functional Materials, Helmholtz-Zentrum-Berlin, Hahn-Meitner-Platz 1, 14109 Berlin, Germany

ARTICLE INFO

Article history:

Received 23 May 2011
Received in revised form 29 July 2011
Accepted 9 August 2011
Available online 18 August 2011

Keywords:

Stratum corneum
Ceramide
Penetration enhancer
Neutron diffraction
Lipid model membrane

ABSTRACT

The present study analyzes the effect of the lipophilic penetration enhancer oleic acid on the bilayer structure of stratum corneum (SC) lipid model membranes based on Ceramide AP by using the neutron diffraction technique. Our results indicate the formation of a single lamellar phase in the presence of oleic acid under the chosen experimental conditions; a separated fluid-like oleic acid-rich phase was not detected in the present study. By comparing the internal membrane structure received from Fourier synthesis with the model system lacking oleic acid, considerable structural changes in terms of impairment of the lamellar order were found after incorporation of the penetration enhancer into the bilayers. In addition, by using specifically deuterated oleic acid we were able to prove the integration of the enhancer molecules into the model bilayers and moreover, to determine the exact position of oleic acid inside the SC lipid model membrane. From the present results we conclude a strong perturbation of lamellar SC lipid arrangement due to the intercalated penetration enhancer which can account for the promoting effects on drug penetration across the SC known for oleic acid.
© 2011 Elsevier B.V. All rights reserved.

1. Introduction

The outermost layer of the skin, the horny layer or stratum corneum (SC) exhibits a unique morphology. It consists of dead flattened cells (corneocytes) enriched with the structural protein keratin which are embedded into a complex intercellular lipid matrix [1]. The latter forms continuous sheets of multiple bilayer stacks made up of free fatty acids (FFA), cholesterol (CHOL) with its derivatives like cholesterol sulfate (ChS), and ceramides (CER) which are classified into 11 subclasses [2–5]. Later it was found that these mortar-like continuous lipid layers constitute the main penetration barrier of the skin [6], whereby the ceramides and the structural arrangement of the lipid bilayers play a key role for the barrier properties and limitation of the water transport [7,8]. Therefore, it is of utmost importance to understand the barrier function of the skin on a molecular level, to learn more about the impact of certain SC lipid subclasses on the lamellar architecture, to study possibilities to influence or moreover improve the barrier characteristics of the SC as well as to modify its properties in terms of penetration enhancement.

Abbreviations: SC, stratum corneum; CER, ceramide; OA, oleic acid; OA-D2, oleic acid-9,10-D2; CER[AP], N-(α -hydroxyoctadecanoyl)-phytosphingosine; FFA, free fatty acid; PA, palmitic acid; CHOL, cholesterol; ChS, cholesterol sulfate; SLD, scattering length density; RH, relative humidity

* Corresponding author at: Martin Luther University Halle-Wittenberg, Institute of Pharmacy, Department of Biopharmacy, Wolfgang-Langenbeck-Straße 4, 06120 Halle (Saale), Germany. Tel.: +49 345 5525025; fax: +49 345 5527292.

E-mail address: annett.schroeter@pharmazie.uni-halle.de (A. Schroeter).

0005-2736/\$ – see front matter © 2011 Elsevier B.V. All rights reserved.
doi:10.1016/j.bbamem.2011.08.012

While early electron microscopy studies of skin morphology focused on excised human skin [9,10], scattering techniques like X-ray scattering were employed later to investigate the lamellar structure of lipid mixtures made up of synthetically derived SC lipids [11]. The use of such synthetic SC lipids with well-defined head group architecture and defined hydrocarbon chain length was found to be more appropriate and can overcome problems like the poor availability of human skin with ethical requirements involved, and the distinct compositional variations of SC lipids (overall lipid content and profile) in different individuals. In recent years, the benefit offered by more simplified systems composed of synthetic SC lipids instead of complex mixtures was proven to be more adequate in numerous works [12,13]. The application of the neutron diffraction technique allowed to elucidate the lamellar assembly of a quaternary model membrane based on CER[AP], CHOL, palmitic acid (PA) and ChS, mass ratio 55/25/15/5. The results emphasized the outstanding role of the short chain and very polar phytosphingosine-based CER[AP] for the formation of a stable bilayer backbone which is summarized in the “armature reinforcement model” [14]. Furthermore, the possibility offered by neutrons to apply specific deuterium labeling in order to exactly localize certain membrane components was highlighted in numerous works [12,15–17].

In some cases, e.g. for the purpose of dermal or transdermal drug administration, the physiological skin barrier properties are prejudicial to the success of drug penetration either into deeper skin layers or through the skin into the systemic circulation. Hence, mechanisms to at least temporarily impair the barrier properties are necessary and have

been reviewed in [18]. Besides physical techniques developed in order to overcome the skin barrier, particularly chemical penetration enhancement by substances denoted as *penetration enhancers* has been studied extensively [19,20]. A plurality of substances from different substance classes exists, known to promote the penetration of different drugs into and through the skin, as e.g. shown for acyclovir [21] and estradiol [22]. However, the exact mechanism of the action of penetration enhancers is not yet fully understood on a molecular scale. Among the numerous penetration enhancers, the monounsaturated *cis*-9-octadecenoic acid (oleic acid, OA) is a well-studied substance [23–25]. The results reported in [25] show a significantly increased penetration of piroxicam after skin treatment with OA. These observations were explained by direct perturbing effects of OA on the SC lipids which also became apparent in decreased phase transition temperatures as well as lowered transition enthalpies revealed by differential scanning calorimetry (DSC) measurements. Another DSC study [26] on 5-fluorouracil (5-FU) permeation through excised skin likewise suggests an OA-induced disruption of skin lipid packing to account for the promotion of drug penetration. Furthermore, the formation of phase-separated fluid domains due to the presence of OA was assumed to strongly contribute to the enhancing effects [25], which was later underlined by other results derived from e.g. ATR-IR studies on human skin [27], ^2H NMR spectroscopy on multilamellar SC lipid dispersions [28] or thermal analysis and freeze fracture electron microscopy on isolated human SC [29]. Finally, a vesicular model system based on the lipid components CER[AP], CHOL, PA and ChS was complemented by OA and subsequently investigated by means of small angle X-ray scattering [30], whereby the induction of phase separation by OA reported before could be corroborated.

Probably due to its particular chemical structure, OA exhibits a distinct perturbing effect on the intercellular lipid layers of the SC. The findings of Separovic and Gawrisch regarding the impairment of lipid chain order upon introduction of unsaturation [31] suggested that the double bond significantly affects the molecular shape of the lipid alkyl chains, and consequently the whole bilayer arrangement. Increase of chain disorder was accompanied by increase of area per lipid molecule [32]. Later it was shown for phospholipid (PL) bilayers that the greatest lamellar-disturbing effect was mediated by unsaturated FFA species featuring *cis* double bonds like OA [33], and that OA was capable of increasing fluidity of the acyl chain region in the PL lamellae. Funari and co-workers considered the molecular shape of OA equaling a boomerang to account for the perturbing effects on the membrane structure [34]. Further molecular dynamics simulations revealed such a *cis* double bond to introduce a skew state to the single bonds surrounding the unsaturation, with parallel increase of *gauche* states of the bonds neighbored to the skew state bonds [35].

The objective of the present study was to analyze the impact of the penetration enhancer OA to the bilayer architecture of a SC lipid model membrane based on CER[AP], CHOL, PA and ChS. We refer to the already established quaternary system described before [14] and complemented it by adding an amount of 10% (mass ratio) of the monounsaturated fatty acid OA. Calculation of the neutron scattering length density profiles allowed for detailed insights into the membrane assembly in order to conclude the influence of OA. By furthermore applying the specifically deuterium-labeled species oleic acid-9,10-D2, we were able to evaluate the exact position of the penetration enhancer inside the model membrane.

2. Materials and methods

2.1. Materials

Ceramide CER[AP] (N-(α -hydroxyoctadecanoyl)-phytosphingosine) was kindly donated by Evonik Goldschmidt GmbH (Essen, Germany). The substance had a purity of $\geq 96\%$ and was used without any further purification. Cholesterol (CHOL), palmitic acid (PA), cholesterol sulfate

(ChS), and the penetration enhancer OA (*cis*-9-octadecenoic acid) were purchased from Sigma Aldrich GmbH (Taufkirchen, Germany), while the specifically deuterated variety (oleic acid-9,10-D2, later referred to as OA-D2) was purchased from Larodan Fine Chemicals (Malmö, Sweden). All substances were used as received. Quartz slides (Spectrosil 2000, $25 \times 65 \times 0.3 \text{ mm}^3$) for the neutron diffraction experiments were purchased from Saint-Gobain (Wiesbaden, Germany). For deposition of the lipids onto the quartz surface, an airbrush instrument (Harder & Steenbeck, Norderstedt, Germany) was used.

2.2. Sample preparation

Planar multilamellar model membranes were prepared according to the method described earlier [36]. Briefly, each lipid species was dissolved in chloroform/methanol (2:1 v/v) and subsequently mixed with the other components in the amount needed to yield sample compositions according to Table 1. The chemical structures of all synthetic SC lipids used for sample preparation are depicted in Fig. 1. Then, a volume of 1.2 ml of the final lipid mixture equalling a total lipid amount of 12 mg was spread over the quartz glass surface by means of an airbrush device. The solvent was allowed to evaporate at room temperature under atmospheric pressure, before the samples were kept under vacuum for 12 h.

After complete removal of solvent, the samples were subjected to alternating heating and cooling cycles under water-saturated atmosphere for the purpose of decreasing the mosaicity of the sample. The necessity of that so-called *annealing* procedure was described in detail before [17]. Furthermore, prior to the measurements the membranes were treated with a buffer solution of pH 9.5, whereby hydration of the membranes was facilitated. Such a procedure resulted in an enhanced lamellar orientation of the SC lipids present in the membrane as exemplary shown in Fig. 2A and B. Here, rocking scans around the first order Bragg peak of the multilamellar sample *Basic_OA* were recorded before (Fig. 2A) and after the buffer treatment was applied (Fig. 2B). Clearly visible is the strong increase in peak intensity and decrease of the broadness of the peak, together with a highly improved signal-to-noise (*s/n*) ratio due to the buffer treatment, indicating that a larger fraction of SC lipids is now oriented in bilayers parallel to the quartz surface. Such an arrangement is essential for further evaluation of the neutron diffraction data as described in the following Section 2.3.

2.3. Neutron diffraction experiment

Neutron diffraction experiments were performed at the V1 membrane diffractometer situated at the cold source of BER II research reactor of the Helmholtz-Zentrum Berlin (HZB, Berlin, Germany). A pyrolytic graphite monochromator was used to adjust the neutron wave length to $\lambda = 5.23 \text{ \AA}$ which was used for our experiment. For recording the scattered neutron intensity, a two-dimensional position-sensitive detector (^3He , $20 \times 20 \text{ cm}^2$ in area, $1.5 \times 1.5 \text{ mm}^2$ spatial resolution) was used. Diffraction data were collected as $\theta - 2\theta$ scans from $2\theta = 0^\circ$ to 45° at a sample to detector distance of 102.38 cm. To check the lamellar orientation and sample quality, test rocking scans were performed prior to the measurement itself. For equilibration and subsequent measurements, the samples were mounted in portable and lockable aluminum chambers where they were kept at fixed temperature (T) and relative humidity (RH).

Table 1
Composition of the investigated multilamellar samples.

SC lipid model system, components	Designation	Ratio (m/m)
1. CER[AP]/CHOL/PA/ChS	Basic	55/25/15/5
2. CER[AP]/CHOL/PA/ChS/OA	Basic_OA	49.5/22.5/13.5/4.5/10
3. CER[AP]/CHOL/PA/ChS/OA-D2	Basic_OA-D2	49.5/22.5/13.5/4.5/10

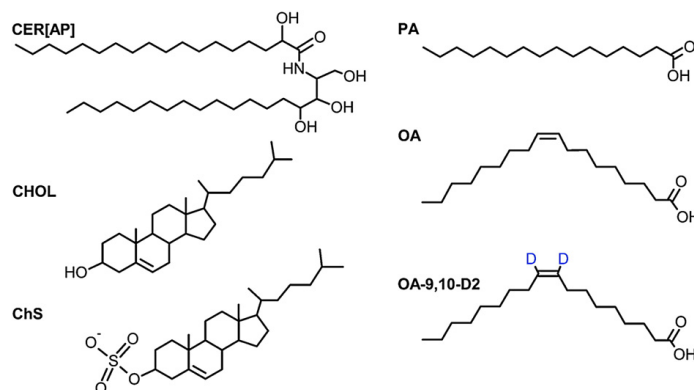


Fig. 1. Chemical structure of the synthetic SC lipids used for preparation of multilamellar lipid model membranes. Abbreviations: CER[AP]: Ceramide AP, CHOL: cholesterol, PA: palmitic acid, ChS: cholesterol sulfate, OA: oleic acid.

Saturated salt solutions were used to adjust the vapor at two different RH as described before [37,38]. For measurements at 57% RH, sodium bromide (NaBr) was used, while potassium sulfate (K_2SO_4) was employed to create a more humid atmosphere of 97% RH. After each change of RH and prior to the measurements, the samples were allowed to equilibrate for 8 to 10 h, while T was fixed at 32 °C to allow for comparability to *in vivo* conditions. Each sample was studied at no less than three different neutron contrasts to vary the neutron scattering length density between the lipids and water. Therefore, the chamber atmosphere was set to three D_2O/H_2O concentrations: 100/0, 50/50 and 8/92 (v/v).

During measurements, the sample was exposed to a monochromatic and collimated incoming neutron beam, with the intensity I of scattered neutrons being recorded as a function of the scattering angle 2θ . The latter is correlated to Q (scattering vector) by $Q = 4 \cdot \pi \cdot \sin \theta / \lambda$, where Q is the resulting vector between incoming wave vector k_i and scattered wave vector k_s , λ is the neutron wavelength, while θ is the angle of incident beam and d is the spacing between the scattering planes. From the positions of a series of equidistant peaks Q_n , the repeat distance d (periodicity) of a lamellar phase was calculated by $d = 2 \cdot \pi / Q_n$, where n is the diffraction order of the peak.

To gain insight into the bilayer structure on a nano-scale, commonly the neutron scattering length density (SLD) profiles $\rho_s(x)$ are calculated by a Fourier synthesis of the structure factors F_h according to Eq. (1):

$$\rho_s(x) = a + b \frac{2}{d} \sum_{h=1}^{h_{\max}} F_h \cdot \cos\left(\frac{2\pi \cdot h \cdot x}{d}\right) \quad (1)$$

Here, a and b are unknown coefficients for the relative normalization of $\rho_s(x)$, d represents the lamellar repeat distance and h is the diffraction order. The absolute value of F_h was calculated by $F_H = \sqrt{h} \cdot J_h \cdot A_h$, where h is the Lorentz correction, A_h is the absorption correction [39] and I_h is the integrated intensity of the h th peak. At least three to four diffraction orders h are needed to reconstruct the $\rho_s(x)$. As the strong incoherent scattering cross section of the large number of hydrogen atoms present in biological material accounts for a poor signal-to-noise (s/n) ratio, well-oriented model membranes are required in order to record diffraction peaks of higher orders.

Peak positions and intensities were determined by Gaussian fits of the peak maxima after background subtraction using the software package IGOR Pro 6.1 (WaveMetrics Inc., Portland, OR, USA). As we assume the SC lipid model bilayers investigated here to be centrosymmetric with the synthetic SC lipids being distributed homogeneously inside the model membrane, the determination of the phase angle and

therewith of the sign of F_h simplifies to the possibilities + or –. The signs of F_h are accessible by contrast variation, which is done by measuring the samples at no less than three different D_2O/H_2O ratios as described previously [40]. For a more detailed description regarding the evaluation procedure of the neutron diffraction data, see [39–41].

For the exact localization of certain molecular groups, one can benefit from the advantage offered by neutrons to distinguish not only between different atoms, but also between isotopes [42]. According to [43], the coherent scattering lengths b_{coh} for hydrogen (1H) and deuterium (2H) are quite different and equal to -0.374 and 0.667×10^{-12} cm, respectively. Hence, specific deuterium labeling of molecular groups can be used to determine the position of lipids inside the SC lipid model membrane [15,16]. In the present study, we used the specifically labeled oleic acid-9,10-D2 (OA-D2) to localize the penetration enhancer.

In order to receive information about the position of the deuterated label, it was necessary to determine the structure factors F_{h_deut} of the “deuterated” sample (*Basic_OA-D2*) as well as the structure factors F_{h_prot} for the “protonated” sample (*Basic_OA*), and subsequently to calculate the difference F_{h_diff} using Eq. (2):

$$F_{h_diff} = F_{h_deut} - F_{h_prot} \quad (2)$$

Then, the difference profiles $\rho_s(x)_{diff}$, which represent the distribution of deuterium density across the bilayer were evaluated as follows:

$$\rho_s(x)_{diff} = \frac{2}{d} \sum_{h=1}^{h_{\max}} F_{h_diff} \cdot \cos\left(\frac{2\pi \cdot h \cdot x}{d}\right) \quad (3)$$

As pointed out before in [15], it is reasonable to only use the structure factors obtained at 8% D_2O for calculating the difference profiles, as the scattering signal resulting from the membrane could be disturbed by the water signal at higher D_2O concentrations. Consequently, the $\rho_s(x)_{diff}$ presented here refer to the structure factors measured at 8% D_2O .

3. Results and discussion

3.1. Lamellar assembly of “Basic” and “Basic_OA”

In this section, the neutron diffraction results obtained for the quaternary sample composed of CER[AP], CHOL, PA and ChS (*Basic*, mass ratio 55/25/15/5), and the sample containing 10% OA (*Basic_OA*) are presented. The corresponding diffraction patterns for both samples

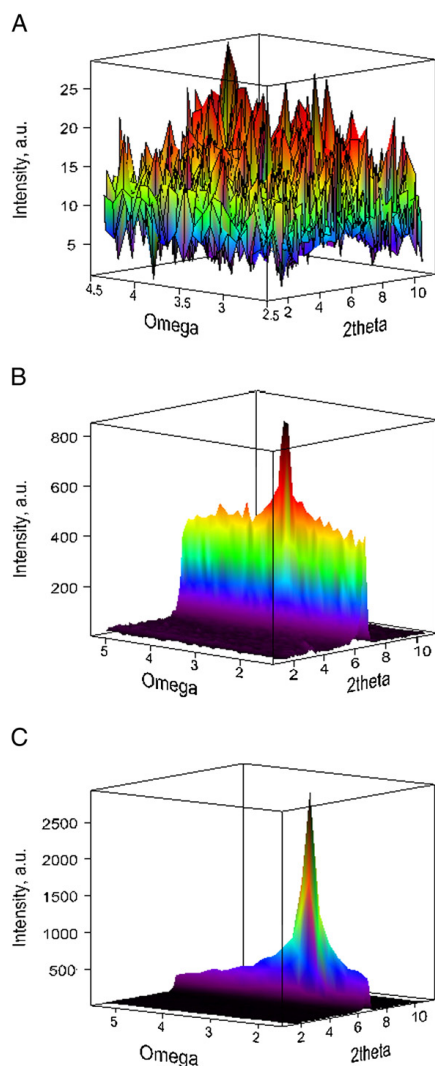


Fig. 2. Rocking scans around the 1st order Bragg peak ($2\theta = 6.6^\circ$) of two different multilamellar samples, which were rotated in an angular range of omega ($\omega = \pm 2^\circ$) to check the mosaicity. A and B: sample composed of CER[AP], CHOL, PA, ChS and OA (ratio 49.5/22.5/13.5/4.5/10 m/m) before (A) and after treatment with buffer pH 9.5 (B). C: rocking scan of the sample containing CER[AP], CHOL, PA and ChS (55/25/15/5 m/m).

recorded at $T = 32^\circ\text{C}$, RH 57% and 8% D_2O are depicted in Fig. 3. Five diffraction peaks attributed to one lamellar phase are detectable for both SC lipid model membranes and indicate a high degree of lamellar order formed under the chosen conditions. Interestingly, neither reflections from phase-separated CHOL crystals which were observed before in such SC models [44,45], nor signals from additional lamellar phases were recorded. The calculated lamellar d -spacings are listed in Table 2. Since we detected a similar repeat distance for the sample *Basic* as has been reported before for the same model system [12], the comparability

of the present results with former findings is proven. An additional peak (see Fig. 3) could not be assigned to a lamellar phase and was attributed to a crystal of Na_2CO_3 or NaHCO_3 due to the peak position at $2\theta = 31^\circ$ indicating a lattice parameter of $\approx 10 \text{ \AA}$. This crystal was maybe introduced during the preparation procedure since the samples were treated with a buffer containing both compounds. Presumably after removal of the buffer solution and drying under atmospheric humidity, a small amount was left and crystallized.

Interestingly, adding 10% (m/m) of the lipophilic penetration enhancer OA does not induce any change of repeat distance d (see Table 2). This is contrary to the results of Zbytovská and co-workers [30], who reported a slight increase in d -spacing upon raising the amount of OA added to a vesicular SC model. They furthermore observed a separated phase occurring at higher OA concentration, i.e. 10–15 mol% [30], which was explained by the formation of a separate domain with more fluid character, containing OA together with other membrane components. Former studies using the FT-IR technique [46] or ^2H NMR [28] to determine the influence of OA on the structure of the SC model systems likewise suggested the OA-induced extraction of certain membrane components with formation of an isotropic separated OA-rich phase, which, however, was not detectable in our study: Since only a single lamellar phase is formed under the chosen experimental conditions, we assume the whole amount of OA to be incorporated into the lipid lamellae of the SC model membrane.

These deviations to the former findings may result from the different techniques applied: Zbytovská and co-workers investigated vesicular SC lipid systems [30], whereas planar multiple SC lipid bilayer stacks were used for our neutron diffraction measurements. Both sample techniques are well established to study the structural assembly of SC lipids but the resulting SC model systems exhibit distinct characteristics. While SC lipid vesicles usually consist of few curved bilayers dispersed in aqueous media, the model membranes used in the present study are made up of several hundred stacked bilayers lacking curvature which are oriented parallel to the planar substrate surface, and hydration is achieved by creation of an atmosphere with certain RH. Such a preparation technique yields hydration properties comparable to *in vivo* conditions of the SC which was found to hold almost no free water in the intercellular lipid matrix as reviewed in [47]. For comparability reasons, we refer to former neutron diffraction studies and used the sample preparation method described in [36]. Summing up, the different techniques presumably account for the observed distinctions in lipid assembly.

We found just a marginal increase in d -spacing at raised RH of 97% as summarized in Table 2 for both samples. Of course, one has to keep in mind that such humidity does not compare with full hydration state, but however, it was shown previously that model membranes based on synthetic CER exhibit extremely poor interlamellar hydration of the hydrophilic head groups and consequently do not show a significant swelling [14,48], like for example phospholipid bilayers do [41]. Kiselev and co-workers suggested the short chain and polar CER [AP] to account for this observation: acting as a kind of molecular “linker” between two adjacent membrane leaflets it pulls the latter together and enables the formation of an extremely stable bilayer backbone [14,48]. Taking into account the specific characteristics found especially for CER[AP] [49] and CER[NP] [50], with their head groups being saturated with intra- and intermolecular hydrogen bonds it seems likely that such a compact bilayer assembly hinders water penetration into the lamellar structures and consequently prohibits swelling. Furthermore, despite the presence of rather ionizable fatty acid species in the model membrane investigated here, only a very small amount of those molecules will in fact be deprotonated due to the comparatively high pK_a of fatty acids inside such ordered lamellar structures [51]. This knowledge could explain the observed poor interlamellar hydration and lack of swelling found in the present study.

Another notable finding is a considerable decrease in the peak intensity detected for sample *Basic_OA* (Fig. 3). While the enhancer-

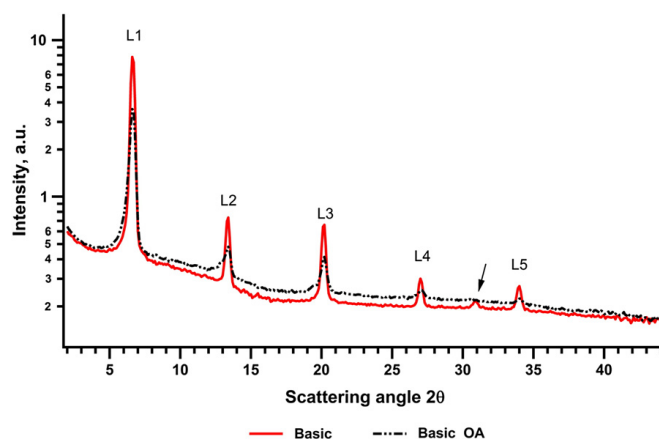


Fig. 3. Neutron diffraction pattern of the model membranes *Basic_OA* and *Basic*. Both samples were measured under equal conditions: 8% D₂O in H₂O, RH 57%. The 1st up to the 5th diffraction order associated to the lamellar phase are denoted as L1–L5. One additional peak (indicated by an arrow) could not be assigned to the reflections of a lamellar structure.

free sample shows high-intense and sharp Bragg peaks, the OA-based model membrane exhibits more broadened, less pronounced diffraction signals under the same measurement conditions. This result indicates an impaired state of lamellar order due to the presence of the penetration enhancer. To corroborate this assumption, the rocking scans around the 1st order Bragg peak for both samples were analyzed. Comparison of Fig. 2B and C, respectively, reveals the following results: the 1st order reflection for sample *Basic_OA* (B) is broadened and less intense, as the scattered intensity is spread over a wider angular range in omega (ω), and sample mosaicity is high [15]. As the Bragg peak is still visible and exhibits a distinct maximum at $\theta = 3.2^\circ$, we conclude a part of the lipids to be arranged in membranes parallel to the substrate surface in presence of OA. However, the decreased peak intensity can result from a distinct surface roughness induced by OA. Due to the lipid disordering effects, the alkyl chains of the SC lipids present in the model membrane experience a certain perturbation or misalignment which results in the observed increase of mosaicity. This is in line with former reports on OA causing increased alkyl chain disorder and disturbing the lamellar assembly of SC lipids in model bilayers [27]. Contrary to this, sample *Basic* exhibits not only a higher reflex intensity, but also a narrower peak shape. Accordingly, mosaicity must be lower compared to sample *Basic_OA*.

Despite the observed impairment of bilayer order in the presence of OA, the detection of five orders of diffraction allowed for the calculation of the neutron SLD profiles $\rho_s(x)$. The signs of F_{h_prot} for sample *Basic_OA* were determined to be $-$, $+$, $-$, $+$, $-$ for the 1st up to the 5th order of diffraction, respectively. As described before [44], the calculation of $\rho_s(x)$ on an absolute scale would produce large errors, consequently, all neutron SLD profiles are presented on a relative scale in arbitrary units (a.u.). The profiles for sample *Basic_OA* at three different D₂O/H₂O ratios (100/0, 50/50 and 8/92 v/v) at 57%

RH are depicted in Fig. 4 and provide insights into the model bilayer assembly:

- The profile represents the neutron scattering length density (SLD) distribution across one bilayer. Thereby, the unit cell features two maxima at the outer edges, indicating the presence of atoms with positive neutron scattering length, i.e. the polar SC lipid head groups. Neighbored bilayers are close to each other which indicates the presence of an extremely small intermembrane space.
- The lipids are pointing their alkyl chains towards the bilayer center as supposed. The high density of hydrogen atoms from terminal methyl groups of the lipid molecules with resulting accumulation of negative scattering length accounts for the formation of the minimum at $x = 0 \text{ \AA}$. A partial interdigitation is also possible as shown before [17].

For the sake of interpretation, two molecules of CER[AP] are added in Fig. 4 to schematically represent the bilayer arrangement. From the Fourier profiles we conclude that the presence of OA does not tremendously alter the expected bilayer structure of the quaternary model membrane. Especially when both samples, *Basic* and *Basic_OA* are compared directly as shown in Fig. 5, the lipid arrangement appears to be comparable in both model systems, as the unit cell has the same size and the head groups are in the same position. For such parallel presentation of the $\rho_s(x)$ for both model systems, the sum of the F_h obtained for each membrane was normalized to 1 and thereby placed on the same relative scale as presented in Table 3.

Small variations in the neutron SLD profiles are visible around the bilayer center with a less pronounced minimum detected for the sample containing OA, indicating that the middle of the bilayer is no more only formed by terminal methyl groups. A reason for this observation could be the presence of OA which is shown to induce a certain state of disorder or even misalignment of the SC lipids. The result might be a larger displacement of a certain number of terminal methyl groups (CH₃) by methylene groups (CH₂) due to the increased alkyl chain disorder. Consequently, the reduced number of hydrogen atoms present in the bilayer center accounts for the lower minimum detected. A similar observation has been reported for a ternary SC model based on CER[EOS], CER[AP], and CHOL [45]. The authors concluded the methylene groups from the outstretched CER[EOS] chain to be extended throughout the

Table 2

Lamellar d -spacings recorded for the model membranes *Basic* and *Basic_OA*. The value for 57% RH was averaged over three D₂O concentrations, while the value for the increased RH represents the mean of two D₂O contrasts.

Sample	57% RH	97% RH
Basic	44.65 ± 0.01 Å	46.86 ± 0.3 Å
Basic_OA	44.66 ± 0.03 Å	47.03 ± 0.2 Å

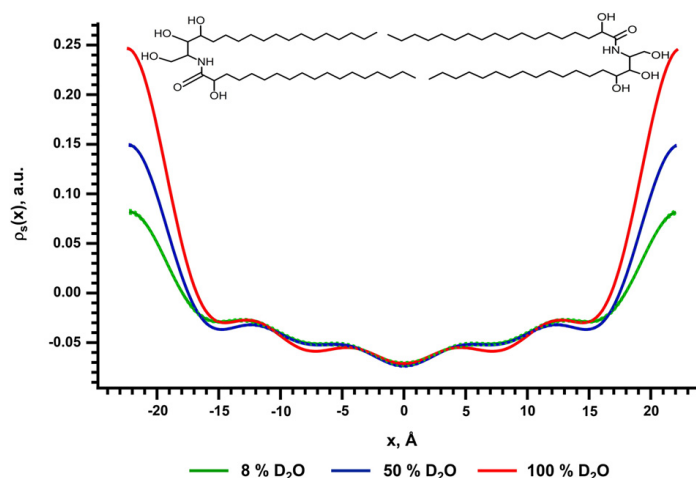


Fig. 4. Neutron scattering length density (SLD) profile $\rho_s(x)$ calculated for sample *Basic_OA* at RH 57% and at three different D_2O/H_2O concentrations: 8% D_2O (green line), 50% D_2O (blue line) and 100% D_2O (red line). For better understanding, the SC lipid arrangement inside the bilayer is indicated by two molecules CER[AP].

membrane and accordingly to diminish the influence of the methyl groups present in the bilayer center, which appeared as less pronounced minimum.

Summarizing, the neutron diffraction data indicate a strongly impaired lattice orientation in the presence of OA which shows in the enormously decreased intensity of the 1st order Bragg peak. This is due to the fact that scattered neutron intensity is spread over a wide angular range in ω , as the lipids are no longer arranged in an exact crystal-like orientation, but are distributed over the quartz substrate in a powder-like structure with a high mosaicity. The postulated perturbing effects of unsaturated fatty acids like OA onto the structure of skin lipids [23,25–27,52] could thus be corroborated by the present results. Additional differential scanning calorimetry (DSC) measurements on the SC lipid

systems *Basic* and *Basic_OA*, respectively, revealed a considerable shift of the main phase transition to lower temperatures for the sample containing 10% OA in comparison to the sample without OA (DSC data not shown). Moreover, the transition peaks are not only occurring at decreased temperatures, but also the heat flux upon phase transition is dramatically decreased in presence of the penetration enhancer. These findings likewise suggest a strong interaction of OA with the SC lipid chains in terms of markedly impaired alkyl chain order.

Although OA caused a distinct perturbation of the state of lipid chain order, our results also indicate the persistence of a stable lamellar structure unaffected in its hydration properties and bilayer size. This stability is most likely due to the influence of the polar CER[AP] enabling the formation of a stable bilayer backbone as illustrated in Fig. 6.

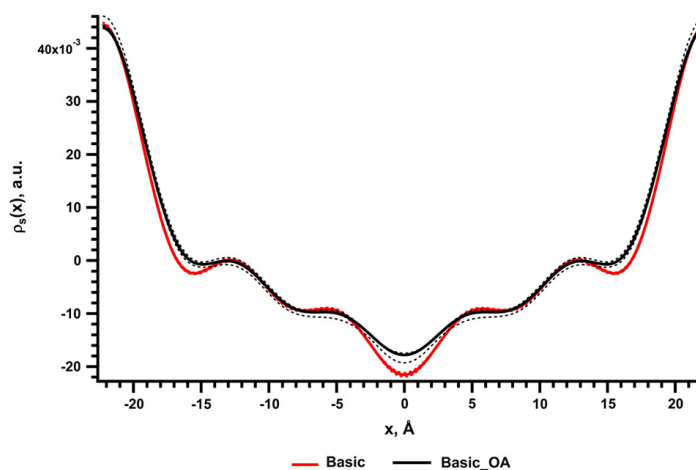


Fig. 5. Comparison of the neutron SLD profiles $\rho_s(x)$ for the sample with OA (*Basic_OA*, black line) and without OA (*Basic*, red line), both measured at 57% RH and 8% D_2O .

2804

T.N. Engelbrecht et al. / Biochimica et Biophysica Acta 1808 (2011) 2798–2806

Table 3

The structure factors F_h normalized to 1 for the model membrane CER[AP]/CHOL/PA/ChS (55/25/15/15 m/m, *Basic*) and the sample composed of 49.5/22.5/13.5/4.5/10 (*Basic_OA*). Both samples were measured at D_2O/H_2O ratio of 8/92 (v/v) and 57% RH.

Diffraction order h	F_h norm Basic	F_h norm Basic_OA
1	-0.439	-0.455
2	0.153	0.177
3	-0.191	-0.168
4	0.103	0.101
5	-0.107	-0.084

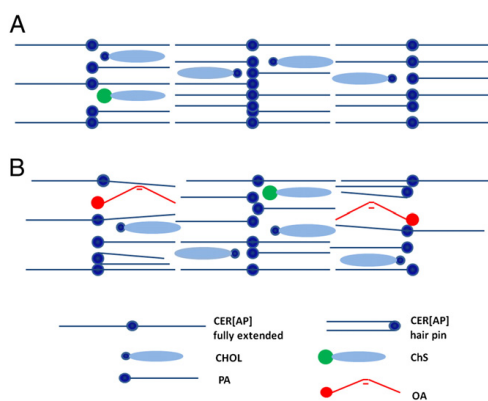


Fig. 6. Sketch of the lamellar SC lipid arrangement in the investigated model systems. A: the *Basic* model containing CER[AP]/CHOL/PA/ChS. B: sample *Basic_OA* additionally containing OA.

3.2. Evidence of OA insertion into the model bilayers

To corroborate the assumption that OA closely interacts *with* and is incorporated *within* the SC lipid model membrane components, we

applied specifically deuterated OA-D2 to the SC model membranes. The multilamellar sample allowed for detection of up to five orders of diffraction (data not shown) assigned to one lamellar phase with $d = 44.39 \pm 0.07 \text{ \AA}$, which is approximately the same value as for the protonated sample. Fig. 7 illustrates the Fourier profiles of both model membranes simultaneously on the same relative scale. As expected, the neutron SLD distribution across the bilayer is in general comparable; however, some significant differences appear in the hydrophobic membrane region, where the $\rho_s(x)$ of sample *Basic_OA-D2* is clearly shifted towards a more positive value. This observation is attributed to the appearance of additional positive neutron scattering length in that membrane region. As the SC lipid model membranes compared here only differ in the presence or absence of 2 deuterons, the observed variations appear due to the localization of the D2 label in that position. To verify this assumption, the difference scattering length density profile $\rho_s(x)_{diff}$ was calculated as described above and is included in Fig. 7 (black solid-dotted line).

The two maxima appearing in this function represent the location of the D2 label within the SC lipid model bilayer, i.e. the *cis* double bond present in OA, where the deuterons are positioned according to Fig. 1. As the membrane is centrosymmetric, the two maxima can be fitted by two identical Gaussian functions, with the position of maximum deuterium density determined to be $|x| = 8.6 \pm 0.04 \text{ \AA}$. The full width at half maximum (FWHM) of the Gaussian was found to be about 5.4 \AA , a bit larger than the nominal resolution of $\Delta d = \frac{d}{2n} = 4.5 \text{ \AA}$ of the experiment. Due to the limited number of diffraction peaks detectable, the resolution of the Fourier synthesis is limited as well. Considering an average C–C bond length for sp^3 hybridized C atoms of 1.5 \AA [53], the carboxyl group of OA pointing towards the head group region of the model membrane is presumably located at about 20 \AA . This value is in good agreement with the calculated position of the head groups of 22.2 \AA , which is defined as $x_{PH} = d/2$ [14].

Summing up, the bilayer architecture of the model membranes with and without the lipophilic penetration enhancer OA was studied on a molecular level. Furthermore, we were able to localize the position of the penetration enhancer inside the lipid lamellae by applying specifically deuterium-labeled OA-D2. The neutron diffraction results prove the incorporation of 10% (m/m) OA into the lipid lamellae, where the penetration enhancer then can interact with the SC lipids. The assumption that OA tends to form

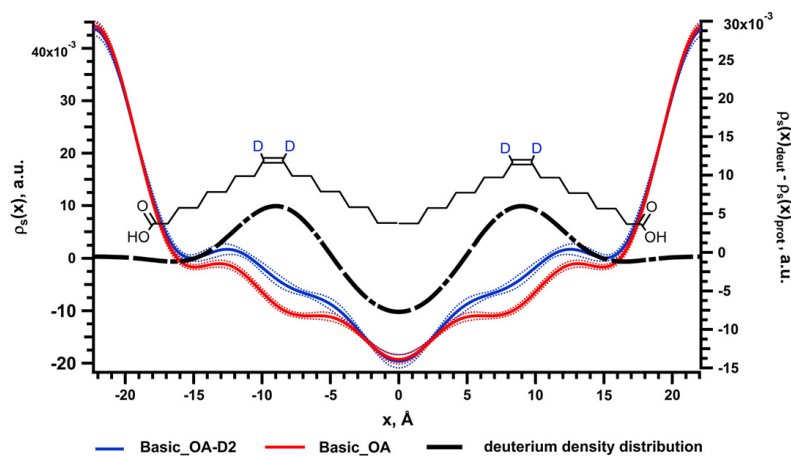


Fig. 7. Neutron SLD profiles at 8% D_2O , RH 57%, of the model membrane containing the deuterated (blue line) and the protonated OA (red line), and the difference scattering length density profile $\rho_s(x)_{diff}$ representing the deuterium distribution across the membrane (black dash-dotted line). The two maxima of $\rho_s(x)_{diff}$ represent the position of the D2 label of OA. For the sake of interpretation, a sketch of the arrangement of two molecules of OA is added.

a separated domain due to its poor miscibility with the other membrane components [30] could not be affirmed by the present neutron diffraction study.

Additionally, the SC lipid membrane composed of CER[AP]/CHOL/PA/ChS which was extensively studied before [12,14,30,48] was shown to serve as an appropriate model for studying the impact of penetration enhancer species like OA to the molecular arrangement of SC lipids by means of the neutron diffraction technique.

4. Conclusions

The present study investigates OA, a lipophilic substance well-known to act as penetration enhancer, and its impact to an SC lipid model membrane extensively analyzed before [12–14]. The neutron diffraction technique enabled to evaluate the bilayer structure on a nano-scale and to compare different membrane characteristics of samples with and without the presence of enhancer molecules, e.g. bilayer thickness and hydration behavior.

Our findings indicate that OA does not provoke a change of bilayer thickness in the model membrane investigated here. In contrast to former reports on OA-induced phase separations due to fluidization effects [28,30,46], the present neutron diffraction data reveal the formation of a single lamellar phase in the presence of 10% m/m OA under the chosen experimental conditions. This finding can be attributed to different techniques applied for preparation of SC model systems. To further analyze whether OA is in fact incorporated into the model matrix bilayers, and to localize the exact position of the penetration enhancer in the membrane, we applied specifically deuterated OA-D2. Our results give direct evidence that the deuterated label and therewith the penetration enhancer is effectively integrated within the model matrix, with the double bond positioned at a distance of about 8.5 Å from the bilayer center. Finally, the diffraction data emphasize the dramatic impact of OA to the state of lamellar order of the SC lipids as already described before [54]. We detected a substantial loss of order when OA is present inside the SC lipid model membrane indicating the perturbation of proper alkyl chain alignment by the lipophilic penetration enhancer, which became apparent in decreased neutron scattering amplitudes. The presence of the *cis* double bond in the OA molecules is probably causing the perturbation of the SC lipid chains which accounts for the observed lamellar disorder. Therefore, we conclude that the intercalation of OA into the lipid lamellae together with the increase of alkyl chain disorder preferentially accounts for the reported enhancing effects of OA on the drug permeation through the skin.

Acknowledgements

The authors would like to express their gratitude to Evonik Goldschmidt GmbH (Essen, Germany) for the donation of CER[AP]. One of the authors, T. Engelbrecht, would like to thank the Graduiertenförderung des Landes Sachsen-Anhalt as well as Evonik Goldschmidt for funding. We gratefully acknowledge granting of beam-time and financial assistance by Helmholtz Zentrum Berlin (HZB, Berlin, Germany).

References

- [1] P.M. Elias, Epidermal lipids, barrier function, and desquamation, *J. Invest. Dermatol.* 80 (Suppl.) (1983) 44s–49s.
- [2] G.M. Gray, H.J. Yardley, Lipid compositions of cells isolated from pig, human, and rat epidermis, *J. Lipid Res.* 16 (1975) 434–440.
- [3] Y. Masukawa, H. Narita, E. Shimizu, N. Kondo, Y. Sugai, T. Oba, R. Homma, J. Ishikawa, Y. Takagi, T. Kitahara, Y. Takema, K. Kita, Characterization of overall ceramide species in human stratum corneum, *J. Lipid Res.* 49 (2008) 1466–1476.
- [4] G.M. Gray, H.J. Yardley, Different populations of pig epidermal-cells – isolation and lipid-composition, *J. Lipid Res.* 16 (1975) 441–447.
- [5] G.M. Gray, R.J. White, Glycosphingolipids and ceramides in human and pig epidermis, *J. Invest. Dermatol.* 70 (1978) 336–341.
- [6] P.W. Wertz, B. van den Bergh, The physical, chemical and functional properties of lipids in the skin and other biological barriers, *Chem. Phys. Lipids* 91 (1998) 85–96.
- [7] S.E. Friberg, I. Kayali, W. Beckerman, L.D. Rhein, A. Simion, Water permeation of reaggregated stratum-corneum with model lipids, *J. Invest. Dermatol.* 94 (1990) 377–380.
- [8] L. Coderch, O. Lopez, A. de la Maza, J.L. Parra, Ceramides and skin function, *Am. J. Clin. Dermatol.* 4 (2003) 107–129.
- [9] D.C. Schwartzendruber, P.W. Wertz, D.J. Kitko, K.C. Madison, D.T. Downing, Molecular models of the intercellular lipid lamellae in mammalian stratum corneum, *J. Invest. Dermatol.* 92 (1989) 251–257.
- [10] K.C. Madison, D.C. Schwartzendruber, P.W. Wertz, D.T. Downing, Presence of intact intercellular lipid lamellae in the upper layers of the stratum corneum, *J. Invest. Dermatol.* 88 (1987) 714–718.
- [11] M.W. de Jager, G.S. Gooris, I.P. Dolbnya, W. Bras, M. Ponc, J.A. Bouwstra, Novel lipid mixtures based on synthetic ceramides reproduce the unique stratum corneum lipid organization, *J. Lipid Res.* 45 (2004) 923–932.
- [12] D. Kessner, M.A. Kiselev, T. Hauss, S. Dante, S. Wartewig, R.H. Neubert, Localisation of partially deuterated cholesterol in quaternary SC lipid model membranes: a neutron diffraction study, *Eur. Biophys. J.* 37 (2008) 1051–1057.
- [13] A. Ruettinger, M.A. Kiselev, T. Hauss, S. Dante, A.M. Balagurov, R.H. Neubert, Fatty acid interdigitation in stratum corneum model membranes: a neutron diffraction study, *Eur. Biophys. J.* 37 (2008) 759–771.
- [14] M.A. Kiselev, N.Y. Ryabova, A.M. Balagurov, S. Dante, T. Hauss, J. Zbytovská, S. Wartewig, R.H.H. Neubert, New insights into the structure and hydration of a stratum corneum lipid model membrane by neutron diffraction, *Eur. Biophys. J.* 34 (2005) 1030–1040.
- [15] S. Dante, T. Hauss, N.A. Dencher, Insertion of externally administered amyloid beta peptide 25–35 and perturbation of lipid bilayers, *Biochemistry* 42 (2003) 13667–13672.
- [16] T. Hauss, G. Buldt, M.P. Heyn, N.A. Dencher, Light-induced isomerization causes an increase in the chromophore tilt in the m-intermediate of bacteriorhodopsin – a neutron-diffraction study, *Proc. Natl. Acad. Sci. U. S. A.* 91 (1994) 11854–11858.
- [17] A. Schroeter, M.A. Kiselev, T. Hauss, S. Dante, R.H.H. Neubert, Evidence of free fatty acid interdigitation in stratum corneum model membranes based on ceramide [AP] by deuterium labelling, *Biochim. Biophys. Acta, Biomembr.* 1788 (2009) 2194–2203.
- [18] H. Trommer, R.H.H. Neubert, Overcoming the stratum corneum: the modulation of skin penetration – a review, *Skin Pharmacol. Physiol.* 19 (2006) 106–121.
- [19] R.B. Walker, E.W. Smith, The role of percutaneous penetration enhancers, *Adv. Drug Deliv. Rev.* 18 (1996) 295–301.
- [20] A.C. Williams, B.W. Barry, Penetration enhancers, *Adv. Drug Deliv. Rev.* 56 (2004) 603–618.
- [21] E.R. Cooper, E.W. Merritt, R.L. Smith, Effect of fatty acids and alcohols on the penetration of acyclovir across human skin in vitro, *J. Pharm. Sci.* 74 (1985) 688–689.
- [22] A.C. Williams, B.W. Barry, The enhancement index concept applied to terpene penetration enhancers for human skin and model lipophilic (estradiol) and hydrophilic (5-fluorouracil) drugs, *Int. J. Pharm.* 74 (1991) 157–168.
- [23] M. Walker, J. Hadgraft, Oleic acid – a membrane ‘fluidiser’ or a fluid within the membrane? *Int. J. Pharm.* 71 (1991) R1–R4.
- [24] E.M. Niaz, Influence of oleic-acid and other permeation promoters on transdermal delivery of dihydroergotamine through rabbit skin, *Int. J. Pharm.* 67 (1991) 97–100.
- [25] M.L. Francoeur, G.M. Golden, R.O. Potts, Oleic acid: its effects on stratum corneum in relation to (trans)dermal drug delivery, *Pharm. Res.* 7 (1990) 621–627.
- [26] M.A. Yamane, A.C. Williams, B.W. Barry, Effects of terpenes and oleic acid as skin penetration enhancers towards 5-fluorouracil as assessed with time; permeation, partitioning and differential scanning calorimetry, *Int. J. Pharm.* 116 (1995) 237–251.
- [27] A. Naik, L.A.R.M. Pechtold, R.O. Potts, R.H. Guy, Mechanism of oleic acid-induced skin penetration enhancement in vivo in humans, *J. Control. Release* 37 (1995) 299–306.
- [28] A.C. Rowat, N. Kitson, J.L. Thewalt, Interactions of oleic acid and model stratum corneum membranes as seen by ²H NMR, *Int. J. Pharm.* 307 (2006) 225–231.
- [29] H. Tanojo, A. Bos-van Geest, J.A. Bouwstra, H.E. Junginger, H.E. Bodde, In vitro human skin barrier perturbation by oleic acid: thermal analysis and freeze fracture electron microscopy studies, *Thermochim. Acta* 293 (1997) 77–85.
- [30] J. Zbytovská, K. Vávrová, M.A. Kiselev, P. Lessieur, S. Wartewig, R.H.H. Neubert, The effects of transdermal permeation enhancers on the thermotropic phase behaviour of a stratum corneum lipid model, *Colloids Surf., A* 351 (2009) 30–37.
- [31] F. Separovic, K. Gawrisch, Effect of unsaturation on the chain order of phosphatidylcholines in a dioleoylphosphatidylethanolamine matrix, *Biophys. J.* 71 (1996) 274–282.
- [32] K. Gawrisch, L.L. Holte, NMR investigations of non-lamellar phase promoters in the lamellar phase state, *Chem. Phys. Lipids* 81 (1996) 105–116.
- [33] J. Prades, S.S. Funari, P.V. Escriba, F. Barcelo, Effects of unsaturated fatty acids and triacylglycerols on phosphatidylethanolamine membrane structure, *J. Lipid Res.* 44 (2003) 1720–1727.
- [34] S.S. Funari, F. Barcelo, P.V. Escriba, Effects of oleic acid and its congeners, elaidic and stearic acids, on the structural properties of phosphatidylethanolamine membranes, *J. Lipid Res.* 44 (2003) 567–575.
- [35] M.T. Hyvönen, P.T. Kovanen, Molecular dynamics simulations of unsaturated lipid bilayers: effects of varying the numbers of double bonds, *Eur. Biophys. J.* 34 (2005) 294–305.
- [36] M. Seul, M.J. Sammon, Preparation of surfactant multilayer films on solid substrates by deposition from organic solution, *Thin Solid Films* 185 (1990) 287–305.
- [37] T.D. Hong, R.H. Ellis, J. Gunn, D. Moore, Relative humidity, temperature, and the equilibrium moisture content of conidia of *Beauveria bassiana* (Balsamo) Vuillemin: a quantitative approach, *J. Stored Prod. Res.* 38 (2002) 33–41.

- [38] P.W. Winston, D.H. Bates, Saturated solutions for the control of humidity in biological-research, *Ecology* 41 (1960) 232–237.
- [39] N.P. Franks, W.R. Lieb, Structure of lipid bilayers and the effects of general anaesthetics: an x-ray and neutron diffraction study, *J. Mol. Biol.* 133 (1979) 469–500.
- [40] D.L. Worcester, N.P. Franks, Structural analysis of hydrated egg lecithin and cholesterol bilayers II. Neutron diffraction, *J. Mol. Biol.* 100 (1976) 359–378.
- [41] J.F. Nagle, S. Tristram-Nagle, Structure of lipid bilayers, *Biochim. Biophys. Acta* 1469 (2000) 159–195.
- [42] B.P. Schoenborn, A.C. Nunes, Neutron scattering, *Annu. Rev. Biophys. Bioeng.* 1 (1972) 529–552.
- [43] D.M. Engelman, P.B. Moore, New method for determination of biological quaternary structure by neutron scattering, *Proc. Natl. Acad. Sci. U. S. A.* 69 (1972) 1997–1999.
- [44] A. Schröter, D. Kessner, M.A. Kiselev, T. Hauss, S. Dante, R.H.H. Neubert, Basic nanostructure of stratum corneum lipid matrices based on ceramides [EOS] and [AP]: a neutron diffraction study, *Biophys. J.* 97 (2009) 1104–1114.
- [45] D. Kessner, M. Kiselev, S. Dante, T. Hauss, P. Lersch, S. Wartewig, R.H. Neubert, Arrangement of ceramide [EOS] in a stratum corneum lipid model matrix: new aspects revealed by neutron diffraction studies, *Eur. Biophys. J.* 37 (2008) 989–999.
- [46] B. Ongpipattanakul, R.R. Burnette, R.O. Potts, M.L. Francoeur, Evidence that oleic acid exists in a separate phase within stratum corneum lipids, *Pharm. Res.* 8 (1991) 350–354.
- [47] P.W. Wertz, Stratum corneum lipids and water, *Exog. Dermatol.* 3 (2004) 53–56.
- [48] M.A. Kiselev, Conformation of ceramide 6 molecules and chain-flip transitions in the lipid matrix of the outermost layer of mammalian skin, the stratum corneum, *Crystallogr. Rep.* 52 (2007) 525–528.
- [49] S. Raudenkolb, S. Wartewig, R.H.H. Neubert, Polymorphism of ceramide 6: a vibrational spectroscopic and X-ray powder diffraction investigation of the diastereomers of N-(alpha-hydroxyoctadecanoyl)-phytosphingosine, *Chem. Phys. Lipids* 133 (2005) 89–102.
- [50] S. Raudenkolb, W. Hubner, W. Rettig, S. Wartewig, R.H.H. Neubert, Polymorphism of ceramide 3. Part 1: an investigation focused on the head group of N-octadecanoylphytosphingosine, *Chem. Phys. Lipids* 123 (2003) 9–17.
- [51] R. Lieckfeldt, J. Villalain, J.C. Gomezfernandez, G. Lee, Apparent pKa of the fatty acids within ordered mixtures of model human stratum corneum lipids, *Pharm. Res.* 12 (1995) 1614–1617.
- [52] B.J. Aungst, Structure/effect studies of fatty acid isomers as skin penetration enhancers and skin irritants, *Pharm. Res.* 6 (1989) 244–247.
- [53] F.H. Allen, O. Kennard, D.G. Watson, L. Brammer, A.G. Orpen, R. Taylor, Tables of bond lengths determined by x-ray and neutron diffraction. 1. Bond lengths in organic compounds, *J. Chem. Soc., Perkin Trans. 2* (1987) S1–S19.
- [54] S.A. Ibrahim, S.K. Li, Chemical enhancer solubility in human stratum corneum lipids and enhancer mechanism of action on stratum corneum lipid domain, *Int. J. Pharm.* 383 (2010) 89–98.

3.2.2 Isopropyl myristate: Influence on the lamellar architecture of oriented SC lipid model membranes and mode of action (Manuscript: Skin Pharmacology and Physiology)

Engelbrecht TN, Demé B, Dobner B, Neubert RHH: **Study of the Influence of the Penetration Enhancer Isopropyl Myristate on the Nanostructure of Stratum Corneum Lipid Model Membranes Using Neutron Diffraction and Deuterium Labelling.** *Skin Pharmacology and Physiology* 2012; 25: 200-207

(DOI: 10.1159/000338538)

Available online:

<http://content.karger.com/ProdukteDB/produkte.asp?doi=10.1159/000338538>

Study of the Influence of the Penetration Enhancer Isopropyl Myristate on the Nanostructure of Stratum Corneum Lipid Model Membranes Using Neutron Diffraction and Deuterium Labelling

T.N. Engelbrecht^a B. Demé^b B. Dobner^a R.H.H. Neubert^a

^aInstitute of Pharmacy, Martin Luther University Halle-Wittenberg, Halle/Saale, Germany; ^bInstitut Laue-Langevin (ILL), Grenoble, France

Key Words

Stratum corneum · Ceramide · Model membrane · Deuterium labelling · Neutron diffraction

Abstract

In order to elucidate the mode of action of the lipophilic penetration enhancer isopropyl myristate (IPM) on a molecular scale, we investigated oriented quaternary stratum corneum (SC) lipid model membranes based on ceramide AP, cholesterol, palmitic acid and cholesterol sulfate containing 10 wt% IPM by means of neutron diffraction. Our results indicate that IPM affects the lamellar lipid assembly in terms of bilayer perturbation and disordering. Phase segregation occurred, indicating that IPM is not likely to mix properly with the other SC lipids due to its branched structure. We used selective deuterium labelling to localize the penetration enhancer, and could successfully prove the presence of IPM in the two coexisting lamellar phases. We conclude that IPM's mode of action as penetration promoter is presumably based on incorporation into the SC lipid matrix, extraction of certain SC lipids into a separate phase and perturbation of the multilamellar lipid assembly.

Copyright © 2012 S. Karger AG, Basel

Introduction

The protecting barrier properties of mammalian skin are generally accepted to be founded on the very thin outermost skin layer, the stratum corneum (SC). A highly ordered intercellular lipid matrix consisting of ceramides (CER), cholesterol (CHOL) with its derivatives and free fatty acids is arranged around protein-filled flat cells, the corneocytes. This coherent system substantially limits uncontrolled transepidermal water loss and prevents the unwanted absorption of substances [1, 2]. At the same time, those barrier properties can be obstructive for the dermal treatment of various skin diseases requiring a certain amount of drug to penetrate into skin. Acceleration of drug absorption can be facilitated by application of so-called penetration enhancers. Enhancer activity is presumably based on interaction with the SC lipid matrix and/or SC protein components, disordering or fluidizing effects on the SC lipids [3], and introduction of phase separation [4]. However, the exact mode of action is not yet fully elucidated on a molecular level. Synergetic effects in terms of drug flux enhancement have also been described, e.g. for myristic acid isopropyl ester (referred to as isopropyl myristate or IPM – a pharmaceutically used

KARGER

Fax +41 61 306 12 34
E-Mail karger@karger.ch
www.karger.com

© 2012 S. Karger AG, Basel
1660–5527/12/0254–0200\$38.00/0

Accessible online at:
www.karger.com/spp

Tanja Engelbrecht
Institute of Pharmacy, Martin Luther University Halle-Wittenberg
Wolfgang-Langenbeck-Strasse 4
DE-06120 Halle/Saale (Germany)
Tel. +49 345 552 5025, E-Mail tanja.engelbrecht@pharmazie.uni-halle.de

Table 1. Composition of the multilamellar SC lipid model membranes investigated by means of neutron diffraction

Sample	SC lipid components	wt%
Basic_IPM	CER[AP]/CHOL/PA/ChS/IPM	49.5/22.5/13.5/4.5/10
Basic_IPM- <i>d</i> ₃	CER[AP]/CHOL/PA/ChS/IPM- <i>d</i> ₃	49.5/22.5/13.5/4.5/10

liquid wax with well-established skin tolerability) in combination with alkanols [5, 6] and with propylene glycol [7]. Although it was also reported that IPM decreases hydrocortisone permeation through human skin [8], the ester is assumed to change the SC microstructure by insertion into the lipid lamellae where it is largely retained due to its high lipophilicity [5, 6]. Furthermore, the wax presumably liquefies the SC lipids due to its branched structure [7], which is supposed to account for the enhancer activity of IPM.

In recent years, the benefits offered by the neutron diffraction technique for the structural investigation of the SC lipid matrix in model membranes were highlighted in numerous works [9–11]. By using a simplistic model, the bilayer architecture of a membrane based on CER[AP], CHOL, palmitic acid (PA) and cholesterol sulfate (ChS) was revealed to be highly dependent on the phytosphingosine type CER[AP] which dictates the bilayer size due to its unique properties [12, 13]. A preceding study elucidated the mode of action of the penetration enhancer oleic acid on a molecular level [14]. It was shown that the position of lipid molecules within the model bilayers can be determined by specific deuterium labelling of molecular groups which can help shedding a light on the mode of enhancer activity on a molecular scale.

In the present work, we investigated the impact of IPM on the structure of a quaternary SC lipid model system based on CER[AP], CHOL, PA, and ChS which has been described before [13], containing either the protonated compound IPM (referred to as sample Basic_IPM) or the specifically deuterated compound IPM-*d*₃ which was received from chemical synthesis (sample Basic_IPM-*d*₃). In order to allow for a sufficient strength of the deuterium label to localize the enhancer, we decided to add an amount of 10 wt% IPM to the model membrane. The composition of the oriented multilamellar model membranes to be investigated by means of neutron diffraction can be found in table 1, and the chemical structures of the synthetic SC lipids used for sample preparation are displayed in figure 1. Local contrast enhance-

ment by the deuterium label enabled us to directly localize the position of the liquid wax inside the membrane lipid lamellae.

Materials and Methods

CER[AP] [N-(α -hydroxyoctadecanoyl)-phytosphingosine] was generously provided by Evonik Goldschmidt GmbH (Essen, Germany). A chromatographic procedure using a silica gel column and chloroform/methanol gradient was applied to increase the purity of the substance above 96% before it was used. PA, CHOL, ChS, and tetradecanoic acid isopropyl ester (IPM) were purchased from Sigma Aldrich GmbH (Taufkirchen, Germany) and used as received. Specifically deuterated 14,14,14-*d*₃-tetradecanoic acid isopropyl ester (IPM-*d*₃) was received from own chemical synthesis [see Synthesis of 14,14,14-*d*₃-Tetradecanoic Acid Isopropyl Ester (IPM-*d*₃)]. All substances used for synthesis were purchased from Sigma Aldrich GmbH (Taufkirchen, Germany) except the deuterated compound, tetradecanoic acid-14,14,14-*d*₃, which was received from Larodan Fine Chemicals (Malmö, Sweden) and used without further purification. The product IPM-*d*₃ was purified by column chromatography using heptane/ether and gradient technique. The isopropanol was dried with sodium before use. All solvents were dried and distilled before use. Thionyl chloride was distilled twice at normal pressure. The ¹H NMR spectrum was recorded on a Varian Inova 500 apparatus (International Equipment Trading Ltd., Vernon Hills, Ill., USA, with an Oxford Instruments Ltd. superconducting magnet) at 27°C and CDCl₃ as internal standard. The mass spectrometric analysis was done using a Q-TOF1 mass spectrometer (Waters Micromass, Manchester, UK). The quartz slides (Spectrosil 2000, 25 × 65 × 0.3 mm) used for the neutron diffraction experiments were received from Saint-Gobain (Wiesbaden, Germany). An airbrush device (Harder & Steenbeck, Norderstedt, Germany) was employed to deposit the lipids onto the quartz surface. All buffer substances used were obtained from Sigma Aldrich.

For the preparation of oriented SC lipid model membranes to be investigated by neutron diffraction, we used a procedure according to the literature [15]. Appropriate amounts of the synthetic SC lipids dissolved in a mixture of chloroform/methanol (2:1 v/v) were combined. Twelve milligrams of the respective final SC lipid mixture (table 1) were sprayed onto the quartz surface using the airbrush device at constant air flow. The solvent was allowed to evaporate first under atmospheric pressure and subsequently under reduced pressure (<50 mbar), where the samples

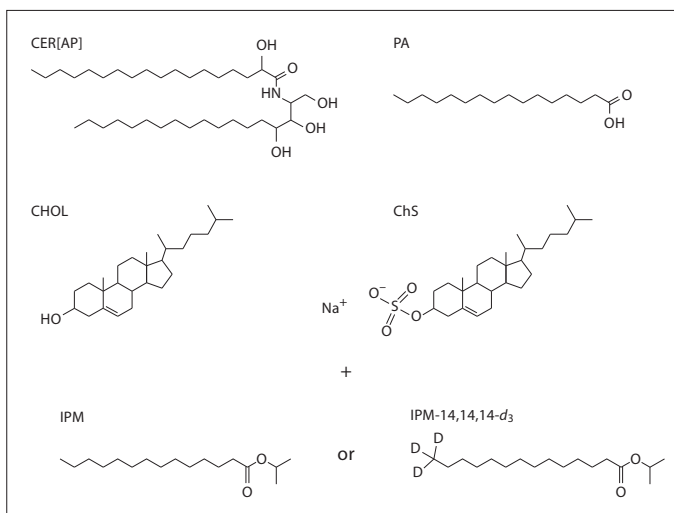


Fig. 1. The molecular structures of the synthetic SC lipids used for sample preparation.

were stored for 10–12 h. After the solvent was removed completely, a subsequent annealing procedure was applied, whereby the samples were heated to 75°C and cooled down to room temperature in water-saturated atmosphere. Subsequently, the samples were hydrated using a buffer solution of pH 9.6, for 5 min, and kept at room temperature until the diffraction measurements.

Synthesis of 14,14,14-d₃-Tetradecanoic Acid Isopropyl Ester (IPM-d₃)

0.43 mmol (100 mg) 14,14,14-d₃ tetradecanoic acid was suspended in 0.5 ml thionyl chloride. The mixture was allowed to stand overnight at room temperature. The excess of thionyl chloride was removed in vacuum. To the oily residue was dropped a mixture of 2.0 mmol (0.12 g) isopropanol and 0.2 mmol (0.16 g) dry pyridine, dissolved in 1 ml dry chloroform at 0°C over a period of 10 min with stirring. After a further hour at that temperature, the mixture was brought to room temperature and stirred for another hour. For workup, the solvent was removed in vacuum and the residue was purified by column chromatography with heptane and ether with a continuous increase of the polarity of the eluent. Yield: 120.4 mg, colorless oil, C₁₇H₃₁D₃O₂ (273.46). ¹H NMR (400 MHz, CDCl₃): δ = 1.19 (d, 6H, 2 × [–CH₃]), 1.21–1.31 (m, 2H, [chain]), 1.55–1.63 (m, 2H, [–CH₂CH₂CO]), 2.2–2.25 (t, 2H, [–CH₂CO]), 4.98 (q, ³J_{H,H} = 6.26, 1H, [–CH(CH₃)₂]). ESI-MS 274.27 [M⁺]+H, 296.24 [M⁺]+Na.

Neutron Diffraction Experiment

Neutron diffraction experiments were carried out using the small momentum transfer diffractometer D16 of the High-Flux Reactor at the Institut Laue-Langevin (Grenoble, France). The neutron wavelength λ was adjusted to 4.752 Å. The scattered neutron intensity was recorded during rocking scans (ω-scans, sam-

Table 2. Calculated *d* spacings (in Å) for both samples investigated by means of neutron diffraction

Sample	Phase A	Phase B
Basic_IPM	46.8 ± 0.14	42.8 ± 0.6
Basic_IPM-d ₃	45.9 ± 0.4	42.5 ± 0.43

ple-to-detector distance: 95.0 cm) by the two-dimensional ³He position-sensitive detector MILAND (area 320 × 320 mm, spatial resolution 1 × 1 mm). The samples were allowed to equilibrate before each measurement in lockable aluminium chambers at fixed temperature of 32°C and a relative humidity of 58%, achieved by a saturated aqueous solution of sodium bromide. Each sample was studied at three different D₂O concentrations in water (100/0, 50/50 and 8/92, v/v D₂O/H₂O) in order to vary the neutron scattering length density between the lipids and water. From a series of equidistant peaks, the spacing between the scattering planes (bilayer repeat distance *d*) was calculated using the correlation $d = 2 \times n \times \pi / Q_n$, where *n* is the diffraction order of the peak and *Q_n* is the scattering vector. The latter is correlated with the scattering angle 2θ by $Q = 4 \times \pi \times \sin \theta / \lambda$. Calculated *d*-spacings are presented in table 2.

For the interpretation of neutron diffraction data, commonly the neutron scattering length density profiles ρ_{*z*}(*x*) are calculated by a Fourier synthesis of the structure factors *F_n* according to

$$\rho_z(x) = a + b \frac{2}{d} \times \sum_{h=1}^{h_{\max}} F_h \times \cos\left(\frac{2\pi hx}{d}\right)$$

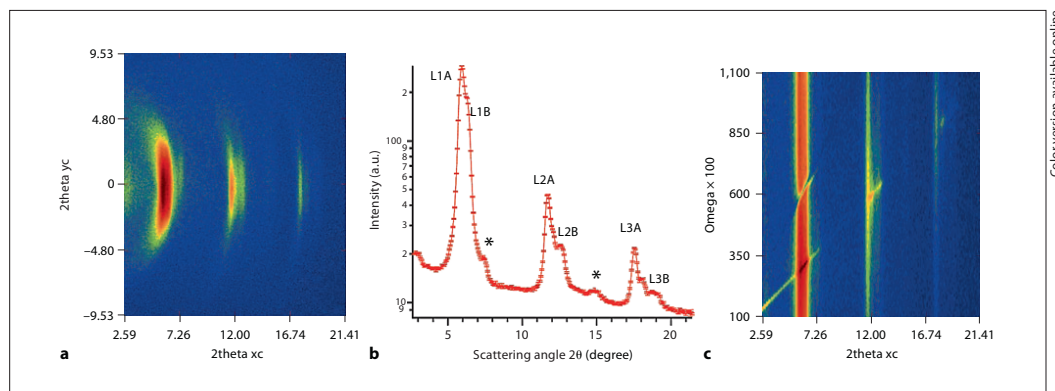


Fig. 2. Neutron diffraction pattern recorded at the first detector position for sample Basic_IPM at 32°C, 58% relative humidity, 100% D₂O. Shown are the 1st to 3rd Bragg reflections of phase A (L1A/L2A/L3A) and phase B (L1B/L2B/L3B), respectively. The first- and second-order diffraction peaks of phase-separated

CHOL crystals ($2\theta = 7.49$ and 14.84°) are marked with an asterisk in **b**. **a** Two-dimensional integrated intensity collected during an omega scan (sample rocking scan as shown in **c**). **b** Integrated intensity, plotted as $\log(I)$ versus 2θ . **c** Omega (ω) dependency of scattered neutron intensity (reciprocal space map).

The $\rho_s(x)$ represent the distribution of neutron scattering length density across one unit cell, i.e. one model bilayer, and therefore provide direct insight into the molecular arrangement of the SC lipids on a nanoscale. The phase of each F_h is determined by the isomorphous replacement method [16]. This is achieved by measuring each sample at least at three different D₂O/H₂O ratios.

The absolute value of F_h is received by

$$|F_h| = \sqrt{h \times I_h \times A_h},$$

where h is the Lorentz correction; A_h is the absorption correction and I_h is the integrated intensity of the h th peak. Data reduction to 2θ versus intensity I was performed with the Large Array Manipulation Program provided by the Institut Laue-Langevin [17], determination of the peak positions and intensities after background subtraction was performed using the software package IGOR Pro 6.1 (WaveMetrics Inc., Portland, Oreg., USA). A more detailed description of the neutron diffraction data evaluation can be found in the literature [18, 19].

Since neutrons are scattered by the atoms' nuclei and not by the electrons, the coherent neutron scattering length b_{coh} can differ markedly for different isotopes. According to the literature, b_{coh} for hydrogen (¹H) equals -0.374×10^{-12} cm and 0.667×10^{-12} cm for its isotope deuterium (²H or D) [20]. Hence, it is possible to distinguish between protonated and deuterated compounds by means of neutron diffraction. For the localization of the deuterium label and therewith of the deuterated penetration enhancer IPM-*d*₃ inside the SC lipid model bilayers, the deuterium density distribution function $\rho_{diff}(x)$ was calculated as difference profile between the deuterated and the protonated sample: $\rho_{diff}(x) = \rho_{deut} - \rho_{prot}$. The maxima in the $\rho_{diff}(x)$ represent the position of the deuterium label within the unit cell.

Results and Discussion

The neutron diffraction pattern of sample Basic_IPM recorded at 32°C, 100% D₂O and 58% relative humidity is shown in figure 2b.

First, the neutron diffraction results reveal the occurrence of phase separation in the investigated model membranes containing 10 wt% IPM. Whereas the enhancer-free model membrane composed of CER[AP], CHOL, PA, and ChS was reported to feature a one-phase system [12, 13], the presence of the penetration enhancer obviously provokes the formation of two clearly pronounced and coexisting lamellar phases referred to as phase A and phase B. For reasons of simplicity, we will further refer to the enhancer-free quaternary model membrane lacking IPM as the reference system. In addition to the two lamellar phases, the 1st- and 2nd-order diffraction signals of crystalline CHOL were detected and are indicated with asterisks in figure 2b. The occurrence of such separate CHOL domains was described before and has been shown not to influence the bilayer assembly of SC lipid model systems [21, 22]. The lamellar repeat distances of the investigated samples were calculated as described above and are listed in table 2. In case of sample Basic_IPM, d equals 46.8 Å for phase A, and 42.8 Å for phase B, respectively. For sample Basic_IPM-*d*₃, the d spacings were determined as 45.9 Å (phase A) and 42.5 Å (phase B). There

is rather good agreement of the d spacings found for the present phase A (table 2) and the reference system of 45.6 Å being reported before [13]. Since just one component, IPM, was added to this model in the present study, it appears reasonable that phase A corresponds with the membrane structure reported for the reference system, and that furthermore the arrangement of the SC lipids in phase A is comparable to the reference system. In contrast, the lamellar spacing of phase B is comparatively smaller. We will refer to that later. Surprisingly, there is a small deviation for the lamellar repeat distance of phase A in sample Basic_IPM and sample Basic_IPM- d_3 . Although the preparation procedures for both membranes were exactly the same, this experimental finding could indicate that there are slight variations in the lipid composition of phase A of both samples, e.g. a slightly higher or lower amount of CHOL and/or fatty acid and/or IPM. Yet the difference is quite small, therefore we regard phase A in both samples to be equivalent.

From these first results, we conclude that the membrane components are not likely to mix properly with each other in the presence of IPM. The branched structure of IPM with a highly mobile terminal isopropyl group probably prevents the other SC lipids to arrange in a densely packed and stable bilayer structure. Phase separation may further indicate that the solubility of the penetration enhancer IPM is limited in the lamellar 45.6-Å structure of the quaternary reference system which corresponds with the present phase A: after a certain limit value of IPM is exceeded, a fraction of the SC lipids is sequestered in the arising new lamellar structure. This emphasizes the impact of only 10% IPM added to the model membrane, and suggests that the enhancer indeed is incorporated into the bilayers and interacts with the SC lipids. To clarify whether IPM is localized in both phase A and phase B, or is accumulated in just one of the lamellar structures, the selectively deuterated IPM- d_3 was applied.

Furthermore, a distinct perturbation of the state of lamellar order was deduced from the shape of the neutron scattering signals in the diffraction pattern displayed in figure 2c. The Bragg sheet intensity is spread over a wider angular range in ω . This observation results from increased lamellar disorder in the model bilayers. Despite the still existing multilamellar assembly of the SC lipids, the bilayers seem to discover a certain perturbation. A possible explanation could be that the alkyl chains are no longer arranged in an *all-trans* zigzag structure, but exhibit an increased number of *gauche* defects. This is due to IPM, which is incorporated into the model bilayers but

presumably requires more space due to its branched structure. The experimental finding of bilayer perturbation is in line with former reports [14], where a similar effect was observed after the addition of 10 wt% of the penetration enhancer oleic acid to the same quaternary model membrane as investigated here. Phase separation was not observed in this former work, but based on the findings the authors concluded that the introduction of *gauche* defects to the SC lipid alkyl chains and SC lipid bilayer perturbation considerably contribute to the enhancer activity of oleic acid [14].

Since the values of the d spacings are in the same order of magnitude for both model membranes studied here, further comparison between the samples Basic_IPM and Basic_IPM- d_3 was drawn. To gain insight into the bilayer architecture on a nanoscale and to prove the incorporation of IPM into the model bilayers, the neutron scattering length density profiles $\rho_s(x)$ were calculated for both samples and are comparatively displayed in figure 3 for phase A and phase B. Generally, both phases exhibit the typical $\rho_s(x)$ found for SC lipid bilayers. The two maxima that correspond with the hydrophilic bilayer region constituted by the SC lipid head groups are surrounding the lipid alkyl chains pointed towards the bilayer center, which is indicated by the central minimum. The difference profiles $\rho_{diff}(x)$ representing the density distribution of the deuterium label across the membrane are added. In comparison to the protonated SC model membrane (fig. 3), the curve progression for the deuterated sample is considerably lifted towards more positive values. This is observed for both, phase A and phase B, and arises from the presence of the d_3 label at the respective position within the membrane unit cell. We conclude from this finding that the deuterium label and therewith the enhancer IPM resides in both observed lamellar phases.

Yet, the *distribution* of the deuterium label itself appears to be different in both phases: whereas $\rho_{diff}(x)$ for phase B exhibits one maximum, three maxima are observed for phase A. This finding indicates that the arrangement of IPM is different within the two lamellar phases. Taking into account that all considerations regarding the molecular arrangement of the SC lipids in the present system are based on a centrosymmetric bilayer assembly, we interpret the diffraction results as follows. As expected from its molecular structure, a certain fraction of IPM points its myristoyl side chain towards the bilayer center, where the accumulation of positive neutron scattering length density due to the presence of three deuterium atoms at the chain end position causes the observed maximum in the $\rho_{diff}(x)$ around $x = 0$. Since the central

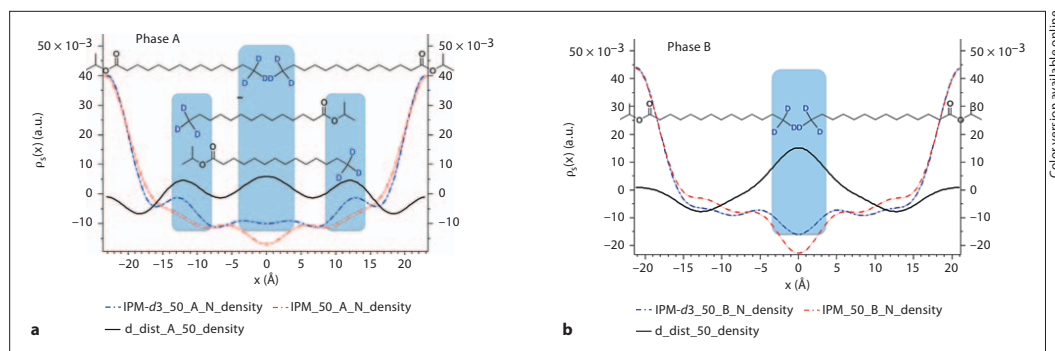


Fig. 3. a The neutron scattering length density profiles for phase A of sample Basic_IPM (red) and sample Basic_IPM- d_3 (blue) at 32°C and 50% D_2O . The difference profile or deuterium density distribution profile is presented as black solid line. For clarity, a sketch of the assumed arrangement of the penetration enhancer is added to the diagram. **b** The neutron scattering length density

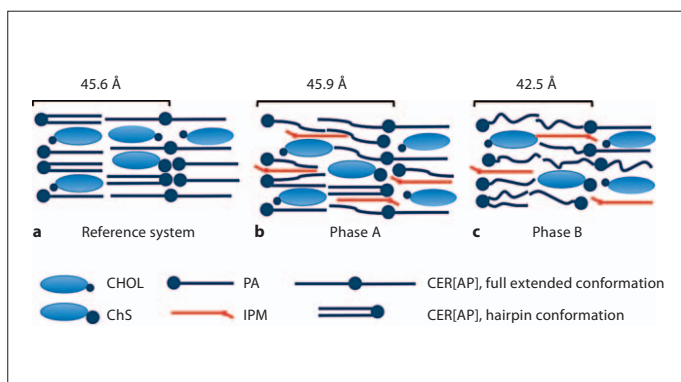
profiles for phase B of sample Basic_IPM (red) and sample Basic_IPM- d_3 (blue) at 32°C and 50% D_2O . The difference profile or deuterium density distribution profile is presented as black solid line. For better understanding, a sketch of two molecules IPM is added to illustrate the presumed enhancer arrangement. Colors refer to the online version only.

maximum is observed in both lamellar structures, this assembly of IPM is conceivable for both, phases A and B. For clarity, a sketch of the proposed assembly of two IPM molecules has been added to figure 3. Due to the hydrophobic match [23], the C14 chain of IPM will have high affinity to the C16 fatty acid (PA) present in the mixture and stretches through one hydrophobic bilayer leaflet. The more hydrophilic ester group most likely lies in the bilayer head group region, where hydrogen bonds with the other SC lipid head groups stabilize this arrangement. The isopropyl group would then be located near the hydrophilic bilayer region. Such an interaction of IPM and the SC intercellular lipid matrix has been proposed before [24]. Due to the limited number of structure factors F_h being available in the neutron diffraction experiment, the resolution of the Fourier synthesis is limited, which probably accounts for the comparatively broad dispersion of the maximum in the $\rho_{diff}(x)$ (fig. 3). The smeared-out maximum might also refer to a relatively broad distribution of the deuterium label itself inside the bilayers. As the C14 alkyl chain of IPM is slightly shortened compared to the C16 PA or the C18 chains of CER[AP], it seems likely that the terminal methyl group of IPM does not exactly reach the bilayer center, and that the CD_3 label therefore is localized slightly beside the position $x = 0$, as schematically presented in figure 3. Furthermore, since the presence of IPM was found to cause *gauche* defects and lamellar disorder, the alkyl chains will possess a certain mobility,

which may result in a kind of delocalization of the deuterated label.

For phase A, the two additional maxima in the $\rho_{diff}(x)$ determined at the position of $|x| = 11.86 \pm 0.39 \text{ \AA}$ suggest that a certain population of IPM is accommodated in the unit cell in a different way as explained above. Based on a centrosymmetric bilayer assembly, we regard both bilayer leaflets as mirrored equals. Surprisingly, the terminal methyl group with the deuterium label seems to be shifted away from the bilayer middle towards the region between center and head group moiety. To explain this observation, we assume that a fraction of the penetration enhancer might be inserted completely into the SC lipid bilayer, stretching the myristoyl chain through the bilayer center towards the neighbor bilayer leaflet, where the deuterated terminal methyl group is localized at the detected position of about 12 Å away from the bilayer center. Consequently, the ester group is no longer localized in the hydrophilic bilayer region, but has to integrate between the more hydrophobic alkyl chain moieties of the other SC lipids. Although this arrangement appears unexpected, such a complete incorporation into the SC lipid bilayers might be conceivable since IPM exhibits a comparatively high lipophilicity and is largely retained in the SC lipid matrix as highlighted before [6]. Moreover, a former neutron diffraction study revealed that CHOL is immersed in the bilayers of a quaternary model membrane in a similar way as proposed here for the molecule IPM,

Fig. 4. Schematic presentation of the assumed lamellar structure in the presence of 10 wt% IPM-*d*₃. **a** Lamellar assembly of the components CER[AP], CHOL, PA and ChS in the short periodicity phase as reported in Kiselev et al. [13]. **b** The assumed bilayer structure of phase A. As described in the text, IPM can be either anchored with its ester group in the hydrophilic head group region, or completely inserted into the hydrophobic membrane region. The bilayer repeat distance is comparable to the quaternary reference system. Remarkable is the increased lamellar disorder. **c** The membrane structure and assembly of IPM in phase B. Note the decreased lamellar spacing, indicating an increased state of lipid fluidity and alkyl chain disorder.



with the hydrophilic OH group positioned inside the hydrophobic membrane region in order to allow for maximum hydrophobic interaction of the steroid ring system with the other membrane components [25]. Furthermore, the penetration enhancer IPM lacks a pronounced *hydrophilic head-hydrophobic tail* structure, for which reason the complete insertion – of at least few IPM molecules – might be possible. At this point, we have no definite explanation why only phase A shows two different arrangements for the penetration enhancer IPM, but it might be due to the larger spacing of phase A.

For a better understanding, the assumed structural assembly of the SC lipids in the two lamellar phases in the presence of IPM is schematically represented in figure 4 and compared to the bilayer nanostructure of the reference system. The latter has been extensively studied and described before [12, 13, 25]. It was shown that the driving force for the highly ordered nanostructure of the CER[AP]-based model membrane is the ceramide itself [13], and that the lamellar repeat distance remains stable even if the fatty acid is replaced by long-chain species [26]. Probably due to strong hydrogen bonds formed between the head groups of the CER molecules, a framework with a high state of lamellar order is built, and the other membrane components such as PA, CHOL and ChS are forced to arrange themselves inside the bilayers of short repeat distance of about 46 Å. We deduce that this bilayer structure is still intact after addition of 10 wt% IPM, since phase A exhibits a comparable repeat distance like reported for the reference system. Consequently, we conclude that CER[AP] remains to be the driving force for the formation of the bilayer structure, even in the presence of the pene-

tration enhancer. Yet, the lamellar arrangement is strongly impaired and alkyl chain disorder is increased, as seen from the neutron diffraction signals. Selective deuteration proved that indeed, IPM is located in this phase A.

The occurrence of an additional phase indicates that a certain threshold of IPM may be exceeded, which separates together with other model membrane components in a new lamellar structure, phase B. The spacing of the latter is clearly decreased, which could further indicate that the presence of the enhancer causes a certain fluidization of the SC lipid alkyl chains arranged in this phase. This leads to stronger interdigitation of the other SC lipids and consequently to a decrease in the lamellar spacing [27]. Moreover, one could speculate that the bilayer-stabilizing impact of CER[AP] is reduced in phase B, maybe due to a slightly smaller amount of CER being present in this newly formed lamellar structure. A bilayer structure altered in such a way with increasingly disordered alkyl chains due to the presence of IPM would consequently offer a diminished resistance against drug flux and could provide an optimal route for the drug molecules traversing the skin barrier. With regard to the mechanism of the enhancer activity of IPM, it is therefore conceivable that the incorporation of IPM together with its significant bilayer disordering effects strongly contribute to IPM's ability to increase drug flux through the skin. It was already suggested by Brinkmann and Mueller-Goymann [24] that IPM is inserted into the SC lipid bilayers with the isopropyl group anchored in the polar region and the myristoyl chain pointing towards the bilayer center. The present results corroborate the assumption of such an arrangement of IPM. In addition, our study suggests that

IPM might also be completely immersed into the SC lipid bilayers, and that IPM causes phase separation in an oriented quaternary SC lipid model based on CER[AP]. The stabilizing influence of the ceramide present in the membrane seems to be outbalanced by the perturbing effect of the penetration enhancer.

In conclusion, we successfully localized the deuterium-labelled penetration enhancer and could therewith prove the incorporation of IPM into the SC lipid model membrane. In the presence of the lipophilic penetration enhancer IPM, a dense lamellar arrangement of all membrane components in a single phase is hindered. Our results provide direct evidence that IPM's mode of action

as penetration enhancer results from affecting the bilayer architecture of the SC lipids, by introducing phase separation, and by direct perturbation of a proper lamellar arrangement.

Acknowledgements

We thank Evonik Goldschmidt GmbH (Essen, Germany) for the donation of CER[AP]. T.N.E. thanks Evonik Goldschmidt GmbH and the Graduiertenförderung des Landes Sachsen-Anhalt for funding. Granting of beam time and financial assistance by Institut Laue-Langevin (Grenoble, France) is gratefully acknowledged.

References

- Elias PM: Epidermal lipids, membranes, and keratinization. *Int J Dermatol* 1981;20:1–19.
- Potts RO, Francoeur ML: The influence of stratum corneum morphology on water permeability. *J Invest Dermatol* 1991;96:495–499.
- Barry BW, Bennett SL: Effect of penetration enhancers on the permeation of mannitol, hydrocortisone and progesterone through human skin. *J Pharm Pharmacol* 1987;39:535–546.
- Ongpipattanakul B, Burnette RR, Potts RO, Francoeur ML: Evidence that oleic acid exists in a separate phase within stratum corneum lipids. *Pharm Res* 1991;8:350–354.
- Goldberg-Cettina M, Liu P, Nightingale J, Kurihara-Bergstrom T: Enhanced transdermal delivery of estradiol in vitro using binary vehicles of isopropyl myristate and short-chain alkanols. *Int J Pharm* 1995;114:237–245.
- Müller-Goymann CC, Mitriakina S: Synergistic effects of isopropyl alcohol (IPA) and isopropyl myristate (IPM) on the permeation of betamethasone-17-valerate from semisolid pharmacopoeia bases. *J Drug Delivery Sci Technol* 2007;17:339–346.
- Arellano A, Santoyo S, Martin C, Ygartua P: Influence of propylene glycol and isopropyl myristate on the in vitro percutaneous penetration of diclofenac sodium from carbopol gels. *Eur J Pharm Sci* 1998;7:129–135.
- Brinkmann I, Mueller-Goymann CC: Role of isopropyl myristate, isopropyl alcohol and a combination of both in hydrocortisone permeation across the human stratum corneum. *Skin Pharmacol Appl Skin Physiol* 2003;16:393–404.
- Engelbrecht T, Hauss T, Suss K, Vogel A, Roark M, Feller SE, Neubert RHH, Dobner B: Characterisation of a new ceramide EOS species: synthesis and investigation of the thermotropic phase behaviour and influence on the bilayer architecture of stratum corneum lipid model membranes. *Soft Matter* 2011;7:8998–9011.
- Groen D, Gooris GS, Barlow DJ, Lawrence MJ, van Mechelen JB, Deme B, Bouwstra JA: Disposition of ceramide in model lipid membranes determined by neutron diffraction. *Biophys J* 2011;100:1481–1489.
- Schröter A, Kessner D, Kiselev MA, Hauss T, Dante S, Neubert RHH: Basic nanostructure of stratum corneum lipid matrices based on ceramides [EOS] and [AP]: a neutron diffraction study. *Biophys J* 2009;97:1104–1114.
- Kiselev MA: Conformation of ceramide 6 molecules and chain-flip transitions in the lipid matrix of the outermost layer of mammalian skin, the stratum corneum. *Crystallogr Rep* 2007;52:525–528.
- Kiselev MA, Ryabova NY, Balagurov AM, Dante S, Hauss T, Zbytovská J, Wartewig S, Neubert RHH: New insights into the structure and hydration of a stratum corneum lipid model membrane by neutron diffraction. *Eur Biophys J* 2005;34:1030–1040.
- Engelbrecht TN, Schroeter A, Hauss T, Neubert RH: Lipophilic penetration enhancers and their impact to the bilayer structure of stratum corneum lipid model membranes: neutron diffraction studies based on the example oleic acid. *Biochim Biophys Acta* 2011;1808:2798–2806.
- Seul M, Sammon MJ: Preparation of surfactant multilayer films on solid substrates by deposition from organic solution. *Thin Solid Films* 1990;185:287–305.
- Franks NP, Lieb WR: Structure of lipid bilayers and the effects of general anaesthetics: an X-ray and neutron diffraction study. *J Mol Biol* 1979;133:469–500.
- Richard D, Ferrand M, Kearley GJ: Analysis and visualisation of neutron-scattering data. *J Neutron Res* 1996;4:33–39.
- Nagle JF, Tristram-Nagle S: Structure of lipid bilayers. *Biochim Biophys Acta* 2000;1469:159–195.
- Worcester DL, Franks NP: Structural analysis of hydrated egg lecithin and cholesterol bilayers. 2. Neutron diffraction. *J Mol Biol* 1976;100:359–378.
- Sears VF: Neutron scattering lengths and cross sections. *Neutron News* 1992;3:26–37.
- Ali MR, Cheng KH, Huang J: Ceramide drives cholesterol out of the ordered lipid bilayer phase into the crystal phase in 1-palmitoyl-2-oleoyl-sn-glycero-3-phosphocholine/cholesterol/ceramide ternary mixtures. *Biochemistry* 2006;45:12629–12638.
- Pata V, Dan N: Effect of membrane characteristics on phase separation and domain formation in cholesterol-lipid mixtures. *Biophys J* 2005;88:916–924.
- Ouimet J, Lafleur M: Hydrophobic match between cholesterol and saturated fatty acid is required for the formation of lamellar liquid ordered phases. *Langmuir* 2004;20:7474–7481.
- Brinkmann I, Mueller-Goymann CC: An attempt to clarify the influence of glycerol, propylene glycol, isopropyl myristate and a combination of propylene glycol and isopropyl myristate on human stratum corneum. *Pharmazie* 2005;60:215–220.
- Kessner D, Kiselev MA, Hauss T, Dante S, Wartewig S, Neubert RH: Localisation of partially deuterated cholesterol in quaternary SC lipid model membranes: a neutron diffraction study. *Eur Biophys J* 2008;37:1051–1057.
- Ruettinger A, Kiselev MA, Hauss T, Dante S, Balagurov AM, Neubert RH: Fatty acid interdigitation in stratum corneum model membranes: a neutron diffraction study. *Eur Biophys J* 2008;37:759–771.
- Zhang RT, Sun WJ, Tristramnagle S, Headrick RL, Suter RM, Nagle JF: Critical fluctuations in membranes. *Phys Rev Lett* 1995;74:2832–2835.

4 FINAL DISCUSSION AND PERSPECTIVES

This thesis aimed at the investigation of structural properties of various oriented SC lipid model membranes with different composition. Furthermore, the impact of CER species with differing head group architecture on the bilayer assembly of the lipid model systems was studied. In addition, the mode of action of two representative penetration-promoting substances with lipophilic character was elucidated on a molecular scale.

4.1 The SC lipid bilayer morphology and the influence of phytosphingosine- and sphingosine-type CER species

For the maintenance of an efficient and penetration-rate limiting skin barrier, the CER fraction of the SC extracellular lipid matrix is generally accepted to play a key role [192], for which reason this outstanding class of SC lipids has been in the focus of extensive research efforts during the past decades [1, 4, 47, 50, 54, 99, 193]. Detailed knowledge about the function of each CER subclass might significantly contribute to a better understanding of structural mechanisms in skin disorders and to the development of new target-oriented concepts for dermal and transdermal treatments. However, the exact relationship between CER structure and function is not yet fully elucidated. Consequently, to provide new insights into this topic the first step was to investigate the importance of different CER species for the formation of a stable lamellar SC lipid assembly, which is regarded as a prerequisite for the maintenance of an efficient skin penetration barrier. Complex biological material as found within the native SC lipid matrix is not suited for such an approach, since the compositional heterogeneity of the SC lipid matrix hinders a systematic evaluation of the influence of particular CER subspecies. Thus, the present work is based on the approach of studying simplistic multilamellar SC lipid model systems.

As reported previously, the bilayer architecture of a quaternary SC model is significantly determined by CER[AP] [3, 4] whose protruding influence was assumed to result from the high polarity of the CER head group and the phytosphingosine backbone. To widen the existing knowledge about the importance of the phytosphingosine-type CER subclass for the barrier integrity, a new ternary SC lipid model matrix was established containing CHOL, stearic acid (SA) and CER[NP], another phytosphingosine-based CER subclass constituting a major part of the CER fraction in

human SC [194]. This CER has only three OH groups in the head group region in comparison to four OH groups in CER[AP]. As the most interesting result of the interdisciplinary approach using neutron diffraction and ^2H NMR spectroscopy, the ternary model membrane CER[NP]/SA/CHOL showed a phase-separated dense and extremely impervious lamellar assembly where water was completely absent. The poor hydration of the SC lipid matrix in human skin is well known [88, 195], but a thin water layer of approximately 1 Å in thickness allows at least for $\text{H}_2\text{O}/\text{D}_2\text{O}$ exchange (contrast variation) in the quaternary model membrane CER[AP]/CHOL/PA/ChS, referred to as *reference system* [3]. This was clearly not the case for the CER[NP]-based model system studied here. Typically, the head group of one CER molecule binds approximately one molecule H_2O [196], but in presence of CER[NP] it seems that water penetration into the head group region is completely hindered. A plausible reason for this observation is most probably the occurrence of phase-separated CER[NP] which prefers a V-shaped arrangement [197, 198] stabilized by the strong network of intra- and intermolecular hydrogen bonds [199, 200]. The resulting dense assembly of V-shaped CER molecules prevents any diffusion of water into the interlamellar spaces and accounts for the lack of D_2O contrast variation that was observed here and already described previously for films made up of CER[NP] [201, 202]. The V-shaped assembly of CER[NP] might furthermore explain the detected increase of the lamellar repeat distance at increased temperature by an expansion of the angle between the CER alkyl chains. The second observed lamellar phase accommodating CHOL, SA and a part of the CER molecules was highly ordered even at 80°C. This finding underlines the stabilizing effects of CER[NP] representing the driving force for the other membrane components to arrange themselves inside the densely packed bilayer assembly. Interestingly, contrast variation was observed for this phase, indicating that the CER[NP] arrangement must differ from the V-shaped structure in such a way that penetration of H_2O into the head group region and its exchange with D_2O is possible. We conclude that CER[NP]'s intra- and intermolecular hydrogen bonds are considerably weakened due to the higher temperature, which facilitates water penetration into the loosened structure at 99 % RH. Due to the highly hydrophobic character of CER[NP], the increased RH induced a distinct hydration pressure to the lipid lamellae, which resulted in the segregation of SC lipids with higher water affinity into the second phase. The reversible formation of this phase at 80°C and 99 % RH, and its disappearance at 80°C and low humidity of 58 % under-

line the distinct hydration characteristics of the CER[NP]-based model, which have never been described before for the CER[AP]-based membranes. In addition, we compared the ternary model membrane based on either CER[NP] or CER[AP] besides CHOL and perdeuterated SA (SA- d_{35}) with regard to the motional freedom of the deuterated fatty acid chain by using ^2H NMR spectroscopy. The results revealed a restricted mobility of SA- d_{35} owing to a condensation of SC lipid packing in presence of CER[NP], which accounts for enhanced alkyl chain rigidity. This effect is most probably mediated by the OH groups of the phytosphingosine-backbone being in an optimal position for the formation of stabilizing intra- and intermolecular hydrogen bonds. The resulting proximity of the CER head groups involves a dense arrangement of the CER alkyl chains reinforcing the bilayer backbone. In contrast, the one additional α -hydroxy group in CER[AP] was shown to perturb the densely packed arrangement and to cause slightly decreased order parameters with a less tight packing of SA- d_{35} . This result impressively underlines that small changes in the head group architecture of the CER species may have pronounced impact on the overall bilayer architecture of the SC lipid model membranes. One can deduce that comparable effects may also occur in the case of unphysiological states of skin accompanied by barrier impairment. Altered SC lipid profiles and absence of CER subclasses enhancing the lipid chain rigidity could result in architectural alterations of the extracellular SC lipid bilayers and a less condensed lipid arrangement. These relationships have already been subject to research efforts, however the mechanisms are not yet fully understood and require further clarification on a molecular scale. The present results may contribute to an enhanced understanding of the nanostructural alterations taking place in the lamellar architecture of the extracellular SC lipid matrix. It would further be of particular interest to enhance the barrier properties in impaired unphysiological states by applying compounds intensifying the SC lipid interactions. Such penetration-retarding characteristics due to increased chain rigidity and condensed lipid packing have been reported [203] and should, based on the actual findings, be also considered for the CER[NP] subclass. Consequently, the development of suitable vehicles for dermal application of e.g. CER[NP] constitutes the remaining challenge [204]. Summing up, the present results highlight the protruding impact of the short-chain phytosphingosine-type CER subspecies for the formation of stable SC lipid bilayer structures. Those effects are most probably founded on the high polarity of the phytosphingosine backbone and the resulting stabilizing hydrogen bond

network. Finally, we could successfully prove that SC research benefits from interdisciplinary approaches in order to gain a more comprehensive insight into the molecular structure of the skin penetration barrier.

Besides confirming the protruding role of the short-chain phytosphingosine-type CER for the bilayer stability, we were interested in the structural properties of model membranes containing both sphingosine- and phytosphingosine-type CER species. Of particular interest is the very long-chain CER[EOS] being often discussed as a prerequisite for the formation of the LPP due to its outstanding chemical structure. Numerous studies on SC lipid model systems containing several CER subspecies exist, with some reporting the existence of a lamellar 130 Å spacing [99, 103, 205, 206], while others do not corroborate the existence of the LPP but again state a protruding role of CER[AP] even in presence of CER[EOS], which is forced to fit into a short periodicity phase (SPP) [1, 102]. In this context, the impact of a novel and artificial CER[EOS] species with a methyl-branched and saturated ω -acyl chain on the bilayer architecture of a quaternary CER[AP]-based SC lipid model membranes was investigated. We were interested whether the protruding influence of CER[AP] can be outbalanced by adding another CER compound with stabilizing effects on the bilayer assembly. Since the new compound denoted as CER[EOS]_branched lacks unsaturation, its very long side chain might exhibit a more rigid character and could hence stabilize the LPP, thereby exceeding the impact of CER[AP] enforcing the SPP. Thus, differences in alkyl chain packing behaviour and consequently in the thermotropic phase behaviour were expected to occur for CER[EOS]_branched and CER[EOS], appearing as e.g. higher temperature of the main phase transition or clear hints for higher alkyl chain order in the case of CER[EOS]_branched. Additionally, there are intimations in literature regarding penetration-reducing effects of fatty acid species with branched structures [207] whose penetration retarder activity presumably results from increased alkyl chain order and rigidity [203]. It was to evaluate if the artificial CER[EOS]_branched also exhibits increased alkyl chain order, and if it consequently has similar reinforcing effects on SC lipid lamellae. Such stabilizing effects could be of importance to prevent or postpone the penetration of harmful agents [104]. Interestingly, DSC and Raman measurements revealed comparable thermotropic phase behaviours for both CER species, neither an increased state of alkyl chain order nor a higher temperature of main phase transition was detected for the artificial compound. Hence, it was concluded that although the two *cis* double

bonds present in naturally occurring CER[EOS] are substituted by a saturated alkyl moiety, the packing behaviour of the CER alkyl chains is not altered. From these findings, penetration retarder effects are not expected for the artificial pendant CER[EOS]_branched. To verify whether also the SC lipid packing in an oriented quaternary model membrane remains unaffected by the exchange of the ω -linoleoyl moiety with an ω -(10-methyl) palmitoyl chain, the oriented model membrane CER[EOS]_branched/CER[AP]/BA/CHOL was studied by means of neutron diffraction. The nanostructural organization of the lipid bilayer was then compared to the model CER[EOS]/CER[AP]/BA/CHOL that was already described previously [102]. Indeed, like already indicated by the DSC and Raman studies, both CER[EOS] species show comparable alkyl chain packing properties and hence induce similar SC lipid arrangements in oriented model membranes. Neither was the LPP observed for the membrane containing the artificial saturated species nor for the one with the naturally occurring compound. Apparently, the methyl-branched ω -acyl chain does not provide the rigidity effects that are probably required for the stabilization of an elongated LPP in presence of the short-chain CER[AP]. The detected lamellar repeat distance of about 48 Å can be interpreted as an SPP assembly, which again is dictated by the polar and short-chain phytosphingosine-type CER subclass according to the structure described previously [1, 102]. The experimental results can be explained with the methyl branching present at the C-10 position of the ω -palmitoyl moiety hindering a rigid and dense assembly of the long acyl chain by introduction of enhanced mobility and *gauche* defects. This hindrance is of the same quality as introduced by the two unsaturated bonds present in the native CER[EOS]. Consequently, CER[AP] remains the driving force dictating the lamellar nanostructure of this quaternary model membrane. Based on the presented experimental findings, an arrangement of the SC lipids in an extended 130 Å phase seems unlikely for the studied quaternary model membrane since the *gauche* defects in the terminal acyl moiety increase mobility, thereby preventing the formation of a sufficiently rigid bilayer backbone required for the stabilization of the long lamellar phase. This result also provides new arguments for the debate regarding the existence of the LPP and underlines that the importance of the ω -acyl-type CER species for the SC lipid bilayer morphology often found in literature [94, 100, 206] might be in some respects overrated. The proposed arrangement of CER[EOS], with its exceptional long-chain structure assembled into the SPP by spanning its amide-bound acyl chain through the whole bilayer unit cell

and extending the ω -acyl moiety through the head group area into the adjacent bilayer [102] likewise applies to the CER[EOS]_branched based model membrane. The proposed arrangement was corroborated by the calculated NSLD profiles, which exhibit slight variations most probably attributed to the chemical variation of the ω -acyl chain, i.e. the varying number of hydrogen atoms due to the presence or absence of the unsaturation and methyl branch. These findings underline the sensitivity of the neutron diffraction technique to small structural alterations of the SC lipids. Finally, all-atom molecular dynamics (MD) simulations proved the accuracy of the proposed structural bilayer arrangement of CER[EOS]_branched stretching through a short CER[AP]-induced lamellar SC lipid assembly. Yet most surprisingly, a small population of the ω -acyl CER obviously inserts its branched acyl chain into the same bilayer by folding back at the ester group position. This assembly of ω -acyl chain CER species has not been described before but might also represent a possibility to insert the long-chain CER present in the SC intercellular matrix into the SPP. Our results demonstrate that the artificial CER[EOS]_branched may serve as pendant to the naturally occurring CER[EOS] for the purpose of structural investigation of oriented SC lipid model membranes. Due to the lack of unsaturated moieties being sensitive to oxidative alterations, the artificial CER species offers improved storage stability being advantageous for preparation and storage of oriented SC lipid model membranes. Handling and processing of the substance is therefore more convenient in terms of chemical stability. In this approach we could again highlight the advantage of combining different techniques to receive more information about the structural properties of the lamellar SC lipid assembly, since the surprising finding of folded CER[EOS] molecules would not have been detected from the diffraction data without computational assistance and MD simulation.

4.2 Mode of action of two representative lipophilic penetration enhancers on the lamellar architecture of SC lipid multilayers

There is substantial interest in dermal or transdermal application of pharmaceuticals, especially for particular groups of patients [208]. In addition to modern carrier systems developed for improving the dermal and transdermal drug delivery, penetration enhancers are used for this purpose as well. Consequently, the second important task of this work was to shed a light on the molecular mechanisms of pene-

tration enhancement activity, whereby the focus was placed in particular on penetration enhancer species influencing the lipophilic penetration pathway and interacting with the intercellular SC lipid matrix. Modelling the lamellar SC lipid assembly with oriented SC lipid membranes and studying their bilayer architecture using neutron diffraction thereby provides detailed insights into the molecular mode of action of the enhancer species within the model bilayers. As representative model compounds, oleic acid (OA) was chosen from the enhancer substance class of unsaturated fatty acids, and isopropyl myristate (IPM) was selected from the group of pharmaceutical waxes. Both penetration enhancer subclasses exhibit a high lipophilicity and therefore have a distinct affinity to the lipophilic SC lipid model membranes. Each of the two selected compounds has been in the focus of previous research efforts, but the presented results are the first received by applying the technique of neutron diffraction combined with selective deuterium labelling. Thereby, the present work could elucidate the mode of action of these penetration promoters on a nanoscale. For comparability reasons, the same quaternary SC lipid model membrane (the *reference system*, CER[AP]/CHOL/PA/ChS) was chosen as basis for studying the effect of both enhancers. Explicit knowledge regarding the detailed molecular mechanisms of penetration enhancing agents interacting with the extracellular SC lipid matrix is essentially needed for the further development of new dermal and transdermal formulations, hence the present results regarding the mode of action of IPM and OA might be of particular interest in this field.

The enhancer activity of *cis*-unsaturated OA is well known [126, 134, 209]. Here, its effect on the molecular structure of oriented SC lipid model membranes was studied for the first time using combined neutron diffraction and deuterium labelling technique. Due to the low scattering intensity resulting from limited neutron flux it was decided to add an amount of 10 % (m/m) of OA allowing for sufficient strength of the deuterium label. Contrary to other reports, the present findings indicate that this amount is completely incorporated into the SC lipid bilayers of the quaternary *reference system* without any indication of co-existing phase-separated lamellar domains as described before [6, 129]. Although the specific molecular structure of OA featuring a kink is likely to provoke phase separation by hindering a simultaneous arrangement of OA in the SC lipid bilayers [6] and extracting some lipid fractions into separate domains [132], such an effect was not observed in this study. This unexpected finding might be attributed to the different sample preparation procedures re-

sulting in SC lipid model systems with different properties in terms of bilayer curvature and state of hydration (curved SC lipid bilayer in the case of vesicle dispersions [6, 132] and planar multilayers in the case of model membranes). We cannot preclude the OA-mediated phase separation under *in vivo* conditions in human SC, but at least for the studied quaternary SC model membrane, this mechanism can be ruled out to contribute to OA's mode of action. Equal values of the lamellar spacing d detected for the enhancer-containing and the corresponding enhancer-free *reference system* indicate the absence of significant lipid alkyl chain fluidization which otherwise would become apparent as shrinking of the periodic spacing of the bilayer unit cell due to increased *gauche* conformers, increased terminal alkyl chain mobility and consequently stronger chain interdigitation. However, the diffraction results revealed a state of severely impaired lamellar order for the OA-based model membrane in comparison to the enhancer-free *reference system*. Although the lamellar SC lipid arrangement is still intact probably due to the stabilizing and reinforcing effects of CER[AP], the presence of OA apparently induces alkyl chain disorder and a distinct perturbation of the lamellar SC lipid assembly resulting in diminished scattering signals. This finding can be explained by the exceptional chemical structure of OA: its *cis* double bond between C9 and C10 results in a bended molecular arrangement, where the terminal alkyl chain possesses a high degree of motional freedom and only the alkyl moiety between carboxyl group and the unsaturation contributes to a dense lipid chain packing [210]. Consequently, the insertion of OA requiring more space due to its kinked structure will change the bilayer lipid arrangement in terms of loosened chain packing. Such a disruption of the continuous lamellar assembly of the other membrane components after insertion of the highly flexible and bended OA molecules as observed here was also reported previously [125]. The SC lipids disordered by OA are less resistant against the diffusion of agents, which would ideally explain the mode of action of this lipophilic penetration enhancer species. Based on the present results we draw the conclusion that intercalation into the SC lipid lamellae, alkyl chain disordering effects and impairment of the bilayer assembly constitute the main mode of action for the penetration enhancer of OA. Further evidence for the lipid-disordering effects of OA was provided by DSC measurements of the SC lipid mixture with and without OA. A shift of the main phase transition towards lower temperature was evident from the thermograms recorded for the SC lipid mixture containing 10 % (see Appendix 6.3), which is in line with former reports [211]. The inser-

tion of the enhancer molecules into the SC lipid bilayers was definitely proven by means of the selectively deuterated compound OA- d_2 . Its application additionally allowed for the exact localization of the enhancer molecules within the lamellar unit cell and revealed OA to be anchored with its carboxyl moiety in the bilayer head group area while pointing its alkyl chain towards the bilayer center. The *cis* double bond is located approximately in the middle of one bilayer leaflet, half the way between central and head group region.

In summary it can be stated that the results presented in this work provide new and interesting insights into the mode of action of the penetration promoter OA on a molecular scale. Former reports of OA inducing phase separation were not corroborated by the present study. However, the articulate bilayer disordering effects of OA reported previously were confirmed by the actual findings, indicating that those mechanisms might significantly contribute to OA's enhancer activity.

As second step, the mode of action of the pharmaceutically used liquid wax IPM was investigated. Here, the diffraction results indeed revealed the occurrence of phase separation apparent as segregated lamellar domains. Applying the selectively deuterated compound IPM- d_3 allowed for proving the presence of the deuterium label and therewith of the penetration enhancer in both coexisting bilayer assemblies. The branched molecular structure of IPM apparently constrains the complete mixing of the enhancer and SC lipids. With 10 % (m/m) IPM added, a certain threshold is exceeded and a fraction of the SC lipids is forced into a new lamellar phase together with a part of IPM. The lamellar *d*-spacing of one of the two phases (Phase A) is in the range of the enhancer-free *reference system*, indicating that CER[AP] is the key compound stabilizing this bilayer structure, and that the lamellar architecture is comparable to the *reference system* [4]. However, compared to the *d*-spacing of the OA-containing model membrane, Phase A of the IPM-based system exhibits a slightly enlarged bilayer size. The incorporation of the wax apparently results in a kind of expansion of the CER[AP]-based assembly. This finding can be explained by the specific position of the IPM molecules within the bilayer unit cell revealed by deuterium labelling. Most interestingly, two different arrangements of IPM are conceivable: Some IPM molecules are anchored with their ester group in the bilayer head group region and point their myristoyl chain towards the bilayer center, but another fraction of the wax is completely embedded in the SC lipid bilayers. The latter assembly causes the more hydrophilic ester group to be immersed in the hydrophobic bilayer

region and the myristoyl chain to be spanned through the central bilayer area into the other membrane leaflet. We conclude from the neutron diffraction results that this assembly is thoroughly possible although it initially appears unexpected due to the consequential exposure of the hydrophilic ester group to a highly hydrophobic environment. The possibility of complete insertion of hydrophilic molecular moieties into lipophilic bilayers has been described before [2], and the fact that IPM lacks the typical amphiphilic head-tail structure might support the observed complete intercalation of the lipophilic enhancer molecules. Hence, the complete insertion of IPM might account for the detected expansion of the bilayer unit cell by pushing apart the membrane leaflets. The second lamellar structure observed for the model membrane, Phase B, shows a clearly smaller d -spacing when compared to Phase A, and the application of the selectively deuterated IPM- d_3 revealed the penetration enhancer to be located just at one single position, with the hydrophilic ester moiety positioned at the SC lipid head groups and the acyl chain arranged in the hydrophobic bilayer area. This arrangement stabilized by hydrogen bonds between the SC lipid head groups and hydrophobic interactions of the hydrocarbon chains corresponds with the assembly also observed for a part of IPM in Phase A and is in line with previous reports [142]. The considerably smaller d -spacing of Phase B observed in the present study was concluded to result from fluidizing effects and stronger alkyl chain interdigitation [212] induced by the presence of IPM. Furthermore, significantly increased bilayer disorder due to the addition of the penetration enhancer was detected for both coexisting phases. This perturbation appears plausible since the enhancer molecules exhibit a branched molecular structure. Although the myristoyl moiety can efficiently interact with the hydrocarbon chains of the SC lipids, the isopropyl group located in proximity to the lipids' head groups is likely to influence the required close packing of the SC lipids. The consequence is a loosened SC lipid assembly and increased lamellar disorder due to IPM's intercalation. Additional FT Raman measurements confirmed the strong impact of IPM on the bilayer stability by revealing a higher state of lamellar disorder in presence of IPM (see Appendix 6.4). Based on the assumption of a SC lipid membrane with significantly disordered bilayer structures, it is easy to imagine that this condition provides easier access for agents penetrating into or traversing this lipid matrix. The presence of phase separation as observed here in presence of IPM might furthermore increase the penetrability of the model membrane, as the coexistence of fluid and gel phases was shown to considerably enhance the perme-

ability of membrane structures by enabling the diffusing agents to cross through the interface between gel and fluid phases [213]. Even if the present simplistic model does not resemble the human SC and cannot represent the physiological state of the extracellular lipid matrix, it yet provides an idea about the processes taking place on a molecular scale when the enhancer IPM is added to oriented multilamellar stacks of SC lipids. In conclusion it can be stated that an amount of 10 % (m/m) IPM affects the lamellar architecture of an oriented CER[AP]-based model membrane in terms of induction of phase separation and bilayer disordering. Based on the present findings received from neutron diffraction it appears reasonable that IPM's penetration enhancer activity is significantly based on these two processes.

4.3 Perspective

The SC intercellular lipid lamellae of mammalian skin contain in sum at least 12 CER subclasses. During the last decades, much research effort was placed on the issue of elucidating the role of single subclasses for the formation and maintenance of the skin barrier. Yet, despite some first insights there are several more CER subspecies whose particular function for the stability of the SC lipid lamellae remains unclear. Of particular interest is the investigation of structure-function relationships in order to determine the impact of characteristics of individual sphingolipid subclasses.

It will be necessary to further clarify the role of different CER head group architectures, which appears to be of outstanding importance for the bilayer stability as indicated by the present findings. In this context special attention should be paid to the respective position of the hydrophilic OH groups in the CER head group. For example, the 6-hydroxysphingosine-type CER species also contain three OH groups in the hydrophilic head, like the phytosphingosine-type CER, but in another molecular position. The SC lipid architecture after exchange of CER[NP], e.g. in the ternary model membrane composed of CER[NP]/CHOL/SA (55/25/20, m/m) by CER[NH] and CER[AH] should therefore be studied by neutron diffraction and compared in terms of hydration properties, occurrence of phase separation, and behaviour at varying temperature conditions. This will provide an insight whether the number or the exact position of the OH groups determines the CER's impact on the SC lipid bilayer structure. As the CER[NP]-based model membrane was shown to exhibit exceptional hydration behaviour, it would be of interest whether a considerable interla-

mellar hydration is possible after a sufficient time period. Time-resolved diffraction measurements might further elucidate the hydration kinetics of the CER[NP]-based ternary model membrane.

There is substantial need for innovative formulations for dermal and transdermal drug delivery, and a reversible reduction of the skin barrier properties using penetration enhancers is a valuable approach to increase the amount of active traversing the barrier. Although numerous substance classes with enhancer activity are known, their exact mode of action on a molecular scale is not fully elucidated. Similar studies as the ones performed in the course of the present thesis could provide knowledge regarding the impact of other enhancer species, e.g. terpenes, other unsaturated fatty acids and pharmaceutically used waxes. In addition, the composition of the SC lipid model matrix should be varied (e.g. exchange of the CER species) to clarify possible differences of enhancer activity in dependency of the architecture of the respective model matrix. As a further point of interest the threshold of IPM in the reference system investigated here before the phase separation occurs should be determined. The use of perdeuterated enhancer molecules for FT Raman or ^2H NMR spectroscopic studies could also prove if separate domains enriched with the enhancer molecules are formed in the SC lipid membranes, which are not detectable by means of neutron diffraction.

Finally, it would be of interest to perform diffusion studies of model drugs through SC lipid model systems containing different enhancer species, or different amounts of one specific enhancer. In combination with information regarding structural alterations of the bilayers obtainable by neutron diffraction, additional insights considering the mode of action of the penetration enhancers can be obtained.

5 SUMMARY

5.1 English version

The penetration barrier of mammalian skin resides in its outermost skin layer, the SC. Since the intercellular SC lipid matrix was recognized to represent the major pathway for drug penetration, this remarkable lamellar structure has increasingly attracted interest during recent years. Oriented SC lipid membranes of simplistic composition as studied in this thesis were shown to represent ideal models resembling the structural conditions of the SC lipid lamellae despite their simplicity. The present work addressed the issue of elucidating the way different lipid species modify the morphology of SC lipid model bilayers. Different methodological approaches were applied such as neutron diffraction combined with deuterium labelling for the study of the molecular bilayer structure, and DSC and FT Raman spectroscopy for the investigation of the thermotropic phase behaviour of the lipids. The experimental findings were confirmed using additional techniques like ^2H NMR spectroscopy and MD simulations. The phytosphingosine-type CER[NP] was shown to induce the formation of an exceptional lamellar architecture in a ternary SC lipid model membrane. This structure is characterized by the occurrence of phase separation, an extremely low interlamellar hydration deviating from the behaviour of the likewise phytosphingosine-based CER[AP], and an outstanding lamellar stability even under thermal stress. The SC lipids were shown to be in a true liquid-crystalline and highly ordered state, clearly exceeding the degree of chain order detected in presence of CER[AP]. Consequently, the phytosphingosine-based ceramide subclasses are concluded to be of utmost importance for the stability of the SC lipid bilayer assembly. Next, the equivalence of an artificial CER[EOS] with a branched and saturated ω -acyl chain ("CER[EOS]_branched") and its natural pendant was verified. DSC and FT Raman spectroscopy proved the phase behaviour of CER[EOS]_branched to be comparable to its naturally occurring pendant CER[EOS]. Moreover, the investigated model membranes containing either the artificial or the natural CER[EOS] species besides CER[AP], CHOL and BA exhibited the same bilayer architecture. The assumption that the saturated ω -acyl chain in CER[EOS]_branched might exceed the stabilizing forces of the polar CER[AP] and induce the formation of the LPP was not corroborated. CER[AP] remained to be the driving force for the lamellar lipid arrangement and constrained all other components to fit into the short bilayer structure. For that pur-

pose the long-chain CER[EOS]_branched either spans the long acyl chain through the whole membrane into the adjacent bilayer unit cell, or surprisingly integrates inside one unit cell by folding back the ω -acyl moiety and bending at the carboxyl group. The latter arrangement was revealed by MD simulations and might also apply for CER[EOS]. These findings also underline the protruding role of the phytosphingosine-type ceramides obviously exceeding the impact of the long-chain ω -acyl ceramide species.

In the second part the modes of action of the lipophilic penetration enhancers OA and IPM on the basis of the quaternary model membrane containing CER[AP], CHOL, PA and ChS were verified. For the unsaturated fatty acid OA a significant perturbation of lamellar order of the SC lipid model bilayers was detected. This was attributed to the bended structure of the *cis* unsaturated enhancer molecules. The position of the enhancer was determined using the specifically deuterated compound. Since phase separation was not observed, the bilayer disordering effects were concluded to constitute the major mode of enhancer activity of OA. On the contrary, the branched ester IPM induces phase separation. A specifically deuterated compound was again used for proving the presence of IPM in both coexisting phases and for determination of its exact position. In one of the coexisting phases IPM is accommodated in a surprising arrangement: in addition to the expected assembly of IPM with its ester group anchored in the bilayer head group region and the myristoyl chain stretched to the bilayer center, a second fraction of IPM is completely immersed in the hydrophobic area of the SC lipid bilayers with the tetradecanoyl moiety stretched through the central region into the other bilayer leaflet. Based on the present experimental findings, IPM's mode of action is predominantly founded on induction of phase separation and the likewise observed bilayer perturbation.

To conclude, the present work verified the mode of action of two penetration enhancers on a molecular scale by means of neutron diffraction. In addition, the impact of two different ceramide subclasses on the lamellar architecture of simplistic SC lipid model systems was investigated. The latter were proven to be the appropriate tool to determine the relevance of single SC lipid species for the bilayer stability. Moreover, the present thesis highlights the benefit offered by using multidisciplinary approaches for the purpose of studying the properties of SC lipid model membranes.

5.2 German version

Die Penetrationsbarriere der menschlichen Haut wird von deren äußerster Schicht, dem Stratum corneum gebildet. Die außergewöhnliche lamellare Struktur seiner interzellulären Lipidmatrix stellt die Hauptroute für penetrierende Stoffe dar und hat in den letzten Jahren außerordentliches Interesse ausgelöst. Orientierte Lipidmembranen mit einfacher Zusammensetzung, wie sie in der vorliegenden Arbeit untersucht wurden, stellen trotz ihrer Einfachheit ausgezeichnete Modelle zur Abbildung der strukturellen Besonderheiten der Lipiddoppelschichten des Stratum corneum dar. Die vorliegende Arbeit widmete sich der Fragestellung, auf welche Art und Weise verschiedene Lipidspezies die Nanostruktur von Stratum corneum-Lipiddoppelschichten modifizieren. Dazu wurden mehrere Methoden genutzt, wie zum Beispiel die Neutronenstreuung zusammen mit spezifischer Deuterium-Markierung für die Strukturaufklärung der molekularen Bilayerstruktur, und DSC sowie FT-Raman-Spektroskopie zur Untersuchung des thermotropen Phasenverhaltens der Lipide. Die experimentellen Befunde wurden durch zusätzliche Techniken wie Deuterium-NMR-Spektroskopie und Molecular Dynamics (MD) Simulationen abgesichert und bestätigt.

Im Rahmen dieser Arbeit konnte gezeigt werden, dass das Phytosphingosinbasierte Ceramid NP die Ausbildung einer außergewöhnlichen lamellaren Struktur in einer ternären Stratum corneum-Lipidmodellmembran bewirkt. Diese Struktur zeichnet sich durch das Auftreten von Phasenseparierungen, eine für Ceramid AP nicht beschriebene marginale interlamellare Hydratisierung, sowie eine besondere Stabilität der Doppelschichten auch unter thermischer Belastung aus. Es stellte sich heraus, dass sich die Lipide in einem flüssigkristallinen Zustand befinden, und dass der lamellare Ordnungsgrad im Ceramid NP-basierten System deutlich höher ist als im Ceramid AP-basierten Modell. Es wurde geschlossen, dass die Phytosphingosin-Ceramidklassen eine besondere Bedeutung für die Stabilität der Stratum corneum-Lipiddoppelschichten haben. Im nächsten Schritt wurde die Äquivalenz eines artifiziellen Ceramid EOS-Abkömmlings mit gesättigter und verzweigter ω -Acyl-Seitenkette (CER[EOS]_branched) und des natürlichen Ceramid EOS bewiesen. Messungen mittels DSC und FT-Raman-Spektroskopie zeigten ein vergleichbares thermotropes Phasenverhalten der beiden Verbindungen. Darüber hinaus wurde für Modellmembranen jeweils bestehend aus Ceramid EOS oder Ceramid EOS_branched in Verbindung mit Ceramid AP, Cholesterol und Behensäure die gleiche Membranstruktur er-

mittelt. Die Vermutung, dass durch die gesättigte ω -ständige Seitenkette der nicht natürlich vorkommenden Substanz Ceramid EOS_branched die stabilisierenden Kräfte des polaren Ceramid AP unter Bildung einer LPP unterbunden werden können, wurde nicht bestätigt. Ceramid AP bleibt die entscheidende Triebkraft, welche die anderen Lipide dazu zwingt, sich in einer kurzen lamellaren Phase anzuordnen. Dabei streckt das künstliche Ceramid EOS_branched seine lange Seitenkette durch die Einheitszelle bis in die benachbarte Doppelschicht, oder es integriert sich interessanterweise durch ein Umknicken an der Estergruppe und entsprechendes Zurückfalten der ω -Acyl-Seitenkette in die ursprüngliche Doppelschicht. Diese molekulare Anordnung wurde mittels MD Simulationen gefunden und ist gleichermaßen denkbar für das natürlich vorkommende Ceramid EOS. Auch diese Ergebnisse stellen die besondere Bedeutung der Phytosphingosin-Ceramidklassen heraus, welche den Einfluss der langkettigen ω -Acylceramide deutlich übertreffen.

Im zweiten Teil der Arbeit wurde der Wirkmechanismus der lipophilen Penetrationenhancer OA und IPM anhand einer quaternären Modellmembran basierend auf Ceramid AP, Cholesterol, Palmitinsäure und Cholesterolsulfat untersucht. Für die ungesättigte Fettsäure OA wurde eine erhebliche Störung der lamellaren Ordnung innerhalb der Lipiddoppelschichten detektiert, was der gekrümmten Struktur der *cis*-konfigurierten ungesättigten Enhancermoleküle zugeschrieben werden kann. Mittels der spezifisch deuterierten Ölsäure-Spezies OA- d_2 konnte die exakte Position des Enhancers bestimmt werden. Phasenseparierungen wurden nicht beobachtet und es wurde geschlossen, dass das Auslösen lamellarer Unordnung den Hauptwirkungsmechanismus des Penetrationenhancers OA darstellt. Im Gegensatz dazu bewirkt die verzweigtkettige Struktur des flüssigen synthetischen Wachses IPM das Auftreten von Phasenseparierungen. Mittels der spezifisch deuterierten Spezies IPM- d_3 wurde der Beweis erbracht, dass die Enhancermoleküle in beiden lamellaren Phasen zugegen sind. Darüber hinaus wurde auch hier die exakte Position des Penetrationenhancers bestimmt. In einer der beiden nebeneinander vorliegenden Phasen ist IPM in ungewöhnlicher Weise angeordnet: zusätzlich zur erwarteten Position, bei der IPM mit seiner Estergruppe im hydrophilen Kopfgruppenbereich der Stratum corneum-Lipiddoppelschicht verankert ist und die Myristoylseitenkette zur Bilayermitte zeigt, existiert noch eine zweite Möglichkeit der Anordnung. Bei dieser sind die Moleküle des synthetischen Wachses IPM vollständig in den hydrophoben Bereich der Lipiddoppelschichten eingelagert. Dabei erstreckt sich die Tetradecanoylseitenkette

über die Bilayermitte hinaus in die andere Hälfte der Doppelschicht. Eine Störung des lamellaren Ordnungszustandes wurde in den experimentellen Ergebnissen für IPM ebenfalls beobachtet, was hier in Kombination mit der Erzwingung von Phase-separation als Hauptmechanismus der Wirkung des synthetischen Wachses IPM als Penetrationsenhancer angesehen wurde.

Abschließend lässt sich sagen, dass im Rahmen der vorliegenden Arbeit die molekularen Wirkmechanismen von zwei Penetrationsenhancer-Spezies mittels Neutronenstreuung aufgeklärt wurden. Darüber hinaus wurde der Einfluss zweier Ceramidsubklassen auf die Morphologie einfacher Stratum corneum-Lipidmodellsysteme untersucht. Es konnte gezeigt werden, dass solche orientierten Systeme einen idealen Ansatz darstellen, um die Bedeutung einzelner Stratum corneum-Lipidspezies für die Stabilität der lamellaren Strukturen zu bestimmen. Darüber hinaus wird durch die vorliegende Arbeit hervorgehoben, dass ein multidisziplinärer Ansatz basierend auf der Kombination mehrerer Methoden von entscheidendem Vorteil für die Strukturuntersuchung von Stratum corneum-Lipidmodellmembranen ist.

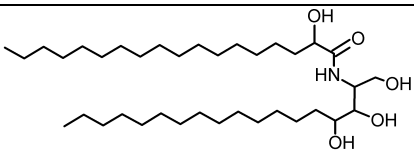
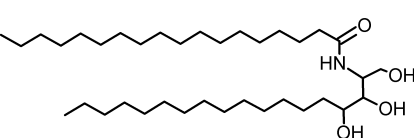
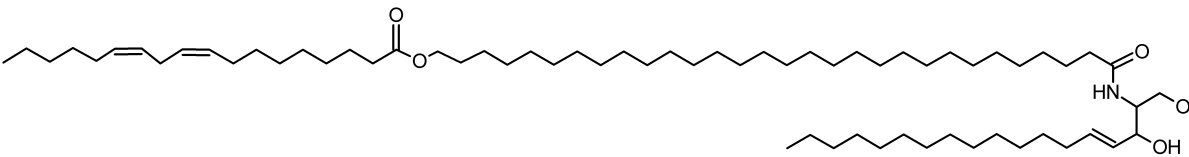
6 APPENDIX

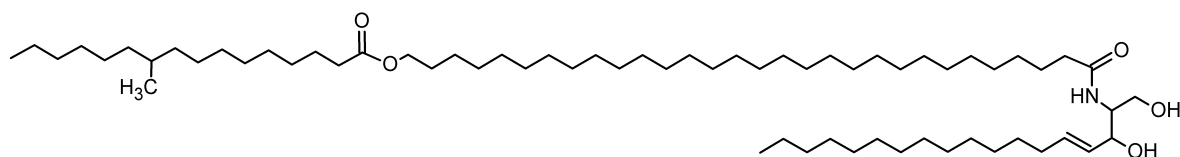
6.1 List of Substances

In this section, all substances used for the experiments performed in the course of the present thesis are listed.

SC lipids used for the preparation of oriented model membranes

The CER species used for preparing oriented multilamellar SC models were generously provided by Evonik Goldschmidt (Essen, Germany), except the artificial CER[EOS]_branched, which was received from a synthetic procedure. The latter, and the origin of all substances used for the chemical synthesis are described in detail in chapter 3.1.2. All chemical structures are listed in Table A 1. The purity of the CER species was $\geq 96\%$, hence the substances were used as received, except for the ω -acyl ceramide CER[EOS]. The substance was purified by middle-pressure liquid chromatography using gradient technique and chloroform/methanol as eluents on a silica gel column to increase the purity. Mass spectrometry was used to prove the identity of the substance.

	<p>N-(α-hydroxy-octadecanoyl)- phytosphingosine, CER[AP]</p>
	<p>N-(octadecanoyl)-phytosphingosine, CER[NP]</p>
 <p>30-linoyloxy-triacontanoyl-sphingosine, CER[EOS]</p>	



30-(10-methylhexadecanoyloxy) triacontanoyl-sphingosine,

CER[EOS]_branched

Table A 1: Chemical structures of the synthetic CER species used for preparing oriented SC lipid model membranes.

The other SC lipids like CHOL, ChS, and the protonated FFA species (behenic acid, palmitic acid, stearic acid, oleic acid) were purchased from Sigma Aldrich (Taufkirchen, Germany) and used as received. The selectively deuterated CHOL-25,26,26,26,27,27,27- d_7 was purchased from Avanti Polar Lipids (Alabaster, AL, USA). The perdeuterated stearic acid (stearic acid- d_{35}) was used as received from Dr. Ehrenstorfer (Augsburg, Germany). The protonated ester isopropyl myristate (IPM) was purchased from Sigma Aldrich (Taufkirchen, Germany) and used as received. The deuterated fatty acid oleic acid-9,10- d_2 (OA- d_2) was received from Larodan Fine Chemicals (Malmö, Sweden) and used without further purification. The specifically deuterated ester isopropyl myristate-14,14,14- d_3 (IPM- d_3) was received from chemical synthesis. A detailed description of the synthetic procedure, and the origin of all materials used for the synthesis can be found in chapter 3.2.2. The deuterated compound myristic acid-14,14,14- d_3 required as precursor was purchased from Larodan Fine Chemicals (Malmö, Sweden) and used as received, while isopropanol, the second precursor for the synthetic procedure was received from Sigma Aldrich (Taufkirchen, Germany) and also used as received. All these lipids are listed in Table A 2.

	cholesterol, CHOL
	sodium cholesteryl sulphate, cholesterol sulphate, ChS

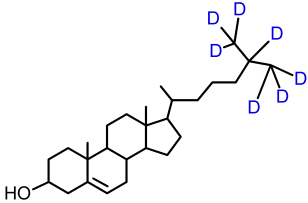
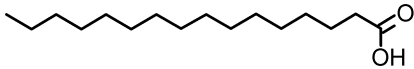
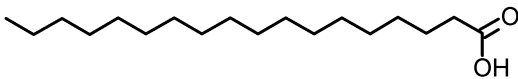
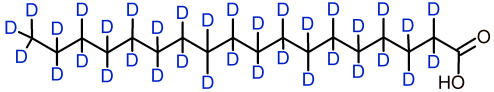
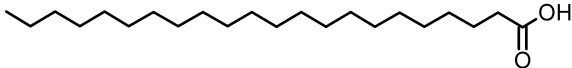
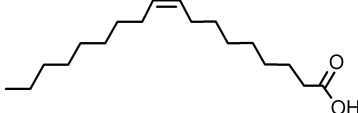
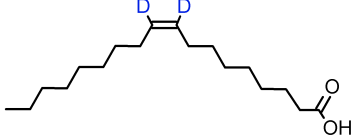
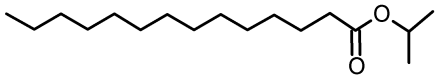
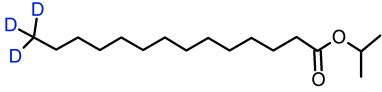
	cholesterol-25,26,26,26,27,27,27- d_7 CHOL- d_7
	palmitic acid, PA
	stearic acid, SA
	stearic acid- d_{35} , SA- d_{35}
	behenic acid, BA
	cis-9-octadecenoic acid, oleic acid, OA
	oleic acid-9,10- d_2 , OA- d_2
	tetradecanoic acid isopropyl ester, isopropyl myristate, IPM
	isopropyl myristate-14,14,14- d_3 , IPM- d_3

Table A 2: A list of the other synthetic SC lipids and penetration enhancers used for sample preparation.

Other substances and equipment used

The solvents used for sample preparation or for the chromatographic purification of the SC lipids (chloroform, methanol, heptane, ether) were of analytical grade. Organic solvents used for the synthetic procedures were of analytical grade and distilled and dried before use. Substances for the synthetic procedures mentioned in the respective chapters 3.1.2 and 3.2.2, the buffer substances for hydrating the oriented

SC lipid model membranes as mentioned in chapter 3.2.1 and 3.2.2, the salts for adjustment of a certain relative humidity during the neutron diffraction experiments, sodium bromide and potassium sulphate, were of analytical grade and received from Sigma Aldrich. Water was demineralized before use. The D₂O for the neutron diffraction experiments was supplied by HZB, Germany (for experiments performed at V1, received from Sigma Aldrich), or supplied by the ILL, France (experiments at D16). An airbrush instrument (Harder & Steenbeck, Norderstedt, Germany) was used with constant air flow for the deposition of the lipids on quartz substrates to create oriented model membranes.

6.2 Composition of the oriented SC lipid model membranes studied in the present thesis

This section provides an overview of the oriented SC lipid model membranes investigated in the course of the present thesis.

Simplistic SC lipid model membranes investigated

In the following table a list of the investigated SC lipid model membranes can be found.

Sample name	Components	Ratio (m/m)
Basic*	CER[AP]/CHOL/PA/ChS	55/25/15/5
Basic_OA	CER[AP]/CHOL/PA/ChS/OA	49.5/22.5/13.5/4.5/10
Basic_OA- <i>d</i> ₂	CER[AP]/CHOL/PA/ChS/OA- <i>d</i> ₂	49.5/22.5/13.5/4.5/10
Basic_IPM	CER[AP]/CHOL/PA/ChS/IPM	49.5/22.5/13.5/4.5/10
Basic_IPM- <i>d</i> ₃	CER[AP]/CHOL/PA/ChS/IPM- <i>d</i> ₃	49.5/22.5/13.5/4.5/10
	CER[NP]/CHOL/SA	55/25/20
	CER[AP]/CHOL/SA	55/25/20
	CER[EOS]/CER[AP]/BA/CHOL	23/10/33/33
	CER[EOS]_branched/CER[AP]/BA/CHOL	23/10/33/33

Table A 3: The sample compositions, all given in mass ratio (*: also termed reference system).

Complex SC lipid model membrane approximating the physiological lipid constitution of human SC

To approximate the physiological state present in the SC intercellular lipid matrix, a model membrane with more complex composition was established and subsequently subjected to neutron scattering experiments. According to literature reports on the SC lipid composition in human SC [194], the following composition (given in mass ratio, m/m) was chosen:

CER fraction		FFA fraction		CHOL	ChS
50		25		20	5
CER[EOS]	20	C16:0	10		
CER[NP]	60	C18:0	10		
CER[AP]	20	C18:1	5		
		C20:0	10		
		C22:0	10		
		C24:0	30		
		C26:0	25		

Table A 4: Lipid composition of the more complex SC model membrane given in mass ratio.

6.3 The effect of OA on the SC lipid architecture: DSC measurements

For the purpose of confirming the bilayer disordering effects of OA, additional DSC measurements were performed to investigate the thermotropic phase behaviour of the SC lipid model system of the composition CER[AP]/CHOL/PA/ChS/OA (49.5/22.5/13.5/4.5/10, m/m). The thermograms were recorded for the first, second and third heating scan and subsequently compared with the thermograms for the enhancer-free reference system as displayed in Fig. A 1. A clear shift of the main phase transition temperature towards lower values indicates a loosened SC lipid packing behaviour. The thermal energy required to “break” the forces stabilizing the bilayer backbone are significantly decreased when OA is present, indicated by lower transition enthalpies and decreased onset temperatures of the transition peaks. This cor-

roborates the results obtained from neutron diffraction suggesting the induction of bilayer disorder as a major mode of action for the penetration enhancer OA.

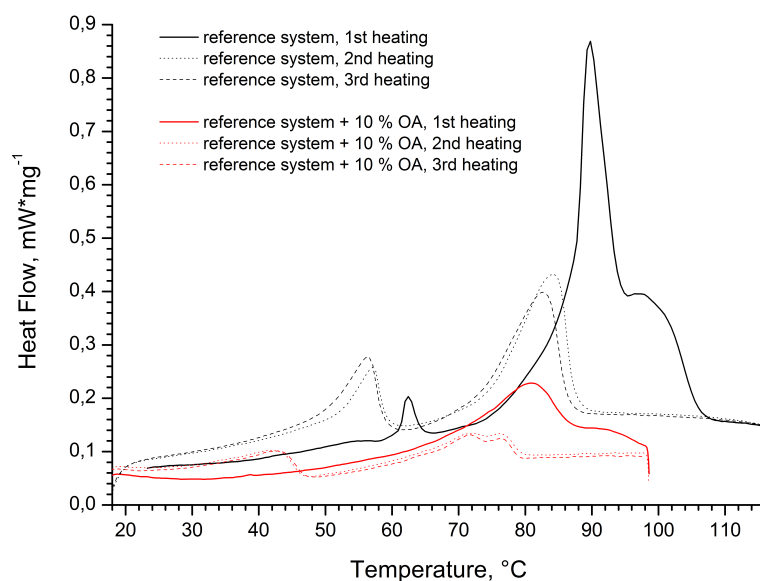


Fig. A 1: Thermograms recorded during the first, second and third heating scan of the enhancer-free reference system and the according model system containing 10 % OA.

6.4 The impact of IPM on the SC lipids: FT Raman spectroscopy

Additional FT Raman spectroscopic measurements were performed in order to verify the impact of IPM on the SC lipid alkyl chain packing and the thermotropic phase behaviour of the model system composed of CER[AP]/CHOL/PA/ChS/IPM (49.5/22.5/13.5/4.5/10, m/m). Data evaluation was focused on the band position of the symmetric CH₂ stretching mode $\nu_{sym}(\text{CH}_2)$ in dependency of T. The lower the band position, the higher the state of order [172, 177], which makes this Raman mode an ideal marker for monitoring the decreasing order upon heating. When the thermal energy applied to the system is sufficiently high, the start of the chain melting appears as abrupt shift of the band position by about 1 cm⁻¹ within a small T range.

While the enhancer-free reference system exhibits a strong shift of the position of $\nu_{sym}(\text{CH}_2)$ around 70-75°C [214], such an abrupt change is not observed for the present SC lipid mixture containing the enhancer IPM where the band position raises more or less constantly, with only a slight implied “jump” beginning around 55°C during the first scan (Fig. A 2). This indicates the disordering influence of IPM, which

induces bilayer perturbation and *gauche* defects. The already disordered bilayers experience thermal influence, and consequently the degree of motional freedom and the number of *gauche* conformers increase, yet not in a sudden but a constant way. During the second heating scan, a small additional “peak” around 45°C might indicate a kind of pre-transition suggesting that a fraction of the SC lipids loses the ordered gel structure and exhibits increased chain disorder already at lower T. A possible explanation could be that a part of SC lipids together with a higher fraction of IPM is located in a separate, maybe fluidized domain, which exhibits less dense chain packing and consequently gets disordered prior to the other SC lipid assembly.

This corroborates the results obtained from neutron diffraction suggesting the induction of bilayer disorder and phase separation as mechanisms of IPM’s enhancer activity.

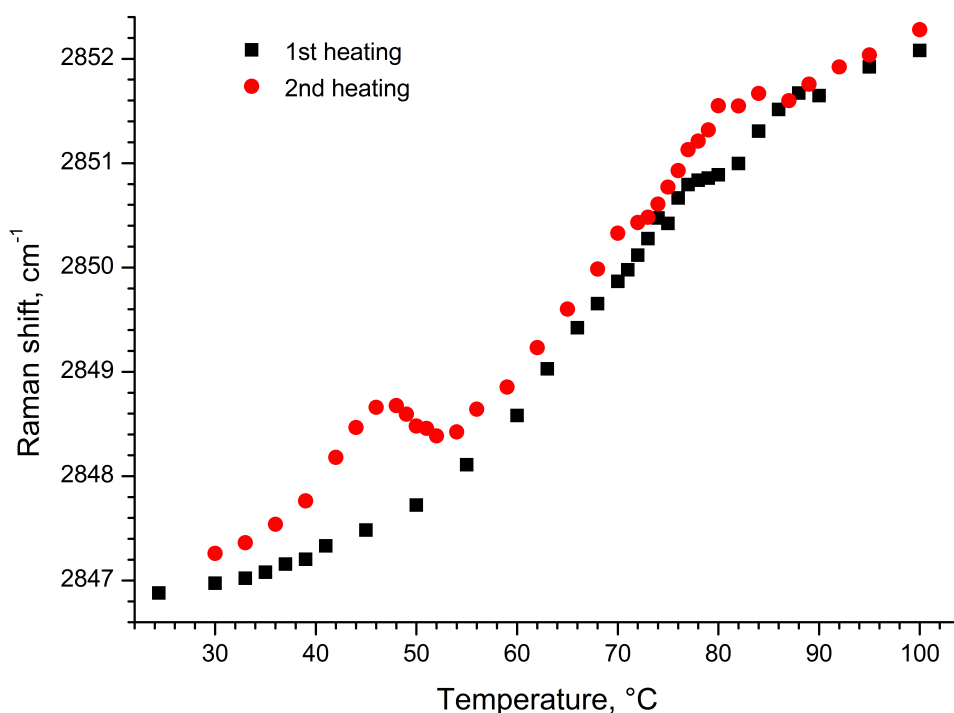


Fig. A 2: Position of the peak attributed to the symmetric CH₂ stretching mode for the sample composed of CER[AP]/CHOL/PA/ChS/IPM (49.5/22.5/13.5/4.5/10, m/m). in relationship to the temperature T.

7 REFERENCES

1. D. Kessner, M. Kiselev, S. Dante, T. Hauss, P. Lersch, S. Wartewig, and R. H. Neubert, *Arrangement of ceramide [EOS] in a stratum corneum lipid model matrix: new aspects revealed by neutron diffraction studies*. European Biophysics Journal, 2008. **37**(6): p. 989-999.
2. D. Kessner, M. A. Kiselev, T. Hauss, S. Dante, S. Wartewig, and R. H. Neubert, *Localisation of partially deuterated cholesterol in quaternary SC lipid model membranes: a neutron diffraction study*. European Biophysics Journal, 2008. **37**(6): p. 1051-1057.
3. M. A. Kiselev, *Conformation of ceramide 6 molecules and chain-flip transitions in the lipid matrix of the outermost layer of mammalian skin, the stratum corneum*. Crystallography Reports, 2007. **52**(3): p. 525-528.
4. M. A. Kiselev, N. Y. Ryabova, A. M. Balagurov, S. Dante, T. Hauss, J. Zbytovská, S. Wartewig, and R. H. H. Neubert, *New insights into the structure and hydration of a stratum corneum lipid model membrane by neutron diffraction*. European Biophysics Journal, 2005. **34**: p. 1030-1040.
5. M. Wegener, R. Neubert, W. Rettig, and S. Wartewig, *Structure of stratum corneum lipids characterized by FT-Raman spectroscopy and DSC. III. Mixtures of ceramides and cholesterol*. Chemistry and Physics of Lipids, 1997. **88**: p. 73-82.
6. J. Zbytovská, K. Vávrová, M. A. Kiselev, P. Lessieur, S. Wartewig, and R. H. H. Neubert, *The effects of transdermal permeation enhancers on thermotropic phase behaviour of a stratum corneum lipid model*. Colloids and Surfaces A: Physicochemical and Engineering Aspects, 2009. **351**: p. 30-37.
7. A. Schroeter, M. A. Kiselev, T. Hauss, S. Dante, and R. H. H. Neubert, *Evidence of free fatty acid interdigitation in stratum corneum model membranes based on ceramide [AP] by deuterium labelling*. Biochimica et Biophysica Acta, Biomembranes, 2009. **1788**(10): p. 2194-2203.
8. G. Thews, E. Mutschler, and P. Vaupel, *Anatomie, Physiologie, Pathophysiologie des Menschen* 1995, ed., Stuttgart: Wissenschaftliche Verlagsgesellschaft mbH.
9. J. Kanitakis, *Anatomy, histology and immunohistochemistry of normal human skin*. European Journal of Dermatology, 2002. **12**(4): p. 390-401.
10. L. T. Smith, K. A. Holbrook, and P. H. Byers, *Structure of the dermal matrix during development and in the adult*. Journal of Investigative Dermatology, 1982. **79 Suppl 1**: p. 93s-104s.
11. C. M. Kielty and C. A. Shuttleworth, *Microfibrillar elements of the dermal matrix*. Microscopy Research and Technique, 1997. **38**(4): p. 413-427.
12. F. H. Silver, J. W. Freeman, and D. DeVore, *Viscoelastic properties of human skin and processed dermis*. Skin Research and Technology, 2001. **7**(1): p. 18-23.
13. Skin Care Forum, *Schematic diagram of the human skin*, in http://www.scf-online.com/english/27_e/Images27_e/skin_verybig27_e.jpg, skin_verybig27_e.jpg, Editor 2001.
14. G. F. Odland, *A Submicroscopic Granular Component in Human Epidermis*. Journal of Investigative Dermatology, 1960. **34**(1): p. 11-15.
15. P. M. Elias and D. S. Friend, *The Permeability Barrier in Mammalian Epidermis*. Journal of Cell Biology, 1975. **65**(1): p. 180-191.
16. R. M. Lavker, *Membrane coating granules: the fate of the discharged lamellae*. Journal of Ultrastructure Research, 1976. **55**(1): p. 79-86.

17. A. G. Matoltsy and P. F. Parakkal, *Membrane-Coating Granules of Keratinizing Epithelia*. *Journal of Cell Biology*, 1965. **24**: p. 297-307.
18. L. Landmann, *The epidermal permeability barrier*. *Anatomy and Embryology*, 1988. **178**(1): p. 1-13.
19. G. K. Menon, K. R. Feingold, and P. M. Elias, *Lamellar Body Secretory Response to Barrier Disruption*. *Journal of Investigative Dermatology*, 1992. **98**(3): p. 279-289.
20. K. A. Holbrook and G. F. Odland, *Regional differences in the thickness (cell layers) of the human stratum corneum: an ultrastructural analysis*. *Journal of Investigative Dermatology*, 1974. **62**(4): p. 415-422.
21. R. J. Scheuplein and L. J. Morgan, *"Bound water" in keratin membranes measured by a microbalance technique*. *Nature*, 1967. **214**(5087): p. 456-458.
22. M. E. Loomans and D. P. Hannon, *An electron microscopic study of the effects of subtilisin and detergents on human stratum corneum*. *Journal of Investigative Dermatology*, 1970. **55**(2): p. 101-114.
23. I. H. Blank and R. J. Scheuplein, *Transport into and within Skin*. *British Journal of Dermatology*, 1969. **S 81**: p. 4-10.
24. R. J. Scheuplein and I. H. Blank, *Permeability of the skin*. *Physiological Reviews*, 1971. **51**(4): p. 702-747.
25. J. C. Mackenzie, *Ordered structure of the stratum corneum of mammalian skin*. *Nature*, 1969. **222**(5196): p. 881-882.
26. E. Candi, R. Schmidt, and G. Melino, *The cornified envelope: a model of cell death in the skin*. *Nature Reviews Molecular Cell Biology*, 2005. **6**(4): p. 328-340.
27. D. C. Swartzendruber, P. W. Wertz, K. C. Madison, and D. T. Downing, *Evidence That the Corneocyte Has a Chemically Bound Lipid Envelope*. *Journal of Investigative Dermatology*, 1987. **88**(6): p. 709-713.
28. P. W. Wertz, D. C. Swartzendruber, D. J. Kitko, K. C. Madison, and D. T. Downing, *The role of the corneocyte lipid envelopes in cohesion of the stratum corneum*. *Journal of Investigative Dermatology*, 1989. **93**(1): p. 169-172.
29. C. R. Harding, *The stratum corneum: structure and function in health and disease*. *Dermatologic Therapy*, 2004. **17 Suppl 1**: p. 6-15.
30. P. M. Elias, *Epidermal lipids, barrier function, and desquamation*. *Journal of Investigative Dermatology*, 1983. **80 (Suppl.)**: p. 44s-49s.
31. P. M. Elias, *Structure and Function of the Stratum-Corneum Permeability Barrier*. *Drug Development Research*, 1988. **13**(2-3): p. 97-105.
32. I. H. Blank, R. J. Scheuplein, and D. J. Macfarlane, *Mechanism of Percutaneous Absorption. 3. Effect of Temperature on Transport of Non-Electrolytes across Skin*. *Journal of Investigative Dermatology*, 1967. **49**(6): p. 582-589.
33. P. M. Elias, J. Goerke, and D. S. Friend, *Mammalian Epidermal Barrier Layer Lipids - Composition and Influence on Structure*. *Journal of Investigative Dermatology*, 1977. **69**(6): p. 535-546.
34. P. M. Elias, E. R. Cooper, A. Korc, and B. E. Brown, *Percutaneous transport in relation to stratum corneum structure and lipid composition*. *Journal of Investigative Dermatology*, 1981. **76**(4): p. 297-301.
35. G. M. Golden, D. B. Guzek, A. H. Kennedy, J. E. McKie, and R. O. Potts, *Stratum corneum lipid phase transitions and water barrier properties*. *Biochemistry*, 1987. **26**(8): p. 2382-2388.

36. G. M. El Maghraby, B. W. Barry, and A. C. Williams, *Liposomes and skin: from drug delivery to model membranes*. European Journal of Pharmaceutical Sciences, 2008. **34**(4-5): p. 203-222.
37. V. M. Meidan, M. C. Bonner, and B. B. Michniak, *Transfollicular drug delivery-is it a reality?* International Journal of Pharmaceutics, 2005. **306**(1-2): p. 1-14.
38. J. Lademann, H. Weigmann, C. Rickmeyer, H. Barthelmes, H. Schaefer, G. Mueller, and W. Sterry, *Penetration of titanium dioxide microparticles in a sunscreen formulation into the horny layer and the follicular orifice*. Skin Pharmacology and Applied Skin Physiology, 1999. **12**(5): p. 247-256.
39. G. M. Gray and H. J. Yardley, *Different Populations of Pig Epidermal-Cells - Isolation and Lipid Composition*. Journal of Lipid Research, 1975. **16**(6): p. 441-447.
40. G. M. Gray and H. J. Yardley, *Lipid Compositions of Cells Isolated from Pig, Human, and Rat Epidermis*. Journal of Lipid Research, 1975. **16**(6): p. 434-440.
41. M. A. Lampe, A. L. Burlingame, J. Whitney, M. L. Williams, B. E. Brown, E. Roitman, and P. M. Elias, *Human stratum corneum lipids: characterization and regional variations*. Journal of Lipid Research, 1983. **24**(2): p. 120-130.
42. N. Nicolaidis, *Skin Lipids. II. Lipid Class Composition of Samples from Various Species and Anatomical Sites*. Journal of the American Oil Chemists' Society, 1965. **42**: p. 691-702.
43. A. Weerheim and M. Ponc, *Determination of stratum corneum lipid profile by tape stripping in combination with high-performance thin-layer chromatography*. Archives of Dermatological Research, 2001. **293**: p. 191-199.
44. G. Grubauer, K. R. Feingold, and P. M. Elias, *Relationship of epidermal lipogenesis to cutaneous barrier function*. Journal of Lipid Research, 1987. **28**(6): p. 746-752.
45. C. A. Lewis, B. J. Hayward, and R. M. Mackenna, *Saturated Hydrocarbons in Skin Surface Lipids*. British Journal of Dermatology, 1965. **77**: p. 303-308.
46. P. W. Wertz and B. van den Bergh, *The physical, chemical and functional properties of lipids in the skin and other biological barriers*. Chemistry and Physics of Lipids, 1998. **91**(2): p. 85-96.
47. Y. Masukawa, H. Narita, E. Shimizu, N. Kondo, Y. Sugai, T. Oba, R. Homma, J. Ishikawa, Y. Takagi, T. Kitahara, Y. Takema, and K. Kita, *Characterization of overall ceramide species in human Stratum corneum*. Journal of Lipid Research, 2008. **49**(7): p. 1466-1476.
48. J. van Smeden, L. Hoppel, R. van der Heijden, T. Hankemeier, R. J. Vreeken, and J. A. Bouwstra, *LC/MS analysis of stratum corneum lipids: ceramide profiling and discovery*. Journal of Lipid Research, 2011. **52**(6): p. 1211-1221.
49. P. W. Wertz and D. T. Downing, *Ceramides of pig epidermis: structure determination*. Journal of Lipid Research, 1983. **24**(6): p. 759-765.
50. P.W. Wertz, M.C. Miethke, S.A. Long, J.S. Strauss, and D.T. Downing, *The composition of the ceramides from human stratum corneum and from comedones*. Journal of Investigative Dermatology, 1985. **84**: p. 410-412.
51. S. Motta, M. Monti, S. Sesana, R. Caputo, S. Carelli, and R. Ghidoni, *Ceramide composition of the psoriatic scale*. Biochimica et Biophysica Acta, 1993. **1182**: p. 147-151.
52. S. Law, P. W. Wertz, D. C. Swartzendruber, and C. A. Squier, *Regional variation in content, composition and organization of porcine epithelial barrier*

- lipids revealed by thin-layer chromatography and transmission electron microscopy*. Archives of Oral Biology, 1995. **40**(12): p. 1085-1091.
53. A. Di Nardo, P. Wertz, A. Giannetti, and S. Seidenari, *Ceramide and cholesterol composition of the skin of patients with atopic dermatitis*. Acta Dermato-Venereologica, 1998. **78**: p. 27-30.
54. S. Motta, M. Monti, S. Sesana, L. Mellesi, R. Ghidoni, and R. Caputo, *Abnormality of water barrier function in psoriasis. Role of ceramide fractions*. Archives of Dermatology, 1994. **130**(4): p. 452-456.
55. K. de Paepe, D. Roseeuw, and V. Rogiers, *Repair of acetone- and sodium lauryl sulphate-damaged human skin barrier function using topically applied emulsions containing barrier lipids*. Journal of the European Academy of Dermatology and Venereology, 2002. **16**(6): p. 587-594.
56. J. Novotny, B. Janusova, M. Novotny, A. Hrabalek, and K. Vavrova, *Short-chain ceramides decrease skin barrier properties*. Skin Pharmacology and Physiology, 2009. **22**(1): p. 22-30.
57. P.W. Wertz, *The nature of the epidermal barrier: biochemical aspects*. Advanced Drug Delivery Reviews, 1996. **18**: p. 283-294.
58. C. Prottey, P. J. Hartop, J. G. Black, and J. I. McCormack, *The repair of impaired epidermal barrier function in rats by the cutaneous application of linoleic acid*. British Journal of Dermatology, 1976. **94**(1): p. 13-21.
59. P. M. Elias, B. E. Brown, and V. A. Ziboh, *The permeability barrier in essential fatty acid deficiency: evidence for a direct role for linoleic acid in barrier function*. Journal of Investigative Dermatology, 1980. **74**(4): p. 230-233.
60. L. Coderch, O. Lopez, A. de la Maza, and J. L. Parra, *Ceramides and skin function*. American Journal of Clinical Dermatology, 2003. **4**(2): p. 107-129.
61. M. Mao-Qiang, P. M. Elias, and K. R. Feingold, *Fatty acids are required for epidermal permeability barrier function*. Journal of Clinical Investigation, 1993. **92**(2): p. 791-798.
62. G. K. Menon, K. R. Feingold, A. H. Moser, B. E. Brown, and P. M. Elias, *De novo sterologenesis in the skin. II. Regulation by cutaneous barrier requirements*. Journal of Lipid Research, 1985. **26**(4): p. 418-427.
63. K. R. Feingold, M. Q. Man, G. K. Menon, S. S. Cho, B. E. Brown, and P. M. Elias, *Cholesterol synthesis is required for cutaneous barrier function in mice*. Journal of Clinical Investigation, 1990. **86**(5): p. 1738-1745.
64. M. Holtje, T. Forster, B. Brandt, T. Engels, W. von Rybinski, and H. D. Holtje, *Molecular dynamics simulations of stratum corneum lipid models: fatty acids and cholesterol*. Biochimica et Biophysica Acta, 2001. **1511**(1): p. 156-167.
65. L. Miao, M. Nielsen, J. Thewalt, J. H. Ipsen, M. Bloom, M. J. Zuckermann, and O. G. Mouritsen, *From lanosterol to cholesterol: structural evolution and differential effects on lipid bilayers*. Biophysical Journal, 2002. **82**(3): p. 1429-1444.
66. R. A. Demel and B. De Kruffyff, *The function of sterols in membranes*. Biochimica et Biophysica Acta, 1976. **457**(2): p. 109-132.
67. J. Zbytovská, M.A. Kiselev, S.S. Funari, V.M. Garamus, S. Wartewig, K. Palát, and R. Neubert, *Influence of cholesterol on the structure of stratum corneum lipid model membrane*. Colloids and Surfaces A: Physicochemical and Engineering Aspects, 2008. **328**: p. 90-99.
68. J. A. Bouwstra, G. S. Gooris, F. E. Dubbelaar, and M. Ponc, *Cholesterol sulfate and calcium affect stratum corneum lipid organization over a wide temperature range*. Journal of Lipid Research, 1999. **40**(12): p. 2303-2312.

69. P. M. Elias, M. L. Williams, M. E. Maloney, J. A. Bonifas, B. E. Brown, S. Grayson, and E. H. Epstein, Jr., *Stratum corneum lipids in disorders of cornification. Steroid sulfatase and cholesterol sulfate in normal desquamation and the pathogenesis of recessive X-linked ichthyosis*. Journal of Clinical Investigation, 1984. **74**(4): p. 1414-1421.
70. D. Webster, J. T. France, L. J. Shapiro, and R. Weiss, *X-linked ichthyosis due to steroid-sulphatase deficiency*. Lancet, 1978. **1**(8055): p. 70-72.
71. A. S. Michaels, S. K. Chandrasekaran, and J. E. Shaw, *Drug Permeation through Human Skin - Theory and Invitro Experimental Measurement*. AIChE Journal, 1975. **21**(5): p. 985-996.
72. P. M. Elias, *Epidermal lipids, membranes, and keratinization*. International Journal of Dermatology, 1981. **20**: p. 1-19.
73. P. M. Elias, *Lipids and the epidermal permeability barrier*. Archives of Dermatological Research, 1981. **270**(1): p. 95-117.
74. A. F. Hayward, *Ultrastructural changes in contents of membrane-coating granules after extrusion from epithelial cells of hamster cheek pouch*. Cell Tissue Res, 1978. **187**(2): p. 323-331.
75. K. C. Madison, D. C. Schwartzenruber, P. W. Wertz, and D. T. Downing, *Presence of intact intercellular lipid lamellae in the upper layers of the stratum corneum*. Journal of Investigative Dermatology, 1987. **88**: p. 714-718.
76. D. C. Swartzendruber, P. W. Wertz, D. J. Kitko, K. C. Madison, and D. T. Downing, *Molecular models of the intercellular lipid lamellae in mammalian stratum corneum*. Journal of Investigative Dermatology, 1989. **92**: p. 251-257.
77. R. O. Potts and M. L. Francoeur, *Lipid biophysics of water loss through the skin*. Proc Natl Acad Sci U S A, 1990. **87**(10): p. 3871-3873.
78. H. Träuble, *The Movement of Molecules Across Lipid Membranes: A Molecular Theory*. Journal of Membrane Biology, 1971. **4**: p. 193-208.
79. B. Forslind, *A domain mosaic model of the skin barrier*. Acta Dermato-Venereologica, 1994. **74**: p. 1-6.
80. L. Norlen, *Molecular skin barrier models and some central problems for the understanding of skin barrier structure and function*. Skin Pharmacology and Applied Skin Physiology, 2003. **16**(4): p. 203-211.
81. B. Forslind, S. Engstrom, J. Engblom, and L. Norlen, *A novel approach to the understanding of human skin barrier function*. Journal of Dermatological Science, 1997. **14**(2): p. 115-125.
82. L. Norlen, *Skin Barrier Structure and Function: The Single Gel Phase Model*. Journal of Investigative Dermatology, 2001. **117**: p. 830-836.
83. J. A. Bouwstra, F. E. R. Dubbelaar, G. S. Gooris, and M. Ponc, *The lipid organisation in the skin barrier*. Acta Dermato-Venereologica, 2000. **Supp 208**: p. 23-30.
84. J. A. Bouwstra, G. S. Gooris, J.A. van der Spek, and W. Bras, *Structural investigations of human stratum corneum by small-angle X-ray scattering*. Journal of Investigative Dermatology, 1991. **97**: p. 1005-1012.
85. S. H. White, D. Mirejovsky, and G. I. King, *Structure of lamellar lipid domains and corneocyte envelopes of murine stratum corneum. An X-ray diffraction study*. Biochemistry, 1988. **27**(10): p. 3725-3732.
86. G. C. Charalambopoulou, T. A. Steriotis, T. Hauss, K. L. Stefanopoulos, and A. K. Stubos, *A neutron-diffraction study of the effect of hydration on stratum corneum structure*. Applied Physics A - Materials Science & Processing, 2002. **74**: p. S1245-S1247.

87. L. Norlen. *New information from cryoelectron microscopy: Speculations versus reality.* in *Gordon Research Conference - Barrier Function of Mammalian Skin.* 2011. Waterville Valley, NH.
88. I. Iwai, H. Han, L. D. Hollander, S. Svensson, L. G. Ofverstedt, J. Anwar, J. Brewer, M. Bloksgaard, A. Laloef, D. Nosek, S. Masich, L. A. Bagatolli, U. Skoglund, and L. Norlen, *The Human Skin Barrier Is Organized as Stacked Bilayers of Fully Extended Ceramides with Cholesterol Molecules Associated with the Ceramide Sphingoid Moiety.* *Journal of Investigative Dermatology*, 2012: p. 1-11.
89. D. Kessner, A. Ruettinger, M. A. Kiselev, S. Wartewig, and R. H. Neubert, *Properties of ceramides and their impact on the stratum corneum structure. Part 2: stratum corneum lipid model systems.* *Skin Pharmacology and Physiology*, 2008. **21**(2): p. 58-74.
90. J. Bouwstra, G. Pilgram, G. Gooris, H. Koerten, and M. Ponec, *New aspects of the skin barrier organization.* *Skin Pharmacology and Applied Skin Physiology*, 2001. **14**: p. 52-62.
91. J. R. Hill and P. W. Wertz, *Molecular models of the intercellular lipid lamellae from epidermal stratum corneum.* *Biochimica et Biophysica Acta-Biomembranes*, 2003. **1616**(2): p. 121-126.
92. A. Al-Amoudi, J. Dubochet, and L. Norlen, *Nanostructure of the epidermal extracellular space as observed by cryo-electron microscopy of vitreous sections of human skin.* *Journal of Investigative Dermatology*, 2005. **124**(4): p. 764-777.
93. T. J. McIntosh, M. E. Stewart, and D. T. Downing, *X-ray diffraction analysis of isolated skin lipids: Reconstitution of intercellular lipid domains.* *Biochemistry*, 1996. **35**(12): p. 3649-3653.
94. J. A. Bouwstra, G. S. Gooris, F. E. R. Dubbelaar, A. M. Weerheim, A. P. Ijzerman, and M. Ponec, *Role of ceramide 1 in the molecular organization of the stratum corneum lipids.* *Journal of Lipid Research*, 1998. **39**(1): p. 186-196.
95. J. A. Bouwstra, G. S. Gooris, F. E. R. Dubbelaar, and M. Ponec, *Phase behavior of stratum corneum lipid mixtures based on human ceramides: The role of natural and synthetic ceramide 1.* *Journal of Investigative Dermatology*, 2002. **118**(4): p. 606-617.
96. J. A. Bouwstra, G. S. Gooris, F. E. R. Dubbelaar, and M. Ponec, *Phase behaviour of lipid mixtures based on human ceramides: coexistence of crystalline and liquid phases.* *Journal of Lipid Research*, 2001. **42**: p. 1759-1770.
97. J. A. Bouwstra, F. E. R. Dubbelaar, G. S. Gooris, A. M. Weerheim, and M. Ponec, *The role of ceramide composition in the lipid organisation of the skin barrier.* *Biochimica et Biophysica Acta-Biomembranes*, 1999. **1419**(2): p. 127-136.
98. M. W. de Jager, G. S. Gooris, I. P. Dolbnya, W. Bras, M. Ponec, and J. A. Bouwstra, *The phase behaviour of skin lipid mixtures based on synthetic ceramides.* *Chemistry and Physics of Lipids*, 2003. **124**(2): p. 123-134.
99. M. W. de Jager, G. S. Gooris, I. P. Dolbnya, W. Bras, M. Ponec, and J. A. Bouwstra, *Novel lipid mixtures based on synthetic ceramides reproduce the unique stratum corneum lipid organization.* *Journal of Lipid Research*, 2004. **45**: p. 923-932.
100. M. W. de Jager, G. S. Gooris, I. P. Dolbnya, M. Ponec, and J. A. Bouwstra, *Modelling the stratum corneum lipid organisation with synthetic lipid mixtures:*

- the importance of synthetic ceramide composition*. Biochimica et Biophysica Acta-Biomembranes, 2004. **1684**: p. 132-140.
101. J. C. Garson, J. Doucet, J. L. Leveque, and G. Tsoucaris, *Oriented structure in human stratum corneum revealed by X-ray diffraction*. Journal of Investigative Dermatology, 1991. **96**(1): p. 43-49.
 102. A. Schröter, D. Kessner, M. A. Kiselev, T. Hauss, S. Dante, and R.H.H. Neubert, *Basic nanostructure of stratum corneum lipid matrices based on ceramides [EOS] and [AP]: a neutron diffraction study*. Biophysical Journal, 2009. **97**: p. 1104-1114.
 103. M. W. de Jager, G. S. Gooris, M. Ponc, and J. A. Bouwstra, *Lipid mixtures prepared with well-defined synthetic ceramides closely mimic the unique stratum corneum lipid phase behavior*. Journal of Lipid Research, 2005. **46**(12): p. 2649-2656.
 104. H. Trommer and R. H. H. Neubert, *Overcoming the stratum corneum: The modulation of skin penetration - A review*. Skin Pharmacology and Physiology, 2006. **19**(2): p. 106-121.
 105. A. Naik, Y. N. Kalia, and R. H. Guy, *Transdermal drug delivery: overcoming the skin's barrier function*. Pharmaceutical Science and Technology Today, 2000. **3**(9): p. 318-326.
 106. B. J. Aungst, N. J. Rogers, and E. Shefter, *Enhancement of Naloxone Penetration through Human Skin In vitro Using Fatty Acids, Fatty Alcohols, Surfactants, Sulfoxides and Amides*. International Journal of Pharmaceutics, 1986. **33**(1-3): p. 225-234.
 107. B. W. Barry, *Lipid-Protein-Partitioning Theory of Skin Penetration Enhancement*. Journal of Controlled Release, 1991. **15**(3): p. 237-248.
 108. T. S. Spencer, C. E. Linamen, W. A. Akers, and H. E. Jones, *Temperature dependence of water content of stratum corneum*. The British Journal of Dermatology, 1975. **93**(2): p. 159-164.
 109. A. C. Williams and B. W. Barry, *Penetration enhancers*. Advanced Drug Delivery Reviews, 2004. **56**(5): p. 603-618.
 110. B. W. Barry, *Mode of action of penetration enhancers in human skin*. Journal of Controlled Release, 1987. **6**(1): p. 85-97.
 111. R. P. Oertel, *Protein conformational changes induced in human stratum corneum by organic sulfoxides: an infrared spectroscopic investigation*. Biopolymers, 1977. **16**(10): p. 2329-2345.
 112. A. N. C. Anigbogu, A. C. Williams, B. W. Barry, and H. G. M. Edwards, *Fourier-Transform Raman-Spectroscopy of Interactions between the Penetration Enhancer Dimethyl-Sulfoxide and Human Stratum-Corneum*. International Journal of Pharmaceutics, 1995. **125**(2): p. 265-282.
 113. R. Notman, W. K. den Otter, M. G. Noro, W. J. Briels, and J. Anwar, *The permeability enhancing mechanism of DMSO in ceramide bilayers simulated by molecular dynamics*. Biophysical Journal, 2007. **93**(6): p. 2056-2068.
 114. R. Notman, M. Noro, B. O'Malley, and J. Anwar, *Molecular basis for dimethylsulfoxide (DMSO) action on lipid membranes*. Journal of the American Chemical Society, 2006. **128**: p. 13982-13983.
 115. A. M. Kligman, *Topical Pharmacology and Toxicology of Dimethyl Sulfoxide .I*. Journal of the American Medical Association, 1965. **193**(10): p. 796-804.
 116. U. T. Lashmar, J. Hadgraft, and N. Thomas, *Topical Application of Penetration Enhancers to the Skin of Nude Mice - a Histopathological Study*. Journal of Pharmacy and Pharmacology, 1989. **41**(2): p. 118-121.

117. P. Liu, T. Kurihara-Bergstrom, and W. R. Good, *Cotransport of estradiol and ethanol through human skin in vitro: understanding the permeant/enhancer flux relationship*. *Pharmaceutical Research*, 1991. **8**(7): p. 938-944.
118. N. S. Thomas and R. Panchagnula, *Transdermal delivery of zidovudine: effect of vehicles on permeation across rat skin and their mechanism of action*. *European Journal of Pharmaceutical Sciences*, 2003. **18**(1): p. 71-79.
119. T. Kai, V. H. W. Mak, R. O. Potts, and R. H. Guy, *Mechanism of Percutaneous Penetration Enhancement - Effect of N-Alkanols on the Permeability Barrier of Hairless Mouse Skin*. *Journal of Controlled Release*, 1990. **12**(2): p. 103-112.
120. L. K. Pershing, L. D. Lambert, and K. Knutson, *Mechanism of Ethanol-Enhanced Estradiol Permeation across Human Skin In vivo*. *Pharmaceutical Research*, 1990. **7**(2): p. 170-175.
121. J. Beastall, R. H. Guy, J. Hadgraft, and I. Wilding, *The Influence of Urea on Percutaneous-Absorption*. *Pharmaceutical Research*, 1986. **3**(5): p. 294-297.
122. B. Bendas, U. Schmalfuss, and R. Neubert, *Influence of Propylene-Glycol as Cosolvent on Mechanisms of Drug Transport from Hydrogels*. *International Journal of Pharmaceutics*, 1995. **116**(1): p. 19-30.
123. E. R. Cooper, E. W. Merritt, and R. L. Smith, *Effect of Fatty Acids and Alcohols on the Penetration of Acyclovir across Human Skin In vitro*. *Journal of Pharmaceutical Sciences*, 1985. **74**(6): p. 688-689.
124. E. M. Niazy, *Influence of Oleic-Acid and Other Permeation Promoters on Transdermal Delivery of Dihydroergotamine through Rabbit Skin*. *International Journal of Pharmaceutics*, 1991. **67**(1): p. 97-100.
125. M. A. Yamane, A. C. Williams, and B. W. Barry, *Effects of Terpenes and Oleic Acid as Skin Penetration Enhancers Towards 5-Fluorouracil as Assessed with Time - Permeation, Partitioning and Differential Scanning Calorimetry*. *International Journal of Pharmaceutics*, 1995. **116**(2): p. 237-251.
126. M. L. Francoeur, G. M. Golden, and R. O. Potts, *Oleic acid: Its effects on stratum corneum in relation to (trans)dermal drug delivery*. *Pharmaceutical Research*, 1990. **7**: p. 621-627.
127. B. W. Barry and S. L. Bennett, *Effect of Penetration Enhancers on the Permeation of Mannitol, Hydrocortisone and Progesterone through Human Skin*. *Journal of Pharmacy and Pharmacology*, 1987. **39**(7): p. 535-546.
128. A. Naik, L. A. R. M. Pechtold, R. O. Potts, and R. H. Guy, *Mechanism of oleic acid-induced skin penetration enhancement in vivo in humans*. *Journal of Controlled Release*, 1995. **37**(3): p. 299-306.
129. B. Ongpipattanakul, R.R. Burnette, R.O. Potts, and M.L. Francoeur, *Evidence that oleic acid exists in a separate phase within stratum corneum lipids*. *Pharmaceutical Research*, 1991. **8**: p. 350-354.
130. G. M. Golden, J. E. McKie, and R. O. Potts, *Role of stratum corneum lipid fluidity in transdermal drug flux*. *Journal of Pharmaceutical Sciences*, 1987. **76**(1): p. 25-28.
131. A. Ortiz and J. C. Gomez-Fernandez, *A differential scanning calorimetry study of the interaction of free fatty acids with phospholipid membranes*. *Chemistry and Physics of Lipids*, 1987. **45**(1): p. 75-91.
132. A.C. Rowat, N. Kitson, and J.L. Thewalt, *Interactions of oleic acid and model stratum corneum membranes as seen by ²H NMR*. *International Journal of Pharmaceutics*, 2006. **307**: p. 225-231.
133. M. A. Stillman, H. I. Maibach, and A. R. Shalita, *Relative irritancy of free fatty acids of different chain length*. *Contact Dermatitis*, 1975. **1**(2): p. 65-69.

134. E. Boelsma, H. Tanojo, H.E. Bodde, and M. Ponec, *Assessment of the potential irritancy of oleic acid on human skin: Evaluation in vitro and in vivo*. *Toxicology in Vitro*, 1996. **10**: p. 729-742.
135. E. Touitou, B. Godin, Y. Karl, S. Bujanover, and Y. Becker, *Oleic acid, a skin penetration enhancer, affects Langerhans cells and corneocytes*. *Journal of Controlled Release*, 2002. **80**(1-3): p. 1-7.
136. S. Santoyo, A. Arellano, P. Ygartua, and C. Martin, *Penetration Enhancer Effects on the in-Vitro Percutaneous Absorption of Piroxicam through Rat Skin*. *International Journal of Pharmaceutics*, 1995. **117**(2): p. 219-224.
137. K. Sato, K. Sugibayashi, and Y. Morimoto, *Effect and Mode of Action of Aliphatic Esters on the Invitro Skin Permeation of Nicorandil*. *International Journal of Pharmaceutics*, 1988. **43**(1-2): p. 31-40.
138. Melinda Goldberg-Cettina, Puchun Liu, James Nightingale, and Tamie Kurihara-Bergstrom, *Enhanced transdermal delivery of estradiol in vitro using binary vehicles of isopropyl myristate and short-chain alkanols*. *International Journal of Pharmaceutics*, 1995. **114**(2): p. 237-245.
139. A. Arellano, S. Santoyo, C. Martin, and P. Ygartua, *Influence of propylene glycol and isopropyl myristate on the in vitro percutaneous penetration of diclofenac sodium from carbopol gels*. *European Journal of Pharmaceutical Sciences*, 1998. **7**(2): p. 129-135.
140. C. S. Leopold and B. C. Lippold, *An Attempt to Clarify the Mechanism of the Penetration Enhancing Effects of Lipophilic Vehicles with Differential Scanning Calorimetry (DSC)*. *Journal of Pharmacy and Pharmacology*, 1995. **47**(4): p. 276-281.
141. I. Brinkmann and C. C. Mueller-Goymann, *Role of isopropyl myristate, isopropyl alcohol and a combination of both in hydrocortisone permeation across the human stratum corneum*. *Skin Pharmacology and Applied Skin Physiology*, 2003. **16**(6): p. 393-404.
142. I. Brinkmann and C. C. Mueller-Goymann, *An attempt to clarify the influence of glycerol, propylene glycol, isopropyl myristate and a combination of propylene glycol and isopropyl myristate on human stratum corneum*. *Pharmazie*, 2005. **60**(3): p. 215-220.
143. D. Friend, P. Catz, and J. Heller, *Transdermal Delivery of Levonorgestrel .3. Simple Alkyl Esters as Skin Permeation Enhancers*. *Journal of Controlled Release*, 1989. **9**(1): p. 33-41.
144. S. N. Tenjarla, R. Kasina, P. Puranajoti, M. S. Omar, and W. T. Harris, *Synthesis and evaluation of N-acetylprolinate esters - novel skin penetration enhancers*. *International Journal of Pharmaceutics*, 1999. **192**(2): p. 147-158.
145. A. C. Williams and B. W. Barry, *The Enhancement Index Concept Applied to Terpene Penetration Enhancers for Human Skin and Model Lipophilic (Estradiol) and Hydrophilic (5-Fluorouracil) Drugs*. *International Journal of Pharmaceutics*, 1991. **74**(2-3): p. 157-168.
146. T. A. Harroun, G. D. Wignall, and J. Katsaras, *Neutron Scattering for Biology*, in *Neutron Scattering in Biology: Techniques and Applications* J. Fitter, T. Gutberlet, and J. Katsaras, Editors. 2006, Springer: Berlin.
147. H. Dachs, *Principles of Neutron Diffraction*, in *Neutron Diffraction*, H. Dachs, Editor 1978, Springer: Berlin.
148. C. R. Cantor and P. R. Schimmel, *Biophysical Chemistry Part II: Techniques for the Study of Biological Structure and Function*. 1980, San Francisco: W. H. Freeman and Co.

149. G. Buldt, H. U. Gally, A. Seelig, J. Seelig, and G. Zaccai, *Neutron diffraction studies on selectively deuterated phospholipid bilayers*. *Nature*, 1978. **271**(5641): p. 182-184.
150. M. Tomita, T. Hasegawa, T. Tsukihara, S. Miyajima, M. Nagao, and M. Sato, *Two concentric protein shell structure with spikes of silkworm Bombyx mori cytoplasmic polyhedrosis virus revealed by small-angle neutron scattering using the contrast variation method*. *The Journal of Biochemistry*, 1999. **125**(5): p. 916-922.
151. T. Gutberlet, U. Heinemann, and M. Steiner, *Protein crystallography with neutrons - status and perspectives*. *Acta Crystallographica, Section B: Structural Crystallography and Crystal Chemistry*, 2001. **57**(Pt 2): p. 349-354.
152. L. de Broglie, *The Reinterpretation of Wave Mechanics*. *Foundations of Physics*, 1970. **1**(1): p. 5-15.
153. P. W. Winston and D. H. Bates, *Saturated Solutions for the Control of Humidity in Biological Research*. *Ecology*, 1960. **41**(1): p. 232-237.
154. G. Zaccai, *Application of Neutron Diffraction to Biological Problems*, in *Neutron Diffraction*, H. Dachs, Editor 1978, Springer: Berlin.
155. C. E. Williams, *Contrast variation in X-ray and neutron scattering*, in *Neutron, X-ray and Light Scattering: Introduction to an Investigative Tool for Colloidal and Polymeric Systems*, P. Lindner and T. Zemb, Editors. 1991, North-Holland: Amsterdam.
156. F. Cser, *About the Lorentz correction used in the interpretation of small angle X-ray scattering data of semicrystalline polymers*. *Journal of Applied Polymer Science*, 2001. **80**(12): p. 2300-2308.
157. N. P. Franks and W. R. Lieb, *Structure of Lipid Bilayers and the Effects of General Anaesthetics: An X-Ray and Neutron Diffraction Study*. *Journal of Molecular Biology*, 1979. **133**(4): p. 469-500.
158. J.F. Nagle and S. Tristram-Nagle, *Structure of lipid bilayers*. *Biochimica et Biophysica Acta*, 2000. **1469**: p. 159-195.
159. D. L. Worcester and N. P. Franks, *Structural Analysis of Hydrated Egg Lecithin and Cholesterol Bilayers II. Neutron Diffraction*. *Journal of Molecular Biology*, 1976. **100**(3): p. 359-378.
160. M. C. Wiener and S. H. White, *Fluid Bilayer Structure Determination by the Combined Use of X-Ray and Neutron-Diffraction. 1. Fluid Bilayer Models and the Limits of Resolution*. *Biophysical Journal*, 1991. **59**(1): p. 162-173.
161. M. C. Wiener, G. I. King, and S. H. White, *Structure of a fluid dioleoylphosphatidylcholine bilayer determined by joint refinement of x-ray and neutron diffraction data. I. Scaling of neutron data and the distributions of double bonds and water*. *Biophysical Journal*, 1991. **60**(3): p. 568-576.
162. J. P. Bradshaw, S. M. Davies, and T. Hauss, *Interaction of substance P with phospholipid bilayers: A neutron diffraction study*. *Biophysical Journal*, 1998. **75**(2): p. 889-895.
163. S. Dante, T. Hauss, and N. A. Dencher, *Beta-amyloid 25 to 35 is intercalated in anionic and zwitterionic lipid membranes to different extents*. *Biophysical Journal*, 2002. **83**(5): p. 2610-2616.
164. M. C. Wiener and S. H. White, *Fluid Bilayer Structure Determination by the Combined Use of X-Ray and Neutron-Diffraction. 2. Composition-Space Refinement Method*. *Biophysical Journal*, 1991. **59**(1): p. 174-185.
165. T. Hauss, G. Buldt, M. P. Heyn, and N. A. Dencher, *Light-Induced Isomerization Causes an Increase in the Chromophore Tilt in the M-Intermediate of Bacteriorhodopsin - a Neutron-Diffraction Study*. *Proceedings*

- of the National Academy of Sciences of the United States of America, 1994. **91**(25): p. 11854-11858.
166. G. Zaccai, G. Buldt, A. Seelig, and J. Seelig, *Neutron Diffraction Studies on Phosphatidylcholine Model Membranes. 2. Chain Conformation and Segmental Disorder*. *Journal of Molecular Biology*, 1979. **134**(4): p. 693-706.
167. M. Seul and M. J. Sammon, *Preparation of Surfactant Multilayer Films on Solid Substrates by Deposition from Organic Solution*. *Thin Solid Films*, 1990. **185**(2): p. 287-305.
168. T. T. Mills, G. E. Toombes, S. Tristram-Nagle, D. M. Smilgies, G. W. Feigenson, and J. F. Nagle, *Order parameters and areas in fluid-phase oriented lipid membranes using wide angle X-ray scattering*. *Biophysical Journal*, 2008. **95**(2): p. 669-681.
169. A. Ruettinger, M. A. Kiselev, T. Hauss, S. Dante, A. M. Balagurov, and R. H. Neubert, *Fatty acid interdigitation in stratum corneum model membranes: a neutron diffraction study*. *European Biophysics Journal*, 2008. **37**(6): p. 759-771.
170. P. J. Hendra, *Fourier transform Raman spectroscopy in pharmaceutical analysis and research*. *American Laboratory*, 1996. **28**(18): p. 13A-13I.
171. N. B. Colthup, L. H. Daly, and S. E. Wiberley, *Introduction to Infrared and Raman Spectroscopy*. 3rd edition ed1990: Academic Press.
172. R. Mendelsohn and D. J. Moore, *Vibrational spectroscopic studies of lipid domains in biomembranes and model systems*. *Chemistry and Physics of Lipids*, 1998. **96**(1-2): p. 141-157.
173. E. Guillard, A. Tfayli, M. Manfait, and A. Baillet-Guffroy, *Thermal dependence of Raman descriptors of ceramides. Part II: Effect of chains lengths and head group structures*. *Analytical and Bioanalytical Chemistry*, 2011. **399**(3): p. 1201-1213.
174. K. Larsson and R. P. Rand, *Detection of changes in the environment of hydrocarbon chains by Raman spectroscopy and its application to lipid-protein systems*. *Biochimica et Biophysica Acta*, 1973. **326**(2): p. 245-255.
175. R. Mendelsohn, S. Sunder, and H. J. Bernstein, *Structural Studies of Biological Membranes and Related Model Systems by Raman Spectroscopy - Sphingomyelin and 1,2-Dilauroyl Phosphatidylethanol-Amine*. *Biochimica et Biophysica Acta*, 1975. **413**(3): p. 329-340.
176. R. F. Schaufele, *Chain Shortening in Polymethylene Liquids*. *Journal of Chemical Physics*, 1968. **49**(9): p. 4168-4175.
177. K. G. Brown, E. Bicknell-Brown, and M. Ladjadj, *Raman-Active Bands Sensitive to Motion and Conformation at the Chain Termini and Backbones of Alkanes and Lipids*. *Journal of Physical Chemistry*, 1987. **91**(12): p. 3436-3442.
178. R. G. Snyder, S. L. Hsu, and S. Krimm, *Vibrational Spectra in C-H Stretching Region and Structure of Polymethylene Chain*. *Spectrochimica Acta, Part A: Molecular and Biomolecular Spectroscopy*, 1978. **34**(4): p. 395-406.
179. R. G. Snyder and J. R. Scherer, *Band-Structure in the C-H Stretching Region of the Raman-Spectrum of the Extended Polymethylene Chain - Influence of Fermi Resonance*. *Journal of Chemical Physics*, 1979. **71**(8): p. 3221-3228.
180. A. Tfayli, E. Guillard, M. Manfait, and A. Baillet-Guffroy, *Thermal dependence of Raman descriptors of ceramides. Part I: Effect of double bonds in hydrocarbon chains*. *Analytical and Bioanalytical Chemistry*, 2010. **397**(3): p. 1281-1296.

181. R. W. Wang, J. Guo, G. Baran, and S. L. Wunder, *Characterization of the state of order of octadecylsilane chains on fumed silica*. *Langmuir*, 2000. **16**(2): p. 568-576.
182. G. W. H. Höhne, W. F. Hemminger, and H.-J. Flammersheim, *Differential Scanning Calorimetry 2003*, Berlin: Springer.
183. Y. Saito, K. Saito, and T. Atake, *Theoretical Analysis of Heat-Flux Differential Scanning Calorimetry Based on a General Model*. *Thermochimica Acta*, 1986. **99**: p. 299-307.
184. R. M. J. Cotterill, *Biophysics - An Introduction 2002*, Chichester John Wiley & Sons Ltd.
185. K. Schmidt-Rohr and H. W. Spiess, *Multidimensional Solid-State NMR and Polymers 1994*, London: Academic Press.
186. J. Grandjean and P. Laszlo, *Deuterium Nuclear Magnetic Resonance Studies of Water Molecules Restrained by Their Proximity to a Clay Surface*. *Clays and Clay Minerals*, 1989. **37**(5): p. 403-408.
187. E. Sternin, M. Bloom, and A. L. Mackay, *De-Pake-ing of NMR Spectra*. *Journal of Magnetic Resonance*, 1983. **55**(2): p. 274-282.
188. J. H. Davis, K. R. Jeffrey, M. Bloom, M. I. Valic, and T. P. Higgs, *Quadrupolar Echo Deuteron Magnetic Resonance Spectroscopy in Ordered Hydrocarbon Chains*. *Chemical Physics Letters*, 1976. **42**(2): p. 390-394.
189. J. H. Davis and K. R. Jeffrey, *Temperature Dependence of Chain Disorder in Potassium Palmitate-Water - A Deuterium NMR Study*. *Chemistry and Physics of Lipids*, 1977. **20**(2): p. 87-104.
190. Y. Takeuchi, Y. Yamaoka, S. Fukushima, K. Miyawaki, K. Taguchi, H. Yasukawa, S. Kishimoto, and M. Suzuki, *Skin penetration enhancing action of cis-unsaturated fatty acids with omega-9, and omega-12-chain lengths*. *Biological & Pharmaceutical Bulletin*, 1998. **21**(5): p. 484-491.
191. A. Tonegawa, A. Michiue, T. Masuda, K. Ohno, H. Matsuura, K. Yamada, and T. Okuda, *Deuterium NMR and Raman spectroscopic studies on conformational behavior of lipophilic chains in the C12E3/decane/water system*. *Zeitschrift für Naturforschung Section A - a Journal of Physical Sciences*, 2002. **57**(6-7): p. 320-326.
192. W. M. Holleran, M. Q. Man, W. N. Gao, G. K. Menon, P. M. Elias, and K. R. Feingold, *Sphingolipids are required for mammalian epidermal barrier function. Inhibition of sphingolipid synthesis delays barrier recovery after acute perturbation*. *Journal of Clinical Investigation*, 1991. **88**(4): p. 1338-1345.
193. G. M. Gray and R. J. White, *Glycosphingolipids and Ceramides in Human and Pig Epidermis*. *Journal of Investigative Dermatology*, 1978. **70**(6): p. 336-341.
194. M. Ponc, A. Weerheim, P. Lankhorst, and P. Wertz, *New acylceramide in native and reconstructed epidermis*. *Journal of Investigative Dermatology*, 2003. **120**: p. 581-588.
195. P.W. Wertz, *Stratum corneum lipids and water*. *Exogenous Dermatology*, 2004. **3**: p. 53-56.
196. C. Faure, J. F. Tranchant, and E. J. Dufourc, *Interfacial hydration of ceramide in stratum corneum model membrane measured by 2H NMR of D2O*. *Journal De Chimie Physique Et De Physico-Chimie Biologique*, 1998. **95**(2): p. 480-486.
197. B. Dahlen and I. Pascher, *Molecular Arrangements in Sphingolipids - Thermotropic Phase Behavior of Tetracosanoylphyto-sphingosine*. *Chemistry and Physics of Lipids*, 1979. **24**(2): p. 119-133.

198. B. Dahlen and I. Pascher, *Molecular Arrangements in Sphingolipids. Crystal Structure of N-Tetracosanoylphyto sphingosine*. Acta Crystallographica, Section B: Structural Crystallography and Crystal Chemistry, 1972. **B 28**(AUG15): p. 2396-2404.
199. P. Garidel, B. Folting, I. Schaller, and A. Kerth, *The microstructure of the stratum corneum lipid barrier: Mid-infrared spectroscopic studies of hydrated ceramide:palmitic acid:cholesterol model systems*. Biophysical Chemistry, 2010. **150**(1-3): p. 144-156.
200. I. Pascher, *Molecular Arrangements in Sphingolipids Conformation and Hydrogen-Bonding of Ceramide and Their Implication on Membrane Stability and Permeability*. Biochimica et Biophysica Acta, 1976. **455**(2): p. 433-451.
201. P. Garidel, *Calorimetric and spectroscopic investigations of phytosphingosine ceramide membrane organisation*. Physical Chemistry Chemical Physics, 2002. **4**(10): p. 1934-1942.
202. M. E. Rerek, H. C. Chen, B. Markovic, D. Van Wyck, P. Garidel, R. Mendelsohn, and D. J. Moore, *Phytosphingosine and sphingosine ceramide headgroup hydrogen bonding: Structural insights through thermotropic hydrogen/deuterium exchange*. Journal of Physical Chemistry B, 2001. **105**(38): p. 9355-9362.
203. J. Hadgraft, J. Peck, D. G. Williams, W. J. Pugh, and G. Allan, *Mechanisms of action of skin penetration enhancers retarders: Azone and analogues*. International Journal of Pharmaceutics, 1996. **141**(1-2): p. 17-25.
204. F. Sahle, *Development and biopharmaceutical evaluation of microemulsions for targeted delivery of ceramides and other Stratum Corneum lipids into the Stratum Corneum (PhD thesis)* 2012, Martin Luther University Halle-Wittenberg: Halle/Saale.
205. M. de Jager, G. Gooris, M. Ponc, and J. Bouwstra, *Acylceramide head group architecture affects lipid organization in synthetic ceramide mixtures*. Journal of Investigative Dermatology, 2004. **123**(5): p. 911-916.
206. D. Groen, G. S. Gooris, and J. A. Bouwstra, *New Insights into the Stratum Corneum Lipid Organization by X-Ray Diffraction Analysis*. Biophysical Journal, 2009. **97**(8): p. 2242-2249.
207. I. M. Schneider, B. Dobner, R. Neubert, and W. Wohlrab, *Evaluation of drug penetration into human skin ex vivo using branched fatty acids and propylene glycol*. International Journal of Pharmaceutics, 1996. **145**(1-2): p. 187-196.
208. A. C. Sintov, I. Krymberk, V. Gavrillov, and R. Gorodischer, *Transdermal delivery of paracetamol for paediatric use: effects of vehicle formulations on the percutaneous penetration*. Journal of Pharmacy and Pharmacology, 2003. **55**(7): p. 911-919.
209. S. S. Funari, F. Barcelo, and P. V. Escriba, *Effects of oleic acid and its congeners, elaidic and stearic acids, on the structural properties of phosphatidylethanolamine membranes*. Journal of Lipid Research, 2003. **44**(3): p. 567-575.
210. P. Tandon, G. Forster, R. Neubert, and S. Wartewig, *Phase transitions in oleic acid as studied by X-ray diffraction and FT-Raman spectroscopy*. Journal of Molecular Structure, 2000. **524**: p. 201-215.
211. H. Tanojo, A. Bos-van Geest, J. A. Bouwstra, H. E. Junginger, and H. E. Bodde, *In vitro human skin barrier perturbation by oleic acid: Thermal analysis and freeze fracture electron microscopy studies*. Thermochemica Acta, 1997. **293**(1-2): p. 77-85.

212. R. T. Zhang, W. J. Sun, S. Tristram-Nagle, R. L. Headrick, R. M. Suter, and J. F. Nagle, *Critical Fluctuations in Membranes*. Physical Review Letters, 1995. **74**(14): p. 2832-2835.
213. S. G. Clerc and T. E. Thompson, *Permeability of Dimyristoyl Phosphatidylcholine/Dipalmitoyl Phosphatidylcholine Bilayer Membranes with Coexisting Gel and Liquid-Crystalline Phases*. Biophysical Journal, 1995. **68**(6): p. 2333-2341.
214. A. Schroeter, *The role of ceramide [AP] for the structural assembly of stratum corneum lipid model membranes (PhD thesis)* 2010, Martin Luther University Halle-Wittenberg: Halle/Saale.

8 PUBLICATIONS

Original articles

- Engelbrecht T, Hauß T, Süß K, Vogel A, Roark M, Feller SE, Neubert RHH, Dobner B: Characterisation of a new ceramide EOS species: synthesis and investigation of the thermotropic phase behaviour and influence on the bilayer architecture of stratum corneum lipid model membranes. *Soft Matter* 2011; 7: 8998-9011 (DOI: 10.1039/c1sm05134b)
- Engelbrecht TN, Schroeter A, Hauß T, Neubert RH: Lipophilic penetration enhancers and their impact to the bilayer structure of stratum corneum lipid model membranes: neutron diffraction studies based on the example oleic acid. *Biochimica et Biophysica Acta, Biomembranes* 2011; 1808: 2798-2806 (DOI: 10.1016/j.bbamem.2011.08.012)
- Engelbrecht TN, Demé B, Dobner B, Neubert RHH: Study of the influence of the penetration enhancer isopropyl myristate on the nanostructure of stratum corneum lipid model membranes using neutron diffraction and deuterium labelling. *Skin Pharmacology and Physiology* 2012; 25: 200-207 (DOI: 10.1159/000338538)
- Engelbrecht TN, Schroeter A, Hauß T, Demé B, Scheidt HA, Huster D, Neubert RHH: The impact of ceramides NP and AP on the nanostructure of stratum corneum lipid bilayers. Part I: neutron diffraction and ^2H NMR studies on multilamellar models based on ceramides with symmetric alkyl chain length distribution. *Soft Matter* 2012; 8: 2599-2607 (DOI: 10.1039/c2sm25420d)
- Schroeter A, Engelbrecht T, Neubert RHH, Goebel ASB: New Nanosized Technologies for Dermal and Transdermal Drug Delivery. A Review. *Journal of Biomedical Nanotechnology* 2010; 6: 1–18
- Schröter A, Engelbrecht T, Wepf R, Neubert, RHH: Neue Einblicke in die morphologische und molekulare Struktur des Stratum corneum. *Pharmazeutische Zeitung* (in press)

Conference contributions

- Engelbrecht T, Hauss T, Neubert RHH: Impact of CER[AP] to the structure of Stratum corneum lipid model membranes. *CRS Meeting*, Halle/Saale, March 2009 (poster)
- Engelbrecht T, Hauss T, Neubert RHH: Investigation of stratum corneum lipid model membranes. *HERCULES course poster presentation*, Grenoble, France, March 2009 (poster)

- Engelbrecht T, Hauss T, Neubert RHH: Investigation of stratum corneum lipid model membranes based on CER[AP]. *5th German-Polish Symposium*, Poznan, Poland, May 2009 (poster)
- Engelbrecht T, Hauss T, Neubert RHH: Impact of CER[AP] to the structure of Stratum Corneum Lipid Model Membranes. *Gordon Research Conference (GRC) on Barrier Function of Mammalian Skin*, Waterville Valley Resort, NH, USA, August 2009 (poster)
- Engelbrecht T, Hauß T, Buchsteiner A, Dobner B, Neubert RHH: Strukturaufklärung von Lipid-Modellmembranen. *Deutsche Tagung für Forschung mit Synchrotronstrahlung, Neutronen und Ionenstrahlen an Großgeräten - SNI Berlin*, Berlin, Germany, February 2010 (poster)
- Engelbrecht T, Hauß T, Buchsteiner A, Dobner B, Neubert RHH: Stratum corneum lipid model membranes investigated by means of neutron diffraction – influence of ceramides. *7th World Meeting on Pharmaceuticals, Biopharmaceuticals and Pharmaceutical Technology 2010*, Valletta, Malta, March 2010 (poster)
- Engelbrecht T, Hauss T, Dobner B, Neubert RHH: Impact of lipophilic penetration enhancers on the bilayer structure of oriented Stratum corneum lipid model membranes as seen by neutron diffraction. *Bilayers at the ILL (BILL 2011)*, Grenoble, France, January 2011 (poster)
- Engelbrecht T, Hauss T, Dobner B, Neubert RHH: Impact of lipophilic penetration enhancers on the bilayer structure of oriented Stratum corneum lipid model membranes as seen by neutron diffraction. *Biophysical Society, 55th Annual Meeting*, Baltimore, USA, March 2011 (poster)
- Engelbrecht T, Scheidt H, Huster D, Demé B, Neubert RHH: Stratum corneum lipid model membranes based on CER[NP] - The bilayer structure as seen by neutron diffraction and 2H-NMR spectroscopy. *APV Skin Forum 12th Annual Meeting*, Frankfurt/Main, Germany, March 2011 (poster and oral presentation)
- Schroeter A, Engelbrecht T, Vogel A, Dobner B, Hauß T, Neubert RHH, Asymmetry in Stratum corneum lipid model membranes based on ceramide [NP], *Gordon Research Conference (GRC) on Barrier Function of Mammalian Skin*, Waterville Valley Resort, NH, USA, August 2011 (poster)
- Engelbrecht T, Hauss T, Dobner B, Neubert RHH: *Impact of Lipophilic Penetration Enhancers on the Bilayer Structure of Oriented Stratum Corneum Lipid Model Membranes as seen by Neutron Diffraction*. *HZB User Meeting*, November 2011, Berlin, Germany (poster)

- Schroeter A, Engelbrecht TN, Vogel A, Hauß T, Dobner B, Neubert RHH: Asymmetry in stratum corneum lipid model membranes based on ceramide [NP]. *HZB User Meeting*, Berlin, Germany, November 2011 (poster)
- Schroeter A, Engelbrecht TN, Vogel A, Hauß T, Dobner B, Neubert RHH: Molecular Structure of the Stratum corneum Lipid Matrix: Impact of Ceramides and Influence of Penetration Enhancers Based on Biophysical in vitro Investigations. *8th World Meeting on Pharmaceutics, Biopharmaceutics and Pharmaceutical Technology*, Istanbul, Turkey, March 2012

Reports

- Engelbrecht T, Schroeter A, Neubert R, Hauß T: Role of ceramide [AP] and ceramide [EOS] in the structural assembly of stratum corneum model membranes. *BENSC Annual Experimental Report*, 2008
- Engelbrecht T, Dobner B, Neubert R, Buchsteiner A, Hauß T: Neutron diffraction study of model membranes with complex Stratum corneum like lipid composition. *HZB (BER II) Annual Experimental Report*, 2009
- Engelbrecht T, Dobner B, Neubert R, Buchsteiner A, Hauß T: Quaternary stratum corneum model membranes with or without penetration enhancers and the impact of pH. *HZB (BER II) Annual Experimental Report*, 2009
- Engelbrecht T, Hauß T, Buchsteiner A, Dobner B, Neubert RHH: Investigation of the effects of penetration enhancers on the lipid assembly in stratum corneum lipid model membranes. *HZB (BER II) Annual Experimental Report*, 2010
- Engelbrecht T, Hauß T, Buchsteiner A, Dobner B, Neubert RHH: Effects of oleic acid on the lipid assembly in stratum corneum lipid model membranes based on asymmetric ceramides. *HZB (BER II) Annual Experimental Report*, 2010
- Schröter A, Engelbrecht T, Neubert RHH, Hauß T: Molecular Structure of the Stratum corneum Lipid Membrane: A New Theoretical Model for the Lipid matrix. *HZB (BER II) Annual Experimental Report*, 2010
- Engelbrecht T, Demé B: Stratum corneum (SC) lipid model membranes: Investigation of the influence of penetration enhancers on the bilayer structure. *Experimental Report for ILL Experiment, proposal no. 8-02-554*, public since 01/12/2011

9 ACKNOWLEDGEMENT

First, I would like to express my sincere gratitude to my advisor, Prof. Dr. R. Neubert for the interesting topic, his enthusiasm and encouragement, for the provision of freedom during all stages of the present PhD work and for his continuous readiness to discuss results.

I'm especially thankful to Dr. Thomas Hauß from Helmholtz Zentrum Berlin für Materialien und Energie (HZB, Berlin, Germany) for his permanent readiness to provide support for the evaluation of the neutron diffraction data and to discuss experimental results. His helpful assistance during the various beam times at V1 and the friendly atmosphere at HZB contributed to the success of this work.

I thank Bruno Demé for his help with experiments at D16, Institut Laue-Langevin (ILL, Grenoble, France) and the assistance during the evaluation of the diffraction data.

I would also like to thank Dr. Holger Scheidt and Prof. Dr. D. Huster (Institute for Medical Physics and Biophysics, University of Leipzig) for their support during performing the ^2H NMR spectroscopic measurements, for the fruitful discussions of the experimental results and for carefully reading the manuscript. I thank Dr. Alexander Vogel (Institute for Medical Physics and Biophysics, University of Leipzig) for contributing the MD simulations to the manuscript and for his helpful comments.

I'm grateful to Dr. Thomas Müller and Dr. Christoph Wagner (Institute of Chemistry, Martin Luther University Halle-Wittenberg) for the help with the X-ray experiments.

Special thanks go to Mrs. Heike Rudolf and Mrs. Kerstin Schwarz for the technical assistance with the FT Raman spectroscopy and DSC experiments.

I thank all members of the Biopharmacy group, in particular Annett Schröter, Alexandra Göbel, Elfi Busse, Sandy Naumann, and all other colleagues for the friendly atmosphere, the helpful discussions and their support.

Furthermore, I would like to thank Evonik Goldschmidt GmbH (Essen, Germany) for funding and for the donation of the ceramides used for all experiments.

I'm especially grateful to Graduiertenförderung des Landes Sachsen-Anhalt for awarding the grant, which provided the required financial support for this work.

Special thanks go to my family and friends, in particular my parents for their permanent support during the last years.

10 CURRICULUM VITAE

Personal Information

Name	Tanja Nadine Engelbrecht
Date of Birth	April 09 th , 1983
Place of Birth	Zschopau, Germany
Nationality	German
Marital status	Not married
Address	Max-Reger-Straße 4, 06110 Halle (Saale)

School Education and Studies

1989 – 1993	Grundschule Martin-Anderson-Nexö, Zschopau, Germany
1993 – 2001	Gymnasium Zschopau, Germany (Abitur)
09/2001 – 07/2005	Pharmacy studies, University of Leipzig, Germany
11/2005 – 04/2006	Practical training, Pelikan-Apotheke, Marienberg, Germany
05/2006 – 10/2006	Practical training, Pharmacy of St. Elisabeth Hospital, Leipzig, Germany
12/2006	Approbation as pharmacist

Professional Experience

11/2006 – 12/2006	Pharmacist, Apotheke Alte Messe, Leipzig, Germany
01/2007 – 06/2007	Pharmacist, Linden-Apotheke, Chemnitz, Germany
06/2007 – 07/2008	Pharmacist, Management of the subsidiary pharmacy Charlotten-Apotheke, Chemnitz, Germany
07/2008 – 01/2012	Ph.D. student in the group of Prof. Dr. R. Neubert, Institute of Pharmacy, Department of Pharmaceutical Technology and Biopharmacy, Martin Luther University Halle-Wittenberg, Halle (Saale), Germany
03/2009 – 04/2009	Participation at HERCULES (H igher E uropean R esearch C ourse for U sers of L arge E xperimental S ystems on neutron and synchrotron radiation in science), Grenoble, France
05/2009 – 05/2012	Pharmacist, Apotheke am Händelhaus, Halle (Saale), Germany

10/2008 – 01/2012

Research and teaching assistant in the group of Prof. Dr. Dr. R. Neubert, Institute of Pharmacy, Department of Pharmaceutical Technology and Biopharmacy, Martin Luther University Halle-Wittenberg, Halle (Saale), Germany

11 EIDESSTATTLICHE ERKLÄRUNG

Hiermit erkläre ich entsprechend § 5 Absatz 2b der Promotionsordnung der Naturwissenschaftliche Fakultät I (Biowissenschaften) der Martin-Luther-Universität Halle-Wittenberg, dass ich die Ergebnisse der vorliegenden Dissertationsarbeit

„Impact of Ceramides and Penetration Enhancers on the Nanostructure of Stratum Corneum Lipid Model Membranes“

am Institut für Pharmazeutische Technologie und Biopharmazie der Martin-Luther-Universität Halle-Wittenberg selbständig und ohne fremde Hilfe erarbeitet und verfasst habe. Ferner habe ich nur die in der Dissertation angegebenen Literaturstellen und Hilfsmittel verwendet und die entnommenen und benutzten Literaturstellen auch als solche kenntlich gemacht. Ich habe mich zu keinem früheren Zeitpunkt um den Dokortitel beworben. Weiterhin habe ich die vorliegende Arbeit bisher keiner anderen Prüfungsbehörde vorgelegt.

Halle (Saale), im Juni 2012

Tanja Engelbrecht